MOLECULAR ANALYSIS OF F_1F_0 ADENOSINE TRIPHOSPHATE SYNTHASE AND RENAL H^+,K^+-ADENOSINE TRIPHOSPHATASES

By

TAMARA CAVISTON OTTO

A DISSERTATION PRESENTED TO THE GRADUATE SCHOOL
OF THE UNIVERSITY OF FLORIDA IN PARTIAL FULFILLMENT
OF THE REQUIREMENTS FOR THE DEGREE OF
DOCTOR OF PHILOSOPHY

UNIVERSITY OF FLORIDA

2001

This dissertation is dedicated to my family and to my husband for their continuous love and support.

ACKNOWLEDGMENTS

I would like to thank my advisor, Dr. Brian Cain. Dr. Cain has been a continuous source of encouragement and support throughout my career as a graduate student. He has provided me with the training and experience necessary for me to become a successful scientist. I would also like to express my gratitude to the other members of my committee--Dr. Michael Kilberg, Dr. Mary Jo Koroly, Dr. Daniel Purich, and Dr. Charles Wingo--for their help and support during my time spent at the University of Florida. I want to thank the members of my lab--Grady Campbell, James Gardner, Paul Sorgen, Debbie Zies, Tammy Bohannon, Michelle Gumz, and Andy Hardy--as well as Sue Lee Kang and Chien Chen of the Yang lab for the stimulating discussions we have shared and for providing a great place to work.

I want to especially thank my family for their love and support throughout these difficult years. They worked long hours to provide me with an excellent education, which has allowed me to achieve my goals. I thank them dearly.

Finally, I wish to thank my dear husband, Scott. Scott has been my best friend and my greatest supporter during the demands of graduate school. He has always been there giving me the strength and courage to continue. I could not have accomplished this great achievement without his support.

TABLE OF CONTENTS

ACKNOWLEDGMENTS..... iii

LIST OF TABLES..... vi

LIST OF FIGURES..... vii

ABBREVIATIONS..... x

ABSTRACT..... xii

CHAPTERS

1 BACKGROUND AND SIGNIFICANCE..... 1

Ion Motive ATPases..... 1
E. coli F_1F_0 ATP Synthase..... 6
unc Operon Genetics..... 8
F_1F_0 ATP Synthase Mechanisms..... 10
b Subunit..... 20
H^+,K^+-ATPase..... 27
Gastric H^+,K^+-ATPase..... 33
Renal H^+,K^+-ATPase..... 43
H^+ Versus Na^+,K^+-ATPase..... 54

2 EXPERIMENTAL PROCEDURES..... 56

Recombinant DNA Techniques..... 56
Plasmid Constructions..... 56
F_1F_0 ATP Synthase Methods..... 73
3' RACE..... 77
5' RACE..... 78
Tissue Culture..... 78
H^+,K^+-ATPase Biochemical Assays..... 80
Northern Analysis..... 83
Immunoblot Analysis..... 83
Immunofluorescence Microscopy..... 85

3 CHARACTERIZATION OF b_{Arg-36} MUTATIONS IN F_1F_0 ATP SYNTHASE FROM *ESCHERICHIA COLI*..... 88

Introduction..... 88
Results..... 90
Discussion.....105

4 AMPLIFICATION OF RABBIT NaKβ_1 cDNA.....109

Introduction..... 109
Results..... 111
Discussion.....118

5 EXPRESSION OF RABBIT RENAL H^+,K^+-ATPases.....126

Introduction..... 126
Results..... 128
Discussion.....151

6 CONCLUSIONS AND FUTURE STUDIES.....158

E. coli F_1F_0 ATP Synthase.....158
Renal H^+,K^+-ATPases.....164

LIST OF REFERENCES.....171

BIOGRAPHICAL SKETCH.....195

LIST OF TABLES

Table 2-1. Primers for the PCR mutagenesis of b_{Arg-36} in the *uncF(b)* gene..... 57

Table 2-2. RT-PCR and RACE primers..... 61

Table 2-3. Mutagenesis primers..... 65

Table 3-1. *E. coli* strains and plasmids..... 95

Table 3-2. *In vivo* and *in vitro* activities of b_{Arg-36} mutants..... 96

Table 3-3. Alterations in F_1 activity associated with b_{Arg-36} substitutions..... 104

Table 4-1. Percent amino acid similarity and identity of rabbit NaKβ_1 with other known NaKβ subunit isoforms..... 122

LIST OF FIGURES

Figure 1-1. Subunit organization of *E. coli* F_1F_0 ATP synthase..... 7

Figure 1-2. Transmembrane organization of H^+,K^+-ATPase..... 29

Figure 1-3. Enzymatic mechanism of H^+,K^+-ATPase..... 32

Figure 1-4. Variation in the N-termini of the $HK\alpha_2$ subunits from rabbit, human, and rat..... 49

Figure 1-5. Distance analysis of HKα and NaKα subunits..... 50

Figure 2-1. Rabbit $HK\alpha_{2a}$ cDNA construction in pREP4..... 60

Figure 2-2. Rabbit $HK\alpha_{2c}$ cDNA construction in pREP4..... 62

Figure 2-3. Rabbit HKβ cDNA construction in pREP8..... 64

Figure 2-4. Rabbit $NaK\beta_1$ cDNA construction in pREP8..... 66

Figure 2-5. Rabbit $HK\alpha_{2c}$ cDNA construction in pBudCE4..... 69

Figure 2-6. Rabbit $HK\alpha_{2a}$ cDNA construction in pBudCE4..... 70

Figure 2-7. Rabbit $NaK\beta_1$ cDNA construction in pBudCE4..... 71

Figure 2-8. Plasmids pTLC47 and pTLC37 expression constructs..... 72

Figure 3-1. Amino acid sequence alignment of bacterial *b* and *b'* subunits..... 91

Figure 3-2. Oligonucleotides for PCR mutagenesis of the *uncF*(*b*) gene..... 92

Figure 3-3. *Mun*I restriction endonuclease analysis of *uncF*(*b*) gene mutations in pKAM14..... 94

Figure 3-4. Complementation of *uncF*(*b*) gene mutants in KM2(Δ*b*)..... 97

Figure 3-5. Immunoblot analysis of *uncF*(*b*) gene mutants..... 99

Figure 3-6. ATP-driven energization of membrane vesicles prepared from *uncF*(*b*) gene mutants..... 101

Figure 3-7. Proton permeabililty of stripped membrane vesicles prepared from *uncF*(*b*) gene mutants..... 103

Figure 4-1. Partial nucleotide sequence alignment of known NaKβ_1 subunits..... 112

Figure 4-2. Agarose gel analysis of rabbit NaKβ_1 cDNA PCR amplifications..... 114

Figure 4-3. Nucleotide sequence alignment of rabbit NaKβ_1 cDNA..... 115

Figure 4-4. Agarose gel analysis of rabbit NaKβ_1 5' RACE reactions..... 117

Figure 4-5. GenBank accession record for rabbit NaKβ_1 cDNA sequence..... 119

Figure 4-6. Western analysis of HEK293c18 cells expressing NaKβ_1 from an episomal vector..... 120

Figure 4-7. Kyte-Doolitle hydropathy plot of rabbit NaKβ_1 amino acid sequence.. 123

Figure 4-8. Amino acid sequence analysis of rabbit NaKβ_1 protein..... 124

Figure 5-1. Episomal expression constructs..... 130

Figure 5-2. Northern analysis of HEK293c18 cells expressing HKα_{2a}, HKα_{2c}, and NaKβ_1 from episomal vectors..... 131

Figure 5-3. Western analysis of HEK293c18 cells expressing NaKβ_1 from an episomal vector..... 133

Figure 5-4. Control plasmid pBudCE4/*lacZ*/CAT expression vector..... 135

Figure 5-5. Western analysis of HEK293 cells stably expressing control plasmid pBudCE4/*lacZ*/CAT..... 137

Figure 5-6. Stable expression constructs..... 138

Figure 5-7. Western analysis of COS-1 cells transiently expressing HKα_{2a}-V5, HKα_{2c}-V5, and NaKβ_1 proteins..... 142

Figure 5-8. Differential expression of rabbit NaKβ_1 protein in stable HEK293 clones..... 143

Figure 5-9. Northern analysis of HEK293 cells stably expressing $HK\alpha_{2a}$ or $HK\alpha_{2c}$ transcripts..... 145

Figure 5-10. Agarose gel analysis of $HK\alpha_2$ RT-PCR reactions from stable HEK293 cells..... 146

Figure 5-11. Localization of $HK\alpha_{2a}$-V5 and $HK\alpha_{2c}$-V5 fusion proteins in COS-1 cells..... 149

Figure 5-12. Western analysis of plasma membranes from COS-1 transient transfections..... 150

Figure 5-13. Western analysis of COS-1 cells transiently expressing rabbit $NaK\beta_3$-*myc* fusion protein..... 152

ABBREVIATIONS

ACMA, 9-amino-6-chloro-2-methoxyacridine

ADP, adenosine-5'-diphosphate

Ap, ampicillin

ATP, adenosine-5'-triphosphate

ATPase, adenosine triphosphatase

$b_{Arg\text{-}36 \rightarrow Ile}$, substitution of isoleucine for arginine at amino acid 36 in the *b* subunit

bp, base pair

CAT, chloramphenicol acetyltransferase

CCCP, carbonyl cyanide-*m*-chlorophenylhydrazone

CCD, cortical collecting duct

CD, collecting duct

Cm, chloramphenicol

CMV, cytomegalovirus

DCCD, dicyclohexylcarbodiimide

D-MEM, Dulbecco's modified Eagle medium

DNA, deoxyribonucleic acid

EBNA-1, Epstein Barr virus nuclear antigen-1

EBV, Epstein Barr virus

E. coli, *Escherichia coli*

FBS, fetal bovine serum

GAP3DH, glyceraldehyde-3-phosphate dehydrogenase

IMCD, inner medullary collecting duct

IPTG, isopropyl-1-thio-β-D-galactoside

kbp, kilobase pair

kD, kilodalton

NADH, β-nicotinamide adenine dinucleotide, reduced form

N. crassa, *Neurospora crassa*

NMR, nuclear magnetic resonance

OMCD, outer medullary collecting duct

PCR, polymerase chain reaction

P. modestum, *Propionigenium modestum*

PMSF, phenylmethylsulfonyl fluoride

RT-PCR, reverse-transcriptase PCR

S. cerevisiae, *Saccharomyces cerevisiae*

SDS, sodium dodecyl sulfate

SR, sarcoplasmic reticulum

UTR, untranslated region

v/v, volume/volume

Abstract of Dissertation Presented to the Graduate School
of the University of Florida in Partial Fulfillment of the
Requirements for the Degree of Doctor of Philosophy

MOLECULAR ANALYSIS OF F_1F_0 ADENOSINE TRIPHOSPHATE SYNTHASE AND RENAL H^+,K^+-ADENOSINE TRIPHOSPHATASES

By

Tamara Caviston Otto

May 2001

Chairman: Brian D. Cain
Major Department: Biochemistry and Molecular Biology

The F_1F_0 ATP synthase is responsible for the production of ATP in almost every cell. The enzyme utilizes the electrochemical gradient of protons to drive ATP synthesis. It is composed of two stalks that attach the F_1 sector to the F_0 sector. The peripheral stalk is composed of a dimer of *b* subunits. A specific *b* subunit arginine, $b_{Arg\text{-}36}$ in *Escherichia coli*, displays evolutionary conservation among bacterial F_1F_0 ATP synthases. Site-directed mutagenesis was used to generate a collection of mutations affecting $b_{Arg\text{-}36}$. The phenotype differed depending upon the substitution, and the $b_{Arg\text{-}36\rightarrow Glu}$ and $b_{Arg\text{-}36\rightarrow Ile}$ substitutions virtually abolished enzyme function. Although total amounts of the enzyme present in membranes prepared from mutant strains were reduced, the primary effect of the $b_{Arg\text{-}36}$ substitutions was on activities of the intact enzyme complexes. The most interesting outcome was that the $b_{Arg\text{-}36\rightarrow Glu}$ substitution results in the uncoupling of a functional F_0 from F_1 ATP hydrolysis activity. This is the first uncoupling mutant identified in the *b* subunit.

The renal H^+,K^+-ATPases are membrane proteins located on apical membranes of specialized epithelial cells in the collecting duct that are largely responsible for potassium conservation in the kidney. The enzymes utilize ATP hydrolysis to transport protons outward in an electroneutral exchange for the inward transport of potassium. There are three H^+,K^+-ATPases in the kidney. Each H^+,K^+-ATPase is composed of an α subunit and a β subunit. Two of the rabbit renal HKα subunits, HKα_{2a} and HKα_{2c}, are very closely related and are the products of one gene. The HKα_{2c} subunit has a sixty-one amino acid extension at its amino-terminus. To study differences between HKα_{2a} and HKα_{2c}, a mammalian transient expression system was established. The rabbit NaKβ_1 subunit was amplified from rabbit medulla using 5' and 3' rapid amplification of cDNA ends to use as the β subunit in the expression system. Later, the NaKβ_3 subunit was also studied. Both HKα_2 subunits were readily identified by Western analysis. The proteins were also seen by immunocytochemistry. However, there was no apparent association with either β subunit. This is in agreement with recent observations reported by other researchers.

CHAPTER 1
BACKGROUND AND SIGNIFICANCE

Ion Motive ATPases

Ion motive ATPases are cellular enzymes that utilize the free energy stored in adenosine-5'-triphosphate (ATP) to generate electrochemical ion gradients. These gradients maintain intracellular ionic or pH balance and stimulate an assortment of processes including absorption, secretion, and transmembrane signaling. Some ATPases are responsible for coupling energy to catalyze processes such as muscle relaxation and receptor recycling. There are three distinct classes of ion motive ATPases. These classes are designated F-type, V-type, and P-type ATPases (177). The work described in this dissertation represents studies conducted on an F-type ATPase and a P-type ATPase. This section will provide a brief overview of the general characteristics of the families of ion motive ATPases. The rest of the chapter will cover in detail the F_1F_0 ATP synthase and the H^+,K^+-ATPase.

Properties of F-type ATPases

F-type ATPases are a family of very large multimeric membrane proteins that contain eight or more different subunits with a complex stoichiometry. The enzymes are responsible for synthesizing the majority of ATP in a cell and are more correctly referred to as F_1F_0 ATP synthases. F_1F_0 ATP synthases are located in the inner mitochondrial membrane, the chloroplast thylakoid membrane, and the bacterial cytoplasmic membrane. Although they vary in oligomeric complexity (125, 251), each of the F_1F_0

ATP synthases from mitochondria, chloroplasts, and bacteria has homologous subunits and share a common molecular architecture. The F_1F_0 ATP synthases are composed of two sectors termed F_1 and F_0. They are routinely separated *in vitro* to facilitate the study of the enzyme. F_1 is a globular head attached to F_0 by an asymmetric central stalk and a peripheral stalk (1, 256). The soluble F_1 sector houses the catalytic subunits for ATP synthesis, and the membrane-bound F_0 sector is responsible for proton translocation.

The chemiosmotic hypothesis, first postulated by Peter Mitchell in the early 1960's, describes the general mechanism of ATP production by the F_1F_0 ATP synthase (158). The hypothesis states that an electrochemical gradient of protons ($\Delta\mu H^+$) is generated during photosynthesis or oxidative phosphorylation. The gradient leads to the energetically favorable movement of protons through F_1F_0 ATP synthase to form ATP. We now know that energy captured from the passage of protons down the electrochemical gradient through the membrane-bound F_0 sector of the enzyme causes the rotation of the central stalk within the F_1 sector. Rotation of the central stalk drives the three nucleotide-binding sites in F_1 through the conformational states to produce ATP (26, 169).

In mitochondria and in chloroplasts, the physiological role of the F_1F_0 ATP synthase is to produce ATP. The enzymes from facultative bacteria, however, have two physiological roles that vary depending on the environmental conditions. In an aerobic environment where $\Delta\mu H^+$ is generated through oxidative phosphorylation, the enzyme utilizes the gradient and synthesizes ATP. Under anaerobic conditions where $\Delta\mu H^+$ is low, the physiological role of the bacterial F_1F_0 ATP synthase is to conduct ATP-driven proton translocation. The enzyme functions in reverse and works as an ATPase,

hydrolyzing cytoplasmic ATP to translocate protons across the membrane generating the proton motive force ($\Delta\mu H^+$). The $\Delta\mu H^+$ is used to power flagellar rotation and proton symporters for nutrient uptake of sugars or amino acids. The ATPase function is inhibited in the mitochondrial and chloroplast enzymes to avoid wasteful ATP hydrolysis *in vivo*. However, purified enzymes from these sources can act as ATPases *in vitro*.

Properties of V-type ATPases

V-type ATPases are very large multimeric membrane protein complexes that have thirteen or more subunits with a complex stoichiometry. The enzymes catalyze ATP-dependent proton translocation in eukaryotic cells and are often called H^+-ATPases (70, 223). H^+-ATPases acidify intracellular compartments, including clathrin-coated vesicles, endosomes, and lysosomes. Acidification of intracellular compartments is responsible for a variety of cellular processes, such as receptor-mediated endocytosis, membrane trafficking, and molecular processing. The enzymes have also been identified in the plasma membranes of specific cells where they are responsible for activities such as urine acidification (128), bone resorption (23), and cytoplasmic pH maintenance (77).

The H^+-ATPase has a similar structural organization to the F_1F_0 ATP synthase, and both enzymes share segments of conserved primary sequence homology in specific subunits. Like the F-type enzymes, the H^+-ATPase is composed of two sectors termed V_1 and V_0. The soluble V_1 sector is responsible for ATP hydrolysis, and the membrane-bound V_0 sector conducts proton translocation. V_1 and V_0 are connected by both a central stalk and a peripheral stalk with additional projections at the base of the central stalk (24, 59). Like the F_1F_0 ATP synthase, the two sectors of the H^+-ATPase can be separated *in vitro*. However, unlike the F_1F_0 ATP synthase, the detached V_1 sector has

very little ATPase activity, and the isolated V_0 sector does not seem to form an open proton pore (86, 267, 270). Although the method by which the H^+-ATPase conducts ATP-dependent proton translocation is not known, it is believed that the mechanism is similar to the rotation that occurs in the F_1F_0 ATP synthase.

Kane (118) demonstrated that fully assembled yeast H^+-ATPase complexes disassembled into inactive V_1 and V_0 sectors *in vivo* in response to changes in carbon source. This disassembly was completely reversible. The process may be a common feature of all H^+-ATPases (86, 227). Indeed, many cells contain pools of free V_1 and V_0 sectors along with fully assembled H^+-ATPase complexes (56, 167, 178, 227, 239). Disassembly of the enzyme probably acts to conserve cytosolic ATP during glucose deprivation. Therefore, the disassembly and reassembly of the enzyme is likely to function as a general regulatory mechanism for the H^+-ATPase.

Properties of P-type ATPases

P-type ATPases are a family of comparatively simple membrane proteins with one to three subunits. These enzymes utilize the energy of ATP hydrolysis to maintain specific transmembrane ion gradients (161, 199). Members of the P-type ATPase family are grouped into two classes, Type I and Type II. Type I P-type ATPases transport transition-metal ions, and Type II P-type ATPases transport alkali cations and other small cations. Type II P-type ATPases are further divided into Type IIA and Type IIB depending on the number of subunits present in the enzyme. In eukaryotic cells, members of the P-type ATPase family include the Ca^{2+}-ATPases involved in cellular regulation of Ca^{2+} and found in plasma membranes and intracellular membrane systems like the sarcoplasmic and endoplasmic reticulums; the Na^+,K^+-ATPases involved in

cellular volume regulation, development of membrane potential, and Na^+ transport in kidney, intestine, and other epithelial tissues; H^+,K^+-ATPases involved in the acidification of the stomach and K^+ reabsorption in the distal colon and renal collecting ducts; and H^+-ATPases in yeast and plant cells responsible for proton-dependent nutrient uptake. The prokaryotic P-type ATPases include the Kdp-ATPases involved in the high affinity K^+-uptake in *E. coli* (8); the Mg^{2+}-ATPases responsible for outward transport of Mg^{2+} in *Salmonella typhimurium* (233); and the Cu^+-ATPases involved in uptake of heavy metals in *Enterococcus hirae* (216).

Each member of the P-type ATPase family contains the catalytic α subunit, which is responsible for ATP hydrolysis. In addition, Type IIB P-type ATPases also have a glycosylated β subunit, which is responsible for trafficking the α subunit to the membrane and for modulating enzymatic activity. The only members of the Type IIB family that have been identified to date are the Na^+,K^+-ATPase and the H^+,K^+-ATPase. In certain tissues, however, the Na^+,K^+-ATPase contains a third membrane protein referred to as the γ subunit. The γ subunit seems to modulate the affinity of the enzyme for ATP, Na^+, and K^+ (11, 235, 236). Although each member of the P-type ATPase family is similar in size, there must be important differences that reflect their specific ion motive properties. The specificity of the translocated ions most likely is characteristic of the non-conserved amino acids of the ion binding domains or channels of these ATPases.

Unlike the F-type and V-type ATPases, enzymes of the P-type form a high-energy aspartyl-phosphoryl-enzyme intermediate during ATP hydrolysis. However, the mechanism by which they utilize ATP hydrolysis and phosphorylation to translocate ions across the membrane is not clearly understood. The most popular model for the catalytic

mechanism of these enzymes is the E_1-E_2 model (51, 108, 117, 206). This mechanism assumes two major conformational states, E_1 and E_2, which are distinguished by their ability to be phosphorylated by ATP and P_i, respectively. Phosphorylation forces the enzyme into the E_2 state and following dephosphorylation, the enzyme returns to the E_1 state. Phosphorylation and dephosphorylation cause changes to occur within the enzyme, and the bound ion is translocated across the membrane and released.

This dissertation describes the molecular analysis of two ion motive ATPases: the F_1F_0 ATP synthase from *E. coli* and the rabbit renal H^+,K^+-ATPase. This chapter will cover both enzymes in detail.

E. coli F_1F_0 ATP Synthase

The *E. coli* F_1F_0 ATP synthase is the simplest and most widely studied F_1F_0 ATP synthase. It has the stoichiometric subunit composition of $\alpha_3\beta_3\delta\varepsilon$ for the F_1 sector (253) and $ab_2c_{10\text{-}12}$ for the F_0 sector (97) (Figure 1-1). The F_1 sector is connected to the F_0 sector by the central stalk and the peripheral stalk (1, 256). The $\gamma\varepsilon$ subunits make up the central stalk, and the *b* subunit dimer forms the peripheral or second stalk. The enzyme can function either as a proton-driven ATP synthase or an ATP-driven proton pump *in vivo* or *in vitro*. Mutants with a defective F_1F_0 ATP synthase cannot support growth on nonfermentable substrates such as succinate because of a lack of oxidative phosphorylation, but are still able to grow aerobically on glycolytic substrates.

The F_1F_0 ATP synthase from bacteria is an advantageous system to study for the following reasons: (1) the genes can be over-expressed from plasmid vectors; (2) molecular techniques can be utilized to change the genes on the chromosome as well as genes cloned into plasmids; (3) *E. coli* can grow by glycolysis permitting study of strains

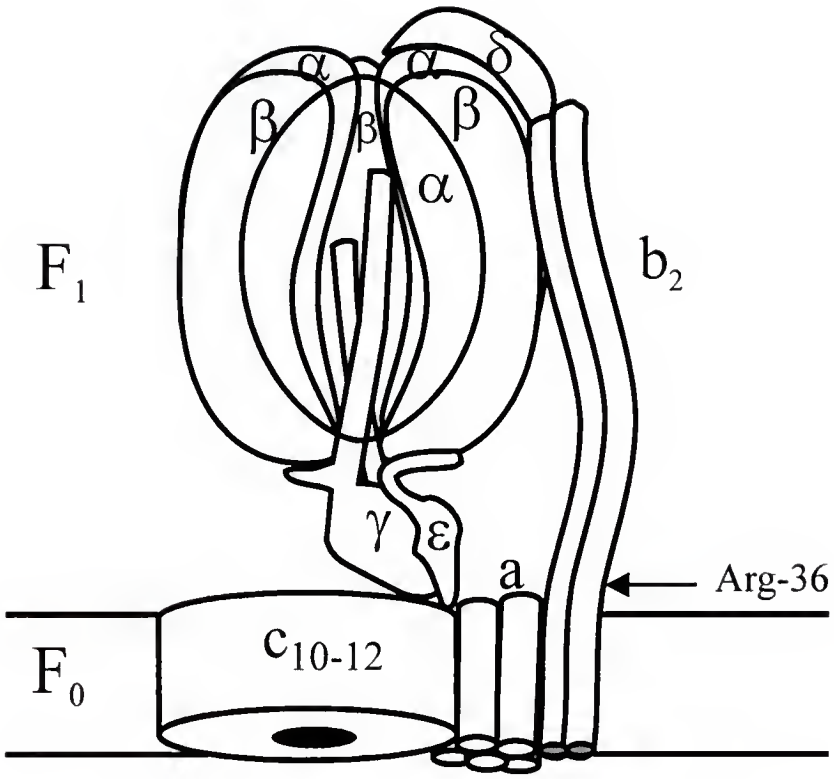

Figure 1-1. Subunit organization of *E. coli* F_1F_0 ATP synthase.

defective in F_1F_0 ATP synthase; (4) the enzyme from *E. coli* is an appropriate model for studying diseases in the human mitochondrial F_1F_0 ATP synthase.

The work described in Chapter 3 addresses the biochemical characterization of the conserved residue $b_{Arg\text{-}36}$ in the *b* subunit of the *E. coli* enzyme. This section will discuss what is currently known about the structure and rotational catalysis of the F_1F_0 ATP synthase and will detail the role of the *b* subunit as the stator of the F_1F_0 ATP synthase.

unc Operon Genetics

Many *E. coli* mutants which are defective in F_1F_0 ATP synthase have been isolated. All mutants mapped in eight complementation groups of the *unc* operon located at about 83 min on the genetic map (58, 76). The order of the structural genes was shown to be *uncB*(*a*), *uncE*(*c*), *uncF*(*b*), *uncH*(δ), *uncA*(α), *uncG*(γ), *uncD*(β), and *uncC*(ε) (90). The gene order of the *unc* operon was confirmed by determining its complete sequence (253). The F_1F_0 ATP synthase genes were preceded by a ninth gene, *uncI*, whose role remains a mystery. The *uncI* gene encoded a basic and hydrophobic protein (253). Using antibodies, the *uncI* gene product has been shown to be located on the cytoplasmic membrane as well as in preparations of F_0 or F_1F_0 (203). However, since the gene was deleted without affecting assembly or activity of the F_1F_0 ATP synthase (82), the protein is not believed to be a subunit of the functional enzyme.

The functional promoter for the genes of the *unc* operon is upstream of *uncI*, two weak promoters are present in the *uncI* reading frame, and the transcriptional terminator is immediately downstream of *uncC*(ε). A single polycistronic mRNA transcript was observed (84, 113, 121, 170). Although there is only one copy of each gene in the

transcript, some subunits, such as *c*, are found in multiple copies in the intact complex, whereas other subunits are present in single copies. How is the expression of the genes regulated so that the final stoichiometries are attained? The regulation is believed to be under translational control. Brusilow *et al.* (28) identified loop and stem structures immediately preceding initiation codons for the *uncF*(*b*), *uncH*(δ) and *uncG*(γ) genes. In each case, these genes follow a more highly expressed gene in the *unc* operon. The RNA secondary structures probably function to lower the expression of the genes immediately downstream.

Ikemura (106, 107) analyzed the order of preference among identical codons and named the most preferred codon the "optimal codon." His theory was that *E. coli* genes encoding for multi-copy proteins used optimal codons selectively whereas other genes used optimal and nonoptimal codons to almost equivalent levels. Kanazawa *et al.* (116) utilized this calculation for the genes of the F_1F_0 subunits and found that the frequency of usage of the optimal codon was indeed higher in the multi-copy subunit than in the single copy subunit, suggesting that the number of subunits is decided at least to some degree by the frequency of codon usage in each gene.

However, regulation of translation is more likely related to RNA secondary structure and ribosome binding efficiency. Schaefer *et al.* (201) used primer extension inhibition or "toeprinting" to analyze ribosome-binding activities of the translation initiation sites of the *unc* operon genes. The toeprint for *uncE*(*c*) was at least twice as strong as those from the other genes. Since there is a direct correlation between the intensity of a toeprint band *in vitro* and the strength of the ribosome-binding site *in vivo*, the *uncE*(*c*) gene has the most efficient ribosome-binding site in the *unc* operon. This

observation is in agreement with the fact that the *c* subunit is the most highly expressed subunit in the F_1F_0 ATP synthase.

Recently, Brusilow's group identified an intragenic ribosome binding site within the *uncB*(*a*) reading frame that preceded a five-codon reading frame that was shifted one base relative to the *uncB*(*a*) reading frame (145). When this binding site was destroyed by mutagenesis, there was a four- to fivefold increase in expression of an *uncB*(*a*)/*lacZ* fusion gene, suggesting that expression of *uncB*(*a*) was lowered by translational frameshifting at this site within the *uncB*(*a*) reading frame.

F_1F_0 ATP Synthase Mechanisms

The F_1F_0 ATP synthase utilizes the energy stored in $\Delta\mu H^+$ to synthesize ATP by a rotary catalytic mechanism. A variety of experimental evidence indicated that proton translocation drives the rotation of the *c* subunit ring that causes rotation of the γ subunit within the α_3/β_3 hexamer. Rotation leads to catalysis of the three catalytic sites in the β subunits because of the asymmetric γ subunit. Proton translocation and rotational catalysis will be discussed separately in this section, although both are required for ATP synthesis.

Proton Translocation

Proton translocation occurs through the F_0 sector, which in the *E. coli* enzyme consists of $ab_2c_{10\text{-}12}$ (Figure 1-1). Although the organization of the subunits in F_0 remains to be elucidated, low resolution electron microscopic and atomic force microscopic images proposed a ring of *c* subunits with the *a* and *b* subunits lying at the periphery of the ring (22, 212, 230). Chemical cross-linking studies have supported this interpretation (69, 111, 149). The crystal structure of the F_1F_0 ATP synthase from *Saccharomyces*

cerevisiae (*S. cerevisiae*) demonstrated that there is indeed a *c* oligomeric ring, and each *c* subunit forms an α-helical hairpin (224). The α-helical hairpin structure correlated well with earlier structural data from nuclear magnetic resonance (NMR) spectroscopy of a monomeric *c* subunit (85). Neither the *a* nor the *b* subunits were resolved in the crystal structure. The *a* subunit has five transmembrane α-helices (243, 249), and one of these helices has been shown to interact with an α-helix of the *c* subunit (111). Chemical cross-linking and direct binding assays showed that the two *b* subunits interact to form a dimer (61, 150, 218) which extends as paired α-helices through the length of the enzyme with interactions inside the lipid bilayer (55).

All three subunits (*a*, *b*, *c*) were required for proton translocation (53). Insertion of the *b* subunit was necessary for proper assembly of the F_0 complex and for insertion of the *a* subunit in the membrane (96, 222, 229). The hydrophilic region of the *b* subunit was not involved in ion translocation because trypsin digestion experiments that removed the soluble portion of the subunit did not affect proton movement through F_0 (98, 179, 180). The *b* subunit does not appear to play a role in the actual translocation of protons across the membrane, but instead may store elastic energy during translocation. This property will be discussed in further detail later in the chapter.

Both the *a* and *c* subunits contain functional groups essential for the transport of protons across the membrane, but the *c* subunit houses the site which undergoes protonation-deprotonation during proton translocation. The conserved residue, $c_{Asp\text{-}61}$ (*E. coli* nomenclature), is buried in the membrane in the center of the second transmembrane helix (85, 224). This amino acid has long been believed to be the site of proton binding in F_0. F_0-mediated proton translocation and ATP-driven proton translocation can be

blocked by reaction of dicyclohexylcarbodiimide (DCCD) with the carboxyl group of $c_{Asp\text{-}61}$. Modification of one *c* subunit is enough to completely inhibit the ATPase activity of the enzyme (97). Mutations affecting $c_{Asp\text{-}61}$ severely limit H^+ translocation. Even the very conservative $c_{Asp\text{-}61\rightarrow Glu}$ mutation had a marked effect on the enzyme, reducing activity to 50% of wild type (155), while the $c_{Asp\text{-}61\rightarrow Asn}$ substitution virtually inactivated the enzyme (102).

Kluge and Dimroth offered the most convincing evidence for the role of $c_{Asp\text{-}61}$ in proton translocation from their studies of the bacterium *Propionigenium modestum* (*P. modestum*). The F_1F_0 ATP synthase from *P. modestum* synthesizes ATP by utilizing a Na^+-gradient. At low Na^+ concentrations, the enzyme switched from Na^+ to H^+ transport, suggesting a common mechanism for the translocation of both ions. The homologous DCCD-sensitive site in the *c* subunit of *P. modestum* is $c_{Glu\text{-}65}$. The extent of DCCD sensitivity was strongly influenced by the pH of the incubation medium. At pH 5-7, where the reaction rate of DCCD is at its maximum, Na^+ weakly protected the site. In contrast, at pH 8-9, where the reaction rate is markedly reduced, Na^+ efficiently protected the enzyme. The authors concluded that the carboxyl group of $c_{Glu\text{-}65}$ was the site of ion binding and that Na^+ only binds to the deprotonated active site residue (129, 130).

Zhang and Fillingame (272) used sequence comparisons between *E. coli* and *P. modestum* to construct multiple mutations in the *E. coli c* subunit near $c_{Asp\text{-}61}$ to generate a Na^+-translocating F_0. One combination of four mutations, $c_{ValAsp\text{-}61AlaIle\rightarrow AlaGlu\text{-}61SerThr}$, did produce an F_0 that, although unable to bind Na^+, did bind Li^+ in a way that inhibited proton translocation. The dependence of protons on Li^+ inhibition suggested competition

for the same binding site. The characteristics of the mutant provided the most direct evidence that $c_{Asp\text{-}61}$ is the proton binding site in the *E. coli* subunit.

The *a* subunit is also believed to play an essential role in proton translocation. Cain and Simoni (30) identified the first two single amino acid substitutions in the *a* subunit, $a_{His\text{-}245\rightarrow Tyr}$ and $a_{Ser\text{-}206\rightarrow Leu}$, that impaired F_0-mediated proton translocation. Neither substitution altered F_1 binding. The site occupied by $a_{His\text{-}245}$ was at a highly conserved position, while $a_{Ser\text{-}206}$ was adjacent to a conserved Leu residue. It seemed likely that the *a* subunit contained at least part of the F_0 channel, and many mutations have been constructed to map out the amino acids that contribute to proton translocation. The only amino acid in the *a* subunit absolutely required for F_1F_0 ATP synthase function was $a_{Arg\text{-}210}$. This amino acid is in the fourth transmembrane helix and in close contact with the expected position of $c_{Asp\text{-}61}$ (111, 243). The site occupied by $a_{Arg\text{-}210}$ could not be substituted by other amino acids without loss of activity (31, 64, 138). Both ATP-driven proton translocation and passive proton translocation were affected. However, the assembly of the enzyme was essentially normal since F_1 retained ATPase activity in the absence of F_0. This observation was corroborated by purifying stable intact enzyme complexes with the $a_{Arg\text{-}210\rightarrow Ile}$ mutation (79).

Mendel-Hartvig and Capaldi (152) demonstrated that during ATP hydrolysis of wild type F_1F_0 ATP synthase, the ε subunit cross-linked to the β subunit and was trypsin insensitive. When the enzyme was substrate inhibited, the ε subunit had little cross-linking to the β subunit and was trypsin sensitive. These observations suggested that the ε subunit changed its position during catalysis, which has been shown to be the result of rotation of the ε subunit within the $\alpha_3\beta_3$ hexamer (122). Examining trypsin sensitivity

and chemical cross-linking of the ε subunit in purified F_1F_0 enzyme complexes with $a_{Arg\text{-}210\rightarrow Ile}$ substitutions revealed a similar observation (79). Therefore, this mutation is an example of a single amino acid substitution that uncouples a functional F_1-ATPase capable of rotation from a nonfunctional F_0 within an intact F_1F_0 complex.

Current models propose that the *a* subunit contains two half-channels that offer access to the site of protonation of $c_{Asp\text{-}61}$ from the periplasmic space and deprotonation of $c_{Asp\text{-}61}$ to the cytoplasm. It is believed that the $a_{Arg\text{-}210}$ residue facilitates a pK_a shift of the $c_{Asp\text{-}61}$ carboxylate to a low pK_a form. Protonation of this form is driven by the high local concentration of protons. Once the site is protonated, a pK_a-dependent conformational change occurs that causes the proton to be released from the other side of the membrane (188).

The exact number of *c* subunits in an intact F_0 complex remains controversial. Radiolabeling experiments originally suggested a possible range of nine to twelve *c* subunits per F_0 (74, 248). Jones and Fillingame (114) conducted cross-linking experiments with *c* subunit dimers and trimers and demonstrated that an F_0 with twelve *c* subunits was functional. This result showed that the stoichiometry could be twelve. However, Schemidt *et al.* (202) established that the stoichiometry of the *c* subunits varied with growth conditions. Translational rates of *uncE*(*c*) were higher in cells grown on glucose but not on succinate. Perhaps the most compelling evidence for the number of *c* subunits came from the crystal structure of the F_1F_0 ATP synthase from *S. cerevisiae*. The crystal structure indicated ten *c* subunits (224). It is possible that some of the *c* subunits were lost during the crystallization process. However, it is more likely that the number of *c* subunits in an intact enzyme complex is not fixed and certainly not fixed at

twelve. The stoichiometry of *c* subunits is important because it dictates the number of protons translocated per ATP synthesized. It is estimated that at least three and maybe four protons are translocated per one ATP molecule synthesized (68, 246). Since there are three catalytic sites in F_1, the most pleasing number of *c* subunits would be a multiple of three, either nine or twelve. This would correspond to a 120 degree rotation of the γ subunit within F_1 (see below).

The ring of *c* subunits has been shown to rotate (195). The authors immobilized *E. coli* F_1F_0 ATP synthase on a Ni^{2+} coverslip through a His-tag linked to the N-terminus of each α subunit. A fluorescently labeled actin filament was attached to the *c* subunit by a cysteine residue. Once MgATP was added, the actin filament rotated, indicating that the *c* subunit rotated during ATP hydrolysis. It is hypothesized that rotation occurs in the opposite direction during ATP synthesis. Based on experimental evidence, the current model for proton translocation is as follows. The $c_{Asp\text{-}61}$ residue is in close proximity to $a_{Arg\text{-}210}$. A proton enters a half-channel in the *a* subunit and protonates $c_{Asp\text{-}61}$. Once $c_{Asp\text{-}61}$ becomes protonated, there is a loss of attraction between $c_{Asp\text{-}61}$ and $a_{Arg\text{-}210}$. This loss of attraction causes the *c* subunit ring to rotate one step, making another $c_{Asp\text{-}61}$ site available for protonation. One proton remains bound to the $c_{Asp\text{-}61}$ residue during rotation until a conformational change causes the proton to be released to the other side through a second half-channel in the *a* subunit. The rotation of the *c* subunit ring is believed to drive the rotation of the γ subunit within the α_3/β_3 hexamer. How rotation is coupled to catalysis will be discussed below.

Rotational Catalysis

Catalysis occurs in the F_1 sector, which in the *E. coli* enzyme contains $\alpha_3\beta_3\gamma\delta\varepsilon$. The catalysis of F_1F_0 ATP synthase relies on a strong cooperativity at the three catalytic sites. Substrate binding at one site occurs simultaneously with product release at the next site. The cooperativity can be explained by the binding change mechanism which states that the structures of the three catalytic sites are always different but cycle through "open," "loose," and "tight" states (27). Experimental evidence has demonstrated that the F_1F_0 ATP synthase is a rotary motor enzyme. Proton translocation through F_0 drives the rotation of the internal γ subunit, producing conformational changes in each catalytic β subunit. The conformational changes lead to cooperativity.

The structure of the F_1 sector has been well documented (Figure 1-1). The high-resolution structural analysis of the bovine mitochondrial F_1 demonstrated that the α and β subunits alternate to form a hexamer (1). The hexamer was the shape of a compacted sphere 80 Å high and 100 Å across. The $\alpha_3\beta_3$ hexamer was arranged around the coiled-coil structure of the γ subunit, often referred to as the central stalk. Reconstitution experiments have demonstrated that the $\alpha_3\beta_3\gamma$ complex is the minimal complex necessary for ATP hydrolysis activity (168). The γ subunit was able to cross-link to the *c* subunit ring, indicating that the γ subunit extends the full length of the stalk (255). The ε subunit was also shown to be present in the central stalk as a two-domain structure (241, 258). Interactions between the C-terminal domain of ε with either the α or the β subunits have been identified (3, 4, 257), as well as interactions between the N-terminal domain of ε with the γ subunit (232, 255) and the *c* subunit ring (273). Oddly, the yeast crystal structure did not show any apparent interaction between the ε subunit and the $\alpha_3\beta_3$

hexamer (224). Therefore, the crystal may not entirely reflect an active state for the enzyme.

Wilkens and Capaldi (256) used electron microscopy to analyze detergent solubilized *E. coli* F_1F_0 ATP synthase. The negatively stained images showed the presence of two narrow stalks 40-45 Å in length that joined F_1 and F_0. One stalk was the central stalk composed of the γ and ε subunits. The peripheral or second stalk extended down the side of the enzyme from F_1 to F_0 and was made up of the δ subunit and *b* subunit dimer. NMR of the δ subunit showed a largely globular α-helical protein (260). Cross-linking studies have determined that δ is attached near the top of F_1 through interactions with an α subunit (139, 173). Cross-linking studies have established that the C-terminal part of the *b* subunit dimer interacts with the C-terminal region of the δ subunit and with both the α and β subunits (62, 148, 149, 191, 192, 198, 256). The second stalk is thought to act as the stator against which the γ, ε, and the ring of *c* subunits rotate relative to the stationary $\alpha_3\beta_3$ hexamer of F_1.

There are six possible nucleotide-binding sites in the F_1 moiety: three non-catalytic sites mainly on the α subunits and three catalytic sites mainly on the β subunits. The bovine mitochondrial F_1 was crystallized in the presence of various nonhydrolyzable analogs and showed that the six nucleotide-binding sites are at the interfaces between the α and β subunits (1). It was clear from the structure that the catalytic sites in the three β subunits exist in differing conformations due to their positions relative to the γ subunit. The structure supported Boyer's hypothesis of the binding change mechanism. The catalytic sites in the β subunits interconvert among three sites: "open," "loose," and "tight." The open site has a very low affinity for ligands and is catalytically inactive, the

loose site loosely binds ligands and is catalytically inactive, while the tight site tightly binds ligands and is catalytically active. Proton translocation leads to conformational changes in each of the β subunits to convert a tight site with bound ATP to an open site, thereby releasing the nucleotide. Concurrently, a loose site with loosely bound ADP and phosphate is transformed to a tight site where ATP forms. Fresh substrate binds to the open site, converting it to a loose site, and the cycle repeats. The steps that require energy are substrate binding and product release. The conformational changes that occur in each of the β subunit are explained by the rotation of the asymmetric γ subunit.

The rotary motion of the γ subunit has been proven experimentally for the isolated F_1 portion acting as an ATPase. Duncan *et al.* (60) made a $\beta_{Asp380 \rightarrow Cys}$ mutant and demonstrated that the Cys residue formed a disulfide bond with γ_{Cys87}. If the bond was reduced, the enzyme allowed to hydrolyze ATP and then put back into oxidizing conditions for bond reformation, the disulfide bond was formed randomly among all three β subunits. If the enzyme was not put under catalyzing conditions, the bond usually formed with the same β subunit. The most logical explanation was that the γ subunit rotated among the β subunits during ATP hydrolysis. Switching of the disulfide bond formation among β subunits could be inhibited by blocking proton transport or oxidative phosphorylation (274, 275). These results established that rotation was linked to transport.

Sabbert *et al.* (193) used another approach to detect rotation. A phosphorescent eosin molecule was attached to the C-terminus of the γ subunit and after photobleaching, the anisotropic decay was followed by polarized absorption recovery. The experiment did not establish rotation, but after analyzing the decay, the results suggested that the

assumed rotation was "stepped." The data best fit a model with the γ subunit acting as a unidirectional three-step rotor.

The most convincing evidence for the rotation of the γ subunit was conducted by Noji *et al.* (172). The authors added a His-tag to the N-terminus of the β subunit and affixed the F_1 complex to a slide coated with Ni^{2+}. They also attached a fluorescently labeled actin filament to the γ subunit. Rotation of the γ subunit could be observed under a fluorescent microscope only with ATP hydrolysis. These experiments proved that only the catalytic domain of the enzyme ($\alpha_3\beta_3\gamma$) was necessary to cause rotation. However, the same results were achieved when the ε subunit was fluorescently labeled in an $\alpha_3\beta_3\gamma\varepsilon$ F_1 complex (122). Rotation was always counterclockwise, as observed from the membranous side of the hexamer. In addition, at nanomolar ATP concentrations, the rotary motion was interrupted. Discrete 120 degree steps were detected with intermittent backward steps. This stepped motion confirmed the model of Sabbert *et al.* (193). At low ATP concentrations, binding of ATP to the catalytic site would be expected to be a rate-limiting step. The binding of ATP facilitated the release of tightly bound ADP, suggesting that ATP binding at one catalytic site promoted release at another (2). The stepped motion at low ATP concentrations suggested that at least two of the three sites had to be filled by nucleotide in order for a 120 degree rotation to occur. This observation implies that rotation is coupled to cooperative catalysis involving more than one catalytic site.

The data suggest a model of energy coupling within the F_1F_0 complex in which rotation of the ring of *c* subunits occurs in one direction for ATP hydrolysis and in the other direction for ATP synthesis. Protons are consecutively translocated for each *c*

subunit across the membrane through associations with the *a* subunit. Because the *c* subunit is in direct contact with the γ and ε subunits (255, 273), the rotation of the *c* subunits is driven in one direction or drives in the other direction the rotation of the γ and ε subunits among catalytic sites.

b Subunit

The F_1 and F_0 sectors of the enzyme are attached by two stalks. The central stalk is composed of the γ and ε subunits and rotates within the $\alpha_3\beta_3$ hexamer to drive conformational changes in the three β subunits during catalysis. The *b* subunit dimer forms the peripheral or second stalk and participates in interactions with δ, α, and β subunits in F_1 (Figure 1-1). The second stalk is believed to act as a stator, holding the $\alpha_3\beta_3$ hexamer against rotating with γε so that the conformational changes can occur.

In *E. coli*, the *b* subunit contains 156 amino acids. There is an N-terminal transmembrane sequence followed by a polar, highly charged region that is predicted to be mostly α-helical. Analysis of the secondary structure of the hydrophilic region of the *b* subunit proposed a random coil between two long α-helices (205, 252). Although these characteristics were apparent in *b* subunit sequences from the mitochondrial and chloroplast enzymes, the *b* subunit has the least primary sequence conservation among all subunits of the F_1F_0 ATP synthase.

Multi-dimensional NMR spectroscopy was used to determine the structure of the synthetic peptide $b_{1\text{-}33}$, which contains the transmembrane region of the *E. coli b* subunit (55). The structure revealed an α-helix between residues $b_{\text{Asn-4}}$ and $b_{\text{Met-22}}$, which was broken by a rigid bend around $b_{\text{Lys-23}}$ to $b_{\text{Trp-26}}$. The α-helix continued at residue $b_{\text{Pro-27}}$ at a 20 degree angle offset. The α-helix stretching from $b_{\text{Asn-4}}$ to $b_{\text{Trp-26}}$ is likely to span the

lipid bilayer to anchor the *b* subunit in the membrane. Single Cys residues were substituted for residues 2-21 of the native *b* subunit, and dimer formation between *b* subunits after cross-linking was tested. High yields of *b* subunit dimers were found at positions 2, 6, and 10, and less intense cross-links were observed at positions 3, 4, 8, 9, 11, 13, 14, 17, and 18. The results demonstrated that the transmembrane domains of the two *b* subunits are capable of close contact with each other. The fact that the less intense cross-links stretch along the α-helices may indicate that the helices are mobile within the membrane. Using cross-linking distance constraints and the NMR data, the authors proposed a model for possible transmembrane *b* subunit interactions. In the model, the transmembrane α-helices of each *b* subunit are at a 23 degree angle to each other. The 20 degree angle offset after the bend may counteract for the 23 degree tilt of the helices so that the following helical segments at an angle more perpendicular to the membrane.

Attempts to determine the high-resolution structure of the cytoplasmic region of the *b* subunit have been unsuccessful. Most of the structural information available on hydrophilic portion of the subunit has been obtained through circular dichroism spectroscopy, analytical centrifugation, and chemical cross-linking experiments. Dunn (61) expressed and purified the cytoplasmic portion of the *E. coli b* subunit ($b_{Val25\text{-}Leu156}$) and termed the protein b_{sol}. The polypeptide displayed characteristics indicative of a highly extended protein during sedimentation equilibrium, and circular dichroism spectroscopy demonstrated that b_{sol} was highly α-helical. Analysis of the molecular weight of the b_{sol} polypeptide by sedimentation equilibrium resulted in a value close to the calculated dimer value. A variety of experiments have demonstrated that b_{sol} can bind

to the F_1 sector (61, 148, 198, 219), but in an intact enzyme complex, dimer formation is necessary for interaction with F_1 (218).

Dimerization interactions between *b* subunits were analyzed by N-terminal deletions and site-directed mutagenesis using the b_{sol} polypeptide (150). When cysteine residues were substituted at positions 124, 128, 132, and 139, disulfide formation occurred with the same residue on the other subunit, implying a parallel α-helical interaction in this area. Adding $b_{solSer60\rightarrow Cys}$ with $b_{solLeu65\rightarrow Cys}$ and $b_{solAla61\rightarrow Cys}$ with $b_{solLeu65\rightarrow Cys}$ resulted in a mixed disulfide formation between pairs of the polypeptides, suggesting a non-parallel α-helical interaction in this region. N-terminal deletion analysis demonstrated that residues 53-66 but not 24-52 are essential for dimerization. The exact boundaries of the dimerization domain are unknown, but probably reside within residues 53-122 (150, 190). The results propose a model in which the two *b* subunits interact in more than one area, but probably not simply as a symmetrical parallel alignment of α-helices.

I observed that F_1F_0 ATP synthase complexes with a two amino acid deletion in the hydrophilic region of the *b* subunit were able to support growth on minimal succinate that was indistinguishable from the wild type enzyme. This result was unexpected. In fact, the only defect of the deletion was reduced assembled complexes. To analyze the effects of larger deletions on the enzyme, our laboratory constructed deletion mutations within the cytoplasmic region of the *b* subunit (219). The deletion mutations were designed to represent deletions of turns in an α-helix. A deletion of two amino acids approximated a half-turn of an α-helix, while a deletion of seven amino acids was roughly two turns of an α-helix. Surprisingly, deletions of up to seven amino acids

resulted in fully functional F_1F_0 ATP synthases, and a deletion of eleven amino acids still produced considerable activity. Removing twelve amino acids, however, destroyed activity. In each case, the major effects of the mutations were on assembly and stability of the enzyme complex. Somehow the *b* subunit was able to compensate for its shortening of up to 16 Å, as would be the case in the deletion of eleven amino acids. The *b* subunit was believed to be a rigid rod-like structure with specific points of contact with F_1 (150, 173). However, the results of the *b* subunit deletions suggested that the *b* subunit has some inherent flexibility and is not necessarily a rigid structure.

To further examine the flexibility of the *b* subunit, our laboratory also constructed insertion mutations in the same area of the subunit (217). In an attempt to retain an α-helical conformation and dimerization between *b* subunits, the amino acid sequence inserted was a duplication of *b* subunit sequence. Insertion of seven amino acids resulted in a virtually normal phenotype, and insertions of up to fourteen amino acids retained significant levels of ATP synthase activity. Any loss of function corresponded to a defect in assembly of the enzyme complex. In fact, the assembly of *b* subunits with an eighteen amino acid insertion was so harsh that no *b* subunit could be found in membrane fractions. Insertion of fourteen amino acids would lengthen the stalk by about 20 Å. These data taken with the comparable results from the deletion analysis strongly suggest that the *b* subunit has significant flexibility to allow such large changes in length. The second stalk observed in the electron micrograph of Wilkens and Capaldi (256) was bent approximately 30 degrees, offering independent evidence for the inherent flexibility of the *b* subunit dimer.

Mutagenesis of the hydrophilic region of the *b* subunit has demonstrated that the *b* subunit plays an important role in the proper assembly of the enzyme. Mutating the conserved residue $b_{Ala\text{-}79}$ prevented the proper assembly of the enzyme due to a failure of *b* subunit dimerization (147, 218). Early termination of the *b* subunit resulted in a nonfunctional F_0 complex even when only $b_{Glu\text{-}155}$ and $b_{Leu\text{-}156}$ were missing at the C-terminus (182, 229). This originally led the field to believe that the *b* subunit bent back toward the membrane. However, in light of the current structural information based on electron microscopy, cross-linking, and nuclear magnetic resonance spectroscopy, the C-terminus of the *b* subunit is thought to extend towards F_1 (191, 218, 256). Mutagenesis affecting $b_{Ala\text{-}128}$ abolished dimerization of the *b* subunits (104).

The residues near the C-terminus of the *b* subunit are necessary for the proper assembly of F_1F_0 ATP synthase *in vivo* (229) and for interaction with F_1 *in vitro* (148). Cross-linking experiments have demonstrated that the δ subunit binds near the top of the $\alpha_3\beta_3$ hexamer (139, 173). The δ subunit was essential for binding F_1 to F_0 (198). Although it was believed that the interaction between the *b* subunit and F_1 was through its association with the δ subunit, cross-linking analysis of the *E. coli* enzyme failed to produce a *b*-δ interaction (10). In the chloroplast enzyme, however, a zero-length cross-linking agent did reveal a subunit I-δ (*E. coli b*-δ) product, suggesting that the subunits are adjacent to each other (18). The *b*-δ interaction in the *E. coli* enzyme has since been demonstrated with the yeast two-hybrid system, NMR spectroscopy, and protease protection experiments (192, 198). Sedimentation equilibrium analysis of purified b_{sol} and δ subunits showed the complex had a stoichiometry of $b_2\delta$, and sedimentation velocity studies revealed the complex was organized in an end-to-end instead of a side-

by-side relationship (62). In order for the *b* subunit to reach up the side of F_1 to the δ subunit, parts of the *b* subunit must be in contact with the α or β subunits. Cross-linking studies have shown that the *b* subunit interacts with both the α and β subunits through parts of the dimerization domain as well as the δ binding domain (149, 191).

The second stalk is believed to act as a stator during rotational catalysis to hold the $\alpha_3\beta_3$ hexamer in place against the rotation of the *c* subunit ring and central stalk. Evidence exists to support this model, but some data seem to conflict with it. These considerations were eloquently explained by Dunn *et al.* (63). The first issue is that of the stability of the second stalk and its relationship to the $\alpha_3\beta_3$ hexamer. Once F_1 is bound to F_0 through the second stalk, the stator is expected to remain associated with one α subunit or αβ pair during catalysis. In support of this idea, Ogilvie *et al.* (173) demonstrated that cross-linking the δ subunit to one of the α subunits at an introduced $\alpha_{Cys\text{-}2}$ did not affect the coupling activity of the F_1F_0 ATP synthase. Linking two *b* subunits together through disulfide bonds also had no effect on coupling (191, 192). These results suggest that the second stalk is a permanent element of the enzyme that is connected to one α subunit or αβ pair. However, Rodgers and Capaldi (191) identified a disulfide bond between the C-terminus of the *b* subunit and $\alpha_{Cys\text{-}90}$ that did block coupling, implying that some flexibility or movement is necessary in the *b*-α association. If the second stalk remains associated with only one α subunit or αβ pair during catalysis, then one would expect a difference among the three αβ pairs, and this difference would presumably affect activity of the enzyme. In light of this idea, Kersten *et al.* (124) used electron spin resonance spectroscopy to examine the effects the *b* subunit has on structural changes within the catalytic nucleotide-binding sites of the β

subunits. The data demonstrated that the hydrophilic region of the *b* subunit affects the conformation of the catalytic sites and puts the sites in a conformation that seems to be consistent with the open state. This result implies that the *b* subunit may play a role in the release of ATP from the catalytic site.

The second issue is the tensile strength of the second stalk. Rotation of the central stalk applies a torque on the $\alpha_3\beta_3$ hexamer that must be opposed by the second stalk so that the hexamer does not rotate with the γ subunit. A rigid rod-like *b* subunit would serve this function well. However, insertion and deletion analyses suggested that the second stalk was a flexible structure (217, 219). The interaction of the *b* subunit with F_1 may add some strength to the second stalk so that it can function as a stator.

The final issue is the elasticity of the second stalk. The flexible *b* subunit, along with $\gamma\varepsilon$, may transiently store energy during rotational catalysis. Junge and colleagues (38) proposed a model where the *b* subunit would tolerate stepwise elastic deformation as protons moved through F_0. The stored energy would then be expended in one step to drive conformational changes which allow the release of ATP from the catalytic site. On the other hand, Oster and Wang (175) have emphasized the importance of the *b* subunit as a flexible, elastic connection coupling F_1 and F_0 so that any torque produced from either proton movement or ATP hydrolysis can be distributed more smoothly to the rest of the enzyme, resulting in increased efficiency. Both models require that the *b* subunit is elastic, although there is no direct evidence to support the elasticity of the *b* subunit. The putative coiled-coil segment in the hydrophilic region could provide several methods for elastic deformation, including bending, stretching, and compression. How energy is

stored in the second stalk may become clear once more structural information is available.

H^+,K^+-ATPase

The H^+,K^+-ATPase utilizes the energy stored in ATP to transport H^+ outward in an electroneutral exchange for the inward transport of K^+ with a stoichiometry of $2H^+:2K^+:1ATP$ (187). The enzyme was first identified in the stomach where its high expression is responsible for luminal gastric acid secretion. Additional H^+,K^+-ATPase isoforms have since been identified in other organs, including the colon, kidney, heart, and skin. The H^+,K^+-ATPase is a Type IIB P-type ATPase and thus consists of a large α subunit and a smaller β subunit. The enzyme most likely exists as an $(\alpha/\beta)_2$ tetramer (186). The α subunit contains the binding sites for ATP, phosphorylation, and inhibitors and is designated the catalytic subunit (99, 244). The β subunit is necessary for efficient targeting of the α subunit from the endoplasmic reticulum to the plasma membrane and also modulates enzymatic activity (43). The Na^+,K^+-ATPase is the only other known Type IIB P-type ATPase, and its α and β subunits are structurally and functionally related to the subunits from the H^+,K^+-ATPase. In fact, much of the information currently available on the H^+,K^+-ATPase has been inferred from studies of the prototypical Na^+,K^+-ATPase.

Enzyme Structure

Hydropathy plots have indicated that the HKα subunit has eight to ten membrane spanning regions with a large cytoplasmic loop (140, 210). Both the N- and C- termini appear to be cytoplasmic, indicating an even number of transmembrane domains between them (204). Limited proteolytic cleavage data showed the presence of at least eight

transmembrane segments (20, 207), while *in vitro* translation experiments suggested the presence of ten transmembrane domains (17). Efforts to crystallize the H^+,K^+-ATPase have produced only low-resolution two-dimensional crystals (95, 184, 266) that have not provided any useful understanding of the overall structure of the α subunit. However, high-resolution structural data have been determined for two Type IIA P-type ATPases. Two-dimensional crystals of the H^+-ATPase of *Neurospora crassa* (*N. crassa*) yielded a three-dimensional map of the enzyme at a resolution of 8 Å (16). Both an 8 Å resolution three-dimensional map (271) and a 2.6 Å resolution atomic model (240) were determined for the sarcoplasmic reticulum (SR) Ca^{2+}-ATPase. The Ca^{2+}-ATPase and the H^+-ATPase had similar structural characteristics. Both enzymes had an extensive mass on the cytoplasmic side, a membrane sector, and a small extracellular region. There were ten clearly defined and tightly packed transmembrane domains, and the arrangement of the transmembrane helices of Ca^{2+}-ATPase was established (240). Although there is generally a low degree of sequence homology across the family of P-type ATPases, they all perform similar functions of ion transport with ATP hydrolysis. Moreover, highly conserved regions most likely related to function or conformation are found in most of the members. Therefore, it seems logical that the common principles determining the relationship between molecular structure and functional properties are preserved within the family, and the HKα subunit almost certainly has ten transmembrane domains with a similar arrangement to that of the Ca^{2+}-ATPase (Figure 1-2A).

All of the known isolated β subunit isoforms from Na^+,K^+-ATPase and H^+,K^+-ATPase share a common molecular architecture: a short N-terminal cytoplasmic segment, a single transmembrane domain, and a large C-terminal extracellular domain

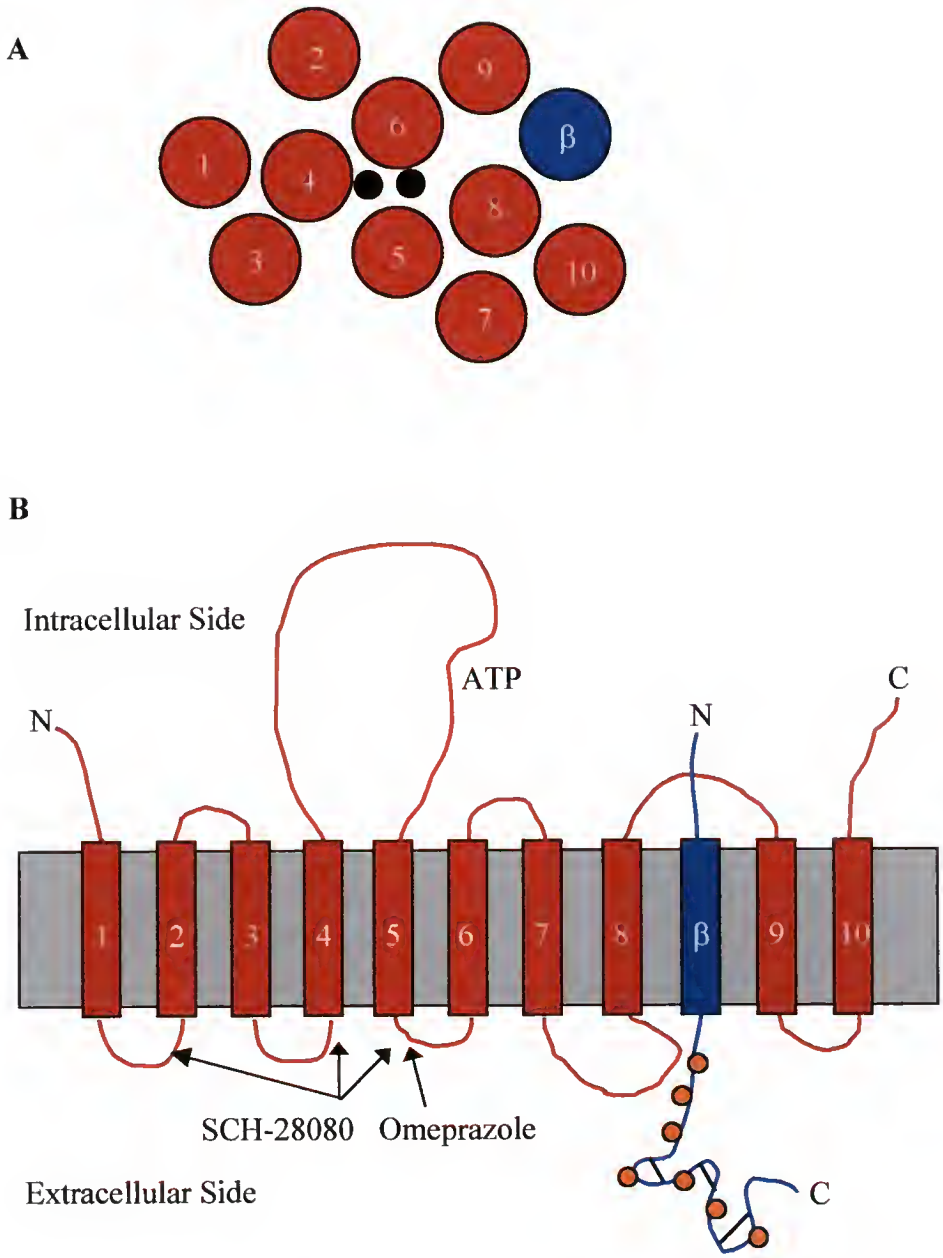

Figure 1-2. Transmembrane organization of H^+,K^+-ATPase. A, The spatial arrangements of the ten transmembrane domains of the HKα subunit, shown in red, have been assigned based on structural data from Ca^{2+}-ATPase. The likely position of the HKβ subunit transmembrane domain is shown in blue. The cation binding sites are represented by black circles. B, The topological structure of the HKα subunit is shown in red with the ten transmembrane domains numbered. The ATP and inhibitor binding sites are indicated. The HKβ subunit is shown in blue. Glycosylation sites are represented by orange circles, and the disulfide bonds are depicted by black lines.

(Figure 1-2B). The extracellular domain is glycosylated and contains six completely conserved cysteine residues that are linked by three internal disulfide bonds (43). The cysteine residues form the bonds in a sequential arrangement (41, 126, 156). Both glycosylation and disulfide bond formation are important in α/β assembly, as well as in the activity of an intact enzyme complex (43).

Wheat germ agglutinin chromatography was used to analyze the areas of interaction between the α and β subunits. Intact gastric vesicles were trypsinized which left the β subunit largely intact. The vesicles were solubilized and passed over a wheat germ agglutinin column to retain the β subunit. The transmembrane domain pair 7 and 8 was retained on the column, suggesting an interaction between α and β within these transmembrane domains (208). The yeast-two hybrid system identified a similar area of interaction between the α and β subunits, namely within $\alpha_{Arg\text{-}898}$ and $\alpha_{Thr\text{-}928}$ (151). This region is flanked by transmembrane domains 7 and 8. Interestingly, a chimera of the Na^+,K^+-ATPase α subunit containing the region from $\alpha_{Gln\text{-}905}$ to $\alpha_{Val\text{-}930}$ of the H^+,K^+-ATPase preferentially assembled with the β subunit of the H^+,K^+-ATPase (254). When comparing the amino acid sequence similarity within the region of both α subunits, a homologous 16 amino acid sequence was identified. There were several sequence differences in the region, such as the position of charged amino acids. The homologous amino acid sequence of the α subunit of the two enzymes is likely a point of contact with the β subunit, and the slight differences in the sequences of this region may explain the selective assembly of the β subunits with their α subunits. Yeast-two hybrid analysis also identified interactions of the α subunit with two areas within the β subunit between $\beta_{Gln\text{-}64}$ to $\beta_{Asn\text{-}130}$ and $\beta_{Ala\text{-}156}$ to $\beta_{Arg\text{-}188}$ (151). Taken together, the data suggest that the

extracellular loop before transmembrane domain 8 of the α subunit interacts with the extracellular domain of the β subunit. Because the single transmembrane domain of the β subunit ends at position 62 and position 64 is included in the interaction between α and β, it is expected that the transmembrane domain of the β subunit is next to transmembrane domain 8 of the α subunit (Figure 1-2B).

Enzyme Mechanism

The mechanism by which the H^+,K^+-ATPase utilizes ATP hydrolysis to translocate H^+ and K^+ across the membrane is not clearly understood. Many experiments have been conducted on other P-type ATPases, including the Na^+,K^+-ATPase and the Ca^{2+}-ATPase, to characterize the transitional steps and mechanism of ion translocation. The most popular model for the catalytic mechanism of all P-type ATPases is the E_1-E_2 model (51, 108, 117, 206). This mechanism assumes two major conformational states, E_1 and E_2, which are distinguished by their affinity for ATP and P_i, respectively. Each state has ion binding sites on opposite sides of the membrane. E_1 binds cytoplasmic ions and E_2 binds luminal ions.

The reaction mechanism of ion transport for the H^+,K^+-ATPase is depicted in Figure 1-3. The enzyme probably transports a proton as a hydronium ion (H_3O^+). H_3O^+ binds with high affinity to the E_1-ATP form. The phosphate from ATP is transferred to a specific Asp residue on the α subunit and transforms the enzyme to the intermediate E_1-P_i-H_3O^+ in which H_3O^+ is occluded. This form is rapidly converted to E_2-P_i-H_3O^+. The E_2-P_i-H3O$^+$ enzyme has a low affinity for H_3O^+ and a high affinity for K^+. Hence, the E_2-P_i-K^+ enzyme is formed, and H_3O^+ is released into the lumen. E_2-P_i-K^+ is rapidly dephosphorylated causing the occlusion of K^+ in the intermediate E_2-K^+ form. ATP

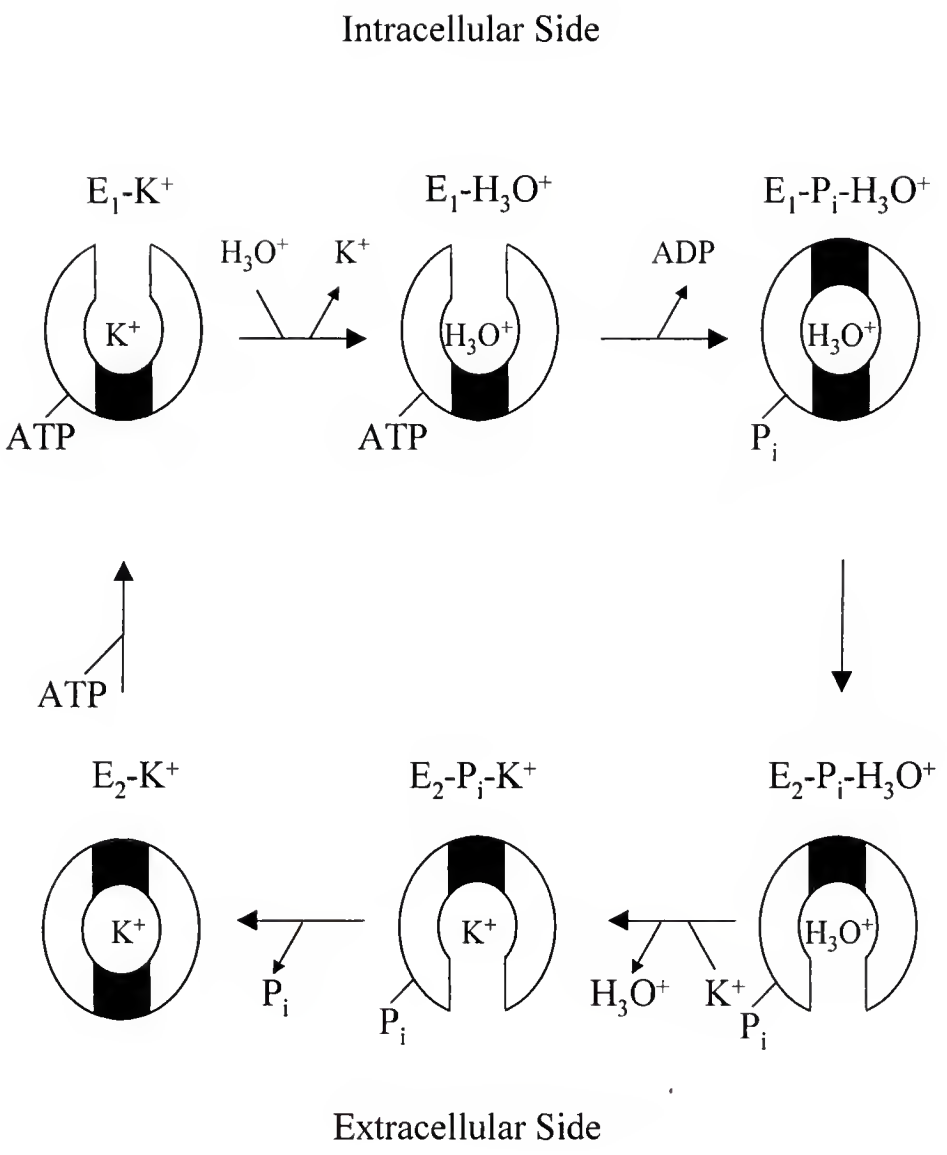

Figure 1-3. Enzymatic mechanism of H^+,K^+-ATPase. Each step of the reaction is described in detail within the text. Adapted from van Driel and Callaghan (244).

binds to E_2-K^+, and the enzyme is converted back to E_1, which releases K^+ into the cytoplasm. E_1 binds to H_3O^+, thereby completing the reaction cycle (244).

The atomic model of SR Ca^{2+}-ATPase was determined with two Ca^{2+} bound in the membrane domain (240). When comparing this structure to that obtained from tubular crystals (271), it was noticed that the cytoplasmic region was more compact in the maps from tubular crystals. The authors fitted the atomic model to the low-resolution map from tubular crystals and concluded that concerted domain motions occur during Ca^{2+} binding. Indeed, direct evidence for the conformational changes between the E_1 and E_2 states has been obtained with extrinsic fluorescent probes. Fluoroscein isothiocyanate, which labels $\alpha_{Lys\text{-}516}$ on the cytoplasmic side of the hog H^+,K^+-ATPase, exhibits a marked decrease in fluorescence in the presence of K^+ and enhanced fluorescence in the presence of Na^+ as a surrogate for H^+ (109, 185). Therefore, the E_1 and E_2 states change the environment of the fluorescein bound in the cytoplasmic domain. The K^+-competitive antagonist arylquinoline MDPQ binds in the region of transmembrane domains 1 and 2 on the extracellular surface of the H^+,K^+-ATPase. Upon binding to the enyzme, the fluorescence of this reagent is enhanced. The phosphorylation of the H^+,K^+-ATPase further increases the fluorescence of MDPQ (183). Consequently, conformational changes occur on both sides of the membrane during the cycling between E_1 and E_2 states.

Gastric H^+,K^+-ATPase

During the 1960's researchers were interested in the mechanism of hydrochloric acid production in the stomach. One theory, the redox theory, was in parallel with the chemiosmotic hypothesis proposed by Mitchell for mitochondria (158). The redox theory

suggested that a system of cytochromes separated protons from electrons and released protons to the outside of the cell. The other theory, the high-energy phosphate theory, was modeled after the Na^+,K^+-ATPase explained by Skou (213). This theory proposed that the chemical energy of ATP was used to drive the uphill transport of protons. The fact that ATP-dependent acidification by membrane vesicles from the stomach was observed offered validation to the ATPase theory. During the 1970's the search began for a proton-transporting ATPase in the stomach. A gastric-specific ATPase was soon identified that was activated by K^+, but not Na^+ and was not inhibited by ouabain, a selective Na^+,K^+-ATPase inhibitor (78, 194). Because maximal transport activity by the ATPase required the presence of K^+ ionophores such as valinomycin (71, 194), the enzyme was distinguished as catalyzing an electroneutral exchange of H^+ for K^+ and consequently called the H^+,K^+-ATPase.

Gastric acid secretion is a regulated process resulting from a complex set of mechanisms acting at the central, peripheral, and cellular levels. A gastric parietal cell is an elaborate arrangement of secretory membranes, where the H^+,K^+-ATPase is highly expressed. The secretory membranes are networks of cytoplasmic helically coiled tubules called tubulovesicles (73, 181). The H^+,K^+-ATPase is inactive in the tubulovesicles due to the impermeability of the vesicles to K^+. When a parietal cell is stimulated, the tubulovesicles incorporate into the apical membrane of the cell to form the secretory canaliculus. The cytoskeleton reorganizes to form microvilli at the canalicular surface. Translocation of the H^+,K^+-ATPase from the tubulovesicles to the canaliculus activates the enzyme because the canaliculus is permeable to K^+ (99).

HKα_1 Subunit Isoform

HKα_1 is the gastric α subunit isoform. The subunit is made up of 1033 amino acids and is encoded by the mouse gene *Atp4a*, which was localized to chromosome 7 (143). The cDNA for HKα_1 has been cloned from a number of species with approximately 90% primary sequence identity. The subunit contains conserved sequences including the phosphorylation site at Asp-386 (250), ATP-protected binding sites for pyridoxal 5-phosphate at Lys-497 (141, 231), and fluoroscein isothiocyanate at Lys-518 (66). These sites are located on the large cytoplasmic loop, which links transmembrane domains 4 and 5 of the HKα_1 subunit. Although HKα_1 is sometimes referred to as the gastric α subunit isoform, HKα_1 has been identified in other organs, including the kidney.

Selective inhibitors of the gastric H^+,K^+-ATPase have been identified. Omeprazole is a substituted pyridyl methylsulfinyl benzimidazole, an acid-activated thiophilic compound, that forms stable disulfide bridges with accessible cysteine residues on the extracellular side of the enzyme. It covalently inhibits the gastric H^+,K^+-ATPase and is often used for the treatment of acid-related diseases. Once administered, the drug becomes protonated in the lumen of the stomach. After protonation, omeprazole is converted to a thiophilic-reactive sulfenamide that can react with accessible cysteine residues of the H^+,K^+-ATPase and inhibit the enzyme. The area of inhibition has been mapped to $\alpha_{Cys\text{-}813}$ (21) (Figure 1-2B).

SCH-28080 is an imidazo-pyridine and inhibits the H^+,K^+-ATPase by competing with K^+ at the extracellular binding site (115, 153, 166). Since the drug is strictly K^+-competitive, it is a reversible inhibitor. The region of inhibition of SCH-28080 was

believed to be within the extracellular loop between transmembrane domains 1 and 2 (165) (Figure 1-2B). A mutation at $\alpha_{Met\text{-}113}$, which lies within this region, did indeed have a large effect on SCH-28080 binding affinity. In contrast, Asano *et al.* (14) demonstrated that the entire extracellular loop between transmembrane domains 1 and 2 of $HK\alpha_1$ could be replaced with the same region from the Na^+,K^+-ATPase α subunit with no loss of SCH-28080 binding. The Na^+,K^+-ATPase is not inhibited by SCH-28080 so the chimeric $HK\alpha_1$ subunit was not acquiring a SCH-28080 binding site from the NaKα subunit sequence. At this time, it is unclear why there is a disagreement in the importance of this loop in SCH-28080 binding.

Interestingly, binding of SCH-28080 prevents inhibition by omeprazole, suggesting an area of overlap of binding sites for the inhibitors (100). Indeed, mutations in transmembrane domain 4 toward the extracellular side of the segment had more significant effects on the affinity of SCH-28080 than at $\alpha_{Met\text{-}113}$ (164), and this surface of the loop had been proposed to bind SCH-28080 (135). Nevertheless, there were no effects on the affinity of the competing ion K^+, and therefore argues that the outer region of transmembrane domain 4, although binding SCH-28080, is not involved in binding K^+. However, binding of K^+ inhibits SCH-28080 binding, signifying a change in this region induced by K^+ binding. Taken together, the data suggest that the outer region of transmembrane domain 4 is a major binding area for SCH-28080, and $\alpha_{Cys\text{-}813}$ at the end of transmembrane domain 5 must also be included in the binding region. This area most likely represents the K^+ binding site. In agreement with this hypothesis, the Ca^{2+}-ATPase crystal structure shows the two Ca^{2+} bound surrounded by transmembrane domains 4 to 6 and transmembrane domain 8 (240).

The function of H^+,K^+-ATPase in the acid secretion of the stomach has been well established. However, studies have suggested that the enzyme may be responsible for the viability and normal development of parietal cells (119). Animals treated with inhibitors of acid secretion normally have parietal cells with dilated canaliculi (94, 119, 120, 137). Treatment with omeprazole caused deterioration of parietal cells and an increase of the number of preparietal cells (119). To study the importance of the H^+,K^+-ATPase in the development, maintenance, and function of the gastric mucosa, mice with a null mutation in the $HK\alpha_1$ subunit gene (*Atp4a*) were generated through homologous recombination (220). Sequences in exon 8 that encoded the phosphorylation site were deleted and replaced with the neomycin resistance gene. Absence of $HK\alpha_1$ transcript and protein were confirmed by Northern analysis and immunohistochemistry. There were no distinguishable differences in physical features or mortality among $Atp4a^{+/+}$, $Atp4a^{+/-}$, and $Atp4a^{-/-}$ mice. Although $HK\alpha_1$ was not produced, the $HK\beta$ subunit mRNA was increased, and the protein was readily detected in the $Atp4a^{-/-}$ mice. However, $Atp4a^{-/-}$ mice had a gastric luminal pH of approximately 7, whereas the pH from $Atp4a^{+/+}$ and $Atp4a^{+/-}$ mice were considerably lower at about pH 3.2 and 3.5, respectively. The secretory canaliculus was much larger and had few microvilli, and the tubulovesicles were larger in diameter in the parietal cells of the $Atp4a^{-/-}$ mice. Nevertheless, there was no indication of an increase in the degeneration of parietal cells in those mice. The number of parietal cells was essentially the same in mutant and wild-type mice. The study demonstrated that expression of $HK\alpha_1$ was required for gastric acid production, but the H^+,K^+-ATPase probably does not play a role in parietal cell differentiation.

HKβ Subunit

Although it was known that the Na^+,K^+-ATPase contained a β subunit, the β subunit of the gastric H^+,K^+-ATPase eluded researchers because it stained weakly with Coomassie Blue and went undetected for some time. Lectin affinity chromatography could be used to isolate the $HK\alpha_1$ subunit, which indicated that the α subunit was closely associated with a 60 to 80 kD glycoprotein (33, 174). Deglycosylation of the protein resulted in a 35 kD core protein which was partially sequenced (91, 189, 238). The sequence shared homology with the β subunits of the Na^+,K^+-ATPase, and the HKβ subunit has since been cloned and sequenced from a variety of species. The HKβ subunit consists of 294 amino acids and is encoded by the mouse gene *Atp4b* located on chromosome 8 (37). The protein has six to seven possible *N*-linked glycoslyation sites, depending on the species (162, 189, 209, 238), and most of the possible sites are used (33, 174, 238)

Co-immunoprecipitation studies using monoclonal antibodies specific for HKβ have shown a physical interaction between HKβ and $HK\alpha_1$ in gastric membranes (112). The α/β association is strong but not covalent. Nonionic detergents solubilize the complex but do not dissociate the subunits, while treatment with more chaotropic detergents results in dissociation of the subunits. The HKβ subunit is necessary for the function of the H^+,K^+-ATPase. Many studies involving the expression of H^+,K^+-ATPase or Na^+,K^+-ATPase in heterologous systems have demonstrated that neither α nor β subunits alone possess ion-transport activity. Only α subunits that assemble with β subunits in the endoplasmic reticulum are stably expressed, acquire their functional

properties, and are transported to the plasma membrane. Indeed, the HKβ subunit may contain trafficking signals required for correct membrane localization in polarized cells.

Interestingly, HKβ can act as a surrogate for the proper assembly of the NaKα subunit isoforms (103), and any of the NaKα subunits can assemble properly with any of the NaKβ or the HKβ subunit isoforms (65). These observations suggest that the α/β interactions must involve homologous regions of the two subunits, and this association must confer a structure which is necessary for function of the enzyme. The fact that mismatching of subunits has not been observed *in vivo* suggests that correct assembly of the enzyme complex involves factors other than the primary amino acid sequence.

The role of glycosylation on the extracellular domain of the HKβ subunit is not completely understood. An early hypothesis suggested that the oligosaccharides offered protection against the acidic gastric conditions (72). A preliminary study demonstrated that glycosylation of HKβ provided resistance against pepsinolysis *in vitro* but to what degree this functions *in vivo* remains uncertain (40). Incubation of HKβ with tunicamycin completely abolished the K^+-ATPase activity and SCH-28080-sensitive phosphorylation of the enzyme when expressed in Sf9 cells (127). However, the assembly of the protein was not affected, suggesting that the sugars were required only for biosynthesis of a functional enzyme. It should be noted, however, that functional wild-type H^+,K^+-ATPase did not traffic properly in Sf9 cells. Catalytically active enzyme complexes were localized to intracellular membranes and not on the plasma membrane.

Recently, Asano *et al.* (13) created a series of mutants that progressively deleted all of the glycosylation sites in HKβ and expressed the constructs in HEK293 cells.

Removing any one of the glycosylation sites had no effect on assembly or enzymatic activity. Progressive removals of the sites on activity were cumulative, and deleting all seven sites resulted in a loss of α/β assembly and function. Interestingly, assembly was not affected when three glycosylation sites were removed, but the surface delivery of the β subunit was hindered, indicating that glycosylation played a role in the delivery mechanism of the enzyme. These results suggested that glycosylation of HKβ plays a role in activity, assembly, and the surface delivery of the enzyme. In contrast, if the glycosylation sites of the $NaK\beta_1$ subunit, which has three *N*-linked sites, were abolished by mutagenesis (19), or if the sugars were removed by tunicamycin (228, 269), the unglycosylated $NaK\beta_1$ subunit still associated with the $NaK\alpha_1$ subunit and produced a fully functional enzyme at the cell surface. However, the β subunit was more susceptible to proteolysis and had a decreased efficiency in assembling with α subunits (19). The observations suggested that the glycosylation sites on the $NaK\beta_1$ subunit were not required for enzyme assembly, function, or protein trafficking but played an important role in the stability and proper folding of the protein.

The six cysteine residues in the extracellular domain of HKβ subunit are completely conserved among all known β subunit isoforms. The residues form disulfide bonds in a sequential arrangement (41, 126, 156). The importance of the disulfide bond formation has been studied with reducing agents. The reduction of the disulfide bonds in HKβ inactivated the H^+,K^+-ATPase,. Similar results were observed with $NaK\beta_1$ (123). Binding of K^+ increased the resistance of disulfide bond reduction in the H^+,K^+-ATPase (41). High concentrations of Na^+ is known to shift the Na^+,K^+-ATPase or H^+,K^+-ATPase to the E_1 state (214), and high concentrations of Na^+ caused the disulfide bonds of HKβ

to be more susceptible to reduction in the presence of K^+ (41). It seems that the strength of disulfide bonds in HKβ increased as the enzyme changed from the E_1 to the E_2K^+ conformation, suggesting that the disulfide bonds offered conformational stability during K^+ transport. A study with a monoclonal antibody that inhibits enzymatic activity provided alternative support for HKβ subunit participation in enzymatic function. Monoclonal antibody 2G11 binds to an epitope within the first 36 N-terminal amino acids of HKβ and inhibits H^+,K^+-ATPase activity (42). The antibody binding altered K^+ binding affinity, thereby supporting the hypothesis that the β subunit aids in the apparent stability of the E_2K^+ conformation.

Each disulfide bond may play a different role in an intact enzyme complex. Noguchi *et al.* (171) reported that eliminating the most N-terminal disulfide bond of *Torpedo* NaKβ_1 produced an inactive α/β complex, and abolishing either of the two most C-terminal disulfide bonds prevented assembly of the α/β complex. Beggah *et al.* (19) conducted a similar study with *Xenopus laevis* NaKβ_1 and confirmed that the two most C-terminal disulfide bonds were important in the assembly of the enzyme complex. However, eliminating only the N-terminal disulfide bond allowed the formation of a small number of functional complexes at the cell surface, which was in disagreement with the data from Noguchi *et al.* (171). The authors believed that the inconsistency in the data was likely due to the sensitivity of the assays used. It appears that the domain comprised between the two most C-terminal disulfide bonds is able to adopt a structure that partially permits correct α/β subunit interaction.

The cytoplasmic tail of the HKβ subunit has a four-residue amino acid sequence that is highly homologous to tyrosine-based endocytosis signals. The signal could be

responsible for the endocytosis and retrieval of the H^+,K^+-ATPase from the secretory canalicular membranes to the tubulovesicles. To determine if the signal was important in the cycling of the enzyme in parietal cells, Courtois-Coutry *et al.* (48) generated transgenic mice expressing HKβ in which the motif's tyrosine residue was mutated to an alanine. The parietal cells from mice expressing the mutant HKβ subunit incessantly secreted acid and constitutively expressed H^+,K^+-ATPase at their cell surfaces. The results suggested that the tyrosine-based signal is required for the endocytosis of the enzyme and for the termination of acid secretion.

The biological role of HKβ was analyzed by a null mutation into the HKβ subunit gene (*Atp4b*) through homologous recombination (200). The mutation disrupted exon 1 so that a functional protein could not be produced. Absence of the HKβ transcript and protein in the stomach were confirmed by RT-PCR, Western analysis, and immunohistochemistry. The protein levels of $HK\alpha_1$ in the *Atp4b*$^{-/-}$ mice were lower than in *Atp4b*$^{+/+}$ and *Atp4b*$^{+/-}$ mice. This was in contrast to what was observed in the *Atp4a*$^{-/-}$ mice (220). There were no distinguishable differences in physical features or mortality among the *Atp4b*$^{+/+}$, *Atp4b*$^{+/-}$, and *Atp4b*$^{-/-}$ mice. However, *Atp4b*$^{-/-}$ mice had a gastric luminal pH of about 7, whereas the pH from *Atp4b*$^{+/+}$ and *Atp4b*$^{+/-}$ mice were considerably lower at pH 3.6 and 4.2, respectively. Sections of the gastric mucosa were examined at various ages of mice, and the appearance of parietal cells occurred more slowly in the *Atp4b*$^{-/-}$ mice than in normal mice. In the *Atp4b*$^{-/-}$ mice, the secretory canaliculus was much larger and had few microvilli, and the tubulovesicles were larger in diameter. The results demonstrated that HKβ was required for the acid secretory activity of the stomach. The fact that the secretory membranes of parietal cells were altered in

the absence of the HKβ subunit implied a membrane structural, and possibly, a biosynthetic role of the H^+,K^+-ATPase.

Renal H^+,K^+-ATPase

Potassium is critical for many cell functions, and its concentration in cells and extracellular fluid is kept constant despite wide variations in dietary K^+ intake. The normal concentration of K^+ in the extracellular fluid is within a narrow range of 3.5 to 5.0 mEq/L. Plasma K^+ levels rising above or dropping below this narrow range produces hyperkalemia or hypokalemia, respectively. Both conditions cause cardiac arrhythmias resulting in life-threatening situations. The kidney plays the major role in K^+ homeostasis by regulating K^+ excretion and functions to conserve K^+ when dietary K^+ intake is reduced. However, the ion pumps and channels that were responsible for K^+ conservation remained obscure into the late 1980's. Doucet and Marcy (57) measured [γ-^{32}P] ATP hydrolysis and detected a K^+-activated ATPase activity in the connecting segment, cortical collecting duct, and outer medullary collecting duct of rabbits and rats. The ATPase had a high affinity for K^+ (K_m=0.2-0.4 mM). The renal ATPase was not inhibited by ouabain, but two known gastric H^+,K^+-ATPase inhibitors, omeprazole and vanadate, were able to inhibit the ATPase activity. Vanadate inhibition indicated that the enzyme was a P-type ATPase. In addition, K^+ depletion increased the K^+-ATPase activity in the outer medullary collecting duct and the cortical collecting duct, making the enzyme a reasonable candidate for active K^+ absorption. Similar results were observed by Garg and Narang (80). Moreover, yet another gastric H^+,K^+-ATPase inhibitor, SCH-28080, also abolished K^+-ATPase activity.

Wingo (262) analyzed dietary K^+ influence on K^+ transport in the kidney. He established rabbits on one of three diets: a K^+-replete diet, a K^+-deplete diet, or a K^+-deplete Na^+-supplemented diet. Both K^+-deplete diets are referred to as K^+-restricted diets. Plasma K^+ levels were significantly less in K^+-deplete animals when compared to K^+-replete and K^+-deplete Na^+-supplemented animals. However, muscular K^+ levels were similar in all animals, demonstrating that significant changes in K^+ excretion occurred without any indication of muscle K^+ depletion. Plasma aldosterone levels were significantly lower in the K^+-deplete Na^+-supplemented rabbits (2.88 ± 0.57 ng/dl) when compared to levels from K^+-deplete rabbits (15.6 ± 5.3 ng/dl) and K^+-replete animals (44.7 ± 14.0 ng/dl). Therefore, any changes in K^+ transport could not be accounted by the effects of aldosterone.

Wingo observed that perfused outer medullary collecting duct from the inner stripe ($OMDC_i$) of the three groups had similar rates of fluid reabsorption and similar transepithelial voltages. However, there was a significant change in K^+ reabsorption, measured as a flux of $^{42}K^+$, in the three groups. K^+ reabsorption nearly tripled in the K^+-restricted rabbits ($17.2 \pm 2.0\%$, K^+-deplete; $20.8 \pm 4.2\%$ K^+-deplete Na^+-supplemented) when compared to the K^+-replete rabbits ($5.9 \pm 0.8\%$). He concluded that K^+ reabsorption in the medullary collecting duct is similar to K^+ secretion in the cortical segments at typical fluid flux rates and could have significant effects on the amount of K^+ excreted in urine. In a later paper, Wingo (261) demonstrated that the $OMCD_i$ had active, omeprazole-sensitive acidification and K^+ absorptive properties and was the first to suggest the presence of an H^+,K^+-ATPase in the kidney.

Chevel *et al.* (39) monitored the ^{86}Rb flux (a radioactive K^+ congener) and K^+-ATPase activities in the cortical and medullary collecting ducts. SCH-28080 inhibited both activities with an IC_{50} of 0.5 μM. Studies were conducted in the presence of 2.5 mM ouabain to inhibit Na^+,K^+-ATPase activity. Evidently, Rb uptake occurred in a manner other than by the Na^+,K^+-ATPase. In fact, structural, functional, and biochemical studies have implicated the H^+,K^+-ATPase in the final regulation of K^+ excretion and absorption in the kidney (263, 265).

Renal HKα Subunit Isoforms

One of the α subunits present in the kidney is the prototypical gastric $HK\alpha_1$. Ahn and Kone (5) used the rat $HK\alpha_1$ sequence to generate a probe to study $HK\alpha_1$ mRNA distribution along the collecting duct by reverse-transcriptase polymerase chain reaction (RT-PCR) on tubule segments and in situ hybridization. Signals showing the presence of $HK\alpha_1$ mRNA were observed from the connecting segment through the inner medullary collecting duct. A similar distribution had been observed by immunohistochemistry using antibodies directed against the $HK\alpha_1$ subunit (264).

The second class of H^+,K^+-ATPases resident in the kidney are the $HK\alpha_2$ subunit containing enzymes. Crowson and Shull (49) generated the first cDNA for a rat HKα colonic subunit. Referred to here as the $HK\alpha_{2a}$ subunit, it is sometimes called the colonic HKα subunit. They noted a weak hybridization signal from the kidney in a tissue distribution Northern analysis, and evidence from other laboratories corroborated this observation (133). The deduced polypeptide consisted of 1036 amino acids and had 63% amino acid identity to $HK\alpha_1$ and 63% identity to the three NaKα subunit isoforms. The cDNA for ATP1AL1 was cloned from human skin axilla with mRNA expression in brain

and kidney (89, 160). The cDNA encoded a 1039 amino acid protein that shared 86% identity to the rat $HK\alpha_{2a}$ protein and 65% amino acid identity to human $HK\alpha_1$. Both the human and rat cDNAs encoded ouabain-sensitive H^+/K^+ exchange activities when expressed in *Xenopus laevis* oocytes (47, 159) and HEK293 cells (87) with the HKβ subunit.

Using 5' rapid amplification of cDNA ends (RACE) from rat kidney and distal colon mRNA with reverse primers for $HK\alpha_{2a}$, Kone and Higham (131) identified two distinct $HK\alpha_2$ mRNAs that were products of the rat $HK\alpha_2$ gene. The first variant, $HK\alpha_{2a}$, was identical to the previously described sequence (49), and the 1036 amino acid protein was encoded by a 4.0 kb mRNA transcribed from the 5'-most promoter. The second variant, $HK\alpha_{2b}$, was a 929 amino acid protein encoded by a 4.0 kb mRNA transcribed from an internal promoter within intron 1 of the $HK\alpha_2$ gene. The $HK\alpha_{2b}$ mRNA contained an unusually large 5' UTR with eight upstream open reading frames. The $HK\alpha_{2b}$ mRNA sequence was identical to $HK\alpha_{2a}$ starting at the codon for Lys-4 of $HK\alpha_{2a}$. However, the first AUG triplet of the $HK\alpha_{2b}$ mRNA that was in a favorable context for translation initiation corresponded to Met-109 of $HK\alpha_{2a}$. Therefore, the predicted $HK\alpha_{2b}$ protein of 929 amino acids lacked the first 108 amino acids of the $HK\alpha_{2a}$ sequence, putting the N-terminus of the $HK\alpha_{2b}$ protein immediately before the first predicted transmembrane domain. The truncation deleted putative protein kinase A and protein kinase C phosphorylation sites present in the rat $HK\alpha_{2a}$ protein. Northern analysis demonstrated that both mRNAs ($HK\alpha_{2b} > HK\alpha_{2a}$) were expressed abundantly in distal colon and less in the proximal colon and kidney. The levels of the two mRNAs increased with K^+ deprivation. Stable expression of $HK\alpha_{2b}$ with the HKβ subunit in

HEK293 cells revealed a K^+ uptake that was SCH-28080-resistant and partially sensitive to ouabain.

Campbell *et al.* (35) identified a different alternatively spliced $HK\alpha_2$ isoform, $HK\alpha_{2c}$, in rabbit renal cortex using RT-PCR and 5' RACE. In contrast to the rat, the alternative splice product of the rabbit yielded an mRNA with a longer open reading frame. The deduced amino acid sequence of $HK\alpha_{2c}$ encoded a protein that was 61 amino acids longer at the N-terminus than the rabbit $HK\alpha_{2a}$ protein. Moreover, there were three short upstream open reading frames in the sequence that may play a role in translational regulation. The extended N-terminal region of the putative $HK\alpha_{2c}$-encoded protein has a casein kinase II phosphorylation motif and a protein kinase a motif. These sites, not present in $HK\alpha_{2a}$, offer potential regulatory sites in the $HK\alpha_{2c}$. Northern and Western analysis demonstrated the presence of both $HK\alpha_{2a}$ and $HK\alpha_{2c}$ mRNAs and protein expression in the rabbit renal cortex. $HK\alpha_{2c}$ protein has been localized to the apical membrane of a small population of cells in the connecting segment, cortical collecting duct and $OMCD_i$ (247). Studies in our laboratory by Deborah Zies demonstrated that both isoforms are the product of a single gene and appear to be under control of one promoter (unpublished observations). Studies of plant Ca^{2+}-ATPase provided evidence for a role of an N-terminal domain of a P-type ATPase in the regulation of pump function. The N-terminal end of the protein was shown to function as an autoinhibitory domain modulated by calmodulin (92). Whether the markedly different N-termini on the rat $HK\alpha_{2b}$ and rabbit $HK\alpha_{2c}$ subunits impart properties differing from the enzymes containing the $HK\alpha_{2a}$ subunits remains to be determined.

It was not immediately clear whether the human ATP1AL1 and the rat $HK\alpha_{2a}$ should be viewed as homologous to one another. Modyanov and his colleagues (89) took the position that it was indeed homologous to rat $HK\alpha_{2a}$. The alternative interpretation was that the sequence identity between ATP1AL1 and rat $HK\alpha_{2a}$ was too low to justify classifying the two genes as homologous. Indeed, the extent of identity between homologous mammalian α subunits of P-type ATPases is usually much higher. For example, the amino acid identity between the human, rat, and rabbit $HK\alpha_1$ subunits exceeds 97%. However, the cloning of the rabbit $HK\alpha_{2a}$ cDNA has helped to clarify the gene homology issue (35). Comparisons of the deduced primary sequences of either the human ATP1AL1 or rat $HK\alpha_{2a}$ to rabbit $HK\alpha_{2a}$ yielded about 87% identity, and much of the sequence diversity between these proteins clustered in the N-terminal 45 amino acids (Figure 1-4). Distance analysis of the complete deduced sequences of the $HK\alpha_{2a}$ and ATP1AL1 subunits suggested that these proteins are more closely related to each other than to either $HK\alpha_1$ or any of the $NaK\alpha$ subunits (Figure 1-5). This supports the argument in favor of assigning the three subunits as the products of homologous genes. Moreover, the 5' mRNA sequences that give rise to the rat $HK\alpha_{2b}$ and rabbit $HK\alpha_{2c}$ sequences appeared to be transcribed from genomic DNA contained in the introns between the first two exons encoding the $HK\alpha_{2a}$ mRNAs in both species. This similar processing of transcripts provided added support for the argument that the rat and rabbit genes are homologous.

To assess the role of the $HK\alpha_{2a}$ subunit in K^+ homeostasis *in vivo*, Meneton *et al.* (154) generated a mouse model carrying a disruption of the $HK\alpha_2$ gene (*cHKa*) and analyzed the ability of the animals to conserve K^+ under normal and K^+-deplete

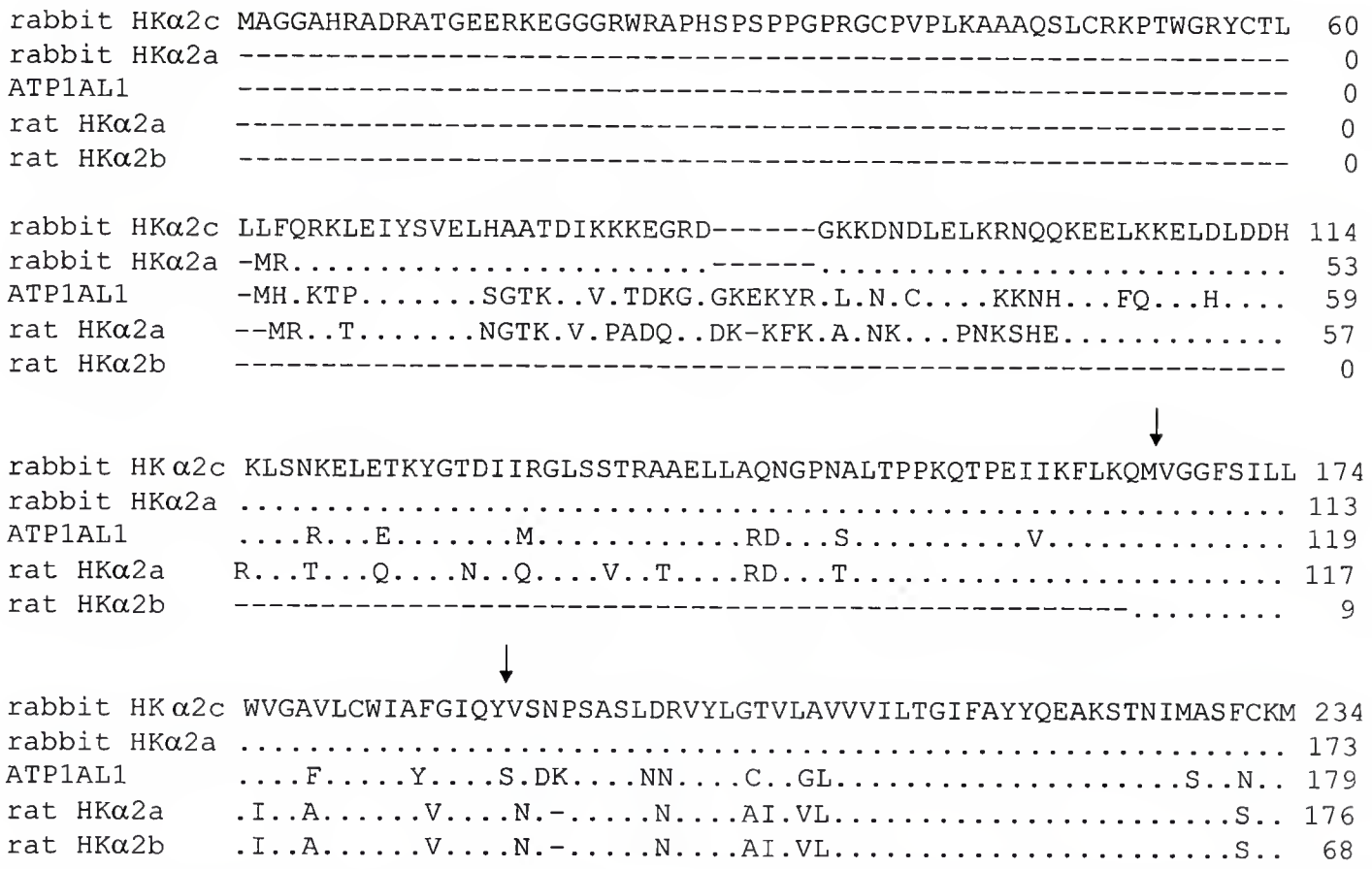

Figure 1-4. Variation in the N-termini of the HKα_2 subunits from rabbit, human, and rat. Sequences were aligned using the CLUSTALW program (237). Species and subunit designations are indicated on the left and amino acid numbers are labeled to the right of each line of sequence. The primary sequence of the rabbit HKα_{2c} subunit is shown using single letter code. Symbols: (●) indicates amino acid identity, (-) indicates the absence of an amino acid at a position; substitutions are shown using single letter code; the arrows indicate the predicted position of the first membrane spanning domain to the bilayer.

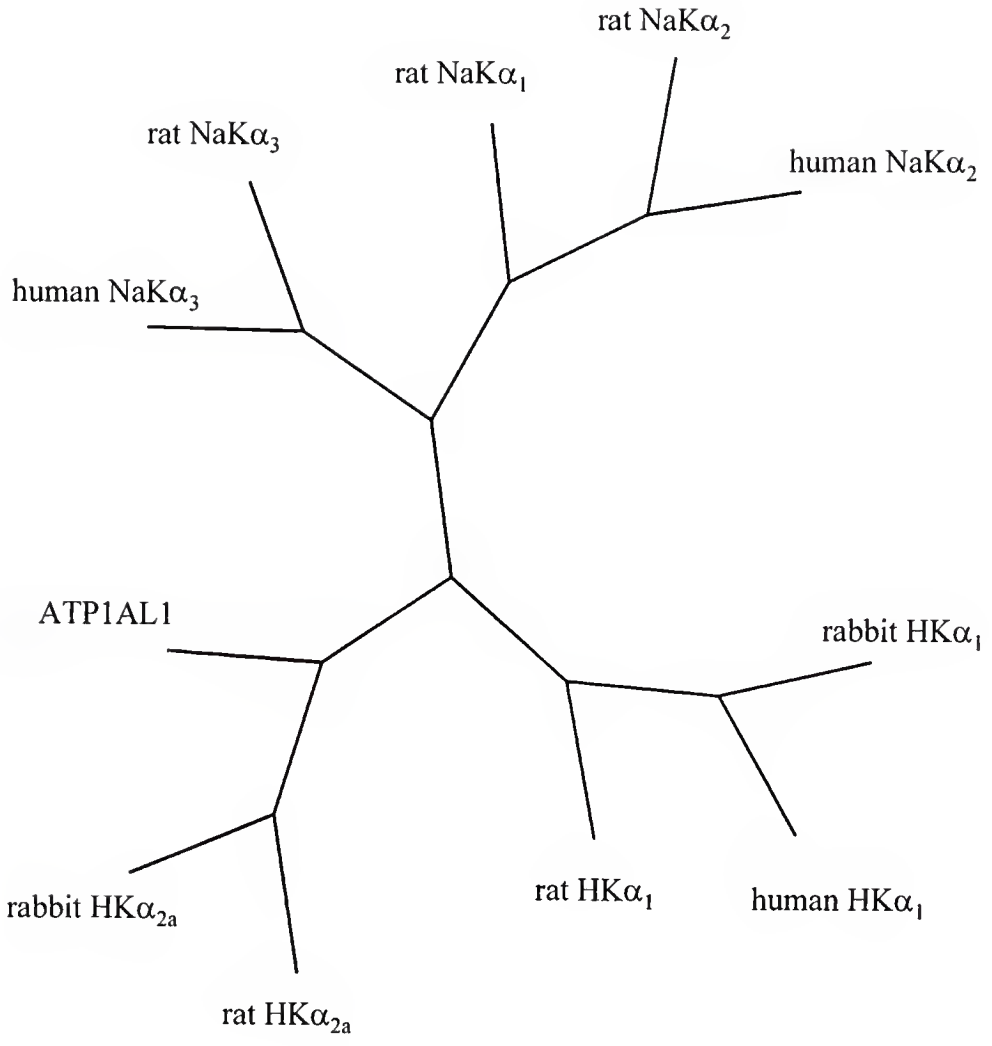

Figure 1-5. Distance analysis of HKα and NaKα subunits. Protein sequences were aligned with CLUSTALW (237). The resulting alignments were used by PHYLIP to determine the relatedness among the subunits. TreeView (176) was used to draw the final tree. The tree is not rooted. The forks indicate closest primary sequence relationships without bias on the length of branches.

conditions. Critical transmembrane domain sequences required for transport activity were replaced with the neomycin resistance gene through homologous recombination. The replacement was confirmed by RT-PCR and sequence analysis. Homozygous *cHKa*$^{-/-}$ mice fed K^+-replete diets had no apparent difficulty with K^+ homeostasis when compared to wild type *cHKa*$^{+/+}$ mice. Urinary K^+ excretion levels were also similar between wild type and homozygous mice fed K^+-replete diets. However, urinary excretion of animals on K^+-restricted diets had dropped over 100-fold, and to similar levels, in both wild type and homozygous mice. The *cHKa*$^{-/-}$ mice suffered a loss in body weight, plasma K^+, and muscle K^+ levels. Although fecal K^+ excretion was decreased in both sets of mice on K^+-restricted diets, *cHKa*$^{-/-}$ mice had a fourfold greater reduction in fecal K^+ excretion. The results indicate that $HK\alpha_{2a}$ plays an important role in K^+ homeostasis during K^+ deprivation, although the effect was primarily in the colon and not in the kidney. It is likely that the gastric $HK\alpha_1$ subunit isoform in the kidney was able to compensate for the loss of $HK\alpha_{2a}$ activity.

Renal β Subunit Isoforms

The identity of the β subunits in renal H^+,K^+-ATPases is much less clear owing to uncertainty about the identity of the β subunits(s) associated with the $HK\alpha_2$ subunits. Three distinct β proteins have been implicated directly or indirectly in renal H^+,K^+-ATPases. These are the HKβ subunit, the $NaK\beta_1$ subunit, and the $NaK\beta_3$ subunit.

Although it has not been rigorously tested in kidney tissue, probably the safest assumption is that the HKβ subunit is the mate to the $HK\alpha_1$ subunit. These two proteins have been conclusively shown to constitute the H^+,K^+-ATPase of the parietal cell (99). Indeed, HKβ subunit mRNA was readily detectable in the kidney by RT-PCR, Northern

analysis, and in situ hybridization (35, 36). The distribution of HKβ mRNA in the connecting segment through the collecting duct was similar to the $HK\alpha_1$ distribution. Transgenic animals were used to show that the HKβ gene promoter directed reporter gene expression in the collecting duct (32). The HKβ subunit also supports H^+,K^+-ATPase activity in *Xenopus laevis* oocyte and tissue culture expression systems for $HK\alpha_{2a}$ subunit pumps (12, 45, 87). However, the HKβ subunit has never been shown to associate with $HK\alpha_{2a}$ *in vivo*.

Two β subunits, which were clearly the products of different genes, have been detected in apparent association with the $HK\alpha_{2a}$ subunit. Two groups independently showed that antibodies directed against the $HK\alpha_{2a}$ subunit co-immunoprecipitated the $NaK\beta_1$ subunit from both colon and kidney tissues (44, 132). The $NaK\beta_1$ subunit was reported to be capable of supporting H^+,K^+-ATPase activity for the $HK\alpha_{2a}$ subunit in an *in vitro* expression system (45, 197). Given the relatively high abundance of the $NaK\beta_1$ subunit in the kidney and its ability to productively associate with $HK\alpha_{2a}$ *in vitro*, it was perhaps not surprising that $NaK\beta_1$ was found in association with $HK\alpha_{2a}$ subunit.

Sangan *et al.* (196) introduced the HKcβ subunit as a potential candidate to serve as a mate for the $HK\alpha_{2a}$ subunit in the colon by using an immunoprecipitation strategy. The HKcβ subunit sequence was identical to the previously identified $NaK\beta_3$ sequence (142) and will be referred to as $NaK\beta_3$ throughout this document. Sangan *et al.* (196) noted the presence of a hybridization signal for $NaK\beta_3$ in a Northern analysis of mRNA from kidney among several other tissues. $NaK\beta_3$ protein expression was up-regulated in the apical membrane of the distal colon in response to K^+ depletion. In a later report

Sangan *et al.* (197) stably expressed rat $HK\alpha_{2a}$ and $NaK\beta_3$ in HEK293 cells. The subunits formed a functional enzyme complex and yielded expression of both ouabain-insensitive H^+,K^+-ATPase activity and ^{86}Rb uptake.

Very recently, Geering *et al.* (83) investigated the association efficiency of human $HK\alpha_{2a}$ (ATP1AL1) with all known β subunit isoforms (HKβ, $NaK\beta_1$, $NaK\beta_2$, $NaK\beta_3$). The authors expressed the subunits in *Xenopus laevis* oocytes and monitored their resistance to cellular and proteolytic degradation and exit from the endoplasmic reticulum (ER). Their results indicated that certain β subunits associated preferentially with ATP1AL1, but that probably none of the known β subunits seemed to fulfill all of the requirements to serve as a real mate to $HK\alpha_{2a}$. ATP1AL1 was well protected against cellular degradation by HKβ and $NaK\beta_2$, and these complexes were able to leave the ER. However, $NaK\beta_1$ interaction was much less efficient and produced few stable enzyme complexes that left the ER. Even though HKβ and $NaK\beta_2$ protected ATP1AL1 from cellular degradation, these enzyme complexes were less resistant to trypsinolysis than authentic α/β complexes such as $NaK\alpha_1/NaK\beta_1$. The authors do point out the possibility that ATP1AL1, when associated with β subunits, may be more sensitive to trypsin than $NaK\alpha_1/NaK\beta_1$ complexes. $NaK\beta_3$ stably associated with ATP1AL1, but the enzyme complexes were moderately trypsin-sensitive and were impaired in their ability to leave the ER. The authors concluded that the incomplete stabilization of $NaK\beta_1$, the trypsin sensitivity of complexes with HKβ or $NaK\beta_2$, and the impaired ER exit of $NaK\beta_3$ complexes suggest that none of the known β subunits is the true mate to the $HK\alpha_2$ subunits. However, at this time no other β subunit candidates have been identified.

H^+ Versus Na^+, K^+-ATPase

Experimental evidence exists which supports the theory that the colonic H^+,K^+-ATPase can also act as a Na^+,K^+-ATPase. Grishin and Caplan (88) analyzed HEK293 cells that stably expressed ATP1AL1 and HKβ. This cell line was relatively resistant to ouabain with a K_i of about 50 μM, whereas only 200 nM ouabain inhibited growth of control cells. Flame photometry was used to determine the steady state levels of intracellular Na^+ levels. Intracellular Na^+ content in cells stably expressing ATP1AL1 and HKβ was half that of control cells. Furthermore, the rate of Na^+ efflux in cells expressing the two subunits was differentially sensitive to the presence of 1 μM ouabain or 1 mM ouabain. However, 1 μM and 1 mM ouabain concentrations inhibited Na^+ efflux to the same extent in control cells. The data strongly suggested that the ATP1AL1/HKβ enzyme complex was able to function as a Na^+,K^+-ATPase. Using an inhibitory antibody to rat $HK\alpha_{2a}$, Codina *et al.* (46) were able to inhibit Na^+-dependent K^+-ATPase activity in native rat distal colon membranes, supporting the position that the colonic H^+,K^+-ATPase can act as a Na^+,K^+-ATPase *in vivo*.

Our laboratory cloned the unique $HK\alpha_{2c}$ subunit isoform from rabbit renal cortex (35). The encoded protein was greater than 90% identical to the published $HK\alpha_{2a}$ sequence. The only difference was a 61 amino acid extension at the N-terminus of $HK\alpha_{2c}$. We had an interest in understanding the importance of the N-terminal extension on the function of the enzyme as an H^+,K^+-ATPase. To analyze its importance, I set out to express both rabbit $HK\alpha_{2a}$ and $HK\alpha_{2c}$ subunit isoforms in a heterologous expression system with the rabbit $NaK\beta_1$ subunit, and later with the $NaK\beta_3$ subunit. This

dissertation describes the expression of these subunits, and the observations that the proteins likely did not form stable enzyme complexes.

CHAPTER 2
EXPERIMENTAL PROCEDURES

Recombinant DNA Techniques

Plasmid DNA was purified by CsCl-ethidium bromide gradient ultracentrifugation (81), by the Qiagen Maxi Prep kit, or by the Qiagen Mini Prep kit (Qiagen, Valencia, CA). Restriction endonuclease reactions, ligation reactions, and transformations were performed according to the recommendations of the suppliers (New England Biolabs, Beverly, MA and Life Technologies, Grand Island, NY). DNA fragments and PCR products were separated by agarose gel electrophoresis, eluted from the agarose, and purified using the QIAquick gel extraction kit (Qiagen). Determination of nucleotide sequences was conducted by the core facilities of the University of Florida Interdisciplinary Center for Biotechnology Research (ICBR). Oligonucleotide synthesis was performed by either Life Technologies or by ICBR.

Plasmid Constructions

$b_{Arg\text{-}36}$ Mutagenesis and Strain Construction

Plasmid pKAM14(*b*) (147) was used to construct mutations of the *uncF*(*b*) gene at the codon for Arg-36. Mutations were generated using PCR mutagenesis essentially as described by Ho *et al.* (101). The primers used to amplify a segment of DNA using pKAM14(*b*) as a template are depicted in Table 2-1. In each case, a silent mutation generating a *Mun*I site was included in the mutagenic primers for screening purposes. The PCR reactions were carried out in a Coy TempCycler II model for 30 cycles. The

Table 2-1. Primers for the PCR mutagenesis of $b_{Arg\text{-}36}$ in the *uncF*(*b*) gene.

Primer Name	Mutagenic Primer Sequence[a]	Encoded Amino Acid Mutation
BC282	5′AAAATAAACAAATAGGGGTTCCGCG3′	
BC280	5′CAGGTTTACGCTCGGCTTCAATTT3′	
BC144 BC281	5′GCAGCAATTGAAAAA**RHA**CAAAAAG3′ 3′CGTCGTTAACTTTTT**YDT**GTTTTTC5′	Glu, Lys, Ile, Thr, Ala, Val
BC307 BC306	5′GCAGCAATTGAAAAA**TVC**CAAAAAG3′ 3′CGTCGTTAACTTTTT**ABG**GTTTTTC5′	Cys, Tyr, Ser
BC309 BC308	5′GCAGCAATTGAAAAA**GAG**CAAAAAG3′ 3′CGTCGTTAACTTTTT**CTC**GTTTTTC5′	Glu

[a]Notation for degenerate nucleotides is that of the International Union of Biochemistry Nomenclature Committee. Unique *Mun*I restriction site is underlined. The nucleotides that encode the mutations at $b_{Arg\text{-}36}$ are in bold.

PCR products were digested with *Aat*II and *Ppu*MI and then ligated to the 2.8 kilobase pair (kbp) *Aat*II/*Ppu*MI fragment of plasmid pKAM14(*b*). Plasmid DNA was prepared from transformants, and recombinant plasmids were selected for the presence of a *Mun*I site. The mutations were identified through nucleotide sequencing.

Plasmids encoding the $b_{Arg\text{-}36}$ mutations in pKAM14(*b*), as well as control plasmids pKAM14(*b*) and pBR322 (25), were transformed into *E. coli* strain KM2(Δ*b*) which has been deleted for the *uncF*(*b*) gene from the chromosome (146). The strains were also transformed with plasmid pKAM16(*lacI*^{q}) to provide improved regulation of the plasmid-encoded *uncF*(*b*) genes (147).

Episomal Expression Plasmid Constructions

The pREP4(*Hyg*^{r}) and pREP8(*His*^{r}) episomal expression vectors were purchased from Invitrogen (Carlsbad, CA). The trans-acting factor Epstein Barr Virus Nuclear Antigen 1 (EBNA-1) required for the Epstein Barr Virus' (EBV) origin of replication was present in both plasmids. Each one of the rabbit HKα_{2a} and HKα_{2c} cDNAs was cloned in the pREP4 plasmid. Rabbit HKβ and NaKβ_1 cDNAs were each cloned in the pREP8 plasmid.

The construction of HKα_{2a} in pREP4 was as follows. The entire coding region of HKα_{2a} (nt 16-4079) had been cloned in the TOPO TA cloning vector (Invitrogen) by Dr. W.G. Campbell, and the plasmid was named pHKa2a53. The plan was to move the coding region of HKα_{2a}, including 5' and 3' UTRs, into pREP4 as a 4.1 kb *Not*I/*Bam*HI fragment. Because of a *Bam*HI site within the nucleotide sequence of HKα_{2a}, conditions which resulted in a partial digest of *Bam*HI were utilized. Plasmid pHKa2a53 was digested to completion with *Not*I and *Bss*HII and partially with *Bam*HI. *Bss*HII was used

to digest the vector backbone to aid in gel purification of the 4.1 kbp *Not*I/*Bam*HI fragment. The fragments were separated by agarose gel electrophoresis, and the 4.1 kbp fragment containing the entire coding region of $HK\alpha_{2a}$ was gel purified and ligated into pREP4. The final plasmid was named pTLC19 (Figure 2-1). There were two start codons present in the multiple cloning region of the TOPO TA cloning vector that were carried with the $HK\alpha_{2a}$ cDNA into pTLC19. These start codons caused the protein to be out of frame. Therefore, pTLC19 did not produce a functional $HK\alpha_{2a}$ protein.

A plasmid containing the entire coding region of rabbit $HK\alpha_{2c}$ did not exist in our laboratory. Because $HK\alpha_{2a}$ and $HK\alpha_{2c}$ only differed at their 5' regions, I decided to use RT-PCR to amplify the unique region of $HK\alpha_{2c}$, including an overlapping region with $HK\alpha_{2a}$, and splice the fragment into pTLC19 to create $HK\alpha_{2c}$ in pREP4. RT-PCR was conducted using RNA isolated from rabbit distal colon with sense primer BC366 and antisense primer BC265 (Table 2-2). These primers amplified a 656 bp fragment of $HK\alpha_{2c}$ with a 260 bp overlap with $HK\alpha_{2a}$ cDNA sequence. The fragment was cloned in TOPO TA cloning vector and named pHKa2c.9 (Figure 2-2). The $HK\alpha_{2c}$ nucleotide sequence was confirmed by nucleotide sequencing. Plasmid pHKa2c.9 was digested to completion with *Afl*II and *Not*I. The 530 bp fragment was separated by agarose gel electrophoresis, gel purified, and ligated into pTLC19 to create pTLC24 (Figure 2-2). This plasmid also had the two start codons from the TOPO TA cloning vector so it did not produce a functional $HK\alpha_{2c}$ protein.

The rabbit HKβ cDNA had been previously amplified in our laboratory by RT-PCR as two overlapping fragments. Each fragment was cloned into TOPO TA cloning vector by Dr. W.G. Campbell. Plasmid pHKβ5H contained the 5' region of HKβ and

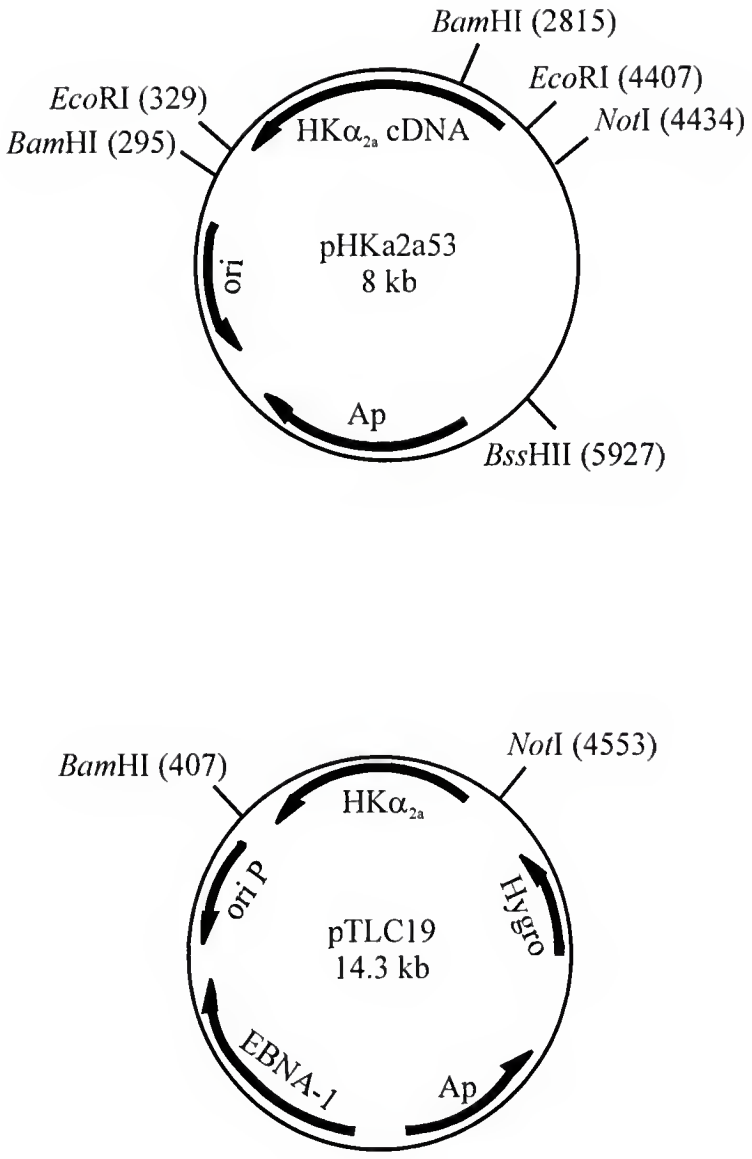

Figure 2-1. Rabbit $HK\alpha_{2a}$ cDNA construction in pREP4. Plasmid pHKa2a53 was digested to completion with *Not*I and *Bss*HII and partially with *Bam*HI. The 4.1 kb *Not*I/*Bam*HI fragment was gel purified and ligated into pREP4 to create pTLC19.

Table 2-2. RT-PCR and RACE primers

Primer Name	Primer Sequence	Use
BC366	$^{5'}$CGGATTCGGAGAAAAGTGCTAGACTGGAGCT$^{3'}$	5' amplification of $HK\alpha_{2c}$ cDNA
BC265	$^{5'}$TTGATGATCTCTGGGGTCTG$^{3'}$	
BC424	$^{5'}$CCATGGCCCGCGGRAAAGCCAAGGA$^{3'}$	$NaK\beta_1$ 3' RACE
AP1	$^{5'}$CCATCCTAATACGACTCACTATAGGGC$^{3'}$	
BC464	$^{5'}$GGTTATACTTCGTTCCTGGGGAAAACT$^{3'}$	$NaK\beta_1$ 5' RACE
BC448	$^{5'}$CCGTCTTTGTAGCCGTAAGTTTCG$^{3'}$	
BC465	$^{5'}$ACTCGGTCCTGGTACGTGGGCTT$^{3'}$	
AP2	$^{5'}$ACTCACTATAGGGCTCGAGCGGC$^{3'}$	

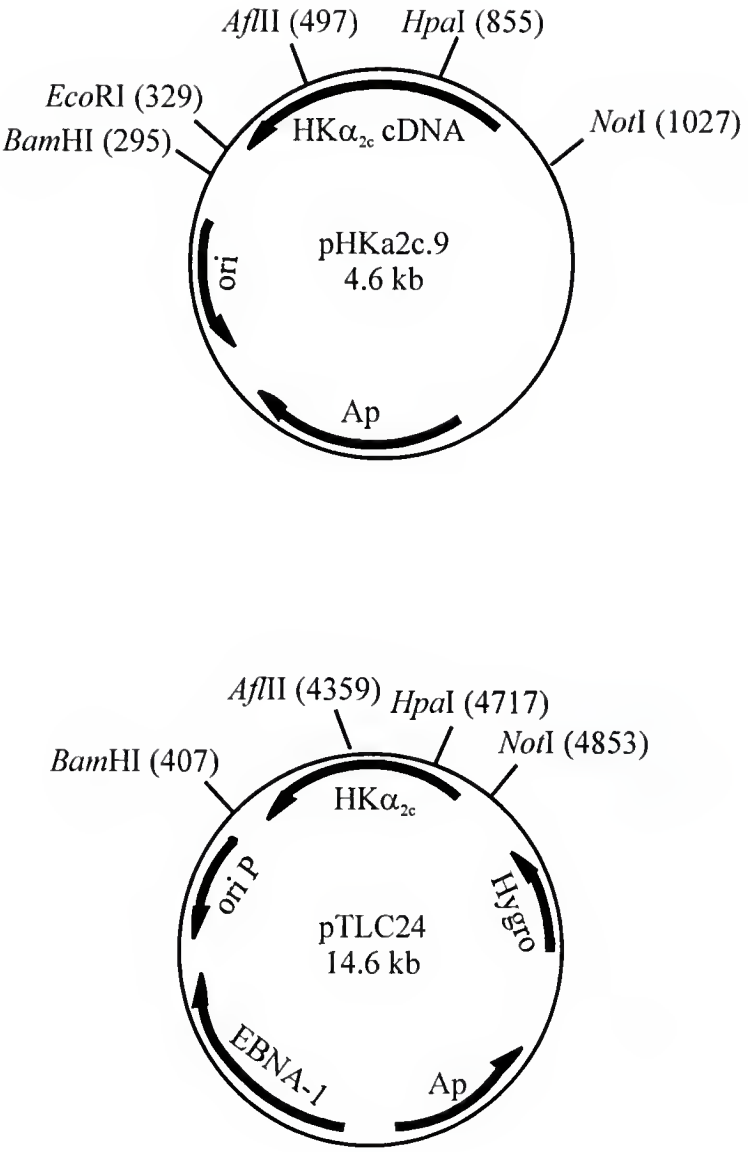

Figure 2-2. Rabbit HKα_{2c} cDNA construction in pREP4. Plasmid pHKa2c.9 was digested to completion with *Not*I and *Afl*II. The 0.5 kb *Not*I/*Afl*II fragment was gel purified and ligated into pTLC19 to create pTLC24.

pHKβ3C contained the 3' region of HKβ. The plan was to construct the full-length cDNA of HKβ in pUC18 and clone the full-length cDNA in pREP8. Plasmid pHKβ3C was digested to completion with *Bam*HI and *Pst*I. The 708 bp fragment was isolated by agarose gel electrophoresis and ligated in pUC18. The plasmid was called pTLC21. The *Bam*HI site in the multiple cloning region of pHKβ5H was destroyed by digesting the plasmid with *Bam*HI, filling in the overhanging ends using Klenow, and religating the plasmid to create pTLC20. Plasmid pTLC20 was digested to completion with *Pst*I and partially with *Hind*III. The resulting 734 bp fragment containing the 5' region of HKβ was isolated and ligated in pTLC21 to generate the full-length HKβ cDNA. This plasmid was named pTLC22. Plasmid pTLC22 was digested with *Kpn*I and *Bam*HI, the 1.4 kb band containing the full-length HKβ was isolated and ligated into pREP8 to create pTLC23 (Figure 2-3).

The rabbit NaKβ_1 cDNA was amplified by RT-PCR using primers with unique restriction sites engineered to aid in the cloning in pREP8. This is discussed in more detail in Chapter 4. The unique restriction sites *Kpn*I and *Nhe*I were engineered at the 5' and 3' ends of NaKβ_1, respectively. The fragment was ligated in TOPO TA cloning vector and named p3A1. QuikChange Mutagenesis (Stratagene, La Jolla, CA) was conducted to correct the mutations at the 3' end of NaKβ_1 using sense primer BC467 and antisense primer BC466 (Table 2-3). The plasmid with the corrected 3' end of rabbit NaKβ_1 was named pNaKβ_1. pNaKβ_1 was digested with *Kpn*I and *Nhe*I, the 0.9 kbp fragment was isolated and ligated in pREP8 to create pTLC25 (Figure 2-4).

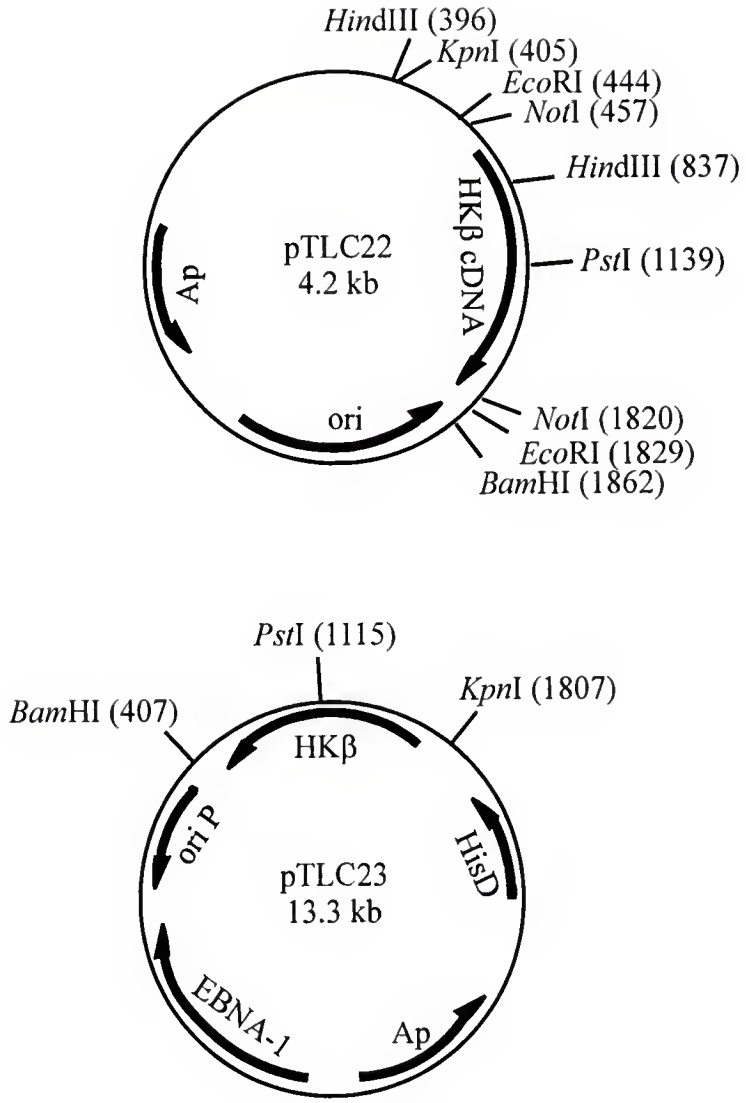

Figure 2-3. Rabbit HKβ cDNA construction in pREP8. Plasmid pTLC22 was digested to completion with *Kpn*I and *Bam*HI. The 1.4 kb *Kpn*I/*Bam*HI fragment was gel purified and ligated into pREP8 to create pTLC23.

Table 2-3. Mutagenesis primers

Primer Name	Primer Sequence[a]	Use
BC466 BC467	5'GCCCTTGCTTGCTCAGCTCTTAACTTCAATTTTTACATCAAAACG3' 5'CGTTTGATGTAAAAATTGAAGTTAAGAGCTGAGCTAGCAAGGGC3'	Repair 3' end of NaKβ_1
TC12 TC13	5'GGGATAAGAACATGTATTACTTCGAACAGGTCTGTCTCTG3' 5'CAGAGACAGACCTGTTCGAAGTAATACATGTTCTTATCCC3	Engineer *Bst*BI site at stop codon of HKα_{2a}
TC18 TC19	5'AACCGCGG**GCGGCCG***CTCGAG*CT3' 5'CTAGAG*CTCGA****G****CGGCCGC*CCGCGGTT3'	Shorten HKα_{2c} 5' UTR
TC24 TC25	5'AATTCTGCAGATAGTTAACCACTGGC3 5'GGCCGCCAGTGGTTAACTATCTGCAG3''	Remove extra ATG's upstream of HKα_{2a}

[a]Restrictions sites designed in primers are underlined, italicized, or in bold.

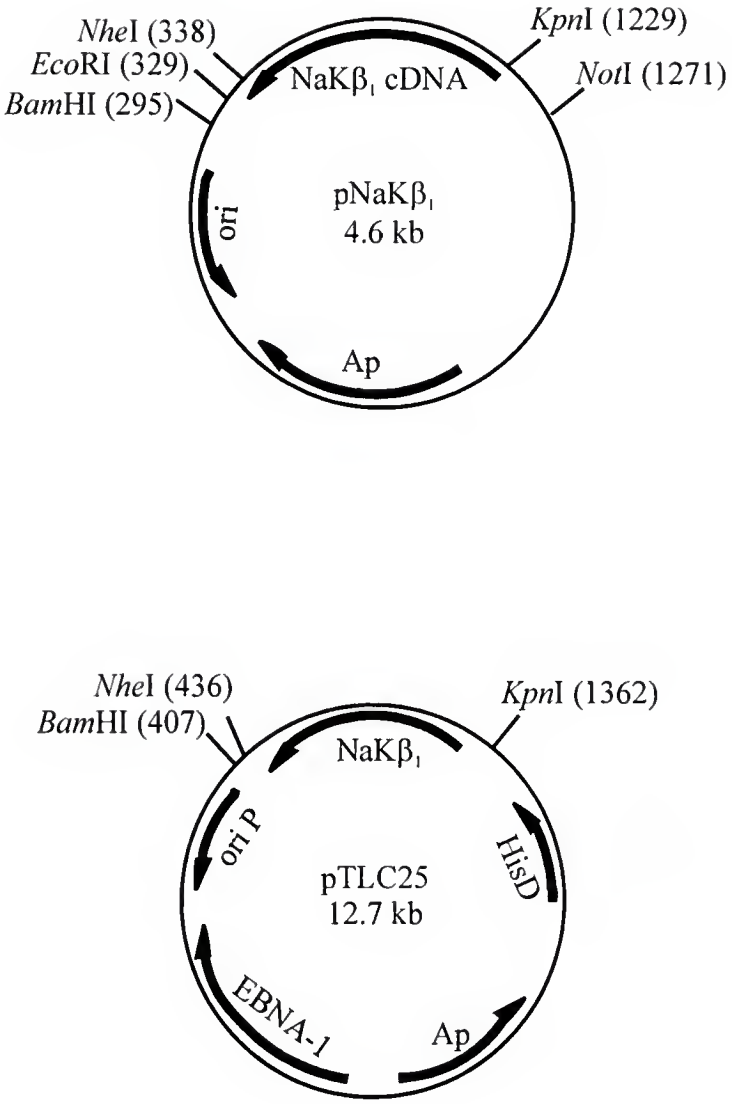

Figure 2-4. Rabbit NaKβ$_1$ cDNA construction in pREP8. Plasmid pNaKβ$_1$ was digested to completion with *Kpn*I and *Nhe*I. The 0.9 kb *Kpn*I/*Nhe*I fragment was gel purified and ligated into pREP8 to create pTLC25.

Stable/Transient Plasmid Construction

The plasmid used for the stable and transient vector construction was pBudCE4 (Invitrogen). This plasmid was unique in that it contained two promoters for cloning two cDNAs, as well as allowing the researcher the ability to clone each cDNA in frame with epitope tags present after each promoter. The $HK\alpha_{2a}$ and $HK\alpha_{2c}$ cDNAs were cloned behind the human EF-1α promoter and in frame with the V5 epitope and polyhistidine (6xHis) metal-binding tag. The $NaK\beta_1$ cDNA was cloned behind the human CMV promoter, but not in frame with the epitope tags since a good commercial anti-rabbit $NaK\beta_1$ antibody was available.

To clone $HK\alpha_{2a}$ and $HK\alpha_{2c}$ in frame with the V5 epitope and 6xHis tag, a *Bst*BI site was engineered at the stop codon of each of the $HK\alpha_2$ cDNAs. The *Bst*BI site was engineered using QuikChange Mutagenesis. pHKa2a53 was digested with *Aat*II and *Kpn*I and the 2 kbp fragment containing the 3' end of $HK\alpha_{2a}$ was ligated in pUC18 to create pTLC29. Primer pairs TC12 and TC13 were used for the QuikChange Mutagenesis to create pTLC30.1 (Table 2-3). The *Bst*BI site in each primer is underlined. The mutations were confirmed by nucleotide sequencing. The DNA fragment with the *BstB*I site was moved back to pHKa2a53 as an *Aat*II/*Kpn*I fragment to regenerate the full-length $HK\alpha_{2a}$ cDNA with the *Bst*BI site. The plasmid was named pTLC31. Plasmid pTLC31 was digested with *Not*I and *Bst*BI, the 3.1 kbp band was gel purified and cloned in pBudCE4 to generate pTLC34. The $HK\alpha_{2a}$ cDNA is in frame with the V5 and polyhistidine epitope tags.

An early hypothesis as to the failure of the episomal expression was the large 5' UTR of $HK\alpha_{2c}$. This was later determined to be due to the start codons carried over from

the TOPO TA cloning vector. Before cloning HKα_{2c} in pBudCE4, the 5' UTR was made shorter through cassette mutagenesis. pHKa2c.9 was digested with *Xba*I and *Hpa*I. The *Hpa*I site was within the 5' UTR of HKα_{2c}, and the *Xba*I site was within the multiple cloning region of TOPO TA vector. Primers TC18 and TC19 were designed with *Xba*I and *Hpa*I complementary ends (Table 2-3). The cassette mutagenesis was confirmed by a loss of an *Nsi*I site. The plasmid was called pTLC32. To create HKα_{2c} in pBudCE4, pTLC32 was digested with *Eco*RV and *Not*I, the 300 bp band was gel purified and ligated into pTLC34. The resulting plasmid was named pTLC35 (Figure 2-5). The HKα_{2c} cDNA is in frame with the V5 and polyhistidine epitope tags..

I determined that two ATG start codons were present on the lower strand in the multiple cloning region of the TOPO TA cloning vector. This would have caused major translational problems. The two start sites carried over during the cloning of HKα_{2a} in pBudCE4. However, the sites were eliminated in HKα_{2c} during the shortening of the 5' UTR. To correct the problem in HKα_{2a}, pTLC34 was digested to completion with *Not*I and partially with *Eco*RI. Cassette mutagenesis was conducted with primer pairs TC24 and TC25 with proper overhangs. A *Hpa*I site was engineered for screening purposes (Table 2-3). The plasmid was called pTLC46 (Figure 2-6).

To clone NaKβ_1 into pBudCE4, pNaKβ_1 was digested with *Bam*HI and *Xba*I, the 0.9 kbp fragment was gel purified and cloned into pBudCE4 to create pTLC33 (Figure 2-7). To clone HKα_{2a} and HKα_{2c} into pTLC33, pTLC46 and pTLC35 were each digested with *Not*I and *Bst*BI, the 3.1 and 3.3 kbp fragments were gel purified, respectively and cloned into pTLC33 which was digested with *Bst*BI and partially with *Not*I to create pTLC47(HKα_{2a}/NaKβ_1) (Figure 2-8A) and pTLC37(HKα_{2c}/NaKβ_1) (Figure 2-8B).

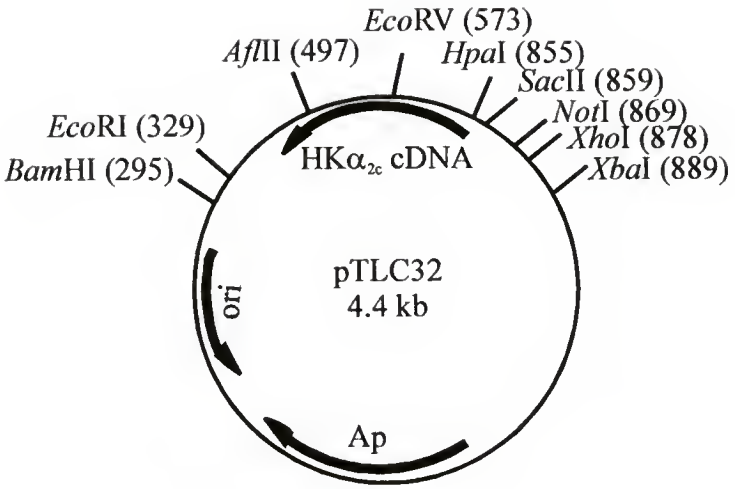

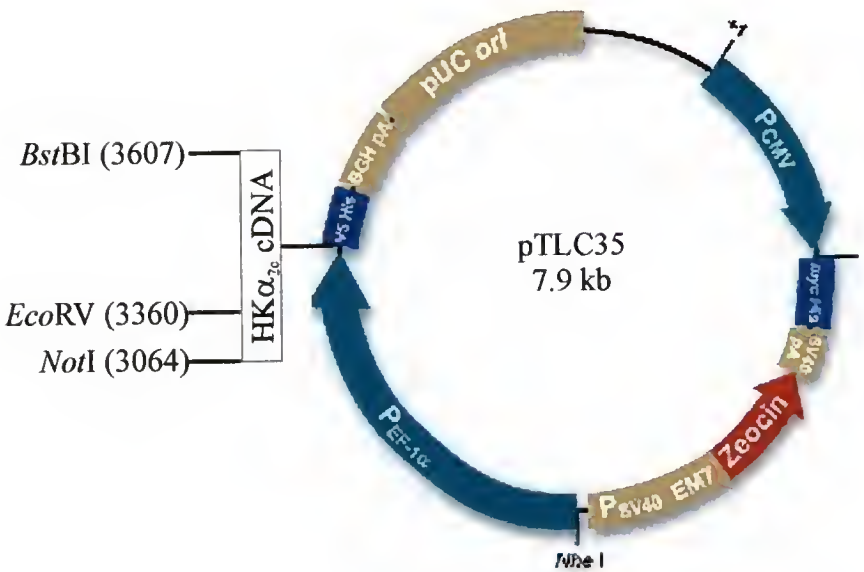

Figure 2-5. Rabbit HKα_{2c} cDNA construction in pBudCE4. Plasmid pTLC32 was digested to completion with *Eco*RV and *Not*I. The 0.3 kb *Eco*RV/*Not*I fragment was gel purified and ligated into pTLC34 to create pTLC35. Figure was adapted from Invitrogen catalog.

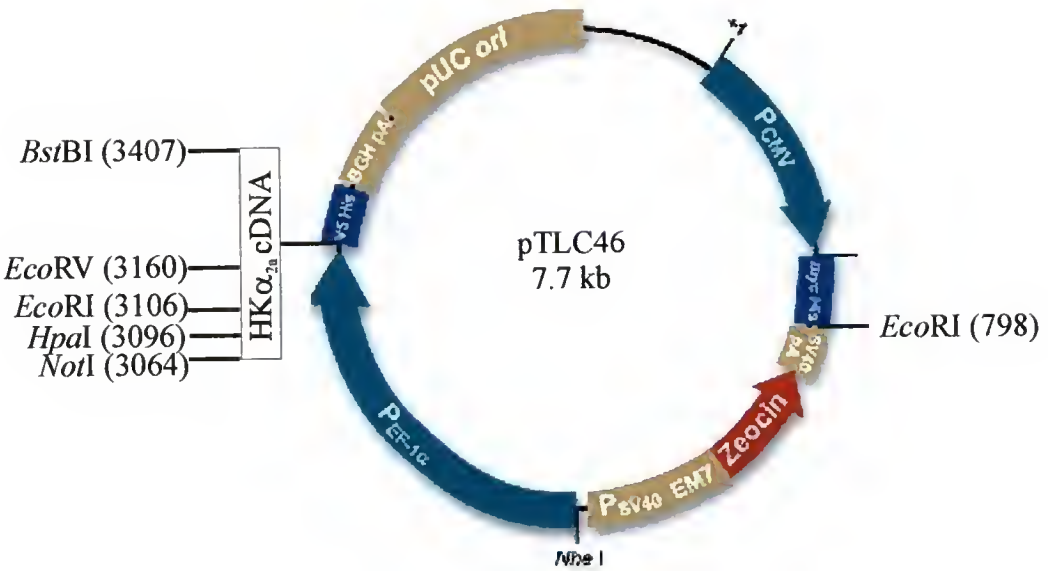

Figure 2-6. Rabbit HKα_{2a} cDNA construction in pBudCE4. Plasmid pTLC34 was digested to completion with *Not*I and partially with *Eco*RI. Primer pairs TC24 and TC25 were ligated into pTLC34 to create pTLC35. Figure was adapted from Invitrogen catalog.

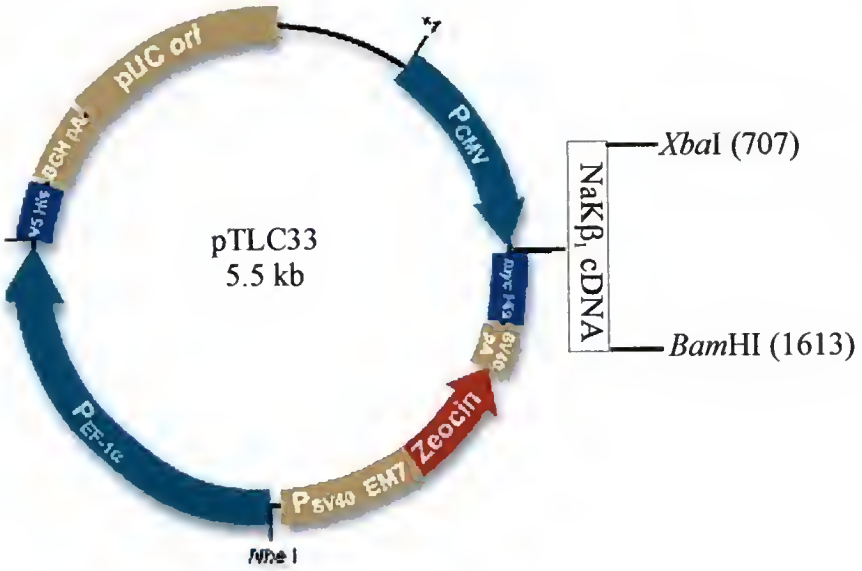

Figure 2-7. Rabbit NaKβ_1 cDNA construction in pBudCE4. Plasmid pNaKβ_1 was digested to completion with *Bam*HI and *Xba*I. The 0.9 kb fragment was gel purified and ligated into pBudCE4 to create pTLC33. Figure was adapted from Invitrogen catalog.

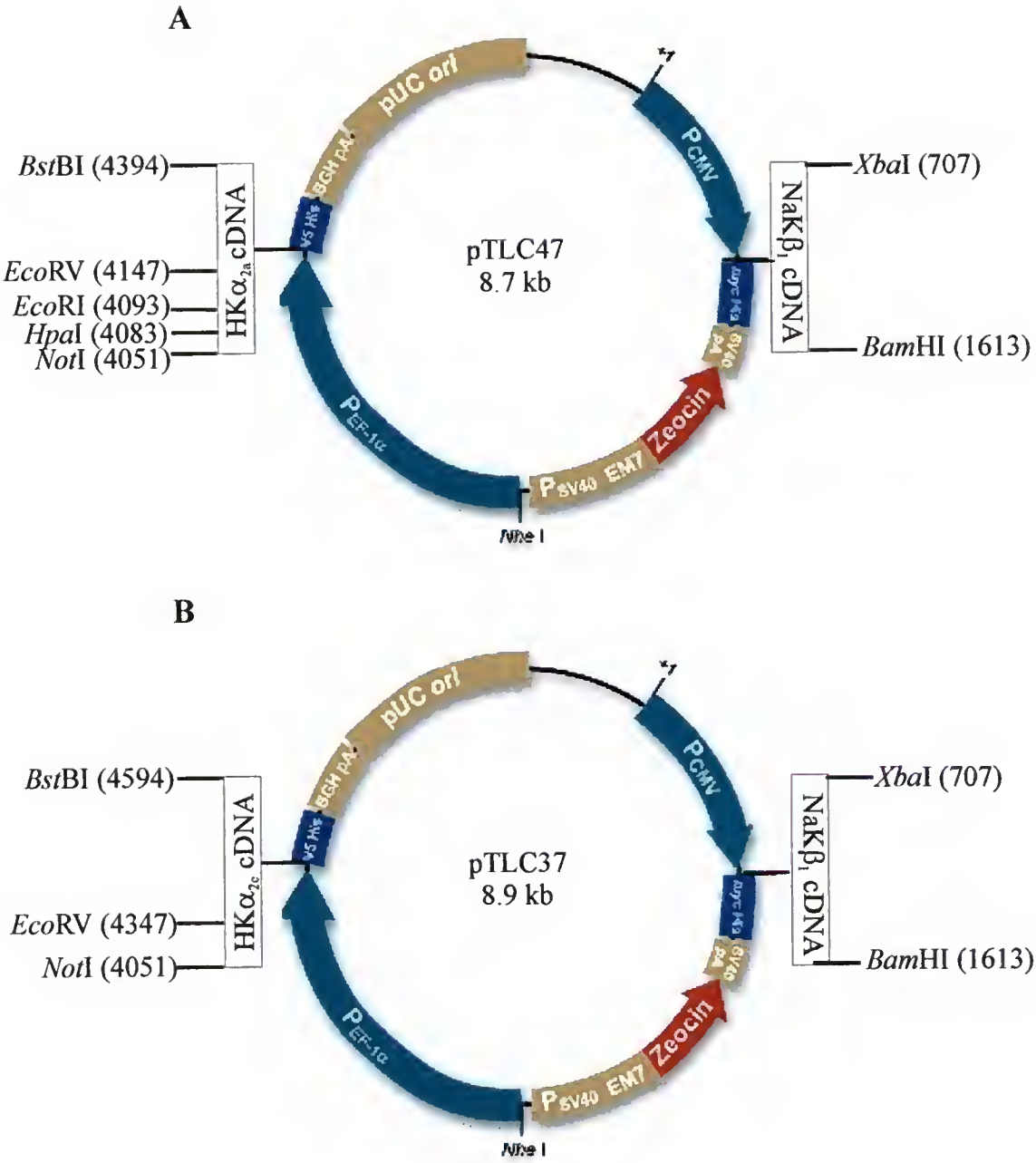

Figure 2-8. Plasmids pTLC47 and pTLC37 expression constructs. A, Plasmid pTLC47 encodes the $HK\alpha_{2a}$ cDNA ,in frame with V5 epitope tag, and $NaK\beta_1$ cDNA. B, Plasmid pTLC37 encodes the $HK\alpha_{2c}$ cDNA, in frame with V5 epitope tag, and $NaK\beta_1$ cDNA. Figures were adapted from Invitrogen catalog.

F_1F_0 ATP Synthase Methods

Bacterial Growth Conditions

Growth media were either Luria broth supplemented with 0.2% (w/v) glucose (LBG) or minimal medium consisting of A salts supplemented with 0.2% (w/v) succinate or 5 mM glucose. Isopropyl-1-thio-β-D-galactoside (IPTG) (0.4-40 μg/ml), ampicillin (Ap) (100 μg/ml), and chloramphenicol (Cm) (30 μg/ml) were added to media as appropriate. Growth of aerobic liquid cultures was performed with constant agitation and monitored using a Klett-Summerson colorimeter. Anaerobic conditions were achieved using a BBL "Gas Pak" (Beckton Dickinson Microbiolobgy Systems, Cockeysville, MD) anaerobic jar which had been flushed with N_2 prior to establishing the anaerobic atomsphere. Unless otherwise indicated, incubations of cultures were at 37°C.

Preparation of Cell Fractions

Inverted membrane vesicles were prepared from cultures grown in 500 ml LBG-Ap-Cm medium containing IPTG (40 μg/ml). Cells were harvested and washed in STEM buffer (0.1 M *N*-tris[hydroxymethyl]-methyl-2-aminoethanesulfonic acid, 20 mM magnesium acetate, 0.25 M sucrose, 0.25 mM [ethylenebis(oxyethylenenitrilo)]tetraacetic acid, 40 mM ε-amino-*n*-caproic acid, pH 7.0), and then resuspended in STEM buffer containing 5 mM *p*-aminobenzamidine, 1 mM dithioerythritol, 1 mM PMSF, and 10 μg/ml deoxyribonuclease. Cells were disrupted using a French Press at 14,000 psi. Unbroken cells and debris were pelleted by two successive centrifugations (8,000 x *g*, 10 min), and the membranes were collected by ultracentrifugation (150,000 x *g*, 1.5 h) in a Beckman Ti-70.1 rotor. Membranes were washed in B_2 buffer (50 mM Tris-HCl, 5 mM $MgSO_4$, 1 mM dithioerythritol, 6 mM *p*-

aminobenzamidine, 10% (v/v) glycerol, pH 7.5). The final membrane pellet was resuspended in B_2 buffer and stored at 4°C. Membrane vesicles stripped of F_1 were prepared essentially as described previously by Hartzog and Cain (93).

Determination of Protein Concentration

Total membrane protein concentration was determined by a modified Lowry procedure (144). Buffer C was made by adding 100 parts of Buffer A (2% Na_2CO_3, 0.4% NaOH, 0.16% sodium potassium tartrate, 1% sodium dodecyl sulfate (SDS)) to one part Buffer B (4% $CuSO_4$). Aliquots from prepared membranes in a total volume of 1 ml were incubated in 3 ml of freshly made Buffer C. After a 15 min incubation at room temperature, 0.3 ml Folin-Ciocalteu phenol reagent, freshly diluted 1:1 with distilled water, was added to the mixture. The solution was incubated for 45 min at room temperature, and OD_{660} was recorded with a Pharmacia spectrophotometer. Each sample was analyzed in triplicate. Bovine serum albumin with a concentration range of 0 to 100 μg of protein was used to generate a standard curve. A correlation coefficient of 0.99 was routinely obtained for the standard curve. Protein concentrations were calculated from the linear range of the standard curve by linear regression.

ATP Hydrolysis Assay

ATP hydrolysis activity of membrane fractions was assayed by the acid molybdate method (211). This assay measures the release of inorganic phosphate from ATP. The reaction consisted of 60 μg membrane protein in a total volume of 4 ml buffer (50 mM Tris-HCl, 1 mM $MgCl_2$, pH 9.1) incubated at 37°C. A 0.435 ml aliquot was removed from the reaction before the addition of ATP so that the background phosphate could be subtracted from the measurement. 150 mM ATP (80 μL) in 25 mM Tris-HCl

(pH 7.5) was added to start the reaction. 0.435 ml aliquots of the reaction mixture were taken at 2, 5, 7, 10, and 15 min, added to 2 ml acid/molybdate solution and were stored on ice. The acid/molybdate solution stopped the reaction and prevented further ATP hydrolysis from occurring. Inorganic phosphate was developed using 0.1 ml of a 1:10 dilution of Eikonogen solution. After incubation for 30 min at room temperature, the absorbance of each sample was determined at 700 nm. A phosphate standard curve was used in the concentration range of 0 to 0.6 μmol. The specific activity was expressed as μmol of ATP hydrolyzed/min/mg membrane protein. Membranes were assayed for determinations of linearity with respect to both time and enzyme concentration.

The ATP hydrolysis data described in Table 3-3 was determined by Dr. C. Ketchum in the laboratory of Dr. R. Nakamoto (University of Virginia). ATP hydrolysis rates (μmol/min/mg) were measured at 30°C in a buffer containing 25 mM HEPES-KOH (pH 7.5), 200 mM KCl, 8 mM $MgSO_4$ (3.1 mM free Mg^{2+}), 10 mM glucose, 1 mM phosphoenolpyruvate, 5 mM ATP, 5 μM carbonyl cyanide-*m*-chlorophenylhydrazone (CCCP), 50 μg/ml pyruvate kinase. The reactions were started with the addition of 0.10 to 0.15 mg/ml *E. coli* membranes. Time points were taken every 2 min up to 8 min and stopped by the addition of 5% SDS. Inorganic phosphate was determined by the method of Taussky and Shorr (234).

Assays of F_1F_0 ATP Synthase Activity

Membrane energization of vesicle preparations was detected by the fluorescence quenching of 9-amino-6-chloro-2-methoxyacridine (ACMA) (9). 250 μg of membrane protein was assayed in buffer (50 mm MOPS, 10 mM $MgCl_2$, pH 7.3). ACMA was added to the reaction mixture at a final concentration of 1 μM. ATP was added to a final

concentration of 0.4 mM. Fluorescence was recorded with an excitation at 410 nm and an emission at 490 nm. Treatment of membrane fractions with 50 μM dicyclohexylcarbodiimide (DCCD) was performed by pre-incubating the membrane fractions for 15 min at 37°C.

Rates of $\Delta\mu H^+$-driven ATP synthesis in Table 3-3 were determined by Dr. C. Ketchum from the laboratory of Dr. R. Nakamoto (University of Virginia) as described by Al-Shawi *et al.* (7). ATP synthesis rates (μmol/min/mg) were measured at 30°C with vigorous shaking in a buffer containing 25 mM HEPES-KOH, 200 mM KCl, 5 mM $MgSO_4$ (3.0 mM free Mg^{2+}), 10 mM glucose, 1 mM ADP, 10 mM $[^{32}P]P_i$, 50 units/ml hexokinase, and 0.12 mg/ml *E. coli* membranes at pH 7.5. The reactions were started with the addition of 2 mM NADH. Time points were taken every 2 min up to 8 min and stopped with ice cold 10 mM H_2SO_4. Inorganic phosphate was preciptated by the method of Sugino and Miyoshi (226), and the radioactivity remaining in the supernatant was determined by Cherenkov counting. Control experiments to determine $\Delta\mu H^+$-independent incorporation of $[^{32}P]P_i$ into the nonprecipitable material was determined in the same conditions but with the presence of 5 μM CCCP and subtracted from the rates obtained in the absence of CCCP.

Immunoblot Analysis

Membrane fractions were suspended in buffer (62.5 mM Tris-HCl, 10% (v/v) glycerol, 5% (v/v) 2-mercaptoethanol, 3% (w/v) SDS, pH 6.8), incubated for 5 min at 95°C, and subjected to polyacrylamide gel electrophoresis on 15% Tris-Glycine BioRad Ready Gels. Proteins were electroblotted using transfer buffer (25 mM Tris-Base, 192 mM glycine, 20% (v/v) methanol, pH 8.3) onto nitrocellulose (0.22 μm). The blot was

blocked for 1 h at room temperature or overnight at 4°C with 5% non-fat dry milk (BioRad) in 10 mM Tris-HCl, 150 mM NaCl, pH 7.2 (TBS). Polyclonal antibodies against SDS-denatured *b* subunit (52, 54) were kindly provided by Drs. K. Altendorf and G. Deckers-Hebesteit (Univeristät Osnabrück). The primary antibody incubation was performed using a 1:5,000 dilution of *b* subunit-specific antibodies in 2.5% non-fat dry milk for 1 h. Secondary antibody incubation was conducted with horseradish peroxidase-linked donkey anti-rabbit antibodies (Amersham Pharmacia Biotech, Piscataway, NJ) at a dilution of 1:50,000 for 1 h. After each antibody incubation, blots were washed three times in TBS, 0.1% (v/v) Tween-20 (TBS-T). Antibody binding was detected by chemiluminescence using the ECL system. Signals were visualized on Hyperfilm-ECL using a Kodak X-OMAT instrument. Strength of signals was quantified with a Kodak image digitizing system (DC120).

3' RACE

3' RACE reactions were performed using the Marathon cDNA Amplification Kit (Clontech, Palo Alto, CA) according to manufacturer's instructions with the following modifications. The reverse transcriptase reactions were conducted with 5 μg total RNA from rabbit renal medulla. The PCR reactions were performed with degenerate primer BC424 and anchor primer AP1 (Table 2-2). The thermal conditions for the PCR reaction were 94°C X 1 min presoak followed by 5 cycles of 94°C X 30 s denaturation and 72°C X 3 min extension, 5 cycles of 94°C X 30 denaturation and 70°C X 3 min extension, 25 cycles of 94°C X 30 s denaturation and 68°C extension with a final 3 min extension at 68°C. Fragments were cloned in TOPO TA cloning vector for sequence analysis.

5' RACE

5' RACE reactions were performed using the Marathon cDNA Amplification Kit according to manufacturer's instructions with the following modifications. The reverse transcriptase reactions were carried out with 5 μg total RNA from rabbit renal medulla. Gene-specific primer BC464 was used to create the cDNA library. The PCR reactions were performed with gene-specific primer BC448 and anchor primer AP1 (Table 2-2). The thermal conditions for the PCR were 94°C X 1min presoak followed by 25 cycles of 94°C X 30 s denaturation, 65°C X 1 min annealing, and 72°C x 2 min extension, with a final 10 min extension at 72°C. One μl of the PCR reaction was used for nested PCR with BC465 and nested anchor primer AP2 (Table 2-2). The thermal conditions for the nested PCR were 94°C X 1 min presoak followed by 25 cycles of 94°C X 30 s denaturation, 56°C X 1 min annealing, and 72°C X 1 min extension, with a final 7 min extension at 72°C. Fragments were cloned in TOPO TA cloning vector for sequence analysis.

Tissue Culture

Three different cell lines were used throughout this dissertation. HEK293 cells are a permanent line of primary human embryonal kidney cells transformed by human adenovirus type 5 DNA. HEK293c18 cells constitutively express EBNA-1 gene product and demonstrate an increase in transfection efficiency of episomal expression vectors over the parent HEK293 cell line. This cell line carries neomycin resistance for the EBNA-1 gene. These cells were a kind gift of Dr. M. Kilberg (University of Florida). COS-1 cells are a SV40 transformed kidney cell line from African green monkey. All cell lines were grown in Dulbecco's modified Eagle medium (DMEM) supplemented

with 10% fetal bovine serum (DMEM-10). All media was filter sterilized with a 0.22 μm cellulose acetate bottle top filter. Cells were maintained in tissue culture flasks in 5% CO_2 atmosphere in a humidified incubator at 37°C.

Episomal Transfection

HEK293c18 cells were grown to 80% confluency in DMEM-10, 250 mg/L G418 in 60 mm dishes. On the day of transfection, 5 μg DNA was diluted to a final volume of 150 μl in serum-free DMEM. Twenty μl Superfect transfection reagent (Qiagen) was added, and the reaction mixture was allowed to incubate at room temperature for 10 min. Cells were rinsed once with PBS, and the PBS was aspirated off the dish. The DNA-Superfect mixture was mixed with 1 ml DMEM-10 and was added dropwise to the cells. Cells were kept in a humidified incubator at 37°C in 5% CO_2 atmosphere for 3 h. After the 3 h incubation, cells were washed four times with PBS, and fresh DMEM-10 was added. After cells had grown for 24 h, DMEM-10 with appropriate antibiotic (10 mM histidinol; 500 μg/ml hygromycin) was added. Selection was complete when cells on control plate had died.

Stable Transfection

HEK293 cells were grown to 80% confluence in 100 mm dishes. On the day of transfection, 10 μl of FuGENE 6 Transfection Reagent (Roche, Indianapolis, IN) was added to 150 μl serum-free DMEM. Linearized plasmid (3.3 μg) was added to the mixture. After a 20 min incubation at room temperature, the DNA-FuGENE mixture was added dropwise to the cells in dishes, and the cells were incubated overnight in the 37°C incubator. Twenty-four hours after transfection, the media was removed and replaced with DMEM-10 containing 100 μg/ml Zeocin (Invitrogen). Clones began to appear

about two weeks post transfection. Single cell clones were isolated with cloning rings and allowed to grow in 24-well plates until cells reached confluency. The clones were expanded into T-25 flasks and ultimately into T-75 flasks for membrane preparation and Western analysis. Clones never appeared on control plates.

Transient Transfection

COS-1 cells were grown to 70% confluence in 150 mm dishes. On the day of transfection, 54 µl of FuGENE was diluted into 1.8 ml serum-free DMEM. Eighteen µg DNA was added to the tube and was incubated for 20 min at room temperature. After the incubation, the DNA-FuGENE mixture was added dropwise to the cells. The cells were placed in the 37°C incubator for 24 h. After the 24 h incubation, the cells were split into three 150 mm dishes and were grown for another 24 h before membrane preparation and analysis.

H^+,K^+-ATPase Biochemical Assays

Plasma Membrane Preparation

Six 150 mm dishes were normally used for a large-scale plasma membrane preparation. Cells were washed two times with 10 ml PBS. The cells were then scraped from dish with 5 ml PBS. This cell solution was added to the next plate, and the procedure was repeated until the last plate had been scraped. This process was repeated two more times resulting in a total volume of 15 ml. Cells were pelleted by centrifugation (1,000 x *g*, 10 min). The cell pellet was resuspended in 2 ml buffer (10 mM Tris, pH 7.5, 1 mM PMSF) and was kept on ice for 10 min. Cells were broken by homogenization with 25 strokes. Two ml homogenization buffer (0.5 M sucrose, 10 mM Tris, pH 7.5, 1 mM PMSF) was added and 25 more strokes were performed. Unbroken

cells and nuclei were pelleted by centrifugation (1,000 x *g*, 10 min). Depending on the size of the pellet, homogenization of the pellet was repeated. Normally, homgenization was repeated two more times. The supernatant was spun at 12,000 x *g* for 15 min to pellet mitochondria and other organelles. The resulting supernatant was spun at 100,000 x *g* for 90 min to recover low density membranes. The final membrane pellet was resuspended in buffer (250 mM sucrose, 5 mM Tris, pH 7.4).

Cell Lysate Preparation

Cells in a T-75 flask were washed once with PBS. Cells were then scraped into 1 ml PBS and pelleted at 1500 x *g* for 5 min. The cell pellet was ressupended in 50 ml Cell Lysis Buffer (50 mM Tris, 150 mM NaCl, 1% Nonidet P-40, pH 7.8). The cell suspension was incubated at 37°C for 10 min to completely lyse the cells. The cell lysate was centrifuged at 10,000 x *g* for 10 min at room temperature to pellet nuclei. The cell lysate was transferred to a new tube.

Bicinchoninic Acid Assay

The bicinchoninic acid assay was used to determine protein concentration as described previously (215). Solution A contained 1% 4,4'-dicarboxy-2,2'-biquinoline, 2% $Na_2CO_3 \cdot H_2O$, 0.16% sodium tartrate, 0.4% NaOH, and 0.95% $NaHCO_3$. Solution B was 4% $CuSO_4 \cdot 5H_2O$. The standard working solution was made fresh by mixing 100 volumes of solution A to 2 volumes of solution B with a final concentration of 1% ultra-pure SDS. Samples were brought to a total volume of 100 µl, and 2 ml of the standard working solution was added to each tube. Samples were incubated in a 37°C water bath for 30 min. After the 30 min incubation, the tubes were kept at room temperature for 10 min. The OD_{562} was recorded with a Pharmacia spectrophotometer. Each sample was

analyzed in duplicate. Bovine serum albumin with a concentration range of 0 to 80 μg of protein was used to generate a standard curve. A correlation coefficient of 0.99 was routinely obtained for the standard curve. Protein concentrations were calculated from the linear range of the standard curve by linear regression.

ATP Hydrolysis Microassay

ATP hydrolysis activity of plasma membrane fractions was assayed by a sensitive acid molybdate method that can detect nanomolar concentrations of phosphate in a solution (245). The reaction consisted of 50 μg plasma membrane protein in a total volume of 1 ml buffer (40 mM Tris-HCl, 3 mM $MgCl_2$, +/- 15 mK KCl, pH 7.4) incubated at 37°C. A 50 μL aliquot was removed from the reaction before the addition of ATP so that the background phosphate could be subtracted from the measurement. Twenty μl of 150 mM ATP (Tris salt or SigmaUltra disodium salt ATP) in 25 mM Tris-HCl (pH 7.5) was added to start the reaction. Fifty μl aliquots of the reaction mixture were taken at 2, 5, 7, 10, and 12 min and added to a tube containing 200 μl 1.75% ammonium heptamolybdate·$4H_2O$ in 6.3 N H_2SO_4 and 950 μL H_2O. The acid/molybdate solution stopped the reaction and prevented further ATP hydrolysis from occurring. Inorganic phosphate was developed using 200 μl of a malachite green solution (0.035% malachite green, 0.35% polyvinyl alcohol). After incubation for 30 min at room temperature, the absorbance of each sample was determined at 610 nm. A phosphate standard curve was used in the concentration range of 0 to 20 nmol. Each reaction, including the standard curve, was done in duplicate. The specific activity was expressed as μmol of ATP hydrolyzed/h/mg membrane protein.

Northern Analysis

Total RNA was isolated from tissue culture cells with the RNeasy kit (Qiagen). Northern blots were conducted according to Davis *et al.* (50). Total RNA (10 μg) was separated by electrophoresis on a 1% agarose, 0.22 M formaldehyde denaturing gel. The gel was soaked in 50 mM NaOH for 30 min to depurinate RNA. The gel was neutralized in 100 mM Tris, pH 7 for 30 min. Finally, the gel was equilibrated in 10X SSC (1.5 M NaCl, 150 mM sodium citrate, pH 7) for 40 min. Capillary transfer to a nylon membrane (Amersham) was performed overnight in 10X SSC. RNA was immobilized on the membrane by baking 1 h at 80°C in a vacuum oven. ^{32}P-labeled probes were prepared by random primer extension with 25 ng DNA according to the RTS RadPrime DNA Labeling System (Life Technologies). Membranes were pre-hybridized for at least 20 min and hybridized with labeled probe for 18 h in hybridization solution (250 mM Na_2HPO_4, 10 mg/ml BSA, 7% SDS) at 65°C. The membranes were washed in buffer (20 mM Na_2HPO_4, 1% SDS, pH 7.2) at 65°C. After washing, membranes were exposed to Kodak BioMax MR film. Exposure was normally 18 h. Glyceraldehyde-3-phosphate dehydrogenase (GAP3DH) was used as a loading control.

Immunoblot Analysis

Membrane fractions were resuspended in buffer (62.5 mM Tris-HCl, 10% (v/v) glycerol, 5% (v/v) 2-mercaptoethanol, 3% (w/v) SDS, pH 6.8) and were incubated for 5 min at 95°C before SDS-PAGE on 10% Tris-glycine gels. Proteins were electroblotted using transfer buffer (25 mM Tris-Base, 192 mM glycine, 20% (v/v) methanol, pH 8.3) onto nitrocellulose (0.22 μm). All antibody incubations were performed at room temperature unless otherwise indicated. Antibody binding was detected by

chemiluminescence using the ECL system. Signals were visualized on Hyperfilm-ECL using a Kodak X-OMAT instrument.

Anti-V5 Antibodies

Membrane fractions were separated by SDS-PAGE using 10% Tris-glycine gels. After the proteins were transferred to nitrocellulose, the blot was blocked for 1 h at room temperature or overnight at 4°C with 5% non-fat dry milk in TBS. The primary antibody incubation was performed using a 1:2,500 dilution of V5-specific monoclonal antibodies (Invitrogen) in 2.5% non-fat dry milk for 1 h. Secondary antibody incubation was conducted with horseradish peroxidase-linked sheep anti-mouse antibodies (Amersham Pharmacia Biotech) at a dilution of 1:10,000 in 2.5% non-fat dry milk for 1 h. After each antibody incubation, blots were washed three times for 5 min in TBS-T.

Anti-Rabbit NaKβ_1 Subunit Antibodies

Membrane fractions were separated by SDS-PAGE on 10% Tris-glycine gels. After proteins were transferred to nitrocellulose, the blot was blocked for 1 h at room temperature or overnight at 4°C with 5% non-fat dry milk in TBS. The primary antibody incubation was performed using 0.5 μg/ml rabbit NaKβ_1 subunit specific mouse monoclonal antibodies (Upstate Biotechnology, Lake Placid, NY) in 2.5% non-fat dry milk overnight at 4°C. Secondary antibody incubation was conducted with horseradish peroxidase-linked sheep anti-mouse antibodies at a dilution of 1:10,000 in 2.5% non-fat dry milk for 1 h. After each antibody incubation, blots were washed three times for 5 min in TBS-T.

Anti-*myc* Antibodies

Membrane fractions were separated by SDS-PAGE on 10% Tris-glycine gels. After proteins were transferred to nitrocellulose, the blot was blocked for 1 h at room temperature or overnight at 4°C with 5% non-fat dry milk in TBS. The primary antibody incubation was performed using 2.5 μg/ml *myc*-specific mouse monoclonal antibodies (Oncogene Research Products, Boston, MA) in 2.5% non-fat dry milk for 1 h. Secondary antibody incubation was conducted with horseradish peroxidase-linked sheep anti-mouse antibodies at a dilution of 1:10,000 in 2.5% non-fat dry milk for 1 h. After each antibody incubation, blots were washed three times for 5 min in TBS-T.

Immunofluorescence Microscopy

Glass coverslips (Corning 22 x 22 mm) were sterilized by placing them in them in a glass petri dish and autoclaving them. The steam cycle of the autoclave was not used, as this caused the coverslips to stick to each other. A sterile Pasteur pipette connected to a vacuum line was used to pick up the coverslip and place it in a 6-well plate. Cells were added to the well and were allowed to adhere for 24 h. The cells were transfected using FuGENE as described in an earlier section. Briefly, plasmid DNA (1 μg) was diluted in 100 μl DMEM containing 3 μl FuGENE. The complex was allowed to form for 20 min and then added to the wells.

After a 24 h incubation time for protein expression, the wells were rinsed three times with PBS. The cells were fixed for 20 min in 3% paraformaldehyde. After fixation was complete, the wells were washed three times (5 min each) with PBS. Free aldehydes resulting from the paraformaldehyde incubation can have fluorescent properties, so cells were incubated for 30 min with 50 mM L-glycine to quench free aldehydes. Wells were

washed three times (5 min each) with PBS. The V5-epitope tag was attached to the C-terminus of the HKα_2 subunits, which is inside the cell. Hence, the cells were permeabilized for 15 min in 0.1% Triton-X-100, 0.1% non-fat dry milk. Cells were blocked overnight at 4°C in 20% normal goat serum, 0.1% Triton-X-100.

A humid box was used for the primary and secondary antibody incubations. A soaked paper towel was placed in the bottom of a small Tupperware container. The paper towel was covered with Parafilm. V5-specific monoclonal antibodies were diluted 1:5000 in 20% normal goat serum, 0.1% Triton-X-100. 100 µl of the diluted antibody solution was placed on the parafilm in the Tupperware container. The coverslips were carefully picked up by the edge with tweezers. The edge of the coverslips were blotted on a Kimwipe and placed with the cell-side down atop the drops of antibody on the parafilm. The lid was placed on the container, and the cells were incubated for 1 h at room temperature. Using tweezers, the coverslips were placed cell-side up back into the 6-well tray and washed three times with 0.1% Triton-X-100, 0.1% non-fat dry milk. Polyclonal goat anti-mouse IgG antibodies conjugated to Texas Red (Molecular Probes, Eugene, OR) were diluted to 1 µg/ml in 20% normal goat serum, 0.1% Triton-X-100. Using the same procedure as the primary antibody incubation, the coverslips were placed cell-side down atop the drops of antibody and were incubated for 1 h at room temperature. From this point forward, the coverslips were shielded from light to avoid bleaching the fluorescence. The coverslips were placed cell-side up back into the 6-well tray and washed three times with 0.1% Triton-X-100, 0.1% non-fat dry milk. The edges of the coverslips were blotted on a Kimwipe and placed cell-side down on a drop of Fluoromount G mounting medium (Fisher Scientific) on glass slides. The slides were

dried for 1 h in the dark. Once dried, the edges of the coverslip were sealed with a layer of nail polish. Confocal images were generated on a BioRad model MRC-1024 confocal laser scanning system. The *xy* sections were generated with a 1.5 μm motor step.

CHAPTER 3
CHARACTERIZATION OF b_{Arg-36} MUTATIONS IN F_1F_0 ATP SYNTHASE FROM *ESCHERICHIA COLI*

Introduction

The two *b* subunits are components of the second stalk of *E. coli* F_1F_0 ATP synthase. The *b* subunits interact to form a dimer in an intact enzyme complex (61, 150). Each protein contains an N-terminal transmembrane domain followed by a polar, highly charged region that extends up the side of F_1. Dmitriev *et al.* (55) used multidimensional NMR spectroscopy to determine the structure of residues 1-34 of the *E. coli b* subunit membrane-spanning region. The structure revealed an α-helix (residues 4-22), proceeded by a bend of about 20° (residues 23-26), and followed by an α-helix (residues 27-34). No high-resolution structure exists for the hydrophilic domain of the *b* subunit. However, circular dichroism spectra indicated that this domain is highly α-helical (61), and secondary structure analysis proposed a random coil between two long α-helices (205, 252).

Experimental evidence exists for *b* subunit interactions with the α subunit (149, 191), the β subunit (10, 149, 259), and the δ subunit (62, 148, 192, 198) of the F_1 sector. Experiments conducted in our laboratory demonstrated that the formation of the *b* subunit dimer is necessary for its interaction with F_1 (218). It is not completely understood how the *b* subunits interact with the *a* or *c* subunits of F_0. The common belief is that the *b* subunits are positioned on the outside of the ring of *c* subunits (22, 212, 230). Cross-linking of purified ATP synthase (10) or F_0 (98, 149) demonstrated that the *a* and *b*

subunits are adjacent to each other. Cysteine residues introduced in the *b* subunit between amino acids 2-18 have a tendency to form disulfide bonds (55), suggesting that the two *b* subunits are next to each other in the membrane.

The δ subunit can be fixed to a specific α subunit without loss of functional enzymatic activity (173). The *b*-δ interaction has been clearly defined through the C-terminal region of the *b* subunit. The rotation of the γε central stalk is well accepted. These three pieces of evidence have led to the suggestion that the *b*-δ interaction is the basis of a stator of F_1F_0 ATP synthase which functions to anchor the α_3/β_3 hexamer, allowing the γε rotor to turn within the F_1 complex.

Early models suggested that the stator should be relatively rigid with fixed points of interaction on F_1 (150, 173). Our laboratory constructed deletion and insertion mutants within the cytoplasmic region of the *b* subunit to address this issue (217, 219). Deleting up to seven amino acids of the *b* subunit resulted in a normal F_1F_0 ATP synthase. Deletions of up to eleven amino acids had substantial activity. Omission of twelve or more amino acids abolished F_1F_0 ATP synthase function. Insertion of up to seven amino acids in the cytoplasmic region of the *b* subunit had no effect on the activity of the enzyme. In fact, adding up to fourteen amino acids resulted in detectable enzyme function. Insertion of eighteen amino acids was enough to abolish F_1F_0 ATP synthase activity. Based on evidence of the α-helical nature of the cytoplasmic region of the *b* subunit, a deletion of eleven amino acids would result in a reduction of the subunit by about 16 Å, and insertion of fourteen amino acid insertion would increase the length of the *b* subunit by about 20 Å. These observations support a model in which the *b* subunit has an intrinsic flexibility and is not necessarily a rigid structure.

Very little amino acid sequence homology exists in the *b* subunit of the enzyme. However, two residues are highly conserved among bacterial F_1F_0 ATP synthases: $b_{Arg\text{-}36}$ and $b_{Ala\text{-}79}$ (*E. coli* nomenclature) (Figure 3-1). The $b_{Ala\text{-}79}$ residue is predicted to be the last amino acid of the first α-helix in the hydrophilic region of the subunit. Mutations at this site resulted in reduced levels of intact F_1F_0 ATP synthase complex in the membrane (147). The substitutions have been correlated with a failure in *b* subunit dimerization (104, 218).

The $b_{Arg\text{-}36}$ residue is located at the base of the second stalk, proximal to the lipid bilayer. I constructed mutations at $b_{Arg\text{-}36}$ in order to investigate its importance in the function of the *b* subunit stator. The site occupied by $b_{Arg\text{-}36}$ proved to be very sensitive to substitution by other amino acids, and the phenotypes differed markedly from previously reported *uncF*(*b*) mutations (104, 110, 147, 182). Although the amount of enzyme complex formed was altered, the major effect of several $b_{Arg\text{-}36}$ mutations was on the activity of the intact F_1F_0 ATP synthase. Included in the collection of mutants is the first *uncF*(*b*) substitution, which uncoupled catalytic activity from proton translocation.

Results

Construction of *uncF*(*b*) Gene Mutations

Analysis of the primary amino acid sequences of a diverse list of *b* subunits showed that $b_{Arg\text{-}36}$ was conserved in bacterial F_1F_0 ATP synthases (Figure 3-1). In order to test the importance of this site for assembly and function of F_1F_0 ATP synthase, a collection of mutations were constructed at $b_{Arg\text{-}36}$ of the *E. coli* subunit by PCR mutagenesis in plasmid pKAM14(*b*). The forward, reverse, and the mutagenic oligonucleotide sequences are described in Figure 3-2. The full-length PCR products

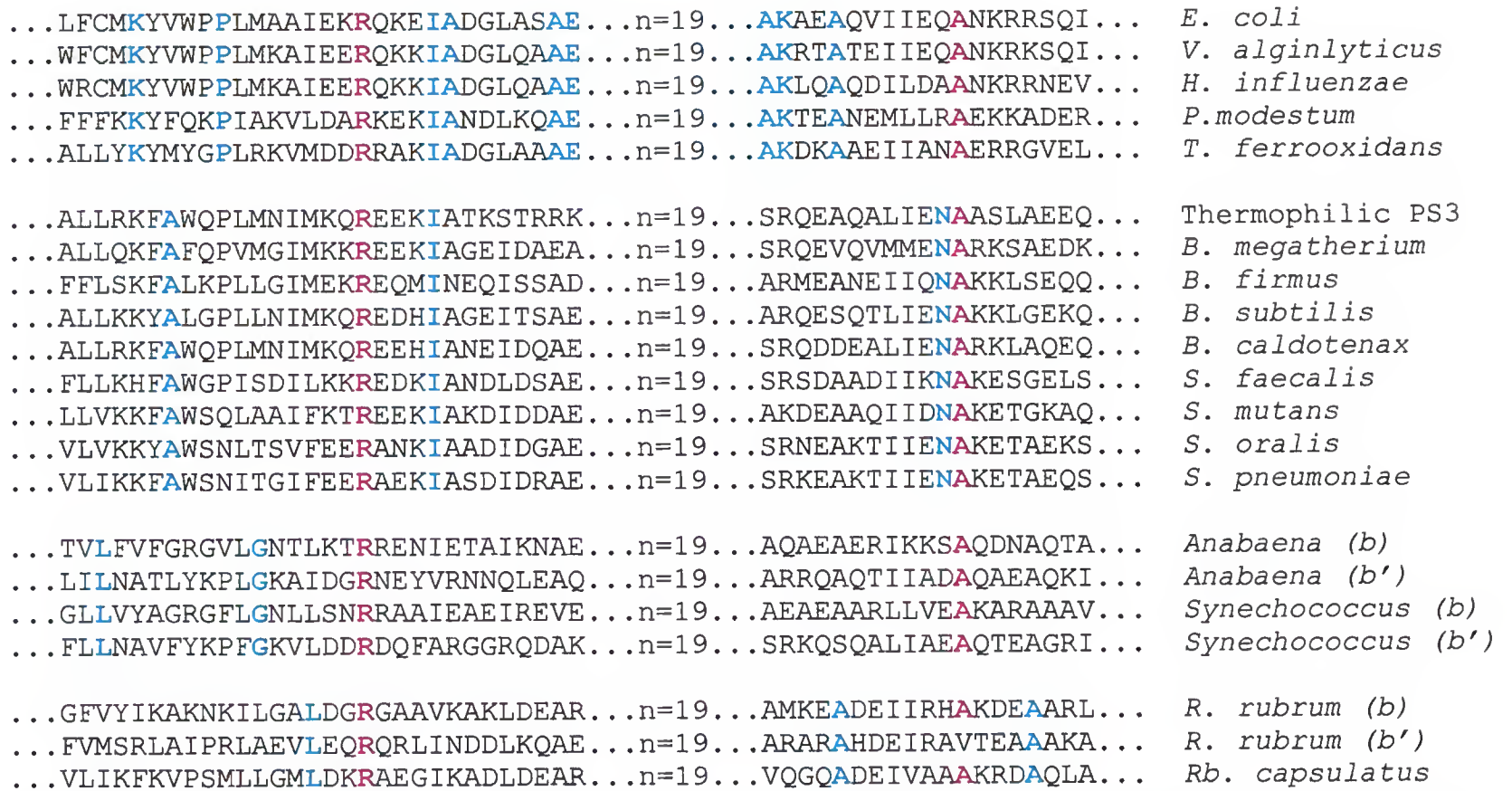

Figure 3-1. Amino acid sequence alignment of bacterial *b* and *b'* subunits. Protein sequences of *b* and *b'* subunits of bacterial F_1F_0 ATP synthases were aligned with respect to where the protein is predicted to exit the membrane. Sequences were plotted consecutively without omission of amino acids. Conserved amino acids are indicated in blue. The highly conserved *E. coli* $b_{Arg\text{-}36}$ and $b_{Ala\text{-}79}$ residues are indicated in pink. The bacterial sequences are grouped based on phylogeny. Sequence data were obtained from GenBank.

A

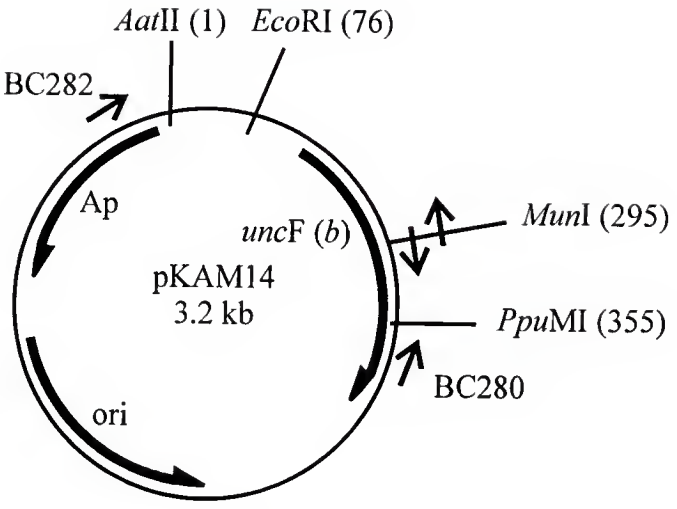


```
          A   A   I   E   K   R   Q   K   E
5'...GCA GCC ATC GAA AAA CGT CAA AAA GAA...3'
3'...CGT CGG TAG CTT TTT GCA GTT TTT CTT...5'
```

B

```
5'AAAATAAACAAATAGGGGTTCCGCG3'  BC282
5'CAGGTTTACGCTCGGCTTCAATTT3'   BC280
```

C

Primer Set 1 — *Mun*I — E, K, I, T, A, V

```
5'GCA GCA ATT GAA AAA RHA CAA AAA G3'   BC144
3'CGT CGT TAA CTT TTT YDT GTT TTT C5'   BC281
```

Primer Set 2 — *Mun*I — C, Y, S

```
5'GCA GCA ATT GAA AAA TVC CAA AAA G3'   BC307
3'CGT CGT TAA CTT TTT ABG GTT TTT C5'   BC306
```

Primer Set 3 — *Mun*I — E

```
5'GCA GCA ATT GAA AAA GAG CAA AAA G3'   BC309
3'CGT CGT TAA CTT TTT CTC GTT TTT C5'   BC308
```

Figure 3-2. Oligonucleotides for PCR mutagenesis of the *uncF*(*b*) gene. A, Plasmid pKAM14(*b*) showing placement of oligonucleotides for mutagenesis. Below plasmid is wild type *b* subunit sequence from residues 31-39. In bold type is $b_{Arg\text{-}36}$. B, Forward and reverse outside primers for PCR mutagenesis. C, Oligonucleotides to create mutations at $b_{Arg\text{-}36}$. The amino acids that each set of degenerate primers encodes is indicated above the primer sets in bold. The unique *Mun*I site created by silent mutations is boxed. Notation for degenerate bases is that of the International Union of Biochemistry Nomenclature Committee.

generated from the PCR mutagenesis were cloned into pKAM14(*b*) as an *Aat*II/*Ppu*MI fragment. Primer Set One resulted in only *Ile* and *Lys* mutations so Primer Sets Two and Three were designed to create the other mutations. Recombinant plasmids were selected for the presence of the unique *Mun*I site that linearized the DNA (Figure 3-3). The mutations were identified through nucleotide sequencing. The effects of the $b_{Arg\text{-}36}$ replacements were studied by complementation of strain KM2(Δ*b*). The plasmids and strains are described in Table 3-1.

Growth Characteristics of Mutants

E. coli strains, which are defective in ATP synthase, cannot derive energy from nonfermentable sources, so growth on succinate minimal medium was used as a qualitative measure of F_1F_0 ATP synthase activity *in vivo*. Strain TC212($b_{Arg\text{-}36\rightarrow Lys}$) supported growth indistinguishable from that of KM200(*b*) at both low and high IPTG concentrations (Table 3-2). Reduced growth was observed from strains TC216($b_{Arg\text{-}36\rightarrow Ser}$), TC217($b_{Arg\text{-}36\rightarrow Cys}$), and TC218($b_{Arg\text{-}36\rightarrow Tyr}$). Strains TC211($b_{Arg\text{-}36\rightarrow Ile}$) and TC215($b_{Arg\text{-}36\rightarrow Glu}$) failed to support growth on succinate minimal medium regardless of inducer concentration. However, under conditions of lower incubation temperature (30°C), strain TC215($b_{Arg\text{-}36\rightarrow Glu}$) produced very small colonies. No conditions were found in which strain TC211($b_{Arg\text{-}36\rightarrow Ile}$) could grow using succinate as a carbon source. Since high levels of IPTG yielded the largest cell mass, 40 μM IPTG was added to media for all subsequent experiments. Figure 3-4 depicts streaks of the $b_{Arg\text{-}36}$ mutant strains on a succinate minimal plate with 40 μM IPTG. Although TC217($b_{Arg\text{-}36\rightarrow Cys}$) does not seem to have colonies in this picture, it is the result of a light streak and repeated experiments revealed clearly visible colonies for this mutant strain.

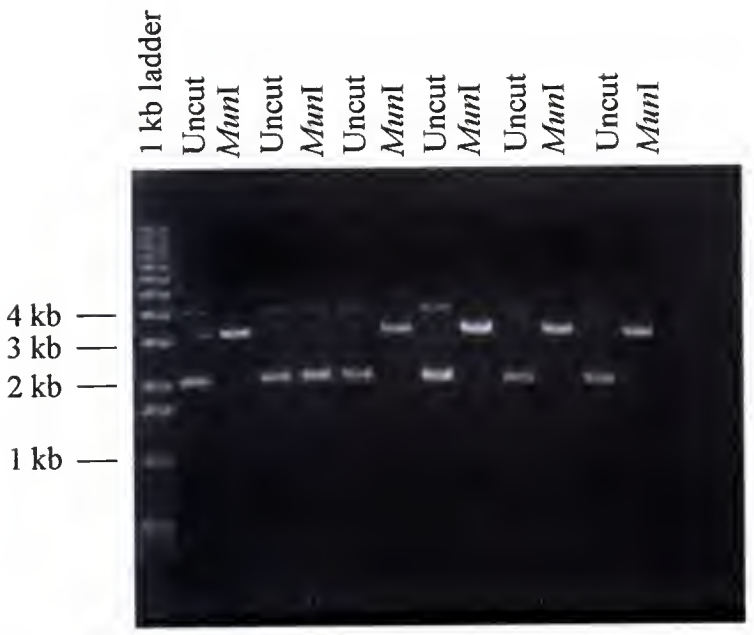

Figure 3-3. *Mun*I restriction endonuclease analysis of *uncF*(*b*) gene mutations in pKAM14(*b*). Plasmid DNA was prepared from positive transformants and analyzed for the presence of a unique *Mun*I restriction site. Undigested and *Mun*I digested DNA lanes are labeled. The absence of a *Mun*I site in pKAM14 was previously confirmed. Plasmid DNA linearized by *Mun*I was analyzed by nucleotide sequencing to determine the encoded mutation at $b_{\text{Arg-36}}$.

Table 3-1: *E. coli* strains and plasmids

Strains or Plasmids	Relevant Genotype or Description	Source or Reference
Strains		
1100	*bgl*R *thi*-1 *rel*-1 HfrPO1	(105)
KM2	1100; *uncF* deletion	(147)
KM200	KM2; pKAM14, pKAM16	(147)
KM322	KM2; pBR322, pKAM16	(147)
TC211	KM2; pTLC11, pKAM16	This study
TC212	KM2; pTLC12, pKAM16	This study
TC215	KM2; pTLC15, pKAM16	This study
TC216	KM2; pTLC16, pKAM16	This study
TC217	KM2; pTLC17, pKAM16	This study
TC218	KM2; pTLC18, pKAM16	This study
Plasmids		
pBR322	Ap^r, Tc^r	(25)
pKAM14	*uncF*, H', Ap^r	(147)
pTLC11	pKAM14; *uncF* (Arg-36→Ile)	This study
pTLC12	pKAM14; *uncF* (Arg-36→Lys)	This study
pTLC15	pKAM14; *uncF* (Arg-36→Glu)	This study
pTLC16	pKAM14; *uncF* (Arg-36→Ser)	This study
pTLC17	pKAM14; *uncF* (Arg-36→Cys)	This study
pTLC18	pKAM14; *uncF* (Arg-36→Tyr)	This study

Table 3-2: *In vivo* and *in vitro* activities of $b_{Arg\text{-}36}$ mutants

Strain	Mutation	IPTG (μM)[a]					ATP hydrolysis[b]
		30°C		37°C			(μmol/min/mg)
		0.4	40	0	0.4	40	
KM200	Wild type	++	+++	++	++	+++	0.90 ± 0.11
KM322	Negative control	-	-	-	-	-	0.15 ± 0.05
TC211	$b_{Arg\text{-}36 \rightarrow Ile}$	-	-	-	-	-	0.53 ± 0.14
TC212	$b_{Arg\text{-}36 \rightarrow Lys}$	++	+++	++	++	+++	0.79 ± 0.17
TC215	$b_{Arg\text{-}36 \rightarrow Glu}$	-	+	-	-	-	0.45 ± 0.05
TC216	$b_{Arg\text{-}36 \rightarrow Ser}$	+	+	-	+	++	0.41 ± 0.08
TC217	$b_{Arg\text{-}36 \rightarrow Cys}$	+	+	-	+	++	0.50 ± 0.07
TC218	$b_{Arg\text{-}36 \rightarrow Tyr}$	+	++	+	+	++	0.54 ± 0.06

[a] *E. coli* strains were grown aerobically on solid succinate minimal media with antibiotics. IPTG was added as indicated. Colony size was scored after 72 h incubation at either 30°C or 37°C as: +++ ≥ 0.4 mm; ++, 0.1-0.4 mm; +, < 0.1 mm; or -, no growth.

[b] ATPase activities were measured as described in Experimental Procedures on membranes obtained from strains grown in LBG-Ap-Cm, 40 mM IPTG at 37°C.

Figure 3-4. Complementation of *uncF*(*b*) gene mutants in KM2(Δ*b*). *E. coli* strain KM2(Δ*b*) was transformed with plasmids, streaked on minimal A succinate medium, and incubated at 37°C for 72 h. Strains: A, KM200(wild type); B, KM322(- control); C, TC211($b_{\text{Arg-36}\rightarrow\text{Ile}}$); D, TC212($b_{\text{Arg-36}\rightarrow\text{Lys}}$); E, TC215($b_{\text{Arg-36}\rightarrow\text{Glu}}$); F, TC216($b_{\text{Arg-36}\rightarrow\text{Ser}}$); G, TC217($b_{\text{Arg-36}\rightarrow\text{Cys}}$); H, TC218($b_{\text{Arg-36}\rightarrow\text{Tyr}}$).

Assembly of F_1F_0 ATP Synthase

The steady-state level of the *b* subunit can be interpreted as indicative of incorporation of the *b* subunit into the F_1F_0 ATP synthase complex, since the subunit is not stable free from the complex (67, 221). An immunoblot analysis using anti-*b* antibodies was performed on membrane vesicles. Membranes derived from all of the $b_{Arg\text{-}36}$ mutants had reduced levels of *b* subunit present (Figure 3-5). Densitometry revealed that the *b* subunit levels ranged from 24% to 60% of wild type levels. For the strains with altered growth characteristics, the *b* subunit levels were 24% of wild type levels for TC215($b_{Arg\text{-}36\rightarrow Glu}$) membranes to 53% for the TC211($b_{Arg\text{-}36\rightarrow Ile}$) samples.

Total membrane-associated F_1 ATP hydrolysis activity is a good test of F_1F_0 ATP synthase complex assembly since F_1 has little affinity for the membrane in the absence of the F_0 subunits. F_1 ATPase activity was determined under high pH conditions to remove the influence of F_0 (31). Reductions in the levels of *b* subunit observed in the immunoblot studies should be reflected in the amount of total F_1 ATPase activity in the membrane. The membranes derived from strain TC212($b_{Arg\text{-}36\rightarrow Lys}$) had the highest level of F_1 ATPase of the mutants tested (85% of wild type KM200(*b*)), and all of the other membranes had between 35% and 52% of activity relative to the strain KM200(*b*) preparations (Table 3-2).

In every case, the levels of *b* subunits and the amounts of F_1 ATPase in membranes prepared from the $b_{Arg\text{-}36}$ mutants should have been sufficient to yield substantial growth if the F_1F_0 ATP synthases containing the altered *b* subunits were fully active. The decrease in F_1F_0 ATP synthase in strain TC212($b_{Arg\text{-}36\rightarrow Lys}$) was apparently not sufficient to reduce the capacity of the cells to generate ATP to the rate-limiting

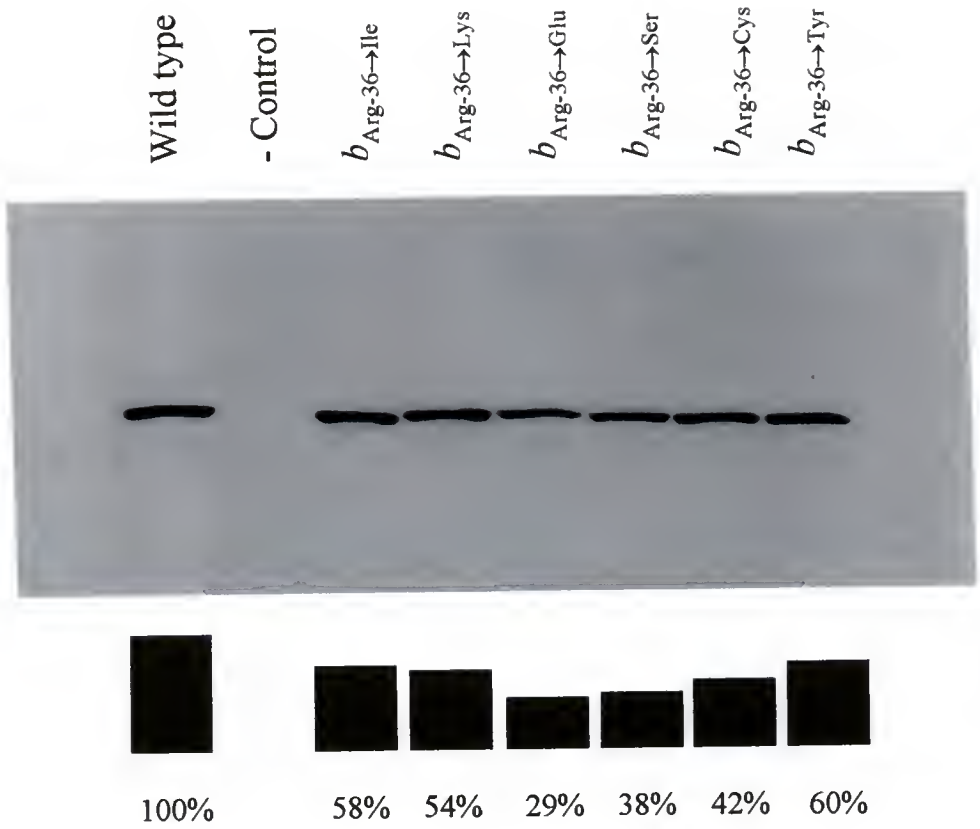

Figure 3-5. Immunoblot analysis of *uncF*(*b*) gene mutants. Membrane fractions were separated on a 15% SDS polyacrylamide Tris-glycine gel. Lanes were loaded with 15 μg total membrane protein. The blot was incubated with *b* subunit-specific antibodies. The secondary antibody was horseradish peroxidase-linked donkey anti-rabbit antibody, and antibody binding was detected by chemiluminescence. The *b* subunit substitutions are indicated above each lane. Strength of signals shown in bar graphs were determined with a Kodak image digitizing system.

threshold for growth. The threshold was also surpassed in strains TC216($b_{Arg\text{-}36\rightarrow Ser}$), TC217($b_{Arg\text{-}36\rightarrow Cys}$) and TC218($b_{Arg\text{-}36\rightarrow Tyr}$). The more interesting observation was that the loss of *in vivo* F_1F_0 ATP synthase function did not correlate with the amount of assembled enzyme complex detected in the membranes of strains TC215($b_{Arg\text{-}36\rightarrow Glu}$) and TC211($b_{Arg\text{-}36\rightarrow Ile}$). Therefore, the losses in F_1F_0 ATP synthase function in these two strains were not simply attributable to a reduction in enzyme levels.

Coupled Activities

F_1F_0 ATP synthase-mediated ATP-driven proton pumping activity in membrane vesicles prepared from the $b_{Arg\text{-}36}$ mutants was used as an initial indication of coupled activity. Acidification of inverted membrane vesicles was monitored by fluorescence of ACMA. The level of NADH-driven fluorescence quenching of ACMA was strong and comparable in all preparations tested, indicating that the membranes were intact, closed vesicles. Membranes derived from strains TC212($b_{Arg\text{-}36\rightarrow Lys}$), TC216($b_{Arg\text{-}36\rightarrow Ser}$), TC217($b_{Arg\text{-}36\rightarrow Cys}$), and TC218($b_{Arg\text{-}36\rightarrow Tyr}$) had reduced ATP-driven proton pumping activity, reflecting the reduced amounts of assembled enzymes present (Figure 3-6). Although the change in fluorescence in this assay is not strictly linear with respect to activity, it can be inferred that the intact F_1F_0 ATP synthase complexes containing the altered *b* subunits were fully competent for coupled activity.

In contrast, ATP-driven proton pumping activity was nearly undetectable in membranes prepared from strain TC211($b_{Arg\text{-}36\rightarrow Ile}$), despite the fact that levels of protein and F_1 activity comparable to the other strains were observed (Figure 3-6). A much more interesting behavior was observed with membranes from strain TC215($b_{Arg\text{-}36\rightarrow Glu}$). These membranes had substantial amounts of ATP-driven proton pumping activity,

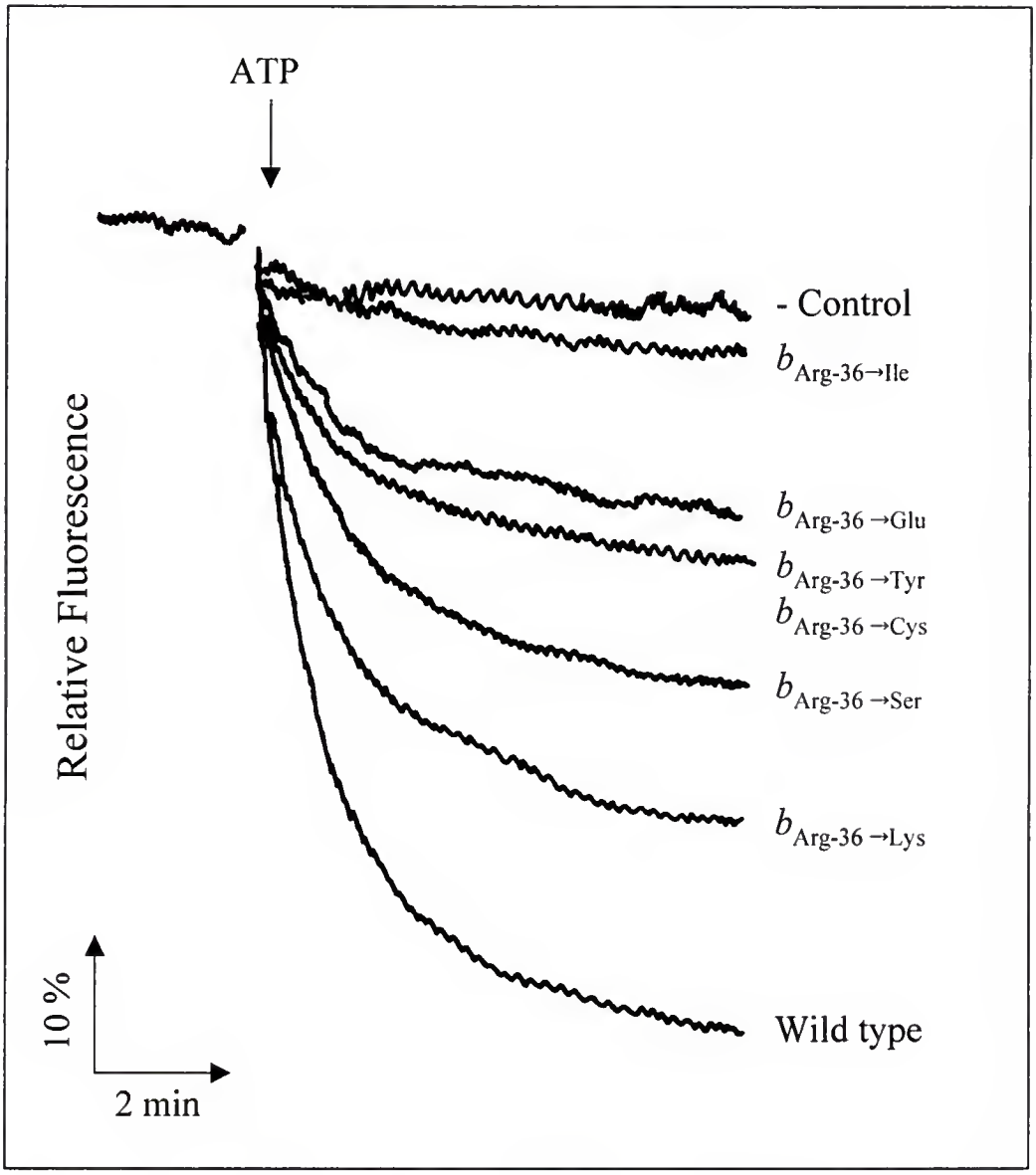

Figure 3-6. ATP-driven energization of membrane vesicles prepared from *uncF*(*b*) gene mutants. 250 μg of membrane protein was suspended in assay buffer (50 mM MOPS, 10 mM $MgCl_2$, pH 7.3). ACMA was added to a final concentration of 1mM, and fluorescence was recorded with an excitation at 410 nm and an emission at 490 nm. ATP was added as indicated to a final concentration of 0.4 mM. The *b* subunit substitutions are labeled next to each trace.

similar to the substitutions that resulted in intermediate growth on succinate minimal media. Since ATP-driven proton pumping is the physiological role of F_1F_0 ATP synthase under anaerobic conditions, strain TC215 ($b_{Arg\text{-}36\rightarrow Glu}$) was tested for growth on glucose in an anaerobic environment. The mutant grew well at 37°C on glucose minimal medium under anaerobic conditions, yielding colony sizes comparable to the positive control strain KM200(*b*). One implication of the data was that the proton conduction mechanism remained intact and functional in F_1F_0 ATP synthase containing the $b_{Arg\text{-}36\rightarrow Glu}$ subunit. This was examined by measuring passive proton translocation through F_0 in stripped membranes prepared from strain TC215($b_{Arg\text{-}36\rightarrow Glu}$) and TC211($b_{Arg\text{-}36\rightarrow Ile}$). As predicted, the stripped membranes from TC215($b_{Arg\text{-}36\rightarrow Glu}$) proved to be leaky when a proton gradient was imposed by addition of NADH (Figure 3-7). Apparently, the $b_{Arg\text{-}36\rightarrow Glu}$ mutation had little effect on proton translocation through the F_0 sector. Membranes from strain TC211($b_{Arg\text{-}36\rightarrow Ile}$) that were stripped of F_1 were somewhat leaky when tested for NADH-driven quenching of ACMA fluorescence. These results suggest that the $b_{Arg\text{-}36\rightarrow Glu}$ substitution resulted in the uncoupling of proton translocation from ATP synthesis.

The coupling efficiencies of strains TC211($b_{Arg\text{-}36\rightarrow Ile}$) and TC215($b_{Arg\text{-}36\rightarrow Glu}$) were determined directly (Table 3-3). The amount of enzyme was adjusted by measuring the level of *a* subunit present in the membrane. Interestingly, the membranes from the negative control strain KM322 which lack the *b* subunit had a small amount of *a* subunits associated but had an extremely high apparent turnover for hydrolysis. More importantly, KM322(negative control) membranes had very little ATP synthesis activity (<5 % of KM200(*b*)). The defective transport function of TC211($b_{Arg\text{-}36\rightarrow Ile}$) was made apparent by its inability to synthesize ATP and a synthesis/hydrolysis ratio equal to the

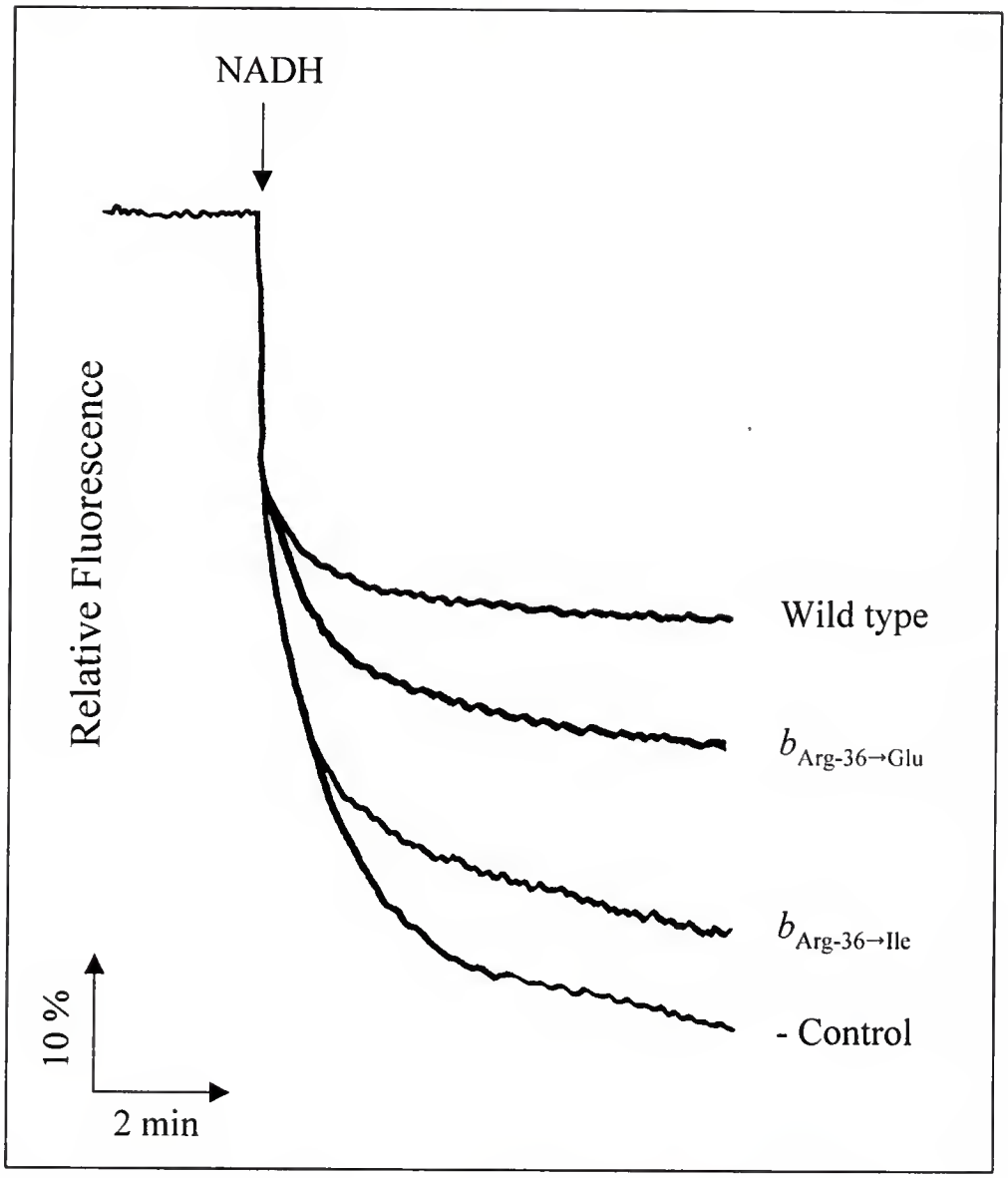

Figure 3-7. Proton permeability of stripped membrane vesicles prepared from *uncF*(*b*) gene mutants. Membrane vesicles were prepared, and F_1 was stripped by gentle agitation in a low ionic strength buffer (1 mM Tris-HCl, 0.5 mM EDTA, 2.5 mM 2-mercaptoethanol, 10 % (v/v) glycerol, pH 8.0). ACMA fluorescence was recorded after the addition of NADH to a final concentration of 0.5 mM. The *b* subunit substitutions are labeled next to each trace.

Table 3-3. Alterations in F_1 activity associated with $b_{Arg\text{-}36}$ substitutions

Strain	Mutation	%F_1[a]	ATP hydrolysis	Turnover[b]	ATP synthesis	Turnover[b]	Synthesis/hydrolysis
KM200	Wild type	2.05	1.55	482	0.219	68.1	0.141
KM322	- control	0.25	0.306	780	0.002	3.4	0.0065
TC211	$b_{Arg\text{-}36\rightarrow Ile}$	0.76	0.624	523	0.004	2.4	0.0065
TC215	$b_{Arg\text{-}36\rightarrow Glu}$	1.10	0.619	358	0.012	6.9	0.0193

[a]Percent of membrane protein represented by F_1 was determined by a quantitative immunoblot as described previously (7).
[b]Turnover (s^{-1}) was calculated using MW of F_1 (382,146 Da).
[c]Ratio was calculated by the turnover number for ATP synthesis divided by the turnover number for ATP hydrolysis.

negative control. Clearly, the catalytic functions of KM322(negative control) and TC211($b_{Arg\text{-}36\rightarrow Ile}$) are fully uncoupled from transport. The F_1F_0 ATP synthase in strain TC215($b_{Arg\text{-}36\rightarrow Glu}$) had a slightly reduced hydrolytic rate and a greater than seven-fold reduction in coupling efficiency relative to the positive control enzyme from KM200(*b*) (Table 3-3). It was apparent that the coupled ATP synthesis function was more defective than the ATP-driven proton pumping in this strain. The activity in the $b_{Arg\text{-}36\rightarrow Glu}$ enzyme was sensitive to both the F_1 inhibitor aurovertin D and the F_0 inhibitor DCCD, indicating that the hydrolytic function remained in communication with the transport mechanism. It should be noted that the absolute values reported for hydrolysis differ from those reported in Table 3-2 because these experiments were performed under different assay conditions chosen to maximize coupling.

Discussion

The *b* subunit dimer is thought to serve as a stator, holding the $\alpha_3\beta_3$ hexamer in place against the rotation of the central stalk and *c* subunit ring. Analysis of primary protein sequence homology suggests that $b_{Arg\text{-}36}$ and $b_{Ala\text{-}79}$ are the most extensively conserved amino acids among all bacterial F_1F_0 ATP synthase *b* subunits. A collection of mutations replacing $b_{Arg\text{-}36}$ was constructed to investigate its functional role in the enzyme. The mutant strains have growth characteristics which indicate deficiencies in oxidative phosphorylation to varying degrees. Substitution of $b_{Arg\text{-}36}$ with *Lys, Ser, Cys*, and *Tyr* resulted in moderate reductions in the steady-state level of F_1F_0 ATP synthase in the membrane. In each case, the intact enzyme with these altered *b* subunits appeared to be functional as shown by growth on succinate minimal media. The $b_{Arg\text{-}36\rightarrow Ile}$ substitution also resulted in a moderate reduction in the level of F_1F_0 ATP synthase

complexes, but the enzyme seemed to be virtually inactive. Apparently, replacing $b_{Arg\text{-}36}$ with a hydrophobic group is incompatible with F_1F_0 ATP synthase activity. This suggests that while $b_{Arg\text{-}36}$ is not essential for F_1F_0 ATP synthase activity, the amino acid at this position exerts significant influence on the function of the enzyme.

A more interesting result is that the $b_{Arg\text{-}36\rightarrow Glu}$ mutation appears to be representative of the small group of mutations affecting the F_0 subunits which uncouple proton translocation from ATP synthesis in F_1. This is the first mutation of this type reported in the *uncF*(*b*) gene. The other uncoupling mutations alter the *c* and *a* subunits which, unlike the *b* subunit, are thought to participate in proton conduction (75, 93, 163, 242). Several observations are consistent with respect to these other missense mutations that yield the uncoupling phenotypes. First, like $b_{Arg\text{-}36}$, all substitutions occur at a strongly conserved position in F_1F_0 ATP synthase. Second, other amino acid substitutions at the same positions do not necessarily cause uncoupling of the enzyme. Third, with the exception of the $c_{Arg\text{-}41\rightarrow Lys}$ mutation (75), the uncoupling mutations are substitutions that result in a more acidic subunit. The effects of the amino acid substitutions in the polar loop of the *c* subunit on coupling can be rationalized by the observation of a direct interaction between one of the uncoupling mutation sites $c_{Gln\text{-}42}$ and the ε subunit (273), which along with the γ subunit, form the rotating stalk of F_1F_0 ATP synthase. The linkage between the rotary stalk and the proton translocation mechanism has apparently been disrupted. Since neither the *a* subunit nor the *b* subunit has been shown to interact with the rotating stalk subunits, another interpretation for those uncoupling mutations may be necessary. Perhaps these substitutions in the F_0

subunits facilitate exit of the proton from the channel along alternate paths not obligately coupled to rotation.

It is most interesting that the defect caused by the $b_{Arg\text{-}36\rightarrow Glu}$ substitution has a greater influence on $\Delta\mu H^+$-driven ATP synthesis than on ATP-driven proton pumping. These results suggest a functional bias in the stator depending on whether the rotor is turning in the direction of hydrolysis or synthesis. In other words, it may be possible that rotation is more efficient in one direction than in the other. Dunn's group (149) has recently conducted cross-linking studies at $b_{Arg\text{-}36}$. Their results indicated a formation of a cross-link between $b_{Arg\text{-}36\rightarrow Cys}$ and the *a* subunit of F_0. The fact that $b_{Arg\text{-}36}$ is in close contact with the *a* subunit suggests that the $b_{Arg\text{-}36\rightarrow Glu}$ substitution may be affecting the proton channel in the *a* subunit.

Junge and his group (38) have developed the idea that the second stalk may serve as an elastic mechanism that stores the energy generated during rotation of γε before the conformational change that allows release of ATP from the catalytic site. How this energy might be stored is not understood. It may be that the $b_{Arg\text{-}36\rightarrow Glu}$ substitution affects the storage of the energy such that the elastic energy cannot be stored during proton transport.

In summary, I have identified the first substitutions in the *b* subunit that yield phenotypes normally associated with subunits of functional importance to proton translocation and coupling of proton translocation to catalysis. The $b_{Arg\text{-}36\rightarrow Glu}$ mutant may be exerting a subtle influence on the conformations of the *a* or *c* subunits resulting in uncoupling. Alternatively, the interaction between the *b* subunit and F_1 may be dynamic,

and the assignment of a purely passive structural role for the *b* subunit in F_1F_0 ATP synthase may be premature.

CHAPTER 4
AMPLIFICATION OF RABBIT NaKβ_1 cDNA

Introduction

The H^+,K^+-ATPases and the Na^+,K^+-ATPases are Type IIB P-type ATPases, distinguished because they exist as heterodimers containing both α subunits and β subunits. The functional activities, including phosphorylation, ATP binding, and inhibitor binding have been associated within the α subunit. More recent studies have indicated that the β subunit has important properties as well, including enzyme stabilization, intracellular trafficking, maturation, and modulation of enzymatic activity.

Three β subunit isoforms have been identified for mammalian Na^+,K^+-ATPases (NaKβ_1, NaKβ_2, NaKβ_3)., whereas only one isoform has been discovered for the H^+,K^+-ATPase (HKβ). Campbell (34) identified two HKβ mRNA species in the rabbit renal medulla. One was essentially identical to the known HKβ cDNA (189), and a second variant mRNA transcript had a different 5' UTR. However, the deduced protein encoded by the second transcript was identical to the published sequence of the rabbit HKβ. All of the known isolated β subunits share a common molecular architecture: a short N-terminal cytoplasmic segment, a single transmembrane domain, and a large C-terminal extracellular domain. The extracellular domain is glycosylated and contains six completely conserved cysteine residues that are linked by three internal disulfide bonds. But, the primary sequence homology between β subunits is very weak.

Co-immunoprecipitation studies using monoclonal antibodies specific for HKβ have shown a physical interaction between HKβ and $HK\alpha_1$ in gastric membranes (112). However, a distinct β subunit associated with $HK\alpha_{2a}$ had not been determined. In fact, the absolute requirement of a β subunit for $HK\alpha_{2a}$ activity has been controversial. Lee *et al.* (136) expressed $HK\alpha_{2a}$ without a β subunit in Sf9 cells and detected K^+- stimulated ATPase activity. However, studies by other laboratories have shown that $HK\alpha_{2a}$ alone did not support $^{86}Rb^+$ uptake, and either HKβ (12, 45, 87, 159) or $NaK\beta_1$ (45, 197) served as a surrogate β subunit for $HK\alpha_{2a}$ in those experiments. Nevertheless, the β subunit that interacted *in vivo* with the colonic HKα subunit isoforms has not been established.

In April of 1998, two independent laboratories used immunoprecipitation experiments to demonstrate that $NaK\beta_1$ associated with $HK\alpha_{2a}$ in the rat kidney (44, 132) and distal colon (44). More recently, Sangan *et al.* (196) demonstrated by immunoprecipitation that $NaK\beta_3$ associated with $HK\alpha_{2a}$ in apical membranes of the rat distal colon. At the time of this work, it appeared that both $NaK\beta_1$ and $NaK\beta_3$ may be paired with $HK\alpha_{2a}$ to form an active enzyme *in vivo*. This was not considered surprising since NaKβ subunits are known to associate with different NaKα subunits (65). Moreover, HKβ has been shown to work in artificial expression systems (12, 45, 87, 159).

The $NaK\beta_1$ subunit was a likely mate to the $HK\alpha_2$ subunits. However, the cDNA sequence for the rabbit $NaK\beta_1$ was not known. Here I report the full-length rabbit $NaK\beta_1$ cDNA sequence. Primers were designed against known $NaK\beta_1$ cDNA sequences to

generate the full-length rabbit sequence by RT-PCR and 5' and 3' rapid amplification of cDNA ends (RACE) using rabbit medulla mRNA as a template.

Results

Degenerate PCR

Immunoprecipitation studies indicated that a likely mate for the $HK\alpha_{2a}$ subunit isoform *in vivo* was the $NaK\beta_1$ subunit (44, 132). In order to establish an expression system of the rabbit $HK\alpha_2$ subunit isoforms, the $NaK\beta_1$ cDNA needed to be cloned, but the $NaK\beta_1$ sequence for rabbit was unknown. The strategy to determine the rabbit $NaK\beta_1$ cDNA was to use RT-PCR and 5' and 3' RACE with degenerative primers designed from known $NaK\beta_1$ subunits from other species.

Human, mouse, rat, and dog $NaK\beta_1$ nucleotide sequences were aligned using the ClustalW multiple sequence alignment program (237). The nucleotide sequence alignment of the coding sequence of mammalian $NaK\beta_1$ subunits showed a high degree of conservation across each species. Sense and antisense primers were designed to anneal at conserved regions near the start and stop codons, respectively (Figure 4-1). Each primer included a unique restriction site to aid in future cloning experiments. The sense primer BC422 was easy to design with only two-fold degeneracy with other $NaK\beta_1$ subunit sequences. The antisense primer proved to be more difficult since the region of the stop codon for the human sequence was slightly different than the other mammalian sequences. I hypothesized that the rabbit sequence would be more similar to the mouse, rat, and dog sequences and designed the antisense primer BC423 in that manner with eight-fold degeneracy. RT-PCR using rabbit medulla RNA was attempted several times with BC422 and BC423, but no product was amplified. This result was likely a

Figure 4-1. Partial nucleotide sequence alignment of known NaKβ_1 subunits. Nucleotide sequences from known NaKβ_1 subunits were aligned using the ClustalW multiple sequence alignment program. A, Sequence alignment near 5' end of cDNAs with degenerate primers below. The start codons are shown in blue. B, Sequence alignment near 3' end of cDNAs with degenerate primer below. The stop codons are indicated in orange. The unique restriction sites in primers are underlined. Symbol: (-) indicates the absence of a nucleotide at a position.

combination of the unique restriction sites and the high degree of degeneracy of primer BC423. Therefore, the sense primer BC422 was redesigned without the *Kpn*I restriction site and was named BC424.

Three independent 3' RACE reactions were performed from a rabbit medulla cDNA library with sense primer BC424 and anchor primer AP1 and analyzed by agarose gel electrophoresis. Based on the placement of primer BC424, the PCR product should have been at least 0.9 kb. Multiple fragments ranging in size from 1 kb to 2 kb were amplified in each reaction (Figure 4-2A). Because these products were the result of a 3' RACE reaction, the different fragment sizes were likely the result of varying lengths of the 3' UTR. Using the PCR products from each of the 3' RACE reactions as templates, a second round of PCR with primers BC422 and BC423 was conducted. These primers were expected to amplify a 0.9 kb fragment. Multiple fragments ranging in size from 0.9 kb to 1.8 kb were amplified during the second round of PCR, but the most abundant fragment was 0.9 kb (Figure 4-2B). The 0.9 kb fragment from each of the three PCR reactions was gel purified and subsequently cloned into the TOPO TA cloning vector for sequence analysis. The sequences were highly homologous to each other when aligned with the ClustalW program (Figure 4-3). When the nucleotide sequences were analyzed against existing sequences in GenBank, they matched $NaK\beta_1$ subunits from other species with a high degree of homology. Therefore, it was likely that the sequences in hand represented the rabbit $NaK\beta_1$ subunit.

RACE

Because the sense and antisense primers used to amplify the sequences were degenerate, 5' and 3' RACE reactions were performed to sequence through those regions

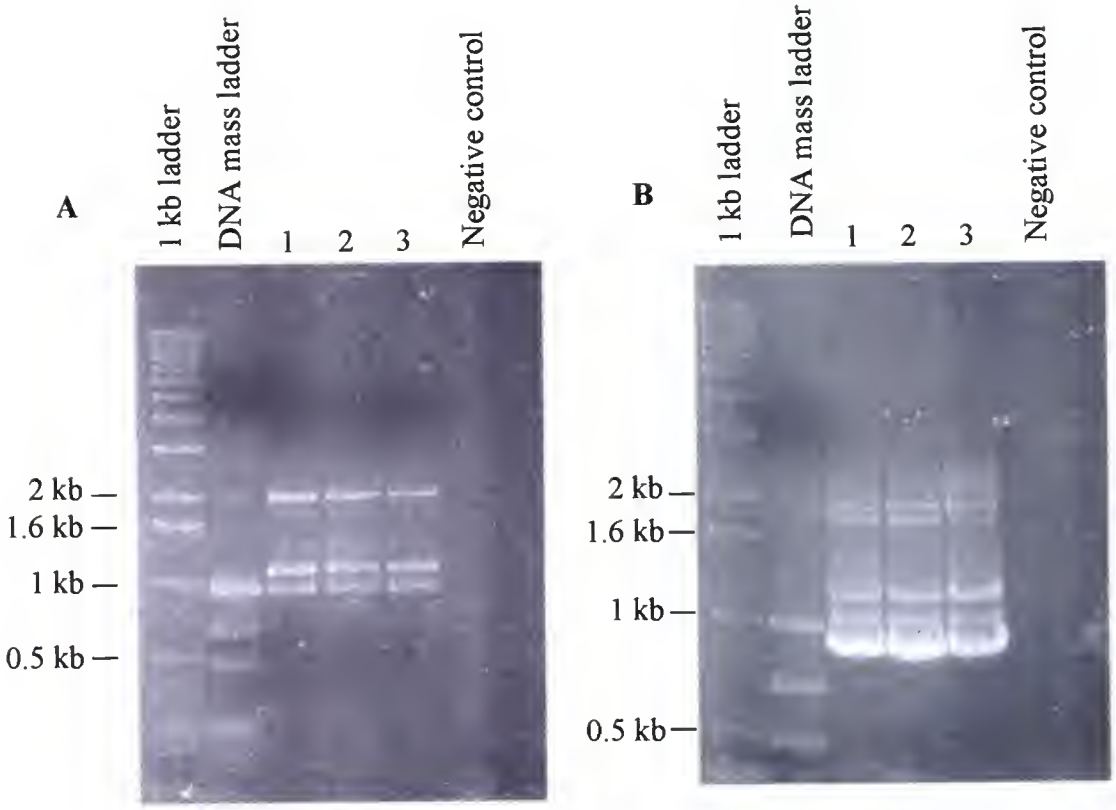

Figure 4-2. Agarose gel analysis of rabbit NaKβ_1 cDNA PCR amplifications. 40% of the PCR samples were analyzed on a 1% agarose gel. A, Analysis of first round of PCR with primers BC424 and AP1. B, Analysis of second round of PCR with primers BC422 and BC423.

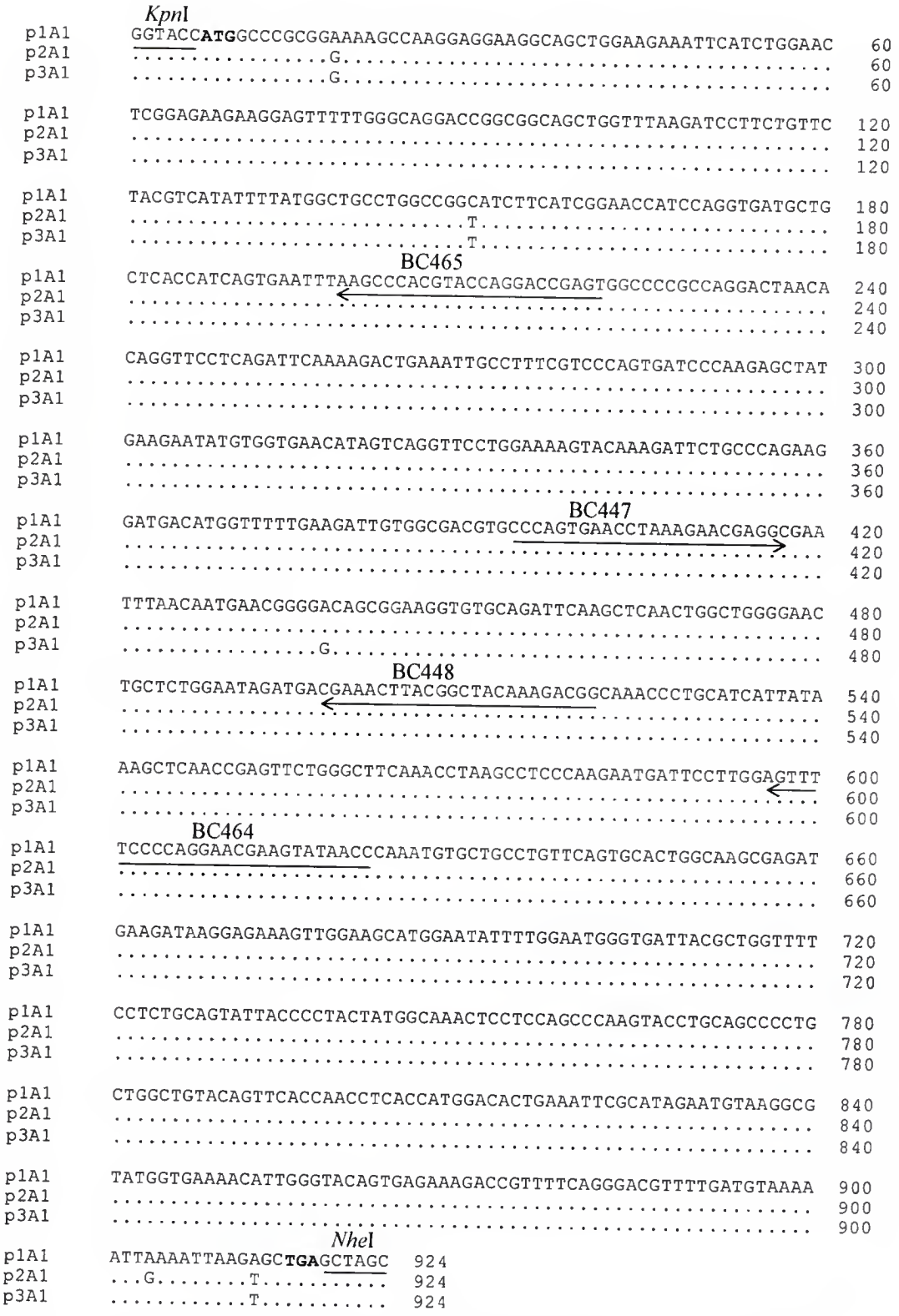

Figure 4-3. Nucleotide sequence alignment of rabbit NaKβ_1 cDNA. Nucleotide sequences from three independent PCR reactions were aligned using ClustalW program. Incorporated restriction sites are underlined. Putative start and stop codons are in bold. Location of primers for RACE reactions are shown by an arrow. Symbol: (.) indicates nucleotide identity.

and obtain the 5' and 3' UTR's. The gene-specific primers designed to obtain the full-length cDNA product are shown in Figure 4-3. Each RACE reaction used a gene-specific primer and anchor primer AP1 with a rabbit medulla cDNA library as a template. The 5' RACE reaction proved to be very difficult. Several gene-specific primers were designed near the 5' end of the sequence, and the annealing temperatures and cycle numbers were repeatedly changed in an attempt to optimize the PCR reaction. However, the reactions consistently produced smears when analyzed by agarose gel electrophoresis. I was successful at amplifying a fragment in the 5' RACE reaction by using gene-specific primer BC464 instead of random hexamers to reconstruct the cDNA library. Using the reconstructed library, three independent 5'RACE reactions were performed with gene-specific primer BC448 and anchor primer AP1. Although this PCR reaction produced a smear, a nested PCR was performed using the products from the first round as a template with gene-specific primer BC465 and anchor primer AP2. This primer pair should have produced 0.2 kb fragment, and when the reactions were analyzed by agarose gel electrophoresis, there was a prominent 0.2 kb fragment in each lane (Figure 4-4). Each of the three fragments was cloned in TOPO TA cloning vector for sequence analysis. The 5' RACE confirmed that the sequence near the start codon of the initial rabbit $NaK\beta_1$ sequences in plasmids p1A1, p2A1, and p3A1 was correct.

Three independent 3' RACE reactions were conducted with gene-specific primer BC447 and anchor primer AP1 using the rabbit medulla cDNA library constructed with random hexamers. This primer pair produced a 0.7 kb fragment. Each fragment was cloned in TOPO TA cloning vector for sequence analysis. The 3' RACE showed that the sequence near the stop codon of the plasmids (p1A1, p2A1, p3A1) was incorrect. The

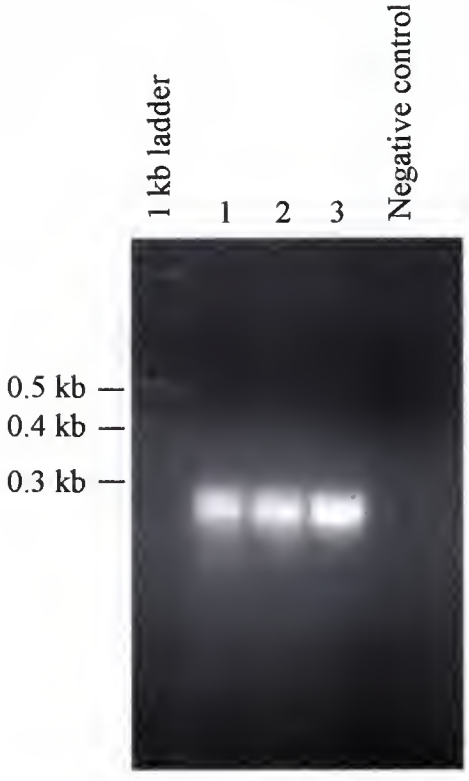

Figure 4-4. Agarose gel analysis of rabbit NaKβ_1 5' RACE reactions. Primer BC465 and nested primer AP2 were used to amplify the 5' end of rabbit NaKβ_1 from an initial 5' RACE reaction. Three independent RACE reactions were performed, and 40% of the reactions were analyzed on a 2% agarose gel.

correct sequence near the stop codon was $^{5'}$GAA GTT AAG AGC **TGA**$^{3'}$. The QuikChange Mutagenesis kit was used to correct the nucleotides in p3A1. The final construct was sequenced again and named pNaKβ_1. The full-length rabbit NaKβ_1 cDNA sequence submitted to GenBank is shown in Figure 4-5.

Western Analysis

The isolation of the full-length rabbit NaKβ_1 cDNA was necessary for expression of the rabbit renal H^+,K^+-ATPases. To determine if mammalian cells could functionally express the NaKβ_1 protein, the cDNA sequence was cloned in the pREP8 mammalian expression vector. The resulting plasmid pTLC25 was maintained episomally in HEK293c18 cells expressing HKα_{2a} from episomal vector pTLC19. Plasma membranes were prepared from these cells, and the expression of NaKβ_1 protein was examined by Western analysis (Figure 4-6). The primary antibody used in the Western analysis was a monoclonal rabbit Na^+,K^+-ATPase antibody which recognizes NaKβ_1. The blot clearly showed the expression of rabbit NaKβ_1 that migrated as a smear of 50-70 kD. These results indicated that the rabbit NaKβ_1 cDNA had been identified since an antibody against rabbit NaKβ_1 was able to detect the expressed protein. The protein was also glycosylated as indicated by the smear on the Western blot.

Discussion

Here I identified the full-length rabbit NaKβ_1 cDNA by RT-PCR and RACE using rabbit renal medulla RNA as the template and degenerate primers based on the 5' and 3' ends of the coding sequences from other mammalian NaKβ_1 cDNAs. The cDNA was highly homologous to other known mammalian NaKβ_1 subunits. Expression of the

```
LOCUS       AF204927     1136 bp    mRNA            MAM       15-DEC-1999
DEFINITION  Oryctolagus cuniculus Na+,K+-ATPase beta 1 subunit mRNA, complete
            cds.
ACCESSION   AF204927
VERSION     AF204927.1  GI:6578920
KEYWORDS    .
SOURCE      European rabbit.
  ORGANISM  Oryctolagus cuniculus
            Eukaryota; Metazoa; Chordata; Craniata; Vertebrata; Euteleostomi;
            Mammalia; Eutheria; Lagomorpha; Leporidae; Oryctolagus.
REFERENCE   1  (bases 1 to 1136)
  AUTHORS   Caviston,T.L., Campbell,W.G., Wingo,C.S. and Cain,B.D.
  TITLE     Molecular identification of the renal H+,K+-ATPases
  JOURNAL   Semin. Nephrol. 19 (5), 431-437 (1999)
  MEDLINE   99439401
   PUBMED   10511383
REFERENCE   2  (bases 1 to 1136)
  AUTHORS   Caviston,T.L., Campbell,W.G., Wingo,C.S. and Cain,B.D.
  TITLE     Direct Submission
  JOURNAL   Submitted (15-NOV-1999) Biochemistry and Molecular Biology,
            University of Florida, P.O. Box 100245, JHMHC, Gainesville, FL
            32610, USA
FEATURES             Location/Qualifiers
     source          1..1136
                     /organism="Oryctolagus cuniculus"
                     /strain="New Zealand White"
                     /db_xref="taxon:9986"
     CDS             16..927
                     /note="P-type ATPase"
                     /codon_start=1
                     /product="Na+,K+-ATPase beta 1 subunit"
                     /protein_id="AAF18134.1"
                     /db_xref="GI:6578921"
                     /translation="MARGKAKEEGSWKKFIWNSEKKEFLGRTGGSWFKILLFYVIFYG
                     CLAGIFIGTIQVMLLTISEFKPTYQDRVAPPGLTQVPQIQKTEIAFRPSDPKSYEEYV
                     VNIVRFLEKYKDSAQKDDMVFEDCGDVPSEPKERGEFNNERGQRKVCRFKLNWLGNCS
                     GIDDETYGYKDGKPCIIIKLNRVLGFKPKPPKNDSLEFSPGTKYNPNVLPVQCTGKRD
                     EDKEKVGSMEYFGMGDYAGFPLQYYPYYGKLLQPKYLQPLLAVQFTNLTMDTEIRIEC
                     KAYGENIGYSEKDRFQGRFDVKIEVKS"
BASE COUNT      350 a    248 c    265 g    273 t
ORIGIN
        1 cgctgacccg ccaccatggc ccgcgggaaa gccaaggagg aaggcagctg gaagaaattc
       61 atctggaact cggagaagaa ggagtttttg ggcaggaccg gcggcagctg gtttaagatc
      121 cttctgttct acgtcatatt ttatggctgc ctggccggta tcttcatcgg aaccatccag
      181 gtgatgctgc tcaccatcag tgaatttaag cccacgtacc aggaccgagt ggccccgcca
      241 ggactaacac aggttcctca gattcaaaag actgaaattg cctttcgtcc cagtgatccc
      301 aagagctatg aagaatatgt ggtgaacata gtcaggttcc tggaaaagta caaagattct
      361 gcccagaagg atgacatggt ttttgaagat tgtggcgacg tgcccagtga acctaaagaa
      421 cgaggcgaat ttaacaatga acgggggcag cggaaggtgt gcagattcaa gctcaactgg
      481 ctggggaact gctctggaat agatgacgaa acttacggct acaaagacgg caaaccctgc
      541 atcattataa agctcaaccg agttctgggc ttcaaaccta agcctcccaa gaatgattcc
      601 ttggagtttt ccccaggaac gaagtataac ccaaatgtgc tgcctgttca gtgcactggc
      661 aagcgagatg aagataagga gaaagttgga agcatggaat attttggaat gggtgattac
      721 gctggttttc ctctgcagta ttacccctac tatggcaaac tcctccagcc caagtacctg
      781 cagcccctgc tggctgtaca gttcaccaac ctcaccatgg acactgaaat tcgcatagaa
      841 tgtaaggcgt atggtgaaaa cattgggtac agtgagaaag accgttttca gggacgtttt
      901 gatgtaaaaa ttgaagttaa gagctgatca caagcacaaa atctttccca ctagccattt
      961 aataagttaa aaaagataca aaaacaaaaa cctactagtc ttgaacaaac tgtcatacgt
     1021 atgggaccta cacttaatct atatgcttta cactagcttt ctgcatttaa taggttagaa
     1081 tgtaaattta aagtgtagca atagcaacaa aatatttatt ctactgtaaa tgacaa
```

Figure 4-5. GenBank accession record for rabbit NaKβ_1 cDNA sequence.

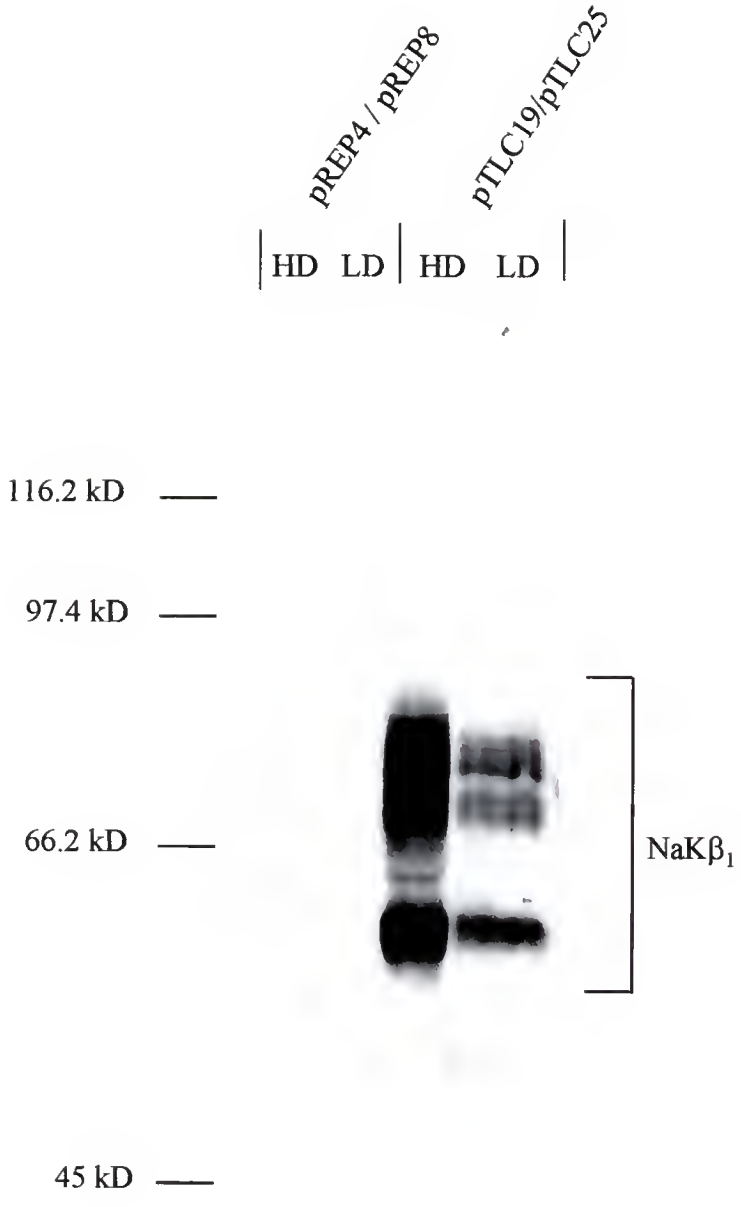

Figure 4-6. Western analysis of HEK293c18 cells expressing NaKβ_1 from an episomal vector. 60 μg protein from a plasma membrane preparation was separated on a 10% Tris-glycine gel, transferred to nitrocellulose, and incubated with mouse anti-rabbit NaKβ_1 antibodies. HD, high-density fraction; LD, low density fraction.

cDNA in an episomal expression system resulted in production of a protein that was recognized by an antibody against rabbit $NaK\beta_1$.

Molecular Toolkit (www.vivo.colostate.edu/molkit), a computer program that searches for and reads every open reading frame in a cDNA sequence, identified an open reading frame of 303 amino acids. An amino acid similarity and homology comparison of this open reading frame with other NaKβ subunit isoforms is shown in Table 4-1. The rabbit $NaK\beta_1$ amino acid sequence was 90% homologous with known $NaK\beta_1$ subunit sequences and showed only 30 to 40% homology with other NaKβ subunit isoforms. All of the known isolated β subunits contain a single transmembrane domain. A Kyte-Doolittle hydropathy plot (134) was used to examine the membrane topology of the rabbit $NaK\beta_1$ amino acid sequence, and a single membrane spanning region was identified between amino acids 35-60 (Figure 4-7). The rabbit $NaK\beta_1$ amino acid sequence is shown in Figure 4-8. All known β subunit isoforms have a glycosylated extracellular domain and six completely conserved cysteine residues linked by internal disulfide bonds. The three *N*-linked glycosylation sites characteristic of all $NaK\beta_1$ subunits and the six conserved cysteine residues were identified. The likely disulfide bonds that form in the native protein were assigned based on experiments that have identified the bonds in $NaK\beta_1$ from other species (126, 157).

At the time this work was conducted, it was widely believed that $NaK\beta_1$ was the likey mate for the $HK\alpha_2$ subunit in the colon and kidney. Two groups independently showed that antibodies directed against the $HK\alpha_2$ subunits co-immunoprecipitated the $NaK\beta_1$ subunit from both colon and kidney tissues (44, 132). The $NaK\beta_1$ subunit has been reported to be capable of supporting of H^+,K^+-ATPase activity for the $HK\alpha_{2a}$

Table 4-1. Percent amino acid similarity and identity of rabbit NaKβ_1 with other known NaKβ subunit isoforms

NaKβ Subunit Isoform	% Identity	% Similarity
Human NaKβ_1	91%	96%
Mouse NaKβ_1	88%	95%
Rat NaKβ_1	90%	96%
Dog NaKβ_1	90%	96%
Human NaKβ_2	39%	55%
Mouse NaKβ_2	39%	54%
Rat NaKβ_2	39%	55%
Human NaKβ_3	37%	53%
Mouse NaKβ_3	33%	50%
Rat NaKβ_3	34%	51%
Rabbit NaKβ_3	36%	53%

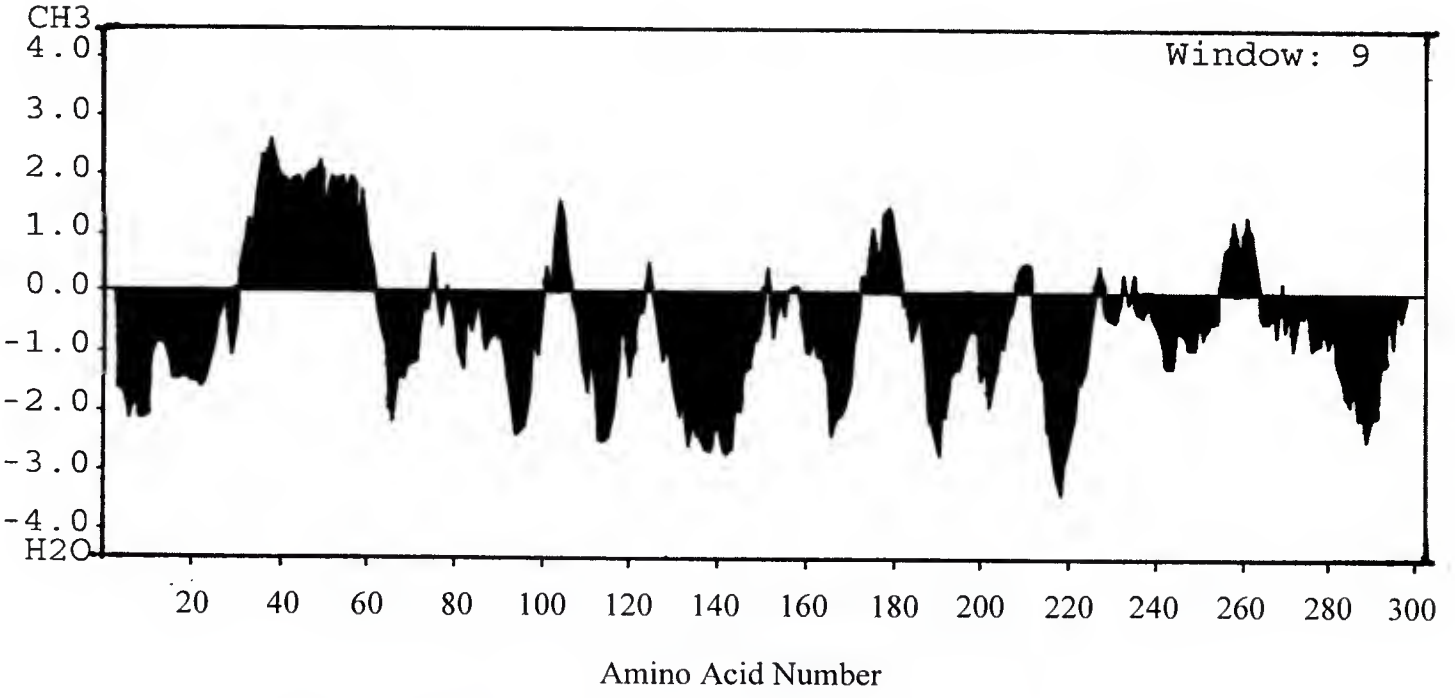

Figure 4-7. Kyte-Doolitte hydropathy plot of rabbit NaKβ_1 amino acid sequence. Amino acid sequence was analyzed according to Kyte and Doolittle (134) with a window of 9. Hydrophobic regions are indicated by the positive numbers on the x-axis.

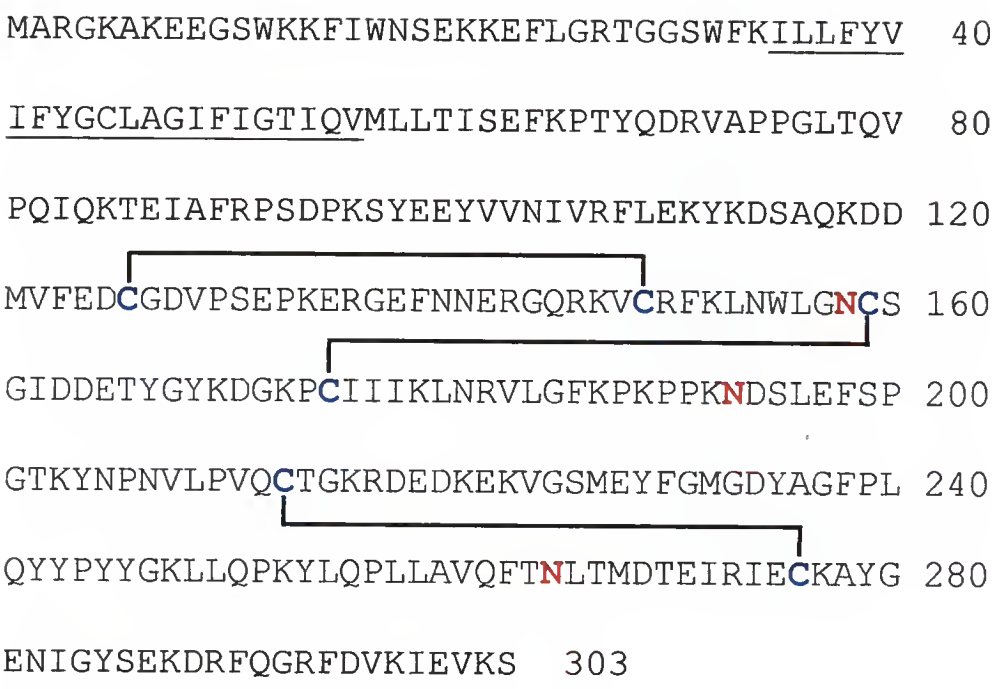

Figure 4-8. Amino acid sequence analysis of rabbit NaKβ_1 protein. The three potential *N*-linked glycosylation sites are indicated in red. The six conserved cysteine residues are shown in blue. The pair of cysteines that likely form disulfide bonds is specified by the black lines. The proposed transmembrane domain is underlined. Single amino acid letter codes are used.

subunit in an *in vitro* expression system (45, 197). Therefore, the rabbit NaKβ_1 was deemed suitable for use in further experiments designed to express the rabbit renal H^+,K^+-ATPase in mammalian tissue culture cells.

CHAPTER 5
EXPRESSION OF RABBIT RENAL H^+,K^+-ATPases

Introduction

Potassium is critical for many cell functions, and its concentration in cells and extracellular fluid is kept constant despite wide variations in dietary K^+ intake. The kidney plays the major role in K^+ homeostasis by regulating urinary K^+ excretion and can conserve K^+ when dietary K^+ intake is reduced. The renal H^+,K^+-ATPase has been implicated in K^+ reabsorption during K^+ depletion. Early experiments established that H^+,K^+-ATPase activity increased in both the cortical collecting duct and OMCD of K^+-restricted animals (57). *In vitro* microperfusion experiments demonstrated that collecting ducts from K^+-restricted animals had net K^+ reabsorption which was blocked by omeprazole and SCH-28080 (261). Normal and K^+-restricted mice may express different isoforms of the H^+,K^+-ATPase. Collecting ducts from normal rats exhibited an H^+,K^+-ATPase activity that was pharmacologically similar to the ouabain-insensitive gastric isoform, which within days of K^+ depletion was replaced by the ouabain-sensitive colonic isoform (29).

Our laboratory was interested in determining the molecular identities of the H^+,K^+-ATPase isoforms in the kidney. Campbell *et al.* (35) identified two $HK\alpha_2$ subunit isoforms from the rabbit kidney: $HK\alpha_{2a}$ and $HK\alpha_{2c}$. The $HK\alpha_{2a}$ cDNA was highly homologous to the human and rat $HK\alpha_{2a}$ cDNAs. The $HK\alpha_{2c}$ cDNA was the result of alternative splicing, resulting in a putative 61 amino acid extension at the N-terminus of

$HK\alpha_{2c}$. Anti-peptide antibodies designed to the unique extension of $HK\alpha_{2c}$ identified a protein of the appropriate mass in rabbit renal cortex. Anti-peptide antibodies designed to the region shared by both $HK\alpha_{2a}$ and $HK\alpha_{2c}$ revealed the presence of a doublet in renal cortex tissue. The larger protein migrated to the same apparent mass of $HK\alpha_{2c}$. The $HK\alpha_{2c}$ protein has been localized to the apical membrane of a small population of cells in the connecting segment, cortical collecting duct and $OMCD_i$ (247). To date, $HK\alpha_{2c}$ has only been observed in the rabbit, but $HK\alpha_{2b}$, another $HK\alpha_2$ variant, appears to arise by the same type of splicing phenomenon in the rat $HK\alpha_2$ gene.

The existence of $HK\alpha_{2c}$ offers the possibility of complex translational regulation of the H^+,K^+-ATPase. The N-terminal extension of $HK\alpha_{2c}$ may provide different enzymatic properties, such as kinetic parameters, degradation rates, or internalization rates. Regulatory proteins may bind the N-terminal extension to activate or inactivate the enzyme. Putative phosphorylation sites may serve a regulatory role as well. The upstream open reading frames in the $HK\alpha_{2c}$ 5' UTR may reduce the efficiency of its translation. To begin to address these questions, an expression system had to be established. However, the β subunit that associated with the $HK\alpha_2$ subunit isoforms remained controversial. Co-immunoprecipitation studies from two independent investigators indicated that the $NaK\beta_1$ subunit isoform associated with $HK\alpha_{2a}$ in the rat kidney and distal colon (44, 132). However, co-immunoprecipitation studies from another group later designated the $NaK\beta_3$ subunit isoform as the mate to $HK\alpha_{2a}$ in the rat distal colon (196). Both NaKβ subunit isoforms have been utilized in heterologous expression systems to study the H^+,K^+-ATPase activities associated with $HK\alpha_{2a}$ (45,

197). This chapter describes the use of episomal, stable, and transient mammalian expression systems in an attempt to functionally express $HK\alpha_{2a}$ and $HK\alpha_{2c}$ with rabbit $NaK\beta_1$ and later with $NaK\beta_3$. Although $HK\alpha_2$ subunits and $NaK\beta_1$ or$NaK\beta_3$ isoforms were expressed in concert, no apparent pump function was observed. The results suggest that a lack of enzymatic activity may be due to a lack of subunit association, in agreement with a very recent publication.

Results

Episomal Expression

The transfer of foreign genes into eukaryotic cells has been vital to our understanding of the functional significance of genes and regulatory sequences. Different mammalian expression vector systems have been designed to facilitate the study of genes. Most expression vectors have the ability to integrate into the host genome at some point in the transfection process. A class of vectors has been developed to avoid positional complications that arise from integration into chromatin. The most notable is the Epstein Barr virus (EBV)-based system (225, 268). This system is designed for enhanced expression and maintenance of genes as an episomal element. EBV-based vectors require two viral elements, the origin of replication and the viral EBV Nuclear Antigen-1 (EBNA-1) gene that facilitates the extrachromosomal maintenance of the vector. Because they are retained as extrachromosomal replicating elements within the nucleus, transgene expression is independent of position effects observed when DNA vectors are randomly integrated. In addition, because the episome is often present as multiple copies, the expression of the transgene can be amplified (6).

The episomal expression system was used as the initial attempts to study the pharmacological profiles of the $HK\alpha_{2a}$ and $HK\alpha_{2c}$ subunit isoforms using the rabbit

$NaK\beta_1$ subunit as the mate. HEK293c18 cells were selected because they were a kidney cell line, and they constitutively expressed EBNA-1, a trans-acting factor required for the EBV origin of replication. The cDNAs for $HK\alpha_{2a}$ and $HK\alpha_{2c}$ were each cloned in the pREP4 vector, which conferred hygromycin resistance, and the cDNA for $NaK\beta_1$ was cloned in the pREP8 vector, which conferred histidinol resistance. Cells were transfected with pTLC19($HK\alpha_{2a}$), pTLC24($HK\alpha_{2c}$), and pTLC25($NaK\beta_1$) (Figure 5-1), and once selection was completed, total RNA was isolated for Northern analysis (Figure 5-2A). Probes specific for $NaK\beta_1$ and for the common region of $HK\alpha_{2a}$ and $HK\alpha_{2c}$ were used to detect the RNA transcripts of the isoforms in the established cells. Control HEK293c18 cells carrying pREP4 and pREP8 vectors did not express any detectable levels of $HK\alpha_{2a}$, $HK\alpha_{2c}$ or $NaK\beta_1$ RNA as indicated by the absence of a signal in control lanes. However, cells that were transfected with plasmid-containing cDNAs did indeed express the expected transcripts, which were recognized by the labeled probes. The probe to the common region of the $HK\alpha_2$ subunits recognized a longer mRNA transcript for $HK\alpha_{2c}$, as expected. However, the $HK\alpha_{2a}$ transcript was detected in higher quantities than the $HK\alpha_{2c}$ transcript. This observation was not a loading defect since a probe to GAP3DH recognized similar amounts of transcript in each lane.

Once it was confirmed that cells transfected with pTLC19($HK\alpha_{2a}$) and pTLC24($HK\alpha_{2c}$) were transcribing the appropriate mRNAs, the cells were then transfected with pTLC25($NaK\beta_1$). After histidinol selection was complete, total RNA was analyzed by Northern analysis (Figure 5-2A). $HK\alpha_{2a}$ and $HK\alpha_{2c}$ transcripts were still produced in the cells, although the levels of transcripts had dropped for both RNAs. Surprisingly, $NaK\beta_1$ transcript was not detected in pTLC24($HK\alpha_{2c}$)/pTLC25($NaK\beta_1$)

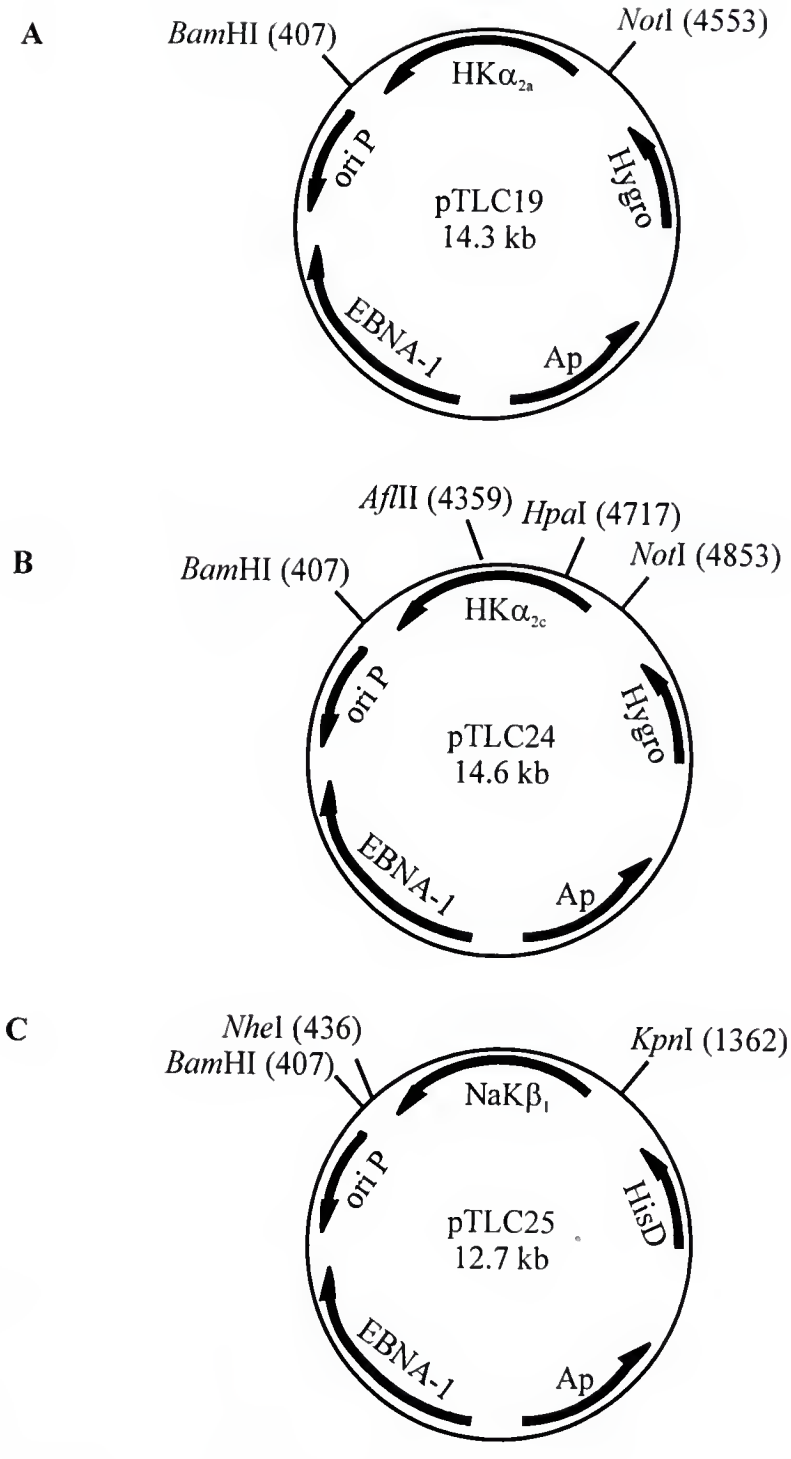

Figure 5-1. Episomal expression constructs. A, Plasmid pTLC19($HK\alpha_{2a}$). B, Plasmid pTLC24($HK\alpha_{2c}$). C, Plasmid pTLC25($NaK\beta_1$)

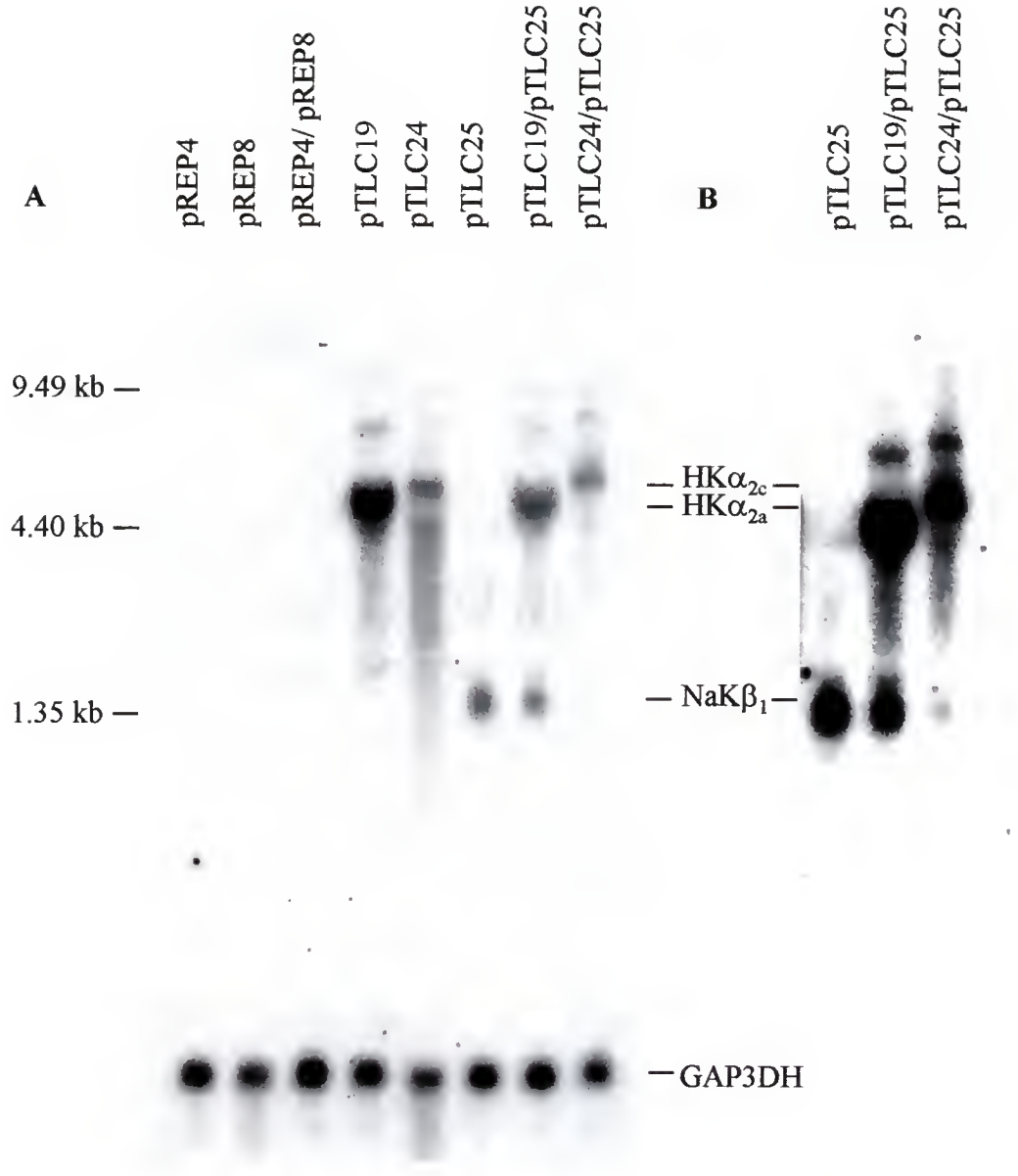

Figure 5-2. Northern analysis of HEK293c18 cells expressing $HK\alpha_{2a}$, $HK\alpha_{2c}$, and $NaK\beta_1$ from episomal vectors. A, Total RNA (10 μg) was separated on a denaturing gel and transferred to nylon membrane. Probes specific for rabbit $NaK\beta_1$ and the common region of $HK\alpha_{2a}$ and $HK\alpha_{2c}$ were randomly labeled with ^{32}P and hybridized to the membrane. A probe for GAP3DH was used as a loading control. B, Blot in A was exposed to film with intensifying screens to increase signal of $NaK\beta_1$ transcript.

cells. However, exposing the film with intensifying screens resulted in a faint band at the expected size for NaKβ_1 in cells expressing pTLC24(HKα_{2c})/pTLC25(NaKβ_1) (Figure 5-2B).

Plasma membranes were prepared from each episomal cell line, and the expression of each isoform was examined by Western analysis. Anti-peptide antibodies to the common region of the HKα_2 subunit isoforms and those specific for HKα_{2c} were unable to detect any proteins in the established cell lines. This was very puzzling, and the cDNAs were sequenced to determine if mutations had occurred to cause the translated proteins to be out of frame. Indeed, the coding sequences were out of frame, but not due to a coding sequence mutation. Two start codons (ATG) were present upstream of the HKα_{2a} and HKα_{2c} cDNAs that caused incorrect proteins to be translated. These start codons originated from the TOPO TA cloning vector's multiple cloning region. However, antibodies to rabbit NaKβ_1 demonstrated that the cells were indeed producing glycosylated NaKβ_1 protein (Figure 5-3). Because pTLC24(HKα_{2c})/pTLC25(NaKβ_1) cells were not producing NaKβ_1 transcript, it was not surprising to observe that the cells had little NaKβ_1 protein when compared to pTLC19(HKα_{2a})/pTLC25(NaKβ_1) cells. We concluded that the likely problem was competition between the two episomal elements in the same cell. Apparently over time, a given cell line developed preferential expression of one or the other plasmid. This was probably a result of differential segregation at mitosis. The episomal system may be appropriate for single proteins, but inclusion of two episomal constructs in the same cell was not successful. Therefore, I elected to abandon the approach as a result of this insurmountable difficulty.

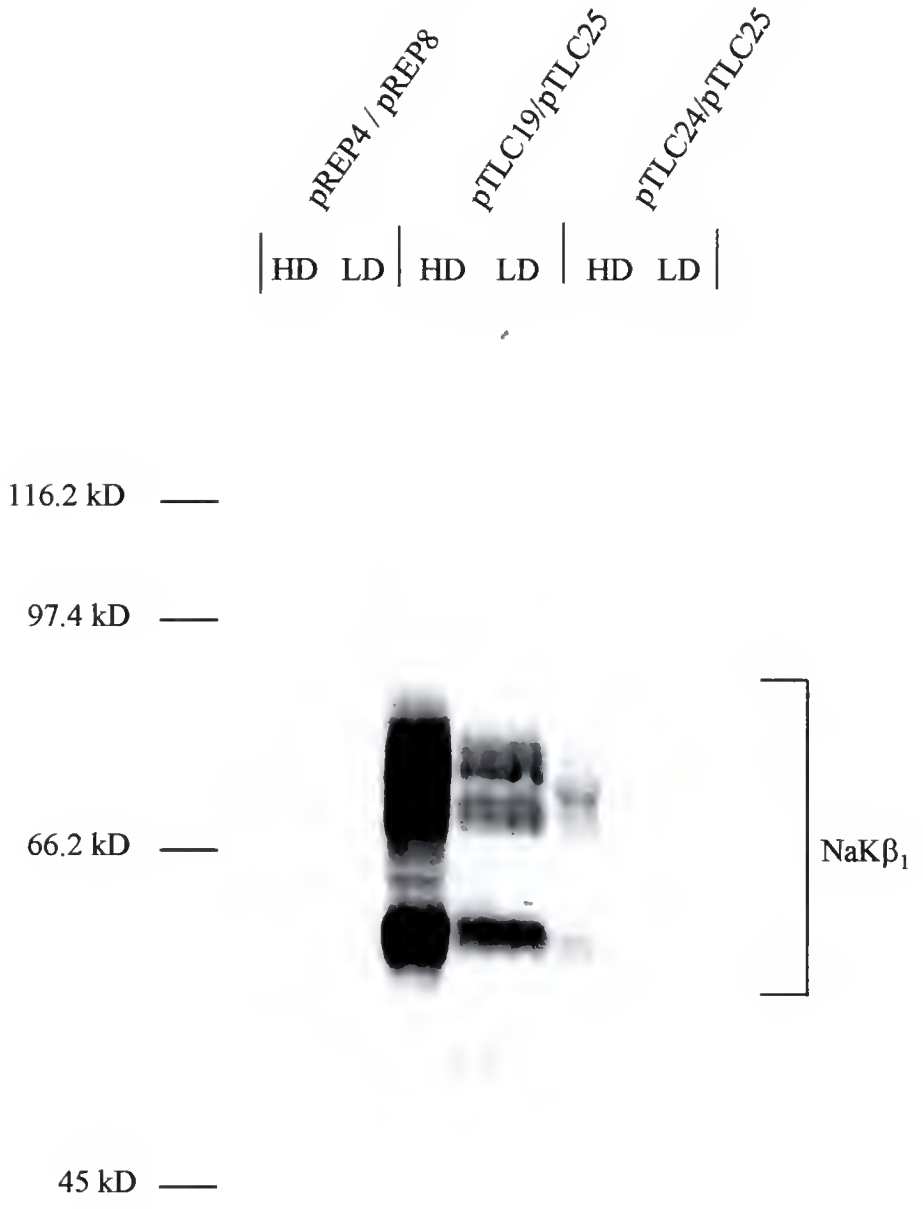

Figure 5-3. Western analysis of HEK293c18 cells expressing NaKβ_1 from an episomal vector. 60 μg protein from a plasma membrane preparation was separated on a 10% Tris-glycine gel, transferred to nitrocellulose, and incubated with mouse anti-rabbit NaKβ_1 antibodies. HD, high-density fraction; LD, low density fraction.

Stable Expression

Foreign DNA can be introduced into the genome of cells through random recombination events. This is the basis of a stable expression system. DNA that contains an antibiotic resistance gene is transfected into mammalian culture cells. The cells are grown under selection under single cell colonies appear. These single cell colonies have the ability to grow in the antibiotic because the DNA has been stably integrated into the cell's genome. The stable expression system has been used in the past to study the H^+,K^+-ATPase in HEK293 cells by others (87, 197) and was used as an alternate approach to establish cells which express the renal H^+,K^+-ATPases. The pBudCE4 mammalian expression vector was chosen as an appropriate vector for this study. The vector contained both the human EF-1α promoter and the human cytomegalovirus (CMV) promoter for high-level constitutive expression of two recombinant proteins. Therefore, both the α and β subunits could be expressed from the same DNA segment. In addition, the plasmid contained C-terminal peptides encoding either the *myc* epitope or the V5 epitope and a polyhistidine metal-binding tag for detection and purification of the recombinant proteins.

Although it was known that the CMV promoter would function in HEK293 cells, inspection of the literature and communication with Invitrogen (pBudCE4 manufacturer) technical services indicated that the human EF-1α promoter had not previously been tested in these cells. To be certain that the promoter could function in these cells, a preliminary experiment was conducted with the control plasmid pBudCE4/*lac*Z/CAT (Figure 5-4). This plasmid had the chloramphenicol acetyltransferase (CAT) gene cloned behind the EF-1α promoter and in frame with the V5 and polyhistidine epitope tags. The

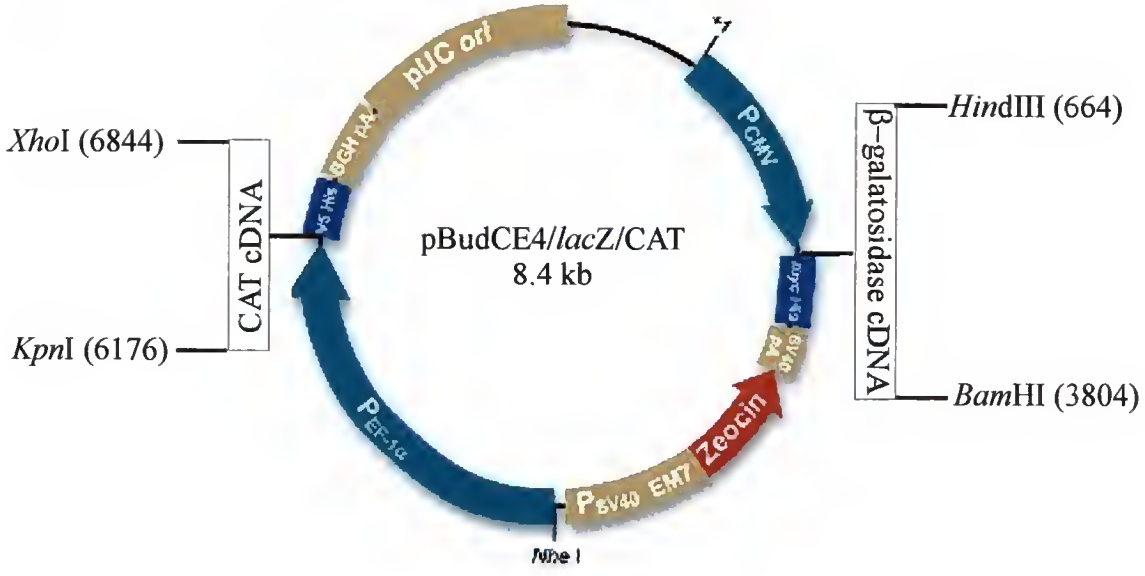

Figure 5-4. Control plasmid pBudCE4/*lac*Z/CAT expression vector. The CAT cDNA was cloned behind the EF-1α promoter and in frame with the V5 epitope tag. The β-galactosidase cDNA was cloned behind the CMV promoter and in frame with the *myc* epitope tag. Figure was adapted from Invitrogen catalog.

gene for β-galactosidase was cloned behind the CMV promoter and in frame with the *myc* and polyhistidine epitope tags. Plasmid pBudCE4/*lac*Z/CAT was transfected into HEK293 cells, and ten single clones were isolated. The cell lysates were analyzed for the presence of CAT and β-galactosidase fusion proteins by Western analysis. Monoclonal V5-specific antibodies recognized the 32 kD CAT fusion protein in two of the three clones depicted in Figure 5-5A, thereby verifying that the EF-1α promoter could function in HEK293 cells. The blot was stripped and re-probed with monoclonal *myc*-specific antibodies. These antibodies detected the 117 kD β-galactosidase fusion protein in two of the three clones screened (Figure 5-5B). Interestingly, two of the isolated clones expressed either fusion protein, whereas only one clone expressed both fusion proteins. This observation suggested that there was a reasonable probability that insertion of the H^+,K^+-ATPase cDNAs would result in expression of both α and β subunits in a single cell line.

The $HK\alpha_{2a}$ and $HK\alpha_{2c}$ cDNAs were cloned behind the EF-1α promoter and in frame with a V5 and polyhistidine epitope tags to aid in their detection by Western analysis. The two start codons that had caused improper translations in the episomal system were removed prior to their cloning in the pBudCE4 vector by cassette mutagenesis. The $NaK\beta_1$ cDNA was cloned behind the CMV promoter, but not in frame with any tag since a good commercial antibody existed for the protein (Figure 5-6). To establish that the constructs expressed the expected sized proteins, COS-1 cells were transiently transfected with plasmids that contained each isoform alone, as well as plasmids with both an α and the β subunit. Crude membrane preparations were analyzed by Western analysis. V5 antibodies readily detected $HK\alpha_{2a}$-V5 and $HK\alpha_{2c}$-V5 fusion

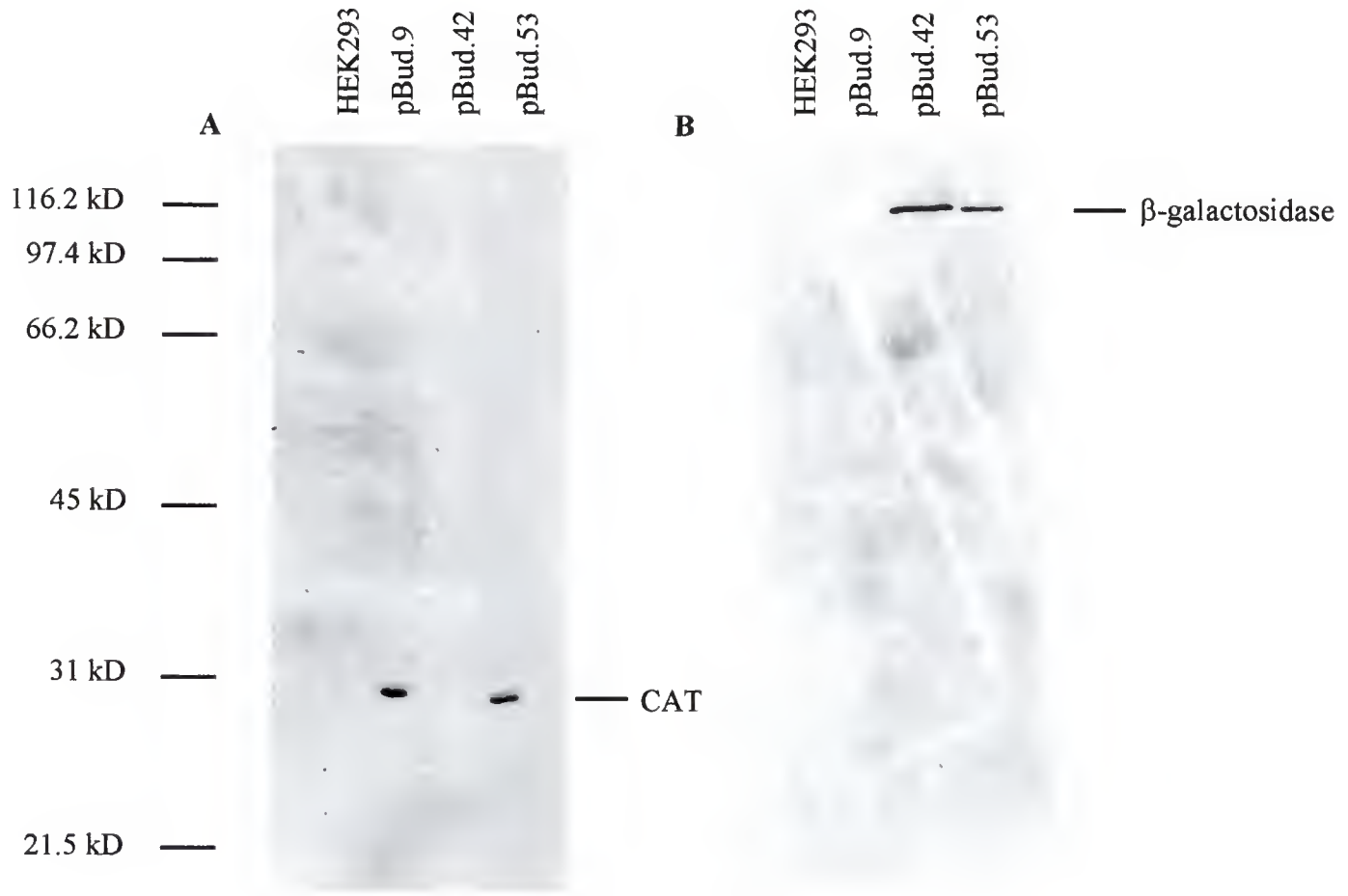

Figure 5-5. Western analysis of HEK293 cells stably expressing control plasmid pBudCE4/*lac*Z/CAT. 50μg protein from cell lysates of Zeocin-resistant clones were separated on a 10% Tris-glycine gel and transferred to nitrocellulose. A, Blot was incubated with anti-V5 antibodies. B, Blot was stripped and probed with anti-*myc* antibodies.

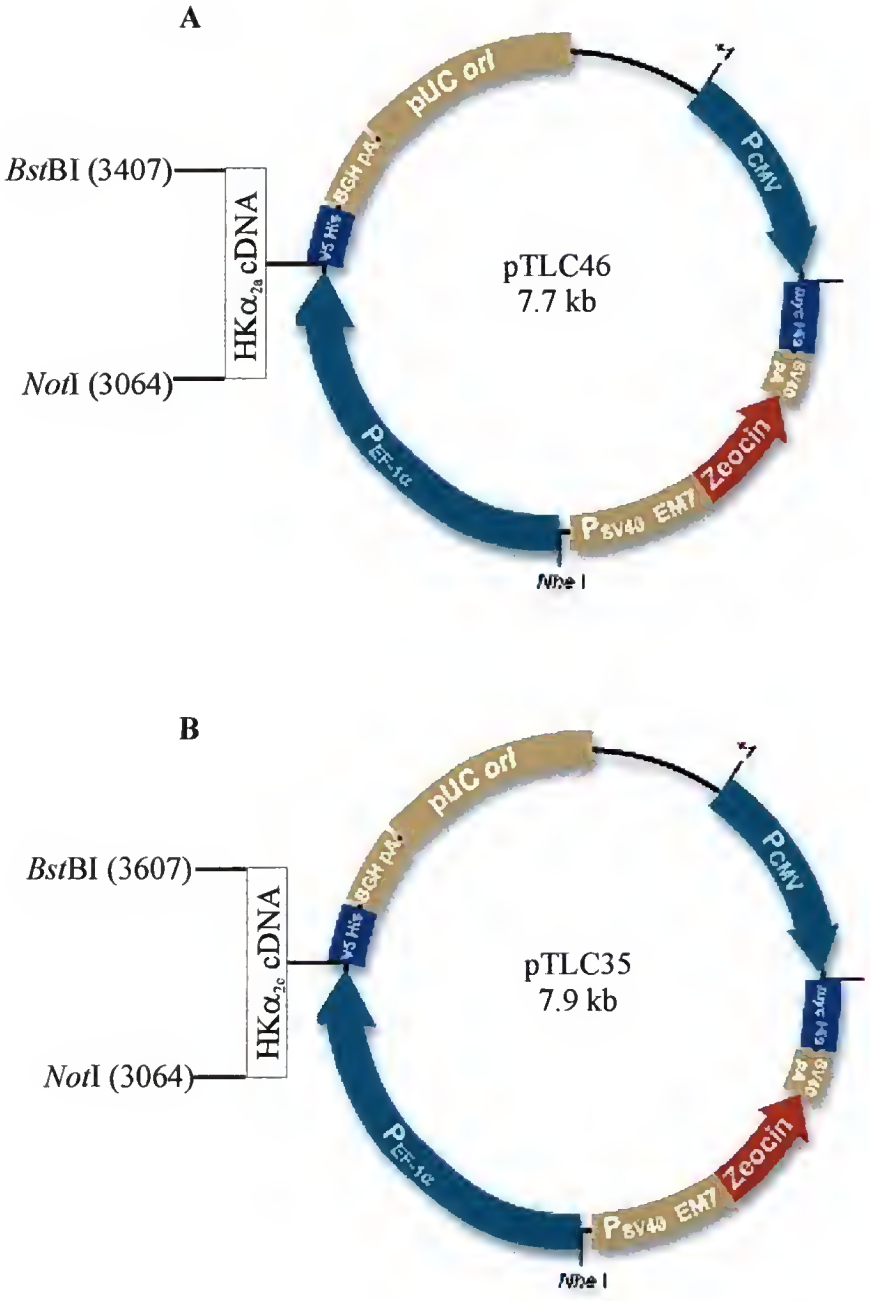

Figure 5-6. Stable expression constructs. A, Plasmid pTLC46($HK\alpha_{2a}$). Plasmid pTLC35($HK\alpha_{2c}$). C, Plasmid pTLC33($NaK\beta_1$). D, Plasmid pTLC47($HK\alpha_{2a}/NaK\beta_1$). E, Plasmid pTLC37($HK\alpha_{2c}/NaK\beta_1$). The $HK\alpha_{2a}$ and $HK\alpha_{2c}$ cDNAs were cloned in frame with the V5 epitope tag. Figure was adapted from Invitrogen catalog.

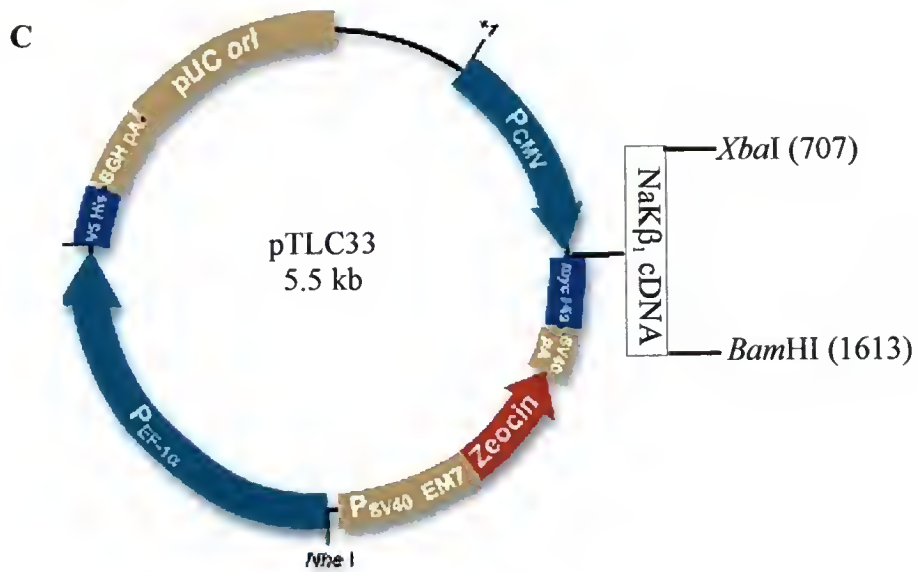

Figure 5-6--continued

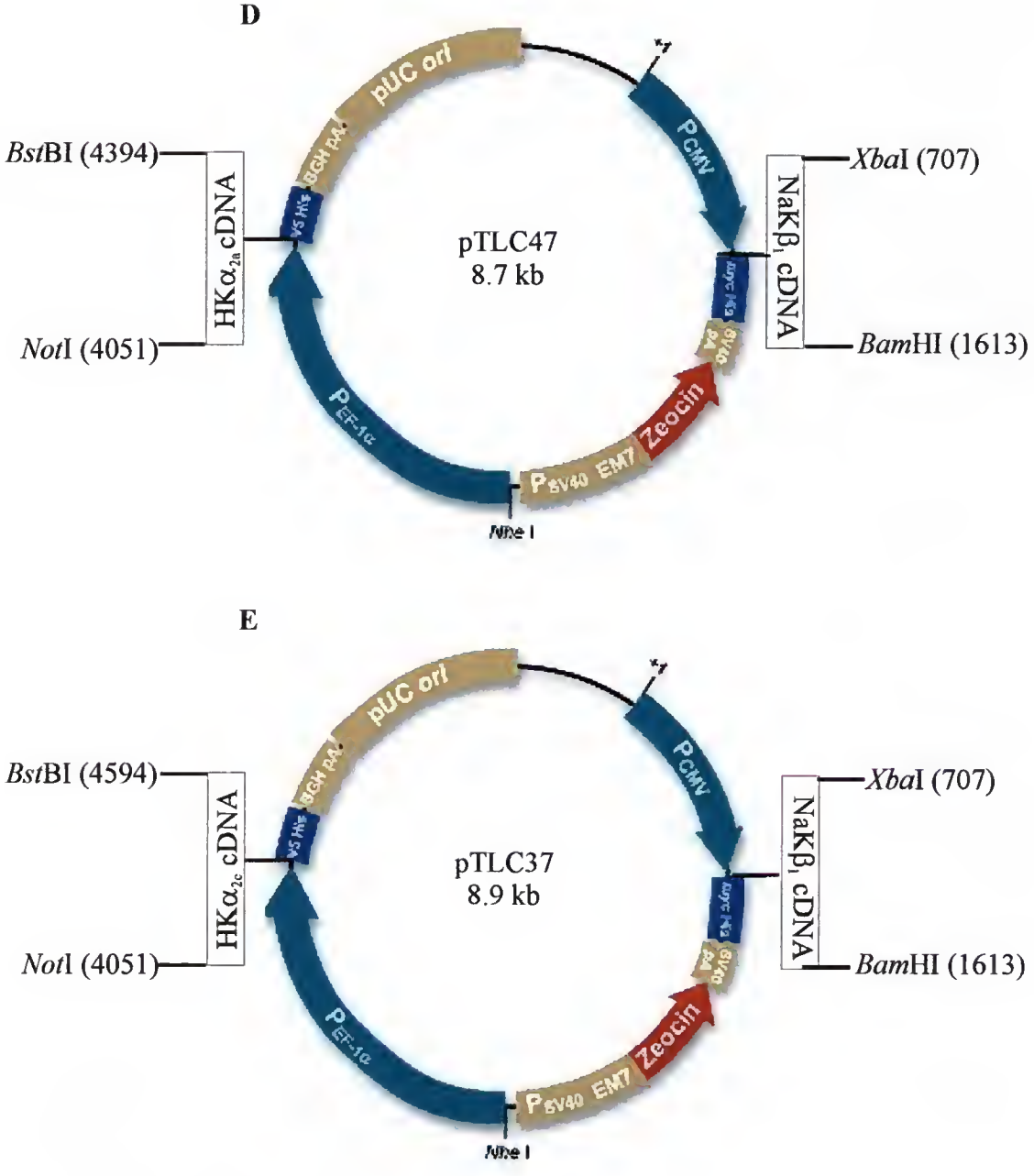

Figure 5-6--continued

proteins (Figure 5-7A). The different mobilities of $HK\alpha_{2a}$-V5 and $HK\alpha_{2c}$-V5 were clearly visible. The blot was stripped and re-probed with $NaK\beta_1$ subunit antibodies (Figure 5-7B). The glycosylated $NaK\beta_1$ protein was detected in lower levels in cells transiently transfected with pTLC33($NaK\beta_1$) versus cells transfected with pTLC47($HK\alpha_{2a}$/$NaK\beta_1$)or pTLC37($HK\alpha_{2c}$/$NaK\beta_1$). This result was reproducible. It appeared that co-expression of the $HK\alpha_2$ subunit isoforms stabilized the $NaK\beta_1$ protein. In any case, the transient transfections demonstrated that the constructs encoded the correct full-length proteins.

HEK293 cells were transfected with linearized plasmids encoding either subunit alone or as a pair of α and β subunits. Stable integration of the plasmids was selected by Zeocin resistance. Single Zeocin-resistant clones were isolated, and the cell lines were expanded for protein analysis. An initial screen of twenty clones for cells stably expressing $NaK\beta_1$ protein alone proved to be highly successful (Figure 5-8). Out of the seven clones that were analyzed, all of the cells were clearly producing glycosylated $NaK\beta_1$ protein to varying levels. Unfortunately, screening for the presence of $HK\alpha_{2a}$-V5 and $HK\alpha_{2c}$-V5 fusion proteins in HEK293 stable cell lines proved to be problematic. Although the transfections produced single clones, none of the cell lines were expressing full-length protein. More than fifty clones were screened in an attempt to find cells that could express the $HK\alpha_2$ fusion proteins. Either chromosomal integration disrupted the $HK\alpha_2$ cDNAs disproportionately or the fusion proteins were unstable during plasma membrane preparations. Indeed, multiple faint bands recognized by V5 antibodies were detected occasionally on Western blots, suggesting instability of the $HK\alpha_2$-V5 fusion proteins during isolation. Several protease inhibitor cocktails were added to the plasma

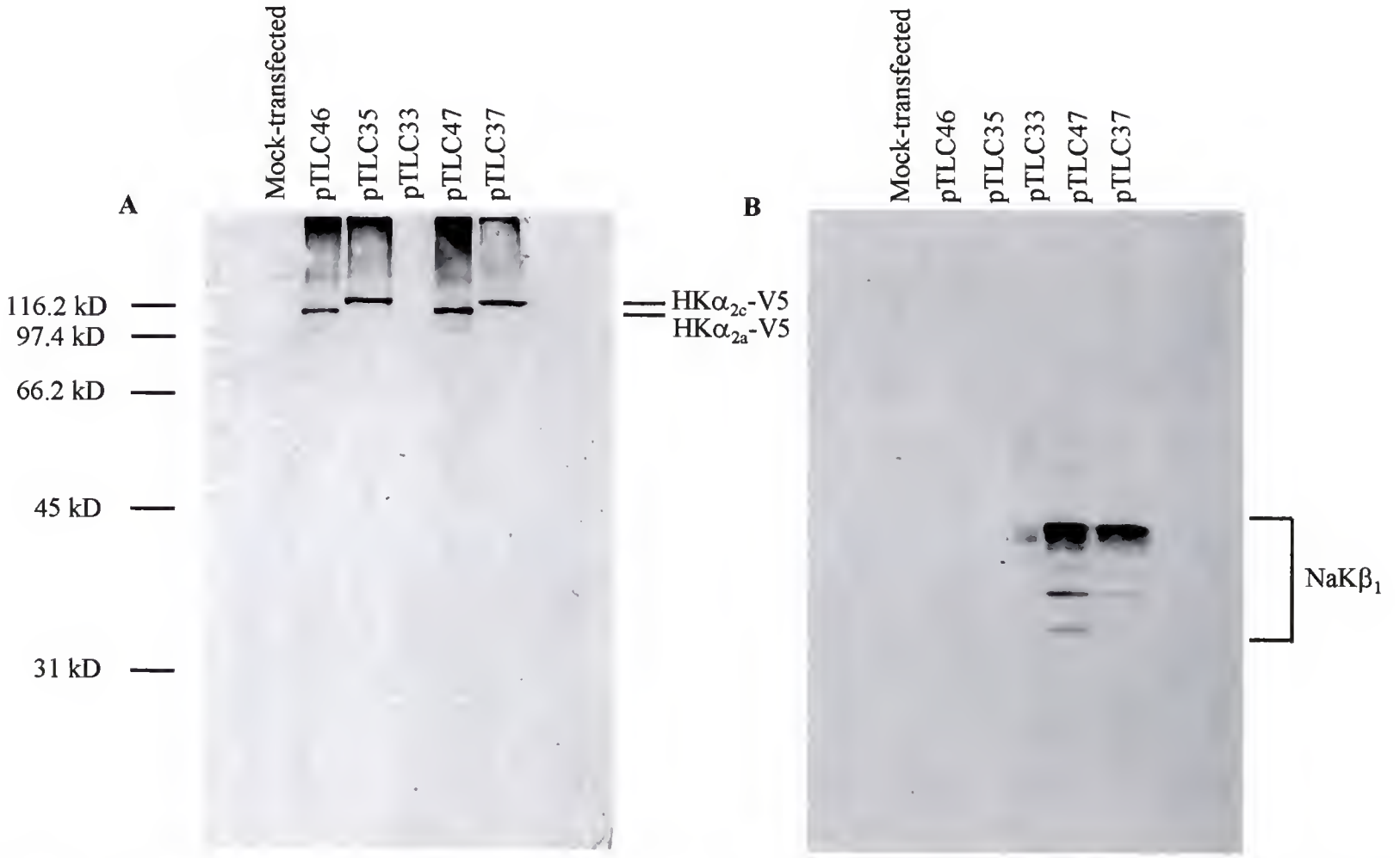

Figure 5-7. Western analysis of COS-1 cells transiently expressing $HK\alpha_{2a}$-V5, $HK\alpha_{2c}$-V5, and $NaK\beta_1$ proteins. COS-1 cells were transiently transfected, and crude membranes were prepared 48 hours after transfection. 50 μg membrane protein was separated on a 10% Tris-glycine gel and transferred to nitrocellulose. A, Blot was incubated with anti-V5 antibodies. B, Blot was stripped and probed with anti-rabbit $NaK\beta_1$ antibodies.

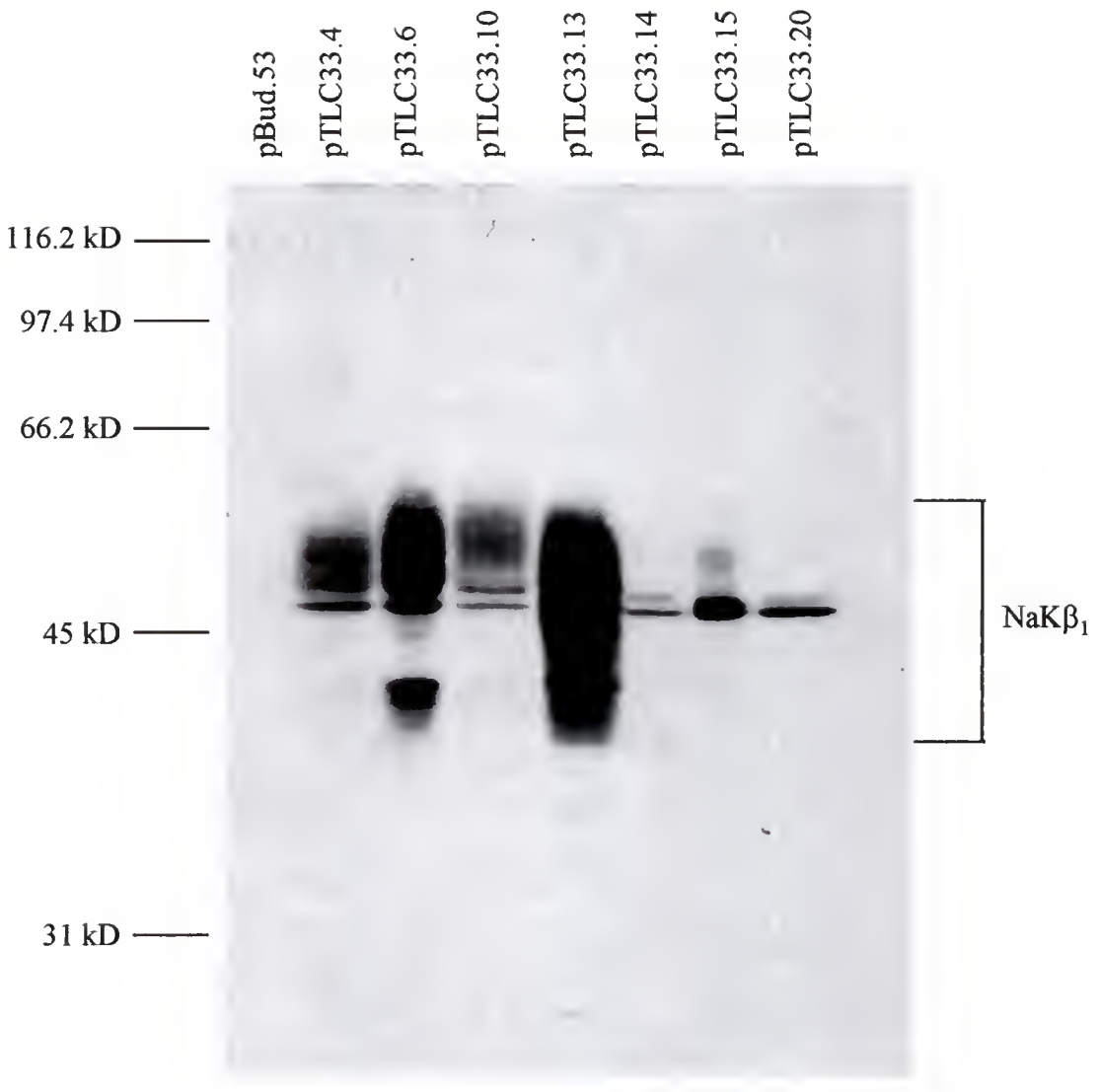

Figure 5-8. Differential expression of rabbit $NaK\beta_1$ protein in stable HEK293 clones. Clones were isolated and protein was analyzed for the presence of $NaK\beta_1$ by western analysis using anti-mouse rabbit $NaK\beta_1$ antibodies.

membrane preparations in an attempt to stabilize the proteins, but similar results were observed.

Another hypothesis for the absence of the $HK\alpha_2$-V5 fusion proteins was the possibility that the cDNAs were either not stably integrating in the genome or that the $HK\alpha_2$ cDNAs were disrupted. To determine if this was the case, total RNA was isolated from several Zeocin-resistant clones transfected with either pTLC47($HK\alpha_{2a}/NaK\beta_1$) or pTLC37($HK\alpha_{2c}/NaK\beta_1$). These clones had previously been screened by Western analysis, and no $HK\alpha_2$-V5 fusion proteins were detected. The total RNA was examined by Northern analysis with a probe to the common region of the $HK\alpha_2$ cDNAs. The presence of what appeared to be a full-length $HK\alpha_2$ transcript was detected in each of the five clones screened (Figure 5-9). To confirm that they were indeed full-length transcripts, RT-PCR was performed to amplify the 3' region of $HK\alpha_{2a}$ and $HK\alpha_{2c}$ cDNAs. Primer BC230 (anneals at nt 1264 in $HK\alpha_{2a}$ cDNA; anneals at nt 1607 in $HK\alpha_{2c}$ cDNA) and primer TC26 (anneals at BGH reverse priming site in pBudCE4) amplified a 2 kb band, as expected in each reaction for this primer pair (Figure 5-10). The PCR reactions were sequenced, and the resulting sequence clearly showed the presence of the two cDNAs with the V5 and polyhistidine epitope tags intact. This strongly suggested that in at least some clones, the $HK\alpha_2$ cDNAs were intact and transcribed. Therefore, it seemed that the problem with the lack of expression of $HK\alpha_{2a}$-V5 and $HK\alpha_{2c}$-V5 fusion proteins in HEK293 cells was not a result of integration difficulties of the subunit cDNAs. A likely explanation was the instability of the fusion proteins during preparation from the HEK293 cells.

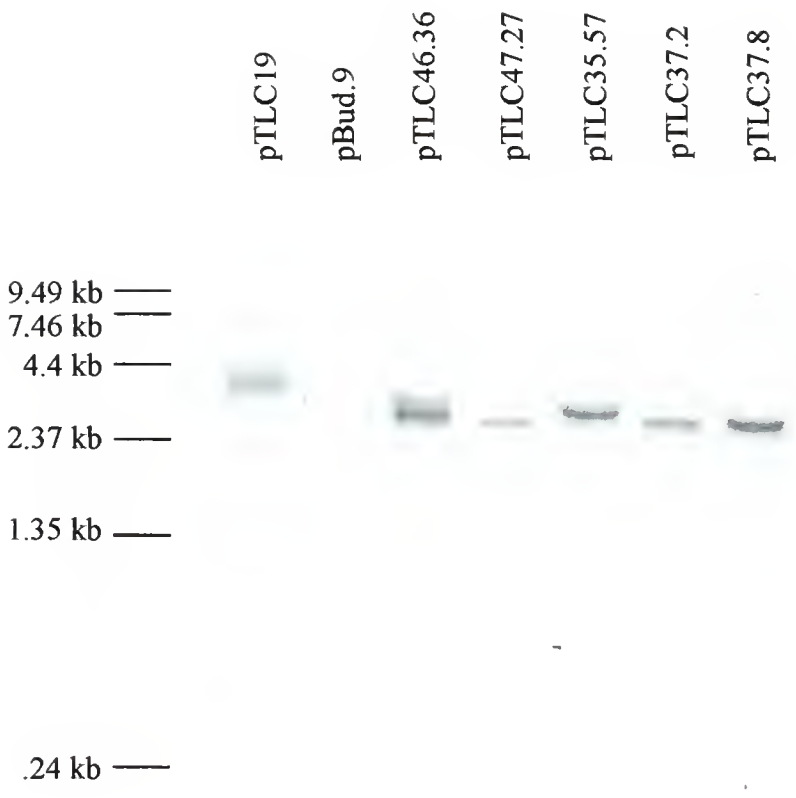

Figure 5-9. Northern analysis of HEK293 cells stably expressing $HK\alpha_{2a}$ or $HK\alpha_{2c}$ transcripts. Total RNA (10 μg) was separated on a denaturing gel and transferred to nylon membrane. A probe specific to the common region of $HK\alpha_{2a}$ and $HK\alpha_{2c}$ was randomly labeled with ^{32}P and hybridized to the membrane. Total RNA from HEK293c18 cells episomally expressing pTLC19($HK\alpha_{2a}$) was used as a positive control.

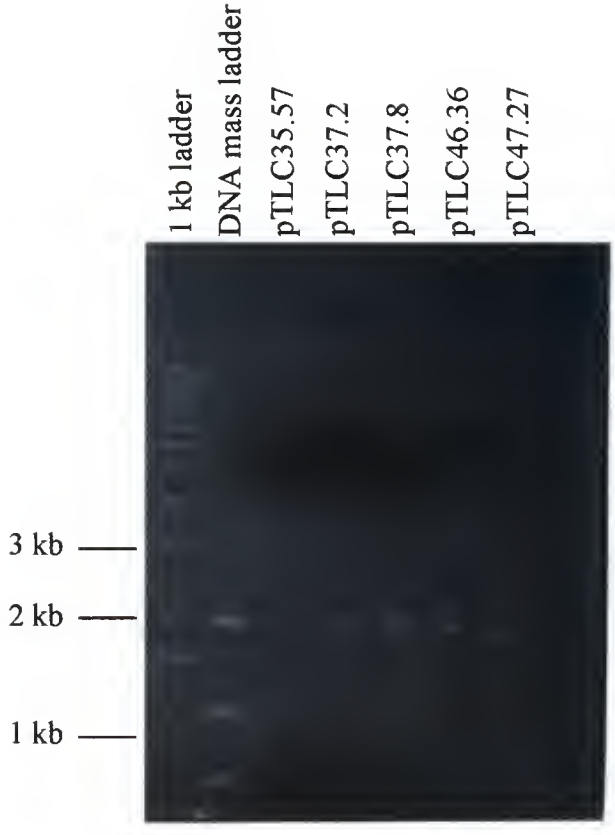

Figure 5-10. Agarose gel analysis of HKα_2 RT-PCR reactions from stable HEK293 cells.Total RNA was isolated from stable clones, and RT-PCR was conducted primers BC230 and TC26. 10% of the PCR reaction was analyzed on a 0.8% agarose gel.

Transient Expression

The $HK\alpha_{2a}$-V5 and $HK\alpha_{2c}$-V5 fusion proteins and $NaK\beta_1$ protein were easily expressed and detected transiently in COS-1 cells (Figure 5-7). Therefore, I chose to use that system to functionally express the renal H^+,K^+-ATPases. ^{86}Rb transport is a common method used to study H^+,K^+-ATPase activity in a heterologous expression system. However, ^{86}Rb is a difficult radioisotope to handle since it is both a high-energy β and γ emitter. ATP hydrolysis is another method that has been used by several investigators to examine H^+,K^+-ATPase activity. Because our laboratory had experience with ATP hydrolysis assays, this method seemed like the obvious choice to use. COS-1 cells were transiently transfected with pTLC47($HK\alpha_{2a}/NaK\beta_1$) or pTLC37($HK\alpha_{2c}/NaK\beta_1$). Plasma membranes were prepared from the cells and tested for ATP hydrolysis activity using a microassay that was sensitive to nanomole concentrations of phosphate. The assay was conducted in the presence and absence of 15 mM KCl. This concentration had been used by other investigators to analyze H^+,K^+-ATPase activity (12, 15, 197). However, no ATP hydrolysis activity could be detected above background levels using Tris-ATP. Since there was evidence to suggest that the H^+,K^+-ATPase may also function as a Na^+,K^+-ATPase, disodium salt ATP was also used., but similar results were obtained.

An early hypothesis as to the absence of the H^+,K^+-ATPase activity was that the α and β subunits were not interacting with each other. Immunofluorescence microscopy was used to analyze the localization of the $HK\alpha_{2a}$-V5 and $HK\alpha_{2c}$-V5 fusion proteins. It was well established that the β subunit was responsible for trafficking the α subunit to the plasma membrane. COS-1 cells were transiently transfected with pTLC46($HK\alpha_{2a}$), pTLC35($HK\alpha_{2c}$), pTLC47($HK\alpha_{2a}/NaK\beta_1$), and pTLC 37($HK\alpha_{2c}/NaK\beta_1$). The

hypothesis was that cells expressing only $HK\alpha_2$ subunits would have different staining patterns than cells expressing both α and β subunits. The $HK\alpha_2$ fusion proteins were visualized with the V5 antibodies and Texas Red secondary antibodies. No background staining was observed in mock-transfected cells (Figure 5-11E). Cells transiently transfected with pTLC46($HK\alpha_{2a}$) or pTLC35($HK\alpha_{2c}$) were clearly producing an abundance of $HK\alpha_{2a}$-V5 and $HK\alpha_{2c}$-V5 fusion proteins, and the staining was consistent with an ER-like localization (Figure 5-11A,B). However, the localization of the fusion proteins did not change dramatically when they were co-expressed with $NaK\beta_1$ (Figure 5-11C,D). These results suggested that the $HK\alpha_2$ fusion proteins were not interacting with $NaK\beta_1$ and moving to the plasma membrane. Western analysis of plasma membrane preparations confirmed that very little, if any, $HK\alpha_{2a}$ or $HK\alpha_{2c}$ fusion proteins were localized to the plasma membrane with $NaK\beta_1$ (Figure 5-12). It appeared that the $HK\alpha_2$-V5 fusion proteins had degraded to some extent, as indicated by mulitple fragments on the Western blot.

The $NaK\beta_3$ subunit isoform had recently been proposed as the mate to the $HK\alpha_2$ subunit isoforms (196), and it was demonstrated to produce a functional H^+,K^+-ATPase in HEK293 cells as assayed by ATP hydrolysis (197). Michelle Gumz, a graduate student in our laboratory, generated the full-length rabbit $NaK\beta_3$ subunit cDNA by RACE and RT-PCR. She cloned the cDNA in pTLC46($HK\alpha_{2a}$) and pTLC35($HK\alpha_{2c}$) behind the CMV promoter and in frame with the *myc* and polyhistidine epitope tags. The Western analysis of plasma membrane preparations from transiently transfected COS-1 cells demonstrated that the cells were capable of producing the $NaK\beta_3$ fusion protein

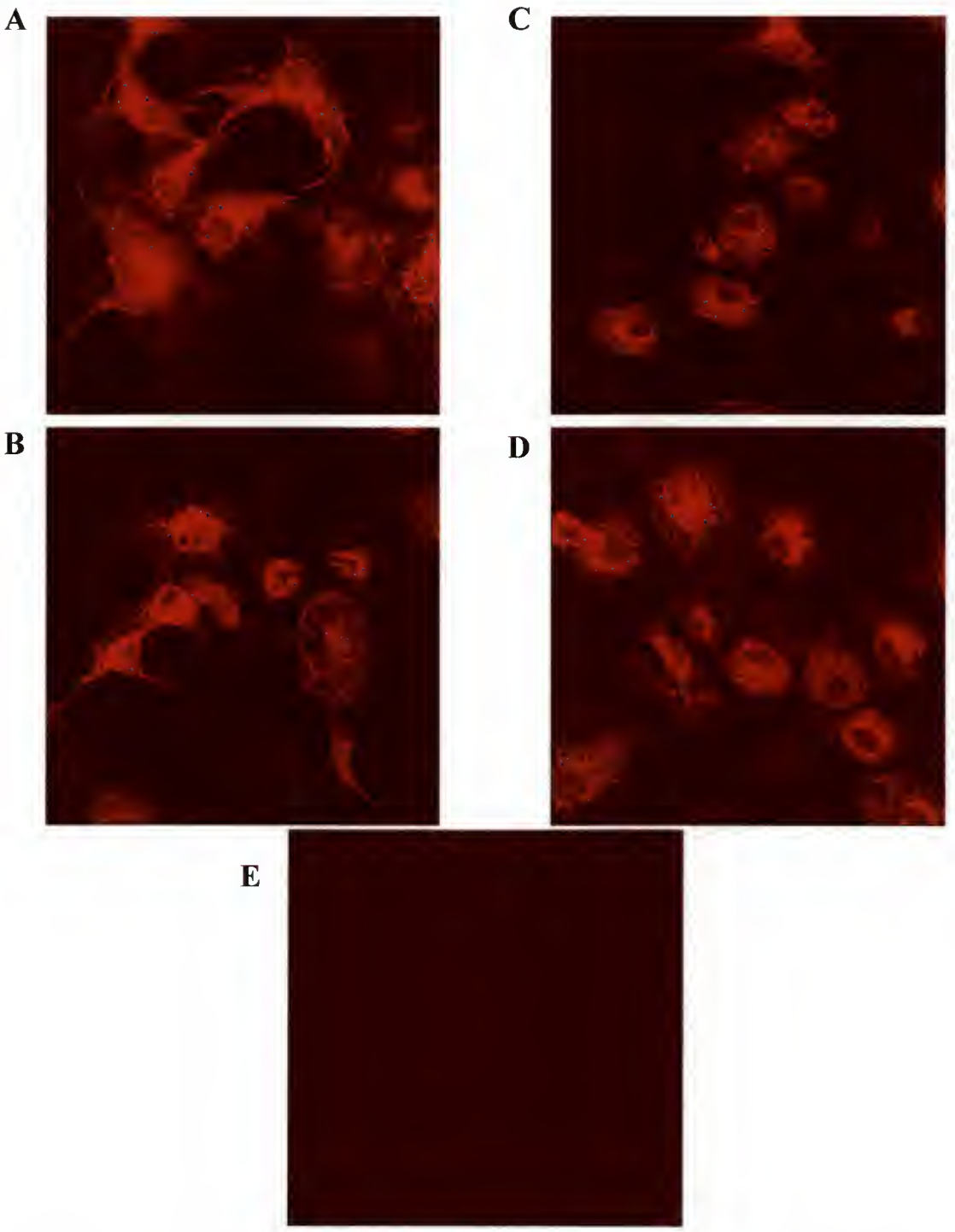

Figure 5-11. Localization of $HK\alpha_{2a}$-V5 and $HK\alpha_{2c}$-V5 fusion proteins in COS-1 cells. Twenty-four hours post transfection, COS-1 cells were stained with anti-V5 antibodies and Texas Red conjugated secondary antibodies. A, Plasmid pTLC46($HK\alpha_{2a}$). B, Plasmid pTLC35($HK\alpha_{2c}$). C, Plasmid pTLC47($HK\alpha_{2a}$/$NaK\beta_1$). D, Plasmid pTLC37($HK\alpha_{2c}$/$NaK\beta_1$). E, Negative control.

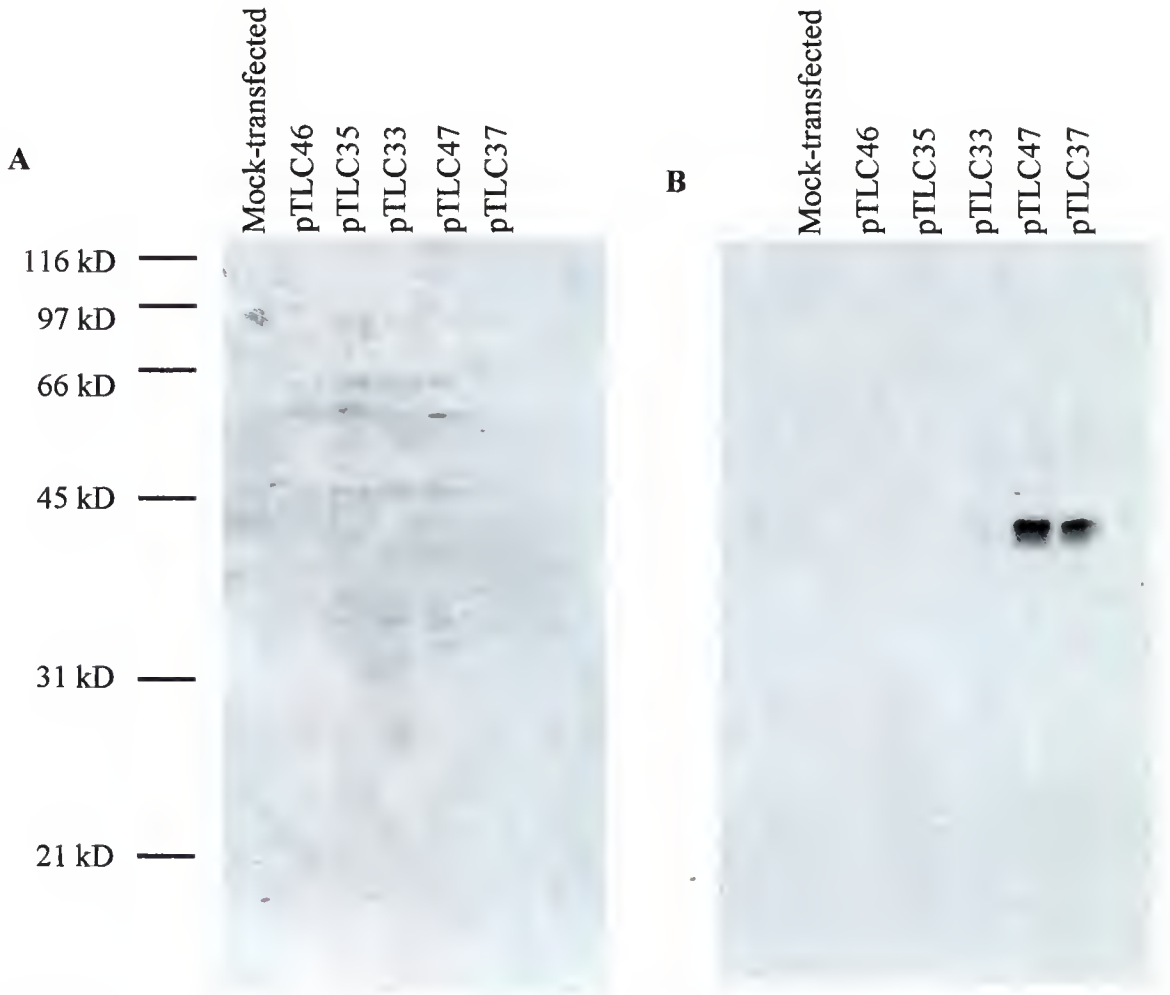

Figure 5-12. Western analysis of plasma membranes from COS-1 transient transfections. Plasma membrane-enriched fractions were isolated from COS-1 cells 48 hours post transfection. 50 μg protein was separated on a 10% Tris-glycine gel and were transferred to nitrocellulose. A. Blot was incubated with anti-V5 antibodies. B, Blot was stripped and incubated with anti-NaKβ_1 antibodies.

(Figure 5-13). However, ATP hydrolysis activity was not detected in COS-1 cells transiently transfected with pMLG24($HK\alpha_{2a}/NaK\beta_3$) or pMLG25($HK\alpha_{2c}/NaK\beta_3$).

Discussion

The episomal expression system was used as an initial attempt to establish cells which expressed the renal H^+,K^+-ATPases. To express the enzyme, both the α and the β subunits must be present. The episomal expression system seemed to be a reasonable method to use since each subunit could be maintained on separate episomes. In theory, there would be no problems with subunits being expressed at lower levels because they would not be integrated in the genome. However, the system had flaws that were not anticipated. HEK293c18 cells were able to readily express the $HK\alpha_{2a}$, $HK\alpha_{2c}$, and $NaK\beta_1$ transcripts when present as single episomes. When the second episome was introduced, however, the cells were unable to express each transcript at comparable levels. This became a problem when trying to detect activity because the expression levels of each subunit greatly varied. It seemed that the trouble with the episomal expression system was due to variances in the copy number of each plasmid. It was obvious that the copy number for each episome was unequal, and it was likely that one episome would be favored over the second episome. This probably arose from unequal segregation of mitosis during establishment of the cell lines.

There was another major problem with the episomal system. The expression of the $HK\alpha_{2a}$ and $HK\alpha_{2c}$ proteins was designed incorrectly. It was later determined that the multiple cloning region of the TOPO TA cloning vector contained two ATG's that serve as start codons. These were not immediately recognized and were left in place during the expression of $HK\alpha_{2a}$ and $HK\alpha_{2c}$. This was disastrous to the translation of the proteins

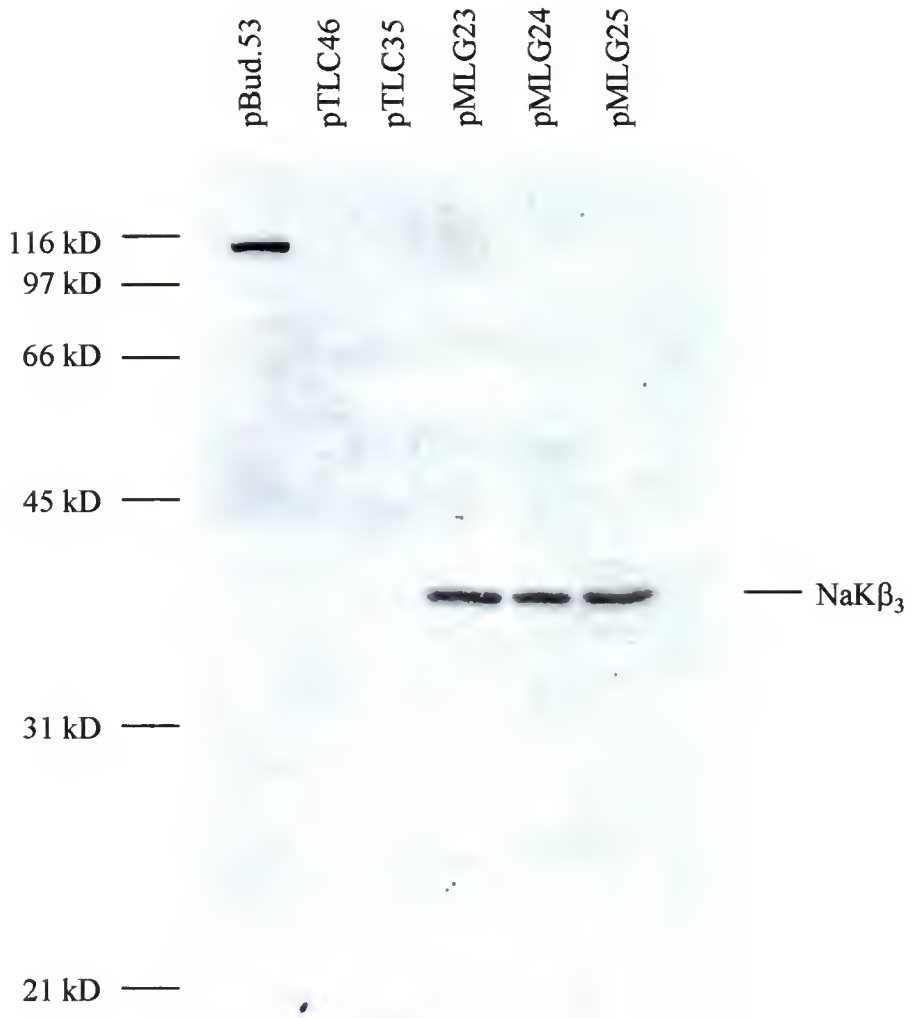

Figure 5-13. Western analysis of COS-1 cells transiently expressing rabbit NaKβ_3-*myc* fusion protein. Plasma membranes were isolated 48 hours post transfection. 50 μg protein was separated on a 10% Tris-glycine gel and transferred to nitrocellulose. Blot was incubated with anti-*myc* antibodies. Cell lysate from clone pBud.53 expressing β-galactosidase-*myc* fusion protein was used as a positive control.

because it caused the products to be out of frame. Although there were correctable problems preventing translation, the distribution of the episomal elements made it clear that this expression system would not work, so it was abandoned.

The stable expression system was used as a second attempt for the expression of the renal H^+,K^+-ATPases. The pBudCE4 expression vector seemed perfect for this system because both the α and the β subunits would be encoded on the same vector. The EF-1α promoter had never been tested in HEK293 cells, so its function needed to be confirmed. Clones were isolated that expressed CAT under the control of the EF-1α promoter, thereby proving that the promoter worked in HEK293 cells.

Clones were screened for the presence of $NaK\beta_1$ protein. Each of the seven clones readily expressed the $NaK\beta_1$ protein. The expression levels varied among the stable cell lines. This result was expected since the level of expression would differ depending on where the cDNA integrated in the genome. The expression of the $HK\alpha_{2a}$ and $HK\alpha_{2c}$ fusion proteins proved to be very difficult in HEK293 cells. No full-length proteins were detected by Western blot. The integration of each cDNA was confirmed by Northern blotting, RT-PCR, and sequence analysis. There was no clear explanation as to why the proteins would be unstable since other researchers have been able to express full-length $HK\alpha_{2a}$ protein in HEK293 cells (12, 87, 197). Sangan *et al.* (197) and Grishin *et al.* (87) established HEK293 cell lines which stably expressed rat and human $HK\alpha_{2a}$ proteins, respectively. Protein expression was demonstrated by Western analysis of crude membrane preparations using anti-$HK\alpha_{2a}$ antibodies. Asano *et al.* (12) transiently expressed guinea pig $HK\alpha_{2a}$ in HEK293 cells and detected the protein by Western

analysis. I compared the methods these researchers utilized to the procedure that I used to isolate proteins from HEK293 cells, and I was unable to discover any major difference.

However, the $HK\alpha_{2a}$-V5 and $HK\alpha_{2c}$-V5 fusion proteins were easily transiently expressed in COS-1 cells. Therefore, the transient expression system was ultimately used to analyze the renal H^+,K^+-ATPases. An ATP hydrolysis microassay was used as an alternative to ^{86}Rb transport for studying the H^+,K^+-ATPase activity. This assay had been validated by several researchers in the field (12, 15, 197). Plasma membrane preparations from COS-1 cells transiently expressing $HK\alpha_{2a}$-V5 or $HK\alpha_{2c}$-V5 fusion proteins with the $NaK\beta_1$ subunit had no detectable ATP hydrolysis activity above background levels. This was in disagreement with published observations by Sangan *et al.* (197). These authors were able to detect ATP hydrolysis in an HEK293 cell line which stably expressed rat $HK\alpha_{2a}$ and $NaK\beta_1$. The ATP hydrolysis activity, expressed as nmol P_i/mg/min, was roughly fifty-fold higher than that found in untransfected HEK293 cells. However, it seems that this group may have been conducting the assay improperly. Instead of taking time points throughout the course of the reaction, the researchers were taking a single endpoint reading. Even high-grade ATP contains some amount of free phosphate that could easily be mistaken for ATP hydrolysis activity if a time course is not conducted. Perhaps the authors were not detecting real H^+,K^+-ATPase activity. Dr. Michael Caplan indicated that his group has never been able to detect H^+,K^+-ATPase activity for ATP1AL1 by the reported methods (personal communication).

It is well established that the β subunit of P-type ATPases traffics the α subunit to the plasma membrane. Grishin *et al.* (87) transiently expressed ATP1AL1 with or without HKβ in COS-1 cells and analyzed the cell surface delivery of ATP1AL1.

Immunofluorescence microscopy demonstrated that ATP1AL1 was retained in the ER unless co-expressed with HKβ. Once HKβ was expressed, ATP1AL1 was found predominantly at the cell surface. This was not the case, however, for the $HK\alpha_2$-V5 fusion proteins reported here. Immunofluorescence microscopy of COS-1 cells transiently expressing the $HK\alpha_2$-V5 fusion proteins and $NaK\beta_1$ demonstrated that the $HK\alpha_2$ proteins were not transported to the plasma membrane, and Western analysis suggested that the proteins remained in the ER. Therefore, the $HK\alpha_2$ fusion proteins were apparently not interacting with the $NaK\beta_1$ subunit, resulting in an absence of detectable H^+,K^+-ATPase hydrolysis activity at the plasma membrane. This conclusion is in direct contrast to the immunopreciptation studies which demonstrated that the $NaK\beta_1$ subunit isoform associated with $HK\alpha_{2a}$ *in vivo* (44, 132). In both studies, subunit assembly was detected as co-immunoprecipitation of $HK\alpha_{2a}$ and a β subunit using an anti-$HK\alpha_{2a}$ antibody. The immunoprecipitated proteins were separated on a polyacrylamide gel and transferred to nitrocellulose for Western analysis. The Western blots were screened with antibodies to known β subunits, and in both cases, the $NaK\beta_1$ antibody detected a protein of the appropriate mass for $NaK\beta_1$. However, since the membranes were not solubilized prior to immunoprecipitation, there is a possibility that the immunoprecipitation pulled down membrane fragments containing Na^+,K^+-ATPases so that $NaK\beta_1$ may not have been in direct association with $HK\alpha_{2a}$. It may be that *in vivo* the $HK\alpha_{2a}$ subunit and $NaK\beta_1$ subunit do not interact and may have a tendency to associate during membrane isolation. These are questions that need to be answered in order to better understand the conflicting results.

The NaKβ_3 subunit isoform had also been implicated as the mate to the HKα_2 subunit isoforms by both immunoprecipitation (196) and functional expression (197). Another graduate student in our laboratory generated the rabbit NaKβ_3 cDNA by RACE and RT-PCR. I examined whether the HKα_2-V5 fusion proteins, when expressed transiently with NaKβ_3, would produce a functional enzyme complex. Again, no detectable ATP hydrolysis activity was observed in COS-1 cells transiently expressing pMLG24(HKα_{2a}/NaKβ_3) or pMLG25(HKα_{2c}/NaKβ_3). This was again in contrast with previously published data (196, 197). The troubles associated with using immunoprecipitation to assign an interaction between the α and β subunits in crude cell lysates, as well as the possible problems with the ATP hydrolysis method have been discussed above. The authors, however, did not have convincing evidence of cell surface delivery of HKα_{2a} with NaKβ_3. Stable HEK293 cell lines expressing only HKα_{2a} showed very little differences in staining patterns when the protein co-expressed with NaKβ_3. The researchers did not address this issue, but the observation is in agreement with a very recent paper discussed below.

My data suggests that the rabbit HKα_{2a} and HKα_{2c} proteins do not interact, or interact at very low levels, with either NaKβ_1 or NaKβ_3, two β subunits believed to associate with the renal HKα_2 subunits *in vivo*. My observations are in agreement with recent data from Geering *et al.* (83). The authors examined subunit interactions between ATP1AL1 with all of the known β subunit isoforms in *Xenopus laevis* oocytes. The NaKβ_1 subunit formed very few stable complexes with ATP1AL1. The NaKβ_3 subunit was able to form complexes with ATP1AL1, but the complexes were impaired in their exit from the ER. This observation corresponds to the absence of a dramatic change in

the cell surface delivery of $HK\alpha_{2a}$ when co-expressed with $NaK\beta_3$ by Sangan *et al.* (197). Based on this study, it is not surprising that the rabbit $HK\alpha_2$ proteins did not form stable complexes with $NaK\beta_1$ or $NaK\beta_3$, as originally believed. In fact, the only β subunits the authors determined were capable of forming efficient stable complexes at the plasma membrane were the HKβ subunit and the $NaK\beta_2$ subunit. However, these complexes exhibited weak interactions and were relatively trypsin-sensitive. The authors concluded that none of the known β subunits is the real mate to ATP1AL1, but an unidentified genuine β subunit should have structural features similar to HKβ and $NaK\beta_2$. Our laboratory has yet to test these β subunits thoroughly. Experiments are currently in progress in our laboratory in an attempt to generate functional enzyme complexes with the $HK\alpha_2$ fusion proteins and the HKβ subunit, as well as with rabbit $NaK\beta_2$.

CHAPTER 6
CONCLUSIONS AND FUTURE STUDIES

E. coli F_1F_0 ATP Synthase

Conclusions

Our laboratory has studied the *b* subunit of the *E. coli* F_1F_0 ATP synthase for over a decade. Although there is little sequence homology between *b* subunits and only a few mutations result in a loss of enzyme function, several functionally significant sites have been identified. Mutagenesis studies established that $b_{Ala\text{-}79}$ was important in both assembly and stability of the enzyme (146, 147). The b_{sol} expression system demonstrated that the major defect of replacements at $b_{Ala\text{-}79}$ was on dimerization of the *b* subunits, and dimerization appeared to be an important event in enzyme assembly (218). By the mid 1990's, the field viewed the *b* subunit dimer as a rigid rod, providing the structural integrity to the peripheral stalk linking F_1 and F_0. Insertion and deletion analysis in the middle of the stalk region of the *b* subunit provided convincing evidence that the second stalk is likely not be a rigid structure (217, 219). In general, mutations in the *b* subunit affected assembly of the F_1F_0 complex. However, the data described in this dissertation offers a more dynamic role to the *b* subunit.

The work presented in Chapter 3 focused on the conserved amino acid $b_{Arg\text{-}36}$. This amino acid was conserved among a diverse group of bacterial *b* subunits. Mutations were constructed at $b_{Arg\text{-}36}$ in order to investigate its importance in the function of the *b* subunit stator. The effects of the $b_{Arg\text{-}36}$ replacements were studied by complementation

of strain KM2(Δ*b*). The mutant strains had growth characteristics that indicated deficiencies in oxidative phosphorylation to varying degrees. Substitution of $b_{Arg\text{-}36}$ with *Lys, Ser, Cys*, and *Tyr* resulted in moderate reductions in the steady-state level of F_1F_0 ATP synthase in the membrane. In each case, the intact enzyme with these altered *b* subunits were functional as shown by growth on succinate minimal media. The $b_{Arg\text{-}36\rightarrow Ile}$ and $b_{Arg\text{-}36\rightarrow Glu}$ substitutions reduced the number of assembled enzyme complexes in the cell, suggesting an assembly defect. However, more importantly, the remaining intact enzyme complexes appeared to be nonfunctional as shown by absence of colony formation on succinate minimal media. This was in stark contrast to almost all other *b* subunit mutations. These results suggested that while $b_{Arg\text{-}36}$ is not essential for F_1F_0 ATP synthase complex formation, the amino acid at this position exerts significant influence on the function of the enzyme.

A more interesting result became clear when ATP-driven proton translocation from cells expressing the $b_{Arg\text{-}36\rightarrow Glu}$ mutation was analyzed. Although the strain was unable to support growth on minimal succinate, the cells had substantial amounts of ATP-driven proton pumping activity. The activity was comparable to other strains that were able to support growth minimal succinate media. The data indicated that the $b_{Arg\text{-}36\rightarrow Glu}$ mutation was representative of the small group of substitutions affecting the F_0 subunits which uncouple proton translocation from ATP synthesis in F_1. This is the first mutation of this type reported in the *uncF*(*b*) gene. Interestingly, the defect caused by the $b_{Arg\text{-}36\rightarrow Glu}$ substitution had a greater influence on $\Delta\mu H^+$-driven ATP synthesis than on ATP-driven proton pumping. This represented a conundrum; the enzyme apparently operated better in the direction of ATP hydrolysis than in the direction of ATP synthesis.

Experimental evidence conclusively demonstrated that the F_1F_0 ATP synthase functions as a rotary motor. Current models propose that proton translocation through F_0 drives the rotation of the *c* subunit ring past the *a* subunit. A proton crosses the membrane as each *c* subunit passes critical sites on the *a* subunit. The energy generated by proton movement is transferred to F_1 through the coupled rotation of γε subunits. The asymmetry of the γ subunit rotating inside the $\alpha_3\beta_3$ hexamer causes conformational changes in the β subunits housing the catalytic sites. The conformational changes in the β subunits permit the binding of ADP + P_i and the release of ATP from catalytic sites. The primary role of the *b* subunit as the second stalk is to serve as a stator, preventing rotation of the $\alpha_3\beta_3$ hexamer with γε, allowing the sequential conformational changes to occur at the catalytic sites.

The $b_{Arg\text{-}36}$ residue is located at the base of the second stalk, proximal to the lipid bilayer. Recently, a $b_{Arg\text{-}36\rightarrow Cys}$ mutant was shown to form a cross-link to the *a* subunit, suggesting that some of the *b* subunit residues near the membrane, including $b_{Arg\text{-}36}$, interact with the cytoplasmic loops of the *a* subunit (149). There are several possible roles for this relationship. The interaction may be important for attaching the *b* dimer to the *a* subunit, thereby preserving the integrity of the stator. Since the *b* subunit is necessary for proper assembly of a functional F_0 channel, the interactions between *b* and *a* at or near $b_{Arg\text{-}36}$ may play a role in assembly of the F_0 complex. However, since the site occupied by $b_{Arg\text{-}36}$ was sensitive to mutations, the interactions between *b* and *a* may have a more functional, rather than structural, influence on coupling. Then what effect does the $b_{Arg\text{-}36\rightarrow Glu}$ substitution have on the stator, and possibly interactions with *a*, so that proton translocation is uncoupled from ATP synthesis?

The *a* subunit contains functional groups essential for the transport of protons across the membrane. However, $a_{Arg\text{-}210}$ is the only amino acid in the *a* subunit that is absolutely required for F_1F_0 ATP synthase function. This amino acid is in the fourth transmembrane helix and in close contact with the expected position of $c_{Asp\text{-}61}$, the site of proton binding. Current models propose that the *a* subunit contains two half-channels that offer access to the site of protonation of $c_{Asp\text{-}61}$ from the periplasmic space and deprotonation of $c_{Asp\text{-}61}$ to the cytoplasm. It is believed that the $a_{Arg\text{-}210}$ residue facilitates a pK_a shift of the $c_{Asp\text{-}61}$ carboxylate to a low pK_a form. Protonation of this form is driven by the high local concentration of protons, and once the site is protonated, a pK_a-dependent conformational change occurs, driving rotation of the *c* subunit ring, and causes the proton to be released from the other side of the membrane. The $b_{Arg\text{-}36\rightarrow Glu}$ substitution, through its interactions with *a*, may cause a conformational change in the *a* subunit so that the two half channels are aligned and short circuits the proton translocation mechanism. Protons would, in theory, freely pass through the channel without driving rotation of the *c* subunit ring, and thereby resulting in an uncoupled enzyme complex.

Counter-clockwise rotation of the *c* subunit ring results in ATP synthesis, whereas clockwise rotation results in ATP hydrolysis. The $b_{Arg\text{-}36\rightarrow Glu}$ mutation might cause rotation of the *c* subunit ring and the central stalk to occur more easily in the direction of ATP hydrolysis than in the direction of ATP synthesis. This theory can be compared to the function of a ratchet wrench. A ratchet can turn in one direction rather easily because there is nothing hindering its rotation. However, the teeth within the ratchet impede rotation in the opposite direction. The $b_{Arg\text{-}36\rightarrow Glu}$ mutation may cause a conformational

change in the *a* subunit or the *c* subunit ring so that rotation is hindered in the direction of ATP synthesis.

Three to four protons are translocated through F_0 before the production of one molecule of ATP. Since protons are thought to be bound and released individually, energy must be stored somewhere in the enzyme for the ATP production. Junge and colleagues proposed that the elastic energy is stored within the inherent flexibility of the *b* subunit (38). It is possible that the negative charge of the glutamic acid residue at the site occupied by $b_{Arg\text{-}36}$ would cause conformational changes in the structure of the *b* subunit. The conformational changes may decrease its energy storage function. Hence, protons would be wastefully translocated across the membrane without ATP synthesis.

Future Studies

The search for second-site suppressors that counteract the effects of the $b_{Arg\text{-}36\rightarrow Glu}$ mutant is an immediate experiment to carry out. Second-site suppressors would likely be identified in the *a* and/or *c* subunits. This approach was attempted in the laboratory by Dr. Paul Sorgen. In a single experiment, he was able to identify several single colony isolates from the $b_{Arg\text{-}36\rightarrow Glu}$ strain that acquired the ability to support growth on minimal succinate media. However, when each clone was sequenced, none of the mutations identified proved capable of directly suppressing the original mutation. In fact, the $b_{Arg\text{-}36\rightarrow Glu}$ mutation carried in the plasmid reverted back to wild type sequence. This result was attributed to the design of the *b* subunit deletion strain. The N-terminal portion of the *b* subunit, including $b_{Arg\text{-}36}$, was left in the chromosome. A cross-over event likely occurred between the small region of the chromosomal *b* subunit and the plasmid *b* subunit to result in wild type sequence. Before second-site suppressors are attempted

again, the $b_{Arg\text{-}36\rightarrow Glu}$ mutation has to be moved to pRPG54, a plasmid encoding the entire *unc* operon. The resulting plasmid could be studied in strain 1100Δ*bc* in which the *unc* operon has been deleted. This should solve the problem originally associated with the search for second-site suppressors. If a second-site suppressor is identified, its location in the enzyme could help to understand the effects of the $b_{Arg\text{-}36\rightarrow Glu}$ substitution.

The results of the uncoupling mutant $b_{Arg\text{-}36\rightarrow Glu}$ suggest a functional bias in the stator depending on whether the rotor is turning in the direction of hydrolysis or synthesis. It would be truly interesting to analyze the effects that the $b_{Arg\text{-}36\rightarrow Glu}$ mutation has on rotation of the *c* subunit ring and γε. Researchers have demonstrated that the central stalk rotates relative to the $\alpha_3\beta_3$ hexamer by a variety of methods. Each one of the methods manipulated the enzyme as an ATPase to illustrate rotation. However, the $b_{Arg\text{-}36\rightarrow Glu}$ mutant is uncoupled in the direction of ATP synthesis. At this time, no one has succeeded in demonstrating rotation coupled to the synthesis of ATP. This is a difficult experiment to perform since a proton gradient must be imposed across the membrane in order to synthesize ATP. The F_1F_0 ATP synthase would be engineered with a His-tag on the α subunits and a fluorescently-labeled actin filament on the *c* subunit ring. F_1F_0 ATP synthase would have to be reconstituted into an artificial membrane bilayer. The enzyme could be attached to a Ni^{2+} slide through interactions with the His-tagged α subunit, as originally described by Noji *et al.* (172) and Sambongi *et al.* (195). Once the enzyme is affixed to the slide, a proton gradient could be induced by manipulating the buffer on either side of the membrane. Then, rotation of the *c* subunit ring could be observed by revolutions of the fluorescent actin filament.

The field of F_1F_0 ATP synthase would be further advanced with a high-resolution structure of the *b* subunit or b_{sol}. However, any high-resolution structural data for the *b* subunit has been unsuccessful, probably due to its inherent flexibility. The structure of the *b* subunit stator and its interactions with other subunits would offer insight as to the potential role of the *b* subunit in energy coupling, as suggested by the uncoupling mutant $b_{Arg\text{-}36\rightarrow Glu}$.

H^+,K^+-ATPase

Conclusions

Our laboratory identified a novel $HK\alpha_2$ subunit isoform in the rabbit kidney that we have termed $HK\alpha_{2c}$ (35). The $HK\alpha_{2c}$ cDNA was the product of an alternative splicing event in the $HK\alpha_2$ gene. This splicing event results in the production of a sixty-one amino acid extension at the N-terminus of the $HK\alpha_{2a}$ protein, resulting in $HK\alpha_{2c}$. The N-terminus of $HK\alpha_{2c}$ has two putative phosphorylation sites, not found in $HK\alpha_{2a}$, that may act to regulate its H^+,K^+-ATPase activity.

A likely mate to the $HK\alpha_2$ subunit isoforms was believed to be the $NaK\beta_1$ subunit as demonstrated by immunoprecipitation studies (44, 132). The work in Chapter 4 describes the isolation of the rabbit $NaK\beta_1$ subunit cDNA. The cDNA was amplified by RT-PCR and 5' and 3' RACE using rabbit renal medulla total RNA. The full-length cDNA was highly homologous to $NaK\beta_1$ cDNAs isolated from other species. Amino acid sequence analysis showed the presence of the three known glycosylation sites conserved in $NaK\beta_1$, six conserved cysteine residues, and single transmembrane domain, which are characteristic of P-type β subunits. The $NaK\beta_1$ cDNA was transfected in a mammalian cell line, and the $NaK\beta_1$ protein was readily detected by Western analysis

using an authentic rabbit NaKβ_1 antibody. This observation provided unambiguous proof that the correct cDNA had been identified.

The expression of the renal H^+,K^+-ATPase has proven to be a very difficult task. The episomal system had a number of faults that were not initially recognized. Ultimately, I proved that it was not a useful method for the coordinate expression of two proteins. The episomes from each subunit were apparently in competition with each other. This led to instability in episomal levels in the cell. There was no way to control for the copy number of each episome. Because H^+,K^+-ATPase activity requires the expression of both the α and β subunits, and these subunits would not have been present in similar amounts, the episomal expression system was abandoned as an appropriate method to use.

The stable expression system with the pBudCE4 expression vector would eliminate of any potential problems associated with the episomal system. Integration into the chromosome dictates the expression levels of the cDNAs. Because both cDNAs were contained on the same plasmid, it was likely that the expression of one subunit would be comparable to the expression of the second subunit. The effects of chromosomal integration on expression were clearly demonstrated when cell lines stably expressing NaKβ_1 were analyzed by Western blot. There were several cell lines that highly expressed the protein, whereas other cell lines on the same blot expressed the protein at much lower levels.

The stable expression of HKα_{2a} and HKα_{2c} proteins in the HEK293 cells was puzzling. The integration of each cDNA was verified through RT-PCR of complete transcripts and sequencing. However, the protein appeared unstable during plasma

membrane preparations. There was no apparent explanation to this observation. Protease inhibitors were used in an attempt to stabilize the proteins during isolation, but the efforts were unsuccessful. Clearly other researchers have reported expression of the $HK\alpha_{2a}$ subunit in this cell line. It remains unclear why the stable expression of the rabbit renal H^+,K^+-ATPase was not successful in our laboratory.

Using a transient expression system in COS-1 cells, the $HK\alpha_{2a}$ and $HK\alpha_{2c}$ fusion proteins were readily identified by Western analysis. Whatever problems that were associated with the stability of these proteins in HEK293 cells apparently disappeared in this host cell system. Therefore, I used this expression system to study the activities of the $HK\alpha_{2a}$ and $HK\alpha_{2c}$. However, it became apparent through immunofluorescence microscopy and Western analysis that the $HK\alpha_2$ subunits were not reaching the plasma membrane. This is a strong indication that the association of the $HK\alpha_2$ subunits with the $NaK\beta_1$ subunit was not occurring. Hence, no H^+,K^+-ATPase activity was observed. This observation may contribute to an explanation as to why the $HK\alpha_2$ subunits were unstable in HEK293 cells. If the $HK\alpha_2$ subunits were not assembled with the $NaK\beta_1$ subunit, the $HK\alpha_2$ subunits may have been more susceptible to recognition by the cell's proteolysis mechanism.

As problems with H^+,K^+-ATPase assembly were appearing in my work, the $NaK\beta_3$ subunit was implicated as the mate to the $HK\alpha_2$ subunits by immunoprecipitation studies in another laboratory (196). Michelle Gumz, a graduate student in our laboratory generated the full-length rabbit $NaK\beta_3$ subunit cDNA by RACE and RT-PCR. Using $NaK\beta_3$, I made attempts to study the H^+,K^+-ATPase activity of the $HK\alpha_2$ subunits in the COS-1 cells. However, similar results were obtained. It appeared that the $HK\alpha_2$ subunits

were not in association with NaKβ_3 either, as indicated by absence of the HKα_2 subunits at the plasma membrane and an absence of ATP hydrolysis activity. My results are in accordance with studies very recently published by Geering *et al.* (83). The authors expressed ATP1AL1 with each one of the known β subunits in *Xenopus laevis* oocytes in order to identify the type of β subunit that best fulfills the criteria as a mate to the HKα_2 subunits. They analyzed the effects of different β subunits on the resistance of ATP1AL1 protein to cellular and proteolytic degradation as well as its exit from the ER. They showed that NaKβ_1 formed very few stable complexes with ATP1AL1. The NaKβ_3 subunit was able to form complexes with ATP1AL1, but the complexes were impaired in their exit from the ER. The only β subunits the authors determined were capable of forming efficient stable complexes at the plasma membrane were the HKβ subunit and the NaKβ_2 subunit. However, these complexes exhibited what they considered to be weak interactions and were relatively trypsin-sensitive, as compared to the interactions between NaKα_1 and NaKβ_1, subunits known to interact *in vivo*. The authors concluded that none of the known β subunits may be the real mate to ATP1AL1, but an unidentified genuine β subunit should have structural features similar to HKβ and NaKβ_2.

Future Studies

I was concerned that the tag at the C-terminus of the HKα_2 subunits may be interfering with the association between the α and the β subunits, and very recently I removed the tag from the subunits. However, conversations very recently with Dr. Michael Caplan have suggested that the tag most likely would not interfere with association since his laboratory can functionally express active ATP1AL1 tagged with the green fluorescent protein at both the N- and C-termini. Based on experiments

conducted in his laboratory and the recent paper by Geering *et al.* (83), I concluded that the HKβ and NaKβ$_2$ subunits are the only appropriate β subunits to use in the expression system. We have in hand the rabbit HKβ cDNA, and efforts are currently underway in the Cain laboratory to generate the full length cDNA for the rabbit NaKβ$_2$ subunit isoform.

It has been documented that cells expressing renal H^+,K^+-ATPase activity have the ability to survive in ouabain, the inhibitor to the Na^+,K^+-ATPase, at a concentration of 1 μM (87). It is believed that the H^+,K^+-ATPase functions as a surrogate Na^+,K^+-ATPase and can maintain the membrane potential so the cells can survive otherwise detrimental conditions. COS-1 and HEK293 cells have been recently transfected with pTLC52(HKα$_{2a}$/HKβ) and were put under selection with Zeocin in attempt to isolate stable clones. Once clones were observed, I added 1 μM ouabain to the media as an initial screen to identify clones which had H^+,K^+-ATPase activity. It is too early to tell if any clones have acquired ouabain resistance.

Clones that do survive the ouabain selection would be isolated to study H^+,K^+-ATPase activity. Western analysis on plasma membrane preparations must be conducted to be certain that the HKα$_2$ subunits are localized to the plasma membrane. It would be interesting to see if ATP hydrolysis activity could be detected on these clones. However, if there is an absence of ATP hydrolysis activity, then ^{86}Rb transport assays must be used. Both ouabain and K^+ sensitivities would need to be examined. I believe that HKα$_{2c}$ should confer an H^+,K^+-ATPase activity that is similar to HKα$_{2a}$. However, the putative phosphorylation sites unique to HKα$_{2c}$ may play a role in the regulation of the enzyme.

Clearly there are discrepancies in the literature as to which β subunit associates with the HKα_2 subunit isoforms *in vivo*. Both the NaKβ_1 and NaKβ_3 subunits have been identified as the mate to the HKα_2 subunits by immunoprecipitation experiments (44, 132, 196). However, results of immunoprecipitation studies with partially solubilized membrane proteins can be difficult to interpret. The yeast two hybrid system is another approach that could be used to identify α/β subunit interactions. The extracytoplasmic loop between transmembrane domains 7 and 8 of the HKα subunit has been proposed to interact with the extracellular region of the β subunit. This loop sequence could be used as an initial "bait" for α/β interactions in a yeast two hybrid system. Of course, if the structure dictated through the disulfide bonds in the extracellular domain of the β subunit is necessary for its interaction with α, a negative result may be obtained by the yeast two hybrid system. The system analyzes intracellular interactions in yeast, and the disulfide bonds would not form in this environment.

Although several investigators utilize ATP hydrolysis to measure H^+,K^+-ATPase activity, the stoichiometry of the cations translocated across the membrane have not been correlated with ATP hydrolysis. In fact, ATPase hydrolysis seems inordinately low in comparison to reported ion translocation values. This experiment would have to be conducted with purified enzymes. Then, the moles of ^{86}Rb transported across the membrane with the amount of ATP hydrolysis could be determined.

The data described in Chapter 5 suggests that the HKα_2 subunits do not associate with either NaKβ_1 or NaKβ_3, as analyzed by Western blotting and immunofluorescence microscopy. However, I was unable to demonstrate a physical lack of association between the two subunits. Because both the anti-V5 and anti-NaKβ_1 antibodies were

made in mouse, co-localization studies of α and β in COS-1 cells could not be conducted.. Antibodies specific to the $HK\alpha_2$ subunit isoforms generated in chicken would be highly valuable. The co-localization experiments could be accomplished, and any problems associated with the C-terminal V5 epitope tag in α/β interactions would be eliminated.

The work described in this dissertation was unable to answer why the $HK\alpha_{2c}$ isoform exists and what role it plays in K^+ conservation. Work in the Cain laboratory is currently in progress to analyze the $HK\alpha_2$ gene structure. Both $HK\alpha_{2a}$ and $HK\alpha_{2c}$ are the product of a single gene and appear to be under control of one promoter. Maybe $HK\alpha_{2c}$ is under different transcriptional control than $HK\alpha_{2a}$ and is up-regulated with changes in K^+ concentration or aldosterone levels. These are questions that remain to be answered. Once the functional expression of $HK\alpha_{2c}$ is complete, we will further our understanding of the role for the enzyme in K^+ homeostasis.

LIST OF REFERENCES

1. **Abrahams, J. P., A. G. Leslie, R. Lutter, and J. E. Walker** 1994. Structure at 2.8 A resolution of F_1-ATPase from bovine heart mitochondria [see comments] Nature. **370:**621-8.

2. **Adolfsen, R., and E. N. Moudrianakis** 1976. Binding of adenine nucleotides to the purified 13S coupling factor of bacterial oxidative phosphorylation Arch Biochem Biophys. **172:**425-33.

3. **Aggeler, R., and R. A. Capaldi** 1996. Nucleotide-dependent movement of the epsilon subunit between alpha and beta subunits in the *Escherichia coli* F_1F_0-type ATPase J Biol Chem. **271:**13888-91.

4. **Aggeler, R., M. A. Haughton, and R. A. Capaldi** 1995. Disulfide bond formation between the COOH-terminal domain of the beta subunits and the gamma and epsilon subunits of the *Escherichia coli* F_1- ATPase. Structural implications and functional consequences J Biol Chem. **270:**9185-91.

5. **Ahn, K. Y., and B. C. Kone** 1995. Expression and cellular localization of mRNA encoding the "gastric" isoform of H(+)-K(+)-ATPase alpha-subunit in rat kidney Am J Physiol. **268:**F99-109.

6. **Aiyar, A., C. Tyree, and B. Sugden** 1998. The plasmid replicon of EBV consists of multiple cis-acting elements that facilitate DNA synthesis by the cell and a viral maintenance element Embo J. **17:**6394-403.

7. **Al-Shawi, M. K., C. J. Ketchum, and R. K. Nakamoto** 1997. The *Escherichia coli* F_0F_1 gammaM23K uncoupling mutant has a higher K0.5 for Pi. Transition state analysis of this mutant and others reveals that synthesis and hydrolysis utilize the same kinetic pathway Biochemistry. **36:**12961-9.

8. **Altendorf, K., A. Siebers, and W. Epstein** 1992. The KDP ATPase of *Escherichia coli* Ann N Y Acad Sci. **671:**228-43.

9. **Aris, J. P., D. J. Klionsky, and R. D. Simoni** 1985. The F_0 subunits of the *Escherichia coli* F_1F_0-ATP synthase are sufficient to form a functional proton pore J Biol Chem. **260:**11207-15.

10. **Aris, J. P., and R. D. Simoni** 1983. Cross-linking and labeling of the *Escherichia coli* F_1F_0-ATP synthase reveal a compact hydrophilic portion of F_0 close to an F_1 catalytic subunit J Biol Chem. **258:**14599-609.

11. **Arystarkhova, E., R. K. Wetzel, N. K. Asinovski, and K. J. Sweadner** 1999. The gamma subunit modulates Na(+) and K(+) affinity of the renal Na,K- ATPase J Biol Chem. **274:**33183-5.

12. **Asano, S., S. Hoshina, Y. Nakaie, T. Watanabe, M. Sato, Y. Suzuki, and N. Takeguchi** 1998. Functional expression of putative H+-K+-ATPase from guinea pig distal colon Am J Physiol. **275:**C669-74.

13. **Asano, S., K. Kawada, T. Kimura, A. V. Grishin, M. J. Caplan, and N. Takeguchi** 2000. The roles of carbohydrate chains of the beta-subunit on the functional expression of gastric H(+),K(+)-ATPase J Biol Chem. **275:**8324-30.

14. **Asano, S., S. Matsuda, S. Hoshina, S. Sakamoto, and N. Takeguchi** 1999. A chimeric gastric H^+,K^+-ATPase inhibitable with both ouabain and SCH 28080 J Biol Chem. **274:**6848-6854.

15. **Asano, S., Y. Tega, K. Konishi, M. Fujioka, and N. Takeguchi** 1996. Functional expression of gastric H+,K(+)-ATPase and site-directed mutagenesis of the putative cation binding site and catalytic center J Biol Chem. **271:**2740-5.

16. **Auer, M., G. A. Scarborough, and W. Kuhlbrandt** 1998. Three-dimensional map of the plasma membrane H+-ATPase in the open conformation Nature. **392:**840-3.

17. **Bamberg, K., and G. Sachs** 1994. Topological analysis of H+,K(+)-ATPase using in vitro translation J Biol Chem. **269:**16909-19.

18. **Beckers, G., R. J. Berzborn, and H. Strotmann** 1992. Zero-length crosslinking between subunits delta and I of the H(+)- translocating ATPase of chloroplasts Biochim Biophys Acta. **1101:**97-104.

19. **Beggah, A. T., P. Jaunin, and K. Geering** 1997. Role of glycosylation and disulfide bond formation in the beta subunit in the folding and functional expression of Na,K-ATPase J Biol Chem. **272:**10318-26.

20. **Besancon, M., J. M. Shin, F. Mercier, K. Munson, M. Miller, S. Hersey, and G. Sachs** 1993. Membrane topology and omeprazole labeling of the gastric H+,K(+)- adenosinetriphosphatase Biochemistry. **32:**2345-55.

21. **Besancon, M., A. Simon, G. Sachs, and J. M. Shin** 1997. Sites of reaction of the gastric H,K-ATPase with extracytoplasmic thiol reagents J Biol Chem. **272:**22438-22446.

22. **Birkenhager, R., M. Hoppert, G. Deckers-Hebestreit, F. Mayer, and K. Altendorf** 1995. The F_0 complex of the *Escherichia coli* ATP synthase. Investigation by electron spectroscopic imaging and immunoelectron microscopy Eur J Biochem. **230:**58-67.

23. **Blair, H. C.** 1998. How the osteoclast degrades bone Bioessays. **20:**837-46.

24. **Boekema, E. J., T. Ubbink-Kok, J. S. Lolkema, A. Brisson, and W. N. Konings** 1997. Visualization of a peripheral stalk in V-type ATPase: evidence for the stator structure essential to rotational catalysis Proc Natl Acad Sci U S A. **94:**14291-3.

25. **Bolivar, F., R. L. Rodriguez, P. J. Greene, M. C. Betlach, H. L. Heyneker, and H. W. Boyer** 1977. Construction and characterization of new cloning vehicles. II. A multipurpose cloning system Gene. **2:**95-113.

26. **Boyer, P. D.** 1997. The ATP synthase--a splendid molecular machine Annu Rev Biochem. **66:**717-49.

27. **Boyer, P. D.** 1993. The binding change mechanism for ATP synthase--some probabilities and possibilities Biochim Biophys Acta. **1140:**215-50.

28. **Brusilow, W. S., D. J. Klionsky, and R. D. Simoni** 1982. Differential polypeptide synthesis of the proton-translocating ATPase of *Escherichia coli* J Bacteriol. **151:**1363-71.

29. **Buffin-Meyer, B., M. Younes-Ibrahim, C. Barlet-Bas, L. Chevel, S. Marsy, and A. Doucet** 1997. K^+ depletion modifies the properties of Sch-28080-sensitive K-ATPase in rat collecting duct Am J Physiol. **272:**F124-131.

30. **Cain, B. D., and R. D. Simoni** 1986. Impaired proton conductivity resulting from mutations in the a subunit of F_1F_0 ATPase in *Escherichia coli* J Biol Chem. **261:**10043-50.

31. **Cain, B. D., and R. D. Simoni** 1989. Proton translocation by the F_1F_0 ATPase of *Escherichia coli*. Mutagenic analysis of the *a* subunit J Biol Chem. **264:**3292-3300.

32. **Callaghan, J. M., S. S. Tan, M. A. Khan, K. A. Curran, W. G. Campbell, A. J. Smolka, B. H. Toh, P. A. Gleeson, C. S. Wingo, B. D. Cain, and et al.** 1995. Renal expression of the gene encoding the gastric H(+)-K(+)-ATPase beta subunit Am J Physiol. **268:**F363-74.

33. **Callaghan, J. M., B. H. Toh, J. M. Pettitt, D. C. Humphris, and P. A. Gleeson** 1990. Poly-N-acetyllactosamine-specific tomato lectin interacts with gastric parietal cells. Identification of a tomato-lectin binding 60-90 X 10(3) Mr membrane glycoprotein of tubulovesicles J Cell Sci. **95:**563-76.

34. **Campbell, W.** 1998.Characterization of the rabbit renal H,K-ATPases. University of Florida. Doctoral Dissertation.

35. **Campbell, W. G., I. D. Weiner, C. S. Wingo, and B. D. Cain** 1999. H-K-ATPase in the RCCT-28A rabbit cortical collecting duct cell line Am J Physiol. **276:**F237-45.

36. **Campbell Thompson, M. L., J. W. Verlander, K. A. Curran, W. G. Campbell, B. D. Cain, C. S. Wingo, and J. E. McGuigan** 1995. In situ hybridization of H-K-ATPase beta subunit mRNA in rat and rabbit kidney Am J Physiol. **269:**F345-354.

37. **Canfield, V. A., and R. Levenson** 1991. Structural organization and transcription of the mouse gastric H+, K(+)- ATPase beta subunit gene Proc Natl Acad Sci U S A. **88:**8247-51.

38. **Cherepanov, D. A., A. Y. Mulkidjanian, and W. Junge** 1999. Transient accumulation of elastic energy in proton translocating ATP synthase FEBS Lett. **449:**1-6.

39. **Chevel, L., C. Barlet-Bas, C. Khadouri, E. Feraille, S. Marsy, and A. Doucet** 1991. K(+)-ATPase-mediated Rb^+ transport in rat collecting tubule: modulation during K^+ deprivation Am J Physiol. **260:**F800-805.

40. **Chow, D., M. Scalley, A. J. Smolka, and J. G. Forte** 1994. Assembly of α-subunit with β-subunit of the H,K-ATPase commences within the endoplasmic reticulum Gastroenterology. **106:**A63.

41. **Chow, D. C., C. M. Browning, and J. G. Forte** 1992. Gastric H(+)-K(+)-ATPase activity is inhibited by reduction of disulfide bonds in β subunit Am J Physiol. **263:**C39-46.

42. **Chow, D. C., and J. G. Forte** 1993. Characterization of the beta-subunit of the H(+)-K(+)-ATPase using an inhibitory monoclonal antibody Am J Physiol. **265:**C1562-70.

43. **Chow, D. C., and J. G. Forte** 1995. Functional significance of the beta-subunit for heterodimeric P-type ATPases J Exp Biol. **198:**1-17.

44. **Codina, J., J. T. Delmas-Mata, and T. D. DuBose, Jr.** 1998. The α-subunit of the colonic H^+,K^+-ATPase assembles with β_1- Na^+,K^+-ATPase in kidney and distal colon J Biol Chem. **273:**7894-9.

45. **Codina, J., B. C. Kone, J. T. Delmas-Mata, and T. D. DuBose, Jr.** 1996. Functional expression of the colonic H+,K+-ATPase alpha-subunit. Pharmacologic properties and assembly with X+,K+-ATPase beta-subunits J Biol Chem. **271:**29759-63.

46. **Codina, J., T. A. Pressley, and T. D. DuBose, Jr.** 1999. The colonic H^+,K^+-ATPase functions as a Na^+-dependent $K^+(NH_4^+)$-ATPase in apical membranes from rat distal colon J Biol Chem. **274:**19693-19698.

47. **Cougnon, M., G. Planelles, M. S. Crowson, G. E. Shull, B. C. Rossier, and F. Jaisser** 1996. The rat distal colon P-ATPase alpha subunit encodes a ouabain-sensitive H+, K+-ATPase J Biol Chem. **271:**7277-80.

48. **Courtois-Coutry, N., D. Roush, V. Rajendran, J. B. McCarthy, J. Geibel, M. Kashgarian, and M. J. Caplan** 1997. A tyrosine-based signal targets H/K-ATPase to a regulated compartment and is required for the cessation of gastric acid secretion Cell. **90:**501-10.

49. **Crowson, M. S., and G. E. Shull** 1992. Isolation and characterization of a cDNA encoding the putative distal colon H+,K(+)-ATPase. Similarity of deduced amino acid sequence to gastric H+,K(+)-ATPase and Na+,K(+)-ATPase and mRNA expression in distal colon, kidney, and uterus J Biol Chem. **267:**13740-8.

50. **Davis, L. G., W. M. Kuehl, and J. F. Battey** 1994. *Basic Methods in Molecular Biology, 2nd edition.* Appleton and Lange, Norwalk.

51. **de Meis, L., and A. L. Vianna** 1979. Energy interconversion by the Ca^{2+}-dependent ATPase of the sarcoplasmic reticulum Annu Rev Biochem. **48:**275-92.

52. **Deckers-Hebestreit, G., and K. Altendorf** 1986. Accessibility of F_0 subunits from *Escherichia coli* ATP synthase. A study with subunit specific antisera Eur J Biochem. **161:**225-31.

53. **Deckers-Hebestreit, G., and K. Altendorf** 1996. The F_0F_1-type ATP synthases of bacteria: structure and function of the F_0 complex Annu Rev Microbiol. **50:**791-824.

54. **Deckers-Hebestreit, G., R. D. Simoni, and K. Altendorf** 1992. Influence of subunit-specific antibodies on the activity of the F_0 complex of the ATP synthase of *Escherichia coli*. I. Effects of subunit *b*-specific polyclonal antibodies J Biol Chem. **267:**12364-9.

55. **Dmitriev, O., P. C. Jones, W. Jiang, and R. H. Fillingame** 1999. Structure of the membrane domain of subunit *b* of the *Escherichia coli* F_0F_1 ATP synthase J Biol Chem. **274:**15598-604.

56. **Doherty, R. D., and P. M. Kane** 1993. Partial assembly of the yeast vacuolar H(+)-ATPase in mutants lacking one subunit of the enzyme J Biol Chem. **268:**16845-51.

57. **Doucet, A., and S. Marsy** 1987. Characterization of K-ATPase activity in distal nephron: Stimulation by potassium depletion Am J Physiol. **253:**F418-423.

58. **Downie, J. A., F. Gibson, and G. B. Cox** 1979. Membrane adenosine triphosphatases of prokaryotic cells Annu Rev Biochem. **48:**103-31.

59. **Dschida, W. J., and B. J. Bowman** 1992. Structure of the vacuolar ATPase from *Neurospora crassa* as determined by electron microscopy J Biol Chem. **267:**18783-9.

60. **Duncan, T. M., V. V. Bulygin, Y. Zhou, M. L. Hutcheon, and R. L. Cross** 1995. Rotation of subunits during catalysis by *Escherichia coli* F_1-ATPase Proc Natl Acad Sci U S A. **92:**10964-8.

61. **Dunn, S. D.** 1992. The polar domain of the *b* subunit of *Escherichia coli* F_1F_0-ATPase forms an elongated dimer that interacts with the F_1 sector J Biol Chem. **267:**7630-6.

62. **Dunn, S. D., and J. Chandler** 1998. Characterization of a $b_2$delta complex from *Escherichia coli* ATP synthase J Biol Chem. **273:**8646-51.

63. **Dunn, S. D., D. T. McLachlin, and M. Revington** 2000. The second stalk of *Escherichia coli* ATP synthase Biochim Biophys Acta. **1458:**356-63.

64. **Eya, S., M. Maeda, and M. Futai** 1991. Role of the carboxyl terminal region of H(+)-ATPase (F_0F_1) a subunit from *Escherichia coli* Arch Biochem Biophys. **284:**71-7.

65. **Fambrough, D. M., M. V. Lemas, M. Hamrick, M. Emerick, K. J. Renaud, E. M. Inman, B. Hwang, and K. Takeyasu** 1994. Analysis of subunit assembly of the Na-K-ATPase Am J Physiol. **266:**C579-89.

66. **Farley, R. A., and L. D. Faller** 1985. The amino acid sequence of an active site peptide from the H,K-ATPase of gastric mucosa J Biol Chem. **260:**3899-901.

67. **Fillingame, R. H.** 1997. Coupling H+ transport and ATP synthesis in F_1F_0-ATP synthases: glimpses of interacting parts in a dynamic molecular machine J Exp Biol. **200:**217-24.

68. **Fillingame, R. H.** 1990. Molecular Mechanics of ATP Synthesis by F_1F_0-Type H+-Transporting ATP Synthases, p. 345-391. In *The Bacteria*,T. A. Krulwich (ed.), vol. XII. Academic Press, New York.

69. **Fillingame, R. H., P. C. Jones, W. Jiang, F. I. Valiyaveetil, and O. Y. Dmitriev** 1998. Subunit organization and structure in the F_0 sector of *Escherichia coli* F_1F_0 ATP synthase Biochim Biophys Acta. **1365:**135-42.

70. **Forgac, M.** 1999. Structure and properties of the vacuolar (H+)-ATPases J Biol Chem. **274:**12951-4.

71. **Forte, J. G., A. Ganser, R. Beesley, and T. M. Forte** 1975. Unique enzymes of purified microsomes from pig fundic mucosa Gastroeneterology. **69:**175-189.

72. **Forte, T. M., and J. G. Forte** 1970. Definition of the extracellular space in secreting and nonsecreting oxyntic cells J Cell Biol. **47:**782-6.

73. **Forte, T. M., T. E. Machen, and J. G. Forte** 1977. Ultrastructural changes in oxyntic cells associated with secretory function: a membrane-recycling hypothesis Gastroenterology. **73:**941-55.

74. **Foster, D. L., and R. H. Fillingame** 1982. Stoichiometry of subunits in the H+-ATPase complex of *Escherichia coli* J Biol Chem. **257:**2009-15.

75. **Fraga, D., J. Hermolin, M. Oldenburg, M. J. Miller, and R. H. Fillingame** 1994. Arginine 41 of subunit *c* of *Escherichia coli* H(+)-ATP synthase is essential in binding and coupling of F_1 to F_0 J Biol Chem. **269:**7532-7.

76. **Futai, M., and H. Kanazawa** 1983. Structure and function of proton-translocating adenosine triphosphatase (F_0F_1): biochemical and molecular biological approaches Microbiol Rev. **47:**285-312.

77. **Futai, M., T. Oka, G. Sun-Wada, Y. Moriyama, H. Kanazawa, and Y. Wada** 2000. Luminal acidification of diverse organelles by V-ATPase in animal cells J Exp Biol. **203 Pt 1:**107-16.

78. **Ganser, A. L., and J. G. Forte** 1973. K^+-stimulated ATPase in purified microsomes of bullfrog oxyntic cells Biochim Biophys Acta. **307:**169-180.

79. **Gardner, J. L., and B. D. Cain** 1999. Amino acid substitutions in the *a* subunit affect the epsilon subunit of F_1F_0 ATP synthase from *Escherichia coli* Arch Biochem Biophys. **361:**302-8.

80. **Garg, L. C., and N. Narang** 1988. Ouabain-insensitive K-adenosine triphosphatase in distal nephron segments of the rabbit J Clin Invest. **81:**1204-1208.

81. **Garger, S. J., O. M. Griffith, and L. K. Grill** 1983. Rapid purification of plasmid DNA by a single centrifugation in a two- step cesium chloride-ethidium bromide gradient Biochem Biophys Res Commun. **117:**835-42.

82. **Gay, N. J.** 1984. Construction and characterization of an *Escherichia coli* strain with a *uncI* mutation J Bacteriol. **158:**820-5.

83. **Geering, K., G. Crambert, C. Yu, T. V. Korneenko, N. B. Pestov, and N. N. Modyanov** 2000. Intersubunit interactions in human X,K-ATPases: role of membrane domains M9 and M10 in the assembly process and association efficiency of human nongastric H,K-ATPase α subunits (ATP1AL1) with known β subunits.

84. **Gibson, F., J. A. Downie, G. B. Cox, and J. Radik** 1978. Mu-induced polarity in the *unc* operon of *Escherichia coli* J Bacteriol. **134:**728-36.

85. **Girvin, M. E., V. K. Rastogi, F. Abildgaard, J. L. Markley, and R. H. Fillingame** 1998. Solution structure of the transmembrane H+-transporting subunit *c* of the F_IF_0 ATP synthase Biochemistry. **37:**8817-24.

86. **Graf, R., W. R. Harvey, and H. Wieczorek** 1996. Purification and properties of a cytosolic V_1-ATPase J Biol Chem. **271:**20908-13.

87. **Grishin, A. V., M. O. Bevensee, N. N. Modyanov, V. Rajendran, W. F. Boron, and M. J. Caplan** 1996. Functional expression of the cDNA encoded by the human ATP1AL1 gene Am J Physiol. **271:**F539-51.

88. **Grishin, A. V., and M. J. Caplan** 1998. ATP1AL1, a member of the non-gastric H,K-ATPase family, functions as a sodium pump J Biol Chem. **273:**27772-27778.

89. **Grishin, A. V., V. E. Sverdlov, M. B. Kostina, and N. N. Modyanov** 1994. Cloning and characterization of the entire cDNA encoded by ATP1AL1--a member of the human Na,K/H,K-ATPase gene family FEBS Lett. **349:**144-50.

90. **Gunsalus, R. P., W. S. Brusilow, and R. D. Simoni** 1982. Gene order and gene-polypeptide relationships of the proton- translocating ATPase operon (*unc*) of *Escherichia coli* Proc Natl Acad Sci U S A. **79:**320-4.

91. **Hall, K., G. Perez, D. Anderson, C. Gutierrez, K. Munson, S. J. Hersey, J. H. Kaplan, and G. Sachs** 1990. Location of the carbohydrates present in the H,K-ATPase vesicles isolated from hog gastric mucosa Biochemistry. **29:**701-6.

92. **Harper, J. F., B. Hong, I. Hwang, H. Q. Guo, R. Stoddard, J. F. Huang, M. G. Palmgren, and H. Sze** 1998. A novel calmodulin-regulated Ca2+-ATPase (ACA2) from Arabidopsis with an N-terminal autoinhibitory domain J Biol Chem. **273:**1099-106.

93. **Hartzog, P. E., and B. D. Cain** 1994. Second-site suppressor mutations at glycine 218 and histidine 245 in the alpha subunit of F_1F_0 ATP synthase in *Escherichia coli* J Biol Chem. **269:**32313-7.

94. **Helander, H. F., H. Mattsson, G. Elm, and S. Ottosson** 1990. Structure and function of rat parietal cells during treatment with omeprazole, SCH 28080, SCH 32651, or ranitidine Scand J Gastroenterol. **25:**799-809.

95. **Herbert, H., Y. Xian, I. Hacksell, and S. Mardh** 1992. Two-dimensional crystals of membrane-bound gastric H,K-ATPase FEBS Lett. **299:**159-62.

96. **Hermolin, J., and R. H. Fillingame** 1995. Assembly of F_0 sector of *Escherichia coli* H+ ATP synthase. Interdependence of subunit insertion into the membrane J Biol Chem. **270:**2815-7.

97. **Hermolin, J., and R. H. Fillingame** 1989. H+-ATPase activity of *Escherichia coli* F_1F_0 is blocked after reaction of dicyclohexylcarbodiimide with a single proteolipid (subunit *c*) of the F_0 complex J Biol Chem. **264:**3896-903.

98. **Hermolin, J., J. Gallant, and R. H. Fillingame** 1983. Topology, organization, and function of the psi subunit in the F_0 sector of the H+-ATPase of *Escherichia coli* J Biol Chem. **258:**14550-5.

99. **Hersey, S. J., and G. Sachs** 1995. Gastric acid secretion Physiol Rev. **75:**155-89.

100. **Hersey, S. J., L. Steiner, J. Mendlein, E. Rabon, and G. Sachs** 1988. SCH28080 prevents omeprazole inhibition of the gastric H^+/K^+-ATPase Biochim Biophys Acta. **956:**49-57.

101. **Ho, S. N., H. D. Hunt, R. M. Horton, J. K. Pullen, and L. R. Pease** 1989. Site-directed mutagenesis by overlap extension using the polymerase chain reaction [see comments] Gene. **77:**51-9.

102. **Hoppe, J., H. U. Schairer, P. Friedl, and W. Sebald** 1982. An Asp-Asn substitution in the proteolipid subunit of the ATP-synthase from *Escherichia coli* leads to a non-functional proton channel FEBS Lett. **145:**21-9.

103. **Horisberger, J. D., P. Jaunin, M. A. Reuben, L. S. Lasater, D. C. Chow, J. G. Forte, G. Sachs, B. C. Rossier, and K. Geering** 1991. The H,K-ATPase beta-subunit can act as a surrogate for the beta-subunit of Na,K-pumps J Biol Chem. **266:**19131-19134.

104. **Howitt, S. M., A. J. Rodgers, P. D. Jeffrey, and G. B. Cox** 1996. A mutation in which alanine 128 Is replaced by aspartic acid abolishes dimerization of the *b*-subunit of the F_0F_1-ATPase from *Escherichia coli* J Biol Chem. **271:**7038-42.

105. **Humbert, R., W. S. Brusilow, R. P. Gunsalus, D. J. Klionsky, and R. D. Simoni** 1983. *Escherichia coli* mutants defective in the *uncH* gene J Bacteriol. **153:**416-22.

106. **Ikemura, T.** 1981. Correlation between the abundance of *Escherichia coli* transfer RNAs and the occurrence of the respective codons in its protein genes J Mol Biol. **146:**1-21.

107. **Ikemura, T.** 1981. Correlation between the abundance of *Escherichia coli* transfer RNAs and the occurrence of the respective codons in its protein genes: a proposal for a synonymous codon choice that is optimal for the *E. coli* translational system J Mol Biol. **151:**389-409.

108. **Inesi, G.** 1985. Mechanism of calcium transport Annu Rev Physiol. **47:**573-601.

109. **Jackson, R. J., J. Mendlein, and G. Sachs** 1983. Interaction of fluorescein isothiocyanate with the ($H^+ + K^+$)-ATPase Biochim Biophys Acta. **731:**9-15.

110. **Jans, D. A., A. L. Fimmel, L. Hatch, F. Gibson, and G. B. Cox** 1984. An additional acidic residue in the membrane portion of the *b*-subunit of the energy-transducing adenosine triphosphatase of *Escherichia coli* affects both assembly and function Biochem J. **221:**43-51.

111. **Jiang, W., and R. H. Fillingame** 1998. Interacting helical faces of subunits *a* and *c* in the F_1F_0 ATP synthase of *Escherichia coli* defined by disulfide cross-linking Proc Natl Acad Sci U S A. **95:**6607-12.

112. **Jones, C. M., B. H. Toh, J. M. Pettitt, T. M. Martinelli, D. C. Humphris, J. M. Callaghan, I. Goldkorn, F. T. Mu, and P. A. Gleeson** 1991. Monoclonal antibodies specific for the core protein of the beta-subunit of the gastric proton pump (H+/K+ ATPase). An autoantigen targetted in pernicious anaemia Eur J Biochem. **197:**49-59.

113. **Jones, H. M., C. M. Brajkovich, and R. P. Gunsalus** 1983. In vivo 5' terminus and length of the mRNA for the proton-translocating ATPase *unc* operon of *Escherichia coli* J Bacteriol. **155:**1279-87.

114. **Jones, P. C., and R. H. Fillingame** 1998. Genetic fusions of subunit *c* in the F_0 sector of H+-transporting ATP synthase. Functional dimers and trimers and determination of stoichiometry by cross-linking analysis J Biol Chem. **273:**29701-5.

115. **Kaminski, J. J., B. Wallmark, C. Briving, and B. M. Anderson** 1991. Inhibition of gastric H^+/K^+-ATPase by substituted imidazo[1,2-a]pyridines and related analogues and its implication in modeling the high affinity potassium ion binding site of the gastric proton pump enzyme J Med Chem. **34:**533-541.

116. **Kanazawa, H., T. Kayano, T. Kiyasu, and M. Futai** 1982. Nucleotide sequence of the genes for beta and epsilon subunits of proton-translocating ATPase from *Escherichia coli* Biochem Biophys Res Commun. **105:**1257-64.

117. **Kanazawa, T., A. Yamada, T. Yamamoto, and Y. Tonomura** 1971. Reaction mechanism of the Ca2 plus-dependent ATPase of sarcoplasmic reticulum from skeletal muscle. V. Vectorial requirements for calcium and magnesium ions of three partial reactions of ATPase: formation and decomposition of a phosphorylated intermediate and ATP-formation from ADP and the intermediate J Biochem (Tokyo). **70:**95-123.

118. **Kane, P. M.** 1995. Disassembly and reassembly of the yeast vacuolar H(+)-ATPase *in vivo* J Biol Chem. **270:**17025-32.

119. **Karam, S. M., and J. G. Forte** 1994. Inhibiting gastric H(+)-K(+)-ATPase activity by omeprazole promotes degeneration and production of parietal cells [see comments] Am J Physiol. **266:**G745-58.

120. **Karasawa, H., N. Tani, and T. Miwa** 1988. The effect of omeprazole on ultrastructural changes in gastric parietal cells Gastroenterol Jpn. **23:**1-8.

121. **Kasimoglu, E., S. J. Park, J. Malek, C. P. Tseng, and R. P. Gunsalus** 1996. Transcriptional regulation of the proton-translocating ATPase (*atpIBEFHAGDC*) operon of *Escherichia coli*: control by cell growth rate J Bacteriol. **178:**5563-7.

122. **Kato-Yamada, Y., H. Noji, R. Yasuda, K. Kinosita, Jr., and M. Yoshida** 1998. Direct observation of the rotation of epsilon subunit in F_1-ATPase J Biol Chem. **273:**19375-7.

123. **Kawamura, M., and K. Nagano** 1984. Evidence for essential disulfide bonds in the beta-subunit of (Na+ + K+)-ATPase Biochim Biophys Acta. **774:**188-92.

124. **Kersten, M. V., S. D. Dunn, J. G. Wise, and P. D. Vogel** 2000. Site-directed spin-labeling of the catalytic sites yields insight into structural changes within the F_0F_1-ATP synthase of *Escherichia coli* Biochemistry. **39:**3856-60.

125. **Kimura, T., K. Nakamura, H. Kajiura, H. Hattori, N. Nelson, and T. Asahi** 1989. Correspondence of minor subunits of plant mitochondrial F_1 ATPase to F_1F_0ATPase subunits of other organisms J Biol Chem. **264:**3183-6.

126. **Kirley, T. L.** 1989. Determination of three disulfide bonds and one free sulfhydryl in the beta subunit of (Na,K)-ATPase J Biol Chem. **264:**7185-92.

127. **Klaassen, C. H., J. A. Fransen, H. G. Swarts, and J. J. De Pont** 1997. Glycosylation is essential for biosynthesis of functional gastric H+,K+- ATPase in insect cells Biochem J. **321:**419-24.

128. **Kleinman, J. G.** 1994. Proton ATPases and urinary acidification J Am Soc Nephrol. **5:**S6-11.

129. **Kluge, C., and P. Dimroth** 1993. Kinetics of inactivation of the F_1F_0 ATPase of *Propionigenium modestum* by dicyclohexylcarbodiimide in relationship to H+ and Na+ concentration: probing the binding site for the coupling ions Biochemistry. **32:**10378-86.

130. **Kluge, C., and P. Dimroth** 1993. Specific protection by Na+ or Li+ of the F_1F_0-ATPase of *Propionigenium modestum* from the reaction with dicyclohexylcarbodiimide J Biol Chem. **268:**14557-60.

131. **Kone, B. C., and S. C. Higham** 1998. A novel N-terminal splice variant of the rat H+-K+-ATPase alpha2 subunit. Cloning, functional expression, and renal adaptive response to chronic hypokalemia J Biol Chem. **273:**2543-52.

132. **Kraut, J. A., J. Hiura, J. M. Shin, A. Smolka, G. Sachs, and D. Scott** 1998. The Na(+)-K(+)-ATPase beta 1 subunit is associated with the HK alpha 2 protein in the rat kidney Kidney Int. **53:**958-62.

133. **Kraut, J. A., F. Starr, G. Sachs, and M. Reuben** 1995. Expression of gastric and colonic H(+)-K(+)-ATPase in the rat kidney Am J Physiol. **268:**F581-7.

134. **Kyte, J., and R. F. Doolittle** 1982. A simple method for displaying the hydropathic character of a protein J Mol Biol. **157:**105-32.

135. **Lambrecht, N., Z. Corbett, D. Bayle, S. J. Karlish, and G. Sachs** 1998. Identification of the site of inhibition by omeprazole of alpha-beta fusion protein of the H,K-ATPase using site-directed mutagenesis J Biol Chem. **273:**13719-13728.

136. **Lee, J., V. M. Rajendran, A. S. Mann, M. Kashgarian, and H. J. Binder** 1995. Functional expression and segmental localization of rat colonic K- adenosine triphosphatase J Clin Invest. **96:**2002-8.

137. **Lehy, T., and M. Dubrasquet** 1972. The secretory, histologic and histochemical effects of acute and subchronic administration of atropine sulfate on the gastric mucosa of the rat Am J Dig Dis. **17:**887-901.

138. **Lightowlers, R. N., S. M. Howitt, L. Hatch, F. Gibson, and G. B. Cox** 1987. The proton pore in the *Escherichia coli* F_0F_1-ATPase: a requirement for arginine at position 210 of the *a* subunit Biochim Biophys Acta. **894:**399-406.

139. **Lill, H., F. Hensel, W. Junge, and S. Engelbrecht** 1996. Cross-linking of engineered subunit δ to $(\alpha\beta)_3$ in chloroplast F-ATPase J Biol Chem. **271:**32737-42.

140. **Maeda, M., J. Ishizaki, and M. Futai** 1988. cDNA cloning and sequence determination of pig gastric (H+ + K+)-ATPase Biochem Biophys Res Commun. **157:**203-9.

141. **Maeda, M., M. Tagaya, and M. Futai** 1988. Modification of gastric (H+ + K+)-ATPase with pyridoxal 5'-phosphate J Biol Chem. **263:**3652-6.

142. **Malik, N., V. A. Canfield, M. C. Beckers, P. Gros, and R. Levenson** 1996. Identification of the mammalian Na,K-ATPase 3 subunit J Biol Chem. **271:**22754-8.

143. **Malo, D., P. Gros, A. Bergmann, B. Trask, H. W. Mohrenweiser, V. A. Canfield, and R. Levenson** 1993. Genes encoding the H,K-ATPase alpha and Na,K-ATPase alpha 3 subunits are linked on mouse chromosome 7 and human chromosome 19 Mamm Genome. **4:**644-9.

144. **Markwell, M. A., S. M. Haas, L. L. Bieber, and N. E. Tolbert** 1978. A modification of the Lowry procedure to simplify protein determination in membrane and lipoprotein samples Anal Biochem. **87:**206-10.

145. **Matten, S. R., T. D. Schneider, S. Ringquist, and W. S. Brusilow** 1998. Identification of an intragenic ribosome binding site that affects expression of the *uncB* gene of the *Escherichia coli* proton- translocating ATPase *unc* operon J Bacteriol. **180:**3940-5.

146. **McCormick, K. A., and B. D. Cain** 1991. Targeted mutagenesis of the *b* subunit of F_1F_0 ATP synthase in *Escherichia coli*: Glu-77 through Gln-85 J Bacteriol. **173:**7240-8.

147. **McCormick, K. A., G. Deckers-Hebestreit, K. Altendorf, and B. D. Cain** 1993. Characterization of mutations in the *b* subunit of F_1F_0 ATP synthase in *Escherichia coli* J Biol Chem. **268:**24683-91.

148. **McLachlin, D. T., J. A. Bestard, and S. D. Dunn** 1998. The *b* and δ subunits of the *Escherichia coli* ATP synthase interact via residues in their C-terminal regions J Biol Chem. **273:**15162-8.

149. **McLachlin, D. T., A. M. Coveny, S. M. Clark, and S. D. Dunn** 2000. Site-directed cross-linking of *b* to the alpha, beta, and a subunits of the *Escherichia coli* ATP synthase J Biol Chem. **275:**17571-7.

150. **McLachlin, D. T., and S. D. Dunn** 1997. Dimerization interactions of the *b* subunit of the *Escherichia coli* F_1F_0-ATPase J Biol Chem. **272:**21233-9.

151. **Melle-Milovanovic, D., M. Milovanovic, S. Nagpal, G. Sachs, and J. M. Shin** 1998. Regions of association between the alpha and the beta subunit of the gastric H,K-ATPase J Biol Chem. **273:**11075-81.

152. **Mendel-Hartvig, J., and R. A. Capaldi** 1991. Nucleotide-dependent and dicyclohexylcarbodiimide-sensitive conformational changes in the epsilon subunit of *Escherichia coli* ATP synthase Biochemistry. **30:**10987-91.

153. **Mendlein, J., and G. Sachs** 1990. Interaction of a K^+-competitive inhibitor, a substituted imidazo[1,2a] pyridine, with the phospho-and dephosphoenzyme forms of H^+,K^+-ATPase J Biol Chem. **265:**5030-5036.

154. **Meneton, P., P. J. Schultheis, J. Greeb, M. L. Nieman, L. H. Liu, L. L. Clarke, J. J. Duffy, T. Doetschman, J. N. Lorenz, and G. E. Shull** 1998. Increased sensitivity to K^+ deprivation in colonic H,K-ATPase-deficient mice J Clin Invest. **101:**536-542.

155. **Miller, M. J., M. Oldenburg, and R. H. Fillingame** 1990. The essential carboxyl group in subunit *c* of the F_1F_0 ATP synthase can be moved and H(+)-translocating function retained Proc Natl Acad Sci U S A. **87:**4900-4.

156. **Miller, R. P., and R. A. Farley** 1988. All three potential N-glycosylation sites of the dog kidney (Na+ + K+)- ATPase beta-subunit contain oligosaccharide Biochim Biophys Acta. **954:**50-7.

157. **Miller, R. P., and R. A. Farley** 1990. Beta subunit of (Na+ + K+)-ATPase contains three disulfide bonds Biochemistry. **29:**1524-32.

158. **Mitchell, P.** 1966. Chemiosmotic coupling in oxidative and photosynthetic phosphorylation Biol Rev. **41:**445-502.

159. **Modyanov, N. N., P. M. Mathews, A. V. Grishin, P. Beguin, A. T. Beggah, B. C. Rossier, J. D. Horisberger, and K. Geering** 1995. Human ATP1AL1 gene encodes a ouabain-sensitive H-K-ATPase Am J Physiol. **269:**C992-7.

160. **Modyanov, N. N., K. E. Petrukhin, V. E. Sverdlov, A. V. Grishin, M. Y. Orlova, M. B. Kostina, O. I. Makarevich, N. E. Broude, G. S. Monastyrskaya, and E. D. Sverdlov** 1991. The family of human Na,K-ATPase genes. ATP1AL1 gene is transcriptionally competent and probably encodes the related ion transport ATPase FEBS Lett. **278:**91-4.

161. **Moller, J. V., B. Juul, and M. le Maire** 1996. Structural organization, ion transport, and energy transduction of P- type ATPases Biochim Biophys Acta. **1286:**1-51.

162. **Morley, G. P., J. M. Callaghan, J. B. Rose, B. H. Toh, P. A. Gleeson, and I. R. van Driel** 1992. The mouse gastric H,K-ATPase beta subunit. Gene structure and co- ordinate expression with the alpha subunit during ontogeny J Biol Chem. **267:**1165-74.

163. **Mosher, M. E., L. K. White, J. Hermolin, and R. H. Fillingame** 1985. H+-ATPase of *Escherichia coli.* An *uncE* mutation impairing coupling between F_1 and F_0 but not F_0-mediated H+ translocation J Biol Chem. **260:**4807-14.

164. **Munson, K., N. Lambrecht, and G. Sachs** 2000. Effects of mutations in M4 of the gastric H^+,K^+-ATPase on inhibition kineticis of SCH28080 Biochemistry. **39:**2997-3004.

165. **Munson, K. B., C. Gutierrez, V. N. Balaji, K. Ramnarayan, and G. Sachs** 1991. Identification of an extracytoplasmic region of H^+,K^+-ATPase labeled by a K^+-competitive photoaffinity inhibitor J Biol Chem. **266:**18976-18988.

166. **Munson, K. B., and G. Sachs** 1988. Inactivation of H^+,K^+-ATPase by a K^+-competitive photoaffinity inhibitor Biochemistry. **27:**3932-3938.

167. **Myers, M., and M. Forgac** 1993. Assembly of the peripheral domain of the bovine vacuolar H(+)-adenosine triphosphatase J Cell Physiol. **156:**35-42.

168. **Nakamoto, R. K.** 1996. Mechanisms of active transport in the F_0F_1 ATP synthase J Membr Biol. **151:**101-11.

169. **Nakamoto, R. K., C. J. Ketchum, and M. K. al-Shawi** 1999. Rotational coupling in the F_0F_1 ATP synthase Annu Rev Biophys Biomol Struct. **28:**205-34.

170. **Nielsen, J., B. B. Jorgensen, K. V. van Meyenburg, and F. G. Hansen** 1984. The promoters of the atp operon of *Escherichia coli* K12 Mol Gen Genet. **193:**64-71.

171. **Noguchi, S., Y. Mutoh, and M. Kawamura** 1994. The functional roles of disulfide bonds in the beta-subunit of (Na,K)ATPase as studied by site-directed mutagenesis FEBS Lett. **341:**233-8.

172. **Noji, H., R. Yasuda, M. Yoshida, and K. Kinosita, Jr.** 1997. Direct observation of the rotation of F_1-ATPase [see comments] Nature. **386:**299-302.

173. **Ogilvie, I., R. Aggeler, and R. A. Capaldi** 1997. Cross-linking of the delta subunit to one of the three alpha subunits has no effect on functioning, as expected if delta is a part of the stator that links the F_1 and F_0 parts of the *Escherichia coli* ATP synthase J Biol Chem. **272:**16652-6.

174. **Okamoto, C. T., J. M. Karpilow, A. Smolka, and J. G. Forte** 1990. Isolation and characterization of gastric microsomal glycoproteins. Evidence for a glycosylated beta-subunit of the H+/K(+)-ATPase Biochim Biophys Acta. **1037:**360-72.

175. **Oster, G., and H. Wang** 2000. Reverse engineering a protein: the mechanochemistry of ATP synthase Biochim Biophys Acta. **1458:**482-510.

176. **Page, R. D. M.** 1996. An application to display phylogenetic trees on personal computers Comput. Appl. Biosci. **12:**357-358.

177. **Pedersen, P. L., and E. Carafoli** 1987. Ion motive ATPases. I. Ubiquity, properties, and significance to cell function TIBS. **12:**146-150.

178. **Peng, S. B., X. Li, B. P. Crider, Z. Zhou, P. Andersen, S. J. Tsai, X. S. Xie, and D. K. Stone** 1999. Identification and reconstitution of an isoform of the 116-kDa subunit of the vacuolar proton translocating ATPase J Biol Chem. **274:**2549-55.

179. **Perlin, D. S., D. N. Cox, and A. E. Senior** 1983. Integration of F_1 and the membrane sector of the proton-ATPase of *Escherichia coli*. Role of subunit "b" (*uncF* protein) J Biol Chem. **258:**9793-800.

180. **Perlin, D. S., and A. E. Senior** 1985. Functional effects and cross-reactivity of antibody to purified subunit *b* (*uncF* protein) of *Escherichia coli* proton-ATPase Arch Biochem Biophys. **236:**603-11.

181. **Pettitt, J. M., D. C. Humphris, S. P. Barrett, B. H. Toh, I. R. van Driel, and P. A. Gleeson** 1995. Fast freeze-fixation/freeze-substitution reveals the secretory membranes of the gastric parietal cell as a network of helically coiled tubule. A new model for parietal cell transformation J Cell Sci. **108:**1127-41.

182. **Porter, A. C., C. Kumamoto, K. Aldape, and R. D. Simoni** 1985. Role of the *b* subunit of the *Escherichia coli* proton-translocating ATPase. A mutagenic analysis J Biol Chem. **260:**8182-7.

183. **Rabon, E., G. Sachs, S. Bassilian, C. Leach, and D. Keeling** 1991. A K^+-competitive fluorescent inhibitor of the H,K-ATPase J Biol Chem. **266:**12395-12401.

184. **Rabon, E., M. Wilke, G. Sachs, and G. Zampighi** 1986. Crystallization of the gastric H,K-ATPase J Biol Chem. **261:**1434-9.

185. **Rabon, E. C., S. Bassilian, G. Sachs, and S. J. Karlish** 1990. Conformational transitions of the H,K-ATPase studied with sodium ions as surrogates from protons J Biol Chem. **265:**19594-19599.

186. **Rabon, E. C., R. D. Gunther, S. Bassilian, and E. S. Kempner** 1988. Radiation inactivation analysis of oligomeric structure of the H,K- ATPase J Biol Chem. **263:**16189-94.

187. **Rabon, E. C., and M. A. Reuben** 1990. The mechanism and structure of the gastric H,K-ATPase Annu Rev Physiol. **52:**321-44.

188. **Rastogi, V. K., and M. E. Girvin** 1999. Structural changes linked to proton translocation by subunit *c* of the ATP synthase [see comments] Nature. **402:**263-8.

189. **Reuben, M. A., L. S. Lasater, and G. Sachs** 1990. Characterization of a beta subunit of the gastric H+/K(+)-transporting ATPase Proc Natl Acad Sci U S A. **87:**6767-71.

190. **Revington, M., D. T. McLachlin, G. S. Shaw, and S. D. Dunn** 1999. The dimerization domain of the *b* subunit of the *Escherichia coli* F_1F_0-ATPase J Biol Chem. **274:**31094-101.

191. **Rodgers, A. J., and R. A. Capaldi** 1998. The second stalk composed of the *b*- and delta-subunits connects F_0 to F_1 via an alpha-subunit in the *Escherichia coli* ATP synthase J Biol Chem. **273:**29406-10.

192. **Rodgers, A. J., S. Wilkens, R. Aggeler, M. B. Morris, S. M. Howitt, and R. A. Capaldi** 1997. The subunit delta-subunit *b* domain of the *Escherichia coli* F_1F_0 ATPase. The *b* subunits interact with F_1 as a dimer and through the delta subunit J Biol Chem. **272:**31058-64.

193. **Sabbert, D., S. Engelbrecht, and W. Junge** 1996. Intersubunit rotation in active F-ATPase Nature. **381:**623-5.

194. **Sachs, G., H. H. Chang, E. Rabon, R. Schackman, M. Lewin, and G. Saccomani** 1976. A nonelectrogenic H^+ pump in plasma membranes of hog stomach J Biol Chem. **251:**7690-7698.

195. **Sambongi, Y., Y. Iko, M. Tanabe, H. Omote, A. Iwamoto-Kihara, I. Ueda, T. Yanagida, Y. Wada, and M. Futai** 1999. Mechanical rotation of the *c* subunit oligomer in ATP synthase (F_0F_1): direct observation [see comments] Science. **286:**1722-4.

196. **Sangan, P., S. S. Kolla, V. M. Rajendran, M. Kashgarian, and H. J. Binder** 1999. Colonic H-K-ATPase beta-subunit: identification in apical membranes and regulation by dietary K depletion Am J Physiol. **276:**C350-60.

197. **Sangan, P., S. Thevananther, S. Sangan, V. M. Rajendran, and H. J. Binder** 2000. Colonic H-K-ATPase α- and β-subunits express ouabain-insensitive H-K-ATPase Am J Physiol Cell Physiol. **278:**C182-9.

198. **Sawada, K., N. Kuroda, H. Watanabe, C. Moritani-Otsuka, and H. Kanazawa** 1997. Interaction of the delta and *b* subunits contributes to F_1 and F_0 interaction in the *Escherichia coli* F_1F_0-ATPase J Biol Chem. **272:**30047-53.

199. **Scarborough, G. A.** 1999. Structure and function of the P-type ATPases Curr Opin Cell Biol. **11:**517-22.

200. **Scarff, K. L., L. M. Judd, B. H. Toh, P. A. Gleeson, and I. R. Van Driel** 1999. Gastric H(+),K(+)-adenosine triphosphatase beta subunit is required for normal function, development, and membrane structure of mouse parietal cells Gastroenterology. **117:**605-18.

201. **Schaefer, E. M., D. Hartz, L. Gold, and R. D. Simoni** 1989. Ribosome-binding sites and RNA-processing sites in the transcript of the Escherichia coli unc operon J Bacteriol. **171:**3901-8.

202. **Schemidt, R. A., J. Qu, J. R. Williams, and W. S. Brusilow** 1998. Effects of carbon source on expression of F_0 genes and on the stoichiometry of the *c* subunit in the F_1F_0 ATPase of *Escherichia coli* J Bacteriol. **180:**3205-8.

203. **Schneppe, B., G. Deckers-Hebestreit, and K. Altendorf** 1991. Detection and localization of the *i* protein in *Escherichia coli* cells using antibodies FEBS Lett. **292:**145-7.

204. **Scott, D. R., K. Munson, N. Modyanov, and G. Sachs** 1992. Determination of the sidedness of the C-terminal region of the gastric H,K-ATPase alpha subunit Biochim Biophys Acta. **1112:**246-50.

205. **Senior, A. E.** 1983. Secondary and tertiary structure of membrane proteins involved in proton translocation Biochim Biophys Acta. **726:**81-95.

206. **Shigekawa, M., and J. P. Dougherty** 1978. Reaction mechanism of Ca2+-dependent ATP hydrolysis by skeletal muscle sarcoplasmic reticulum in the absence of added alkali metal salts. III. Sequential occurrence of ADP-sensitive and ADP-insensitive phosphoenzymes J Biol Chem. **253:**1458-64.

207. **Shin, J. M., M. Besancon, A. Simon, and G. Sachs** 1993. The site of action of pantoprazole in the gastric H+/K(+)-ATPase Biochim Biophys Acta. **1148:**223-33.

208. **Shin, J. M., and G. Sachs** 1994. Identification of a region of the H,K-ATPase alpha subunit associated with the beta subunit J Biol Chem. **269:**8642-6.

209. **Shull, G. E.** 1990. cDNA cloning of the beta-subunit of the rat gastric H,K-ATPase J Biol Chem. **265:**12123-6.

210. **Shull, G. E., and J. B. Lingrel** 1986. Molecular cloning of the rat stomach (H+ + K+)-ATPase J Biol Chem. **261:**16788-91.

211. **Simoni, R. D., and A. Shandell** 1975. Energy transduction in *Escherichia coli.* Genetic alteration of a membrane polypeptide of the (Ca2+,Mg2+)-ATPase J Biol Chem. **250:**9421-7.

212. **Singh, S., P. Turina, C. J. Bustamante, D. J. Keller, and R. Capaldi** 1996. Topographical structure of membrane-bound *Escherichia coli* F_1F_0 ATP synthase in aqueous buffer FEBS Lett. **397:**30-4.

213. **Skou, J. C.** 1957. The influence of some cations on an adenosine triphosphatase from peripheral nerves Biochim Biophys Acta. **23:**394-401.

214. **Skou, J. C.** 1982. The (Na+ + K+)-ATPase: coupling of the reaction with ATP to the reaction with Na+ and K+ Ann N Y Acad Sci. **402:**169-84.

215. **Smith, P. K., R. I. Krohn, G. T. Hermanson, A. K. Mallia, F. H. Gartner, M. D. Provenzano, E. K. Fujimoto, N. M. Goeke, B. J. Olson, and D. C. Klenk** 1985. Measurement of protein using bicinchoninic acid [published erratum appears in Anal Biochem 1987 May 15;163(1):279] Anal Biochem. **150:**76-85.

216. **Solioz, M., A. Odermatt, and R. Krapf** 1994. Copper pumping ATPases: common concepts in bacteria and man FEBS Lett. **346:**44-7.

217. **Sorgen, P. L., M. R. Bubb, and B. D. Cain** 1999. Lengthening the second stalk of F_1F_0 ATP synthase in *Escherichia coli* J Biol Chem. **274:**36261-6.

218. **Sorgen, P. L., M. R. Bubb, K. A. McCormick, A. S. Edison, and B. D. Cain** 1998. Formation of the *b* subunit dimer is necessary for interaction with F_1-ATPase Biochemistry. **37:**923-32.

219. **Sorgen, P. L., T. L. Caviston, R. C. Perry, and B. D. Cain** 1998. Deletions in the second stalk of F_1F_0-ATP synthase in *Escherichia coli* J Biol Chem. **273:**27873-8.

220. **Spicer, Z., M. L. Miller, A. Andringa, T. M. Riddle, J. J. Duffy, T. Doetschman, and G. E. Shull** 2000. Stomachs of mice lacking the gastric H,K-ATPase alpha -subunit have achlorhydria, abnormal parietal cells, and ciliated metaplasia J Biol Chem. **275:**21555-65.

221. **Stack, A. E., and B. D. Cain** 1994. Mutations in the delta subunit influence the assembly of F_1F_0 ATP synthase in *Escherichia coli* J Bacteriol. **176:**540-2.

222. **Steffens, K., E. Schneider, G. Deckers-Hebestreit, and K. Altendorf** 1987. F_0 portion of *Escherichia coli* ATP synthase. Further resolution of trypsin-generated fragments from subunit *b* J Biol Chem. **262:**5866-9.

223. **Stevens, T. H., and M. Forgac** 1997. Structure, function and regulation of the vacuolar (H+)-ATPase Annu Rev Cell Dev Biol. **13:**779-808.

224. **Stock, D., A. G. Leslie, and J. E. Walker** 1999. Molecular architecture of the rotary motor in ATP synthase [see comments] Science. **286:**1700-5.

225. **Sugden, B., K. Marsh, and J. Yates** 1985. A vector that replicates as a plasmid and can be efficiently selected in B-lymphoblasts transformed by Epstein-Barr virus Mol Cell Biol. **5:**410-3.

226. **Sugino, Y., and Y. Miyoshi** 1964. The specific precipitation of orthophosphate and some biochemical applications J Biol Chem. **239:**2360-2364.

227. **Sumner, J. P., J. A. Dow, F. G. Earley, U. Klein, D. Jager, and H. Wieczorek** 1995. Regulation of plasma membrane V-ATPase activity by dissociation of peripheral subunits J Biol Chem. **270:**5649-53.

228. **Takeda, K., S. Noguchi, A. Sugino, and M. Kawamura** 1988. Functional activity of oligosaccharide-deficient (Na,K)ATPase expressed in *Xenopus* oocytes FEBS Lett. **238:**201-4.

229. **Takeyama, M., T. Noumi, M. Maeda, and M. Futai** 1988. F_0 portion of *Escherichia coli* H+-ATPase. Carboxyl-terminal region of the *b* subunit is essential for assembly of functional F_0 J Biol Chem. **263:**16106-12.

230. **Takeyasu, K., H. Omote, S. Nettikadan, F. Tokumasu, A. Iwamoto-Kihara, and M. Futai** 1996. Molecular imaging of *Escherichia coli* F_0F_1-ATPase in reconstituted membranes using atomic force microscopy FEBS Lett. **392:**110-3.

231. **Tamura, S., M. Tagaya, M. Maeda, and M. Futai** 1989. Pig gastric (H+ + K+)-ATPase. Lys-497 conserved in cation transporting ATPases is modified with pyridoxal 5'-phosphate J Biol Chem. **264:**8580-4.

232. **Tang, C., and R. A. Capaldi** 1996. Characterization of the interface between gamma and epsilon subunits of *Escherichia coli* F_1-ATPase J Biol Chem. **271:**3018-24.

233. **Tao, T., P. F. Grulich, L. M. Kucharski, R. L. Smith, and M. E. Maguire** 1998. Magnesium transport in *Salmonella typhimurium*: biphasic magnesium and time dependence of the transcription of the mgtA and mgtCB loci Microbiology. **144:**655-64.

234. **Taussky, H., and E. Shorr** 1953. A microcolorimetric method for the determination of inorganic phosphorus J. Biol. Chem. **202:**675-685.

235. **Therien, A. G., R. Goldshleger, S. J. Karlish, and R. Blostein** 1997. Tissue-specific distribution and modulatory role of the gamma subunit of the Na,K-ATPase J Biol Chem. **272:**32628-34.

236. **Therien, A. G., S. J. Karlish, and R. Blostein** 1999. Expression and functional role of the gamma subunit of the Na, K-ATPase in mammalian cells J Biol Chem. **274:**12252-6.

237. **Thompson, J., D. Higgins, and T. Gibson** 1994. CLUSTALW: improving the sensitivity of progressive multiple sequence alignment through sequence weighing, position-specific gap penalties and weight matrix choice Nucl. Acid Res. **22:**4673-4680.

238. **Toh, B. H., P. A. Gleeson, R. J. Simpson, R. L. Moritz, J. M. Callaghan, I. Goldkorn, C. M. Jones, T. M. Martinelli, F. T. Mu, D. C. Humphris, and et al.** 1990. The 60- to 90-kDa parietal cell autoantigen associated with autoimmune gastritis is a beta subunit of the gastric H+/K(+)-ATPase (proton pump) Proc Natl Acad Sci U S A. **87:**6418-22.

239. **Tomashek, J. J., J. L. Sonnenburg, J. M. Artimovich, and D. J. Klionsky** 1996. Resolution of subunit interactions and cytoplasmic subcomplexes of the yeast vacuolar proton-translocating ATPase J Biol Chem. **271:**10397-404.

240. **Toyoshima, C., M. Nakasako, H. Nomura, and H. Ogawa** 2000. Crystal structure of the calcium pump of sarcoplasmic reticulum at 2.6 A resolution [see comments] Nature. **405:**647-55.

241. **Uhlin, U., G. B. Cox, and J. M. Guss** 1997. Crystal structure of the epsilon subunit of the proton-translocating ATP synthase from *Escherichia coli* Structure. **5:**1219-30.

242. **Valiyaveetil, F. I., and R. H. Fillingame** 1997. On the role of Arg-210 and Glu-219 of subunit *a* in proton translocation by the *Escherichia coli* F_0F_1-ATP synthase J Biol Chem. **272:**32635-41.

243. **Valiyaveetil, F. I., and R. H. Fillingame** 1998. Transmembrane topography of subunit *a* in the *Escherichia coli* F_1F_0 ATP synthase J Biol Chem. **273:**16241-7.

244. **van Driel, I. R., and J. M. Callaghan** 1995. Proton and potassium transport by H+/K(+)-ATPases Clin Exp Pharmacol Physiol. **22:**952-60.

245. **Van Veldhoven, P. P., and G. P. Mannaerts** 1987. Inorganic and organic phosphate measurements in the nanomolar range Anal Biochem. **161:**45-8.

246. **Van Walraven, H. S., H. Strotmann, O. Schwarz, and B. Rumberg** 1996. The H+/ATP coupling ratio of the ATP synthase from thiol-modulated chloroplasts and two cyanobacterial strains is four FEBS Lett. **379:**309-13.

247. **Verlander, J. W., R. M. Moudy, W. G. Campbell, B. D. Cain, and C. S. Wingo** 1998. Immunohistochemical localization of $HK\alpha_{2c}$ in rabbit kidney J Am Soc Nephrol. **9:**13A.

248. **von Meyenburg, K., B. B. Jorgensen, J. Nielsen, F. G. Hansen, and O. Michelsen** 1982. The membrane bound ATP synthase of *Escherichia coli*: a review of structural and functional analyses of the atp operon Tokai J. Exp. Clin. Med. **7 (suppl.):**23-31.

249. **Wada, T., J. C. Long, D. Zhang, and S. B. Vik** 1999. A novel labeling approach supports the five-transmembrane model of subunit *a* of the *Escherichia coli* ATP synthase J Biol Chem. **274:**17353-7.

250. **Walderhaug, M. O., R. L. Post, G. Saccomani, R. T. Leonard, and D. P. Briskin** 1985. Structural relatedness of three ion-transport adenosine triphosphatases around their active sites of phosphorylation J Biol Chem. **260:**3852-9.

251. **Walker, J. E., M. J. Runswick, and L. Poulter** 1987. ATP synthase from bovine mitochondria. The characterization and sequence analysis of two membrane-associated sub-units and of the corresponding cDNAs J Mol Biol. **197:**89-100.

252. **Walker, J. E., M. Saraste, and N. J. Gay** 1982. *E. coli* F_1-ATPase interacts with a membrane protein component of a proton channel Nature. **298:**867-9.

253. **Walker, J. E., M. Saraste, and N. J. Gay** 1984. The *unc* operon. Nucleotide sequence, regulation and structure of ATP- synthase Biochim Biophys Acta. **768:**164-200.

254. **Wang, S. G., K. A. Eakle, R. Levenson, and R. A. Farley** 1997. Na+-K+-ATPase alpha-subunit containing Q905-V930 of gastric H+-K+- ATPase alpha preferentially assembles with H+-K+-ATPase beta Am J Physiol. **272:**C923-30.

255. **Watts, S. D., C. Tang, and R. A. Capaldi** 1996. The stalk region of the *Escherichia coli* ATP synthase. Tyrosine 205 of the gamma subunit is in the interface between the F_1 and F_0 parts and can interact with both the epsilon and *c* oligomer J Biol Chem. **271:**28341-7.

256. **Wilkens, S., and R. A. Capaldi** 1998. Electron microscopic evidence of two stalks linking the F_1 and F_0 parts of the *Escherichia coli* ATP synthase Biochim Biophys Acta. **1365:**93-7.

257. **Wilkens, S., and R. A. Capaldi** 1998. Solution structure of the epsilon subunit of the F_1-ATPase from *Escherichia coli* and interactions of this subunit with beta subunits in the complex J Biol Chem. **273:**26645-51.

258. **Wilkens, S., F. W. Dahlquist, L. P. McIntosh, L. W. Donaldson, and R. A. Capaldi** 1995. Structural features of the epsilon subunit of the *Escherichia coli* ATP synthase determined by NMR spectroscopy [see comments] Nat Struct Biol. **2:**961-7.

259. **Wilkens, S., S. D. Dunn, and R. A. Capaldi** 1994. A cryoelectron microscopy study of the interaction of the *Escherichia coli* F_1-ATPase with subunit *b* dimer FEBS Lett. **354:**37-40.

260. **Wilkens, S., S. D. Dunn, J. Chandler, F. W. Dahlquist, and R. A. Capaldi** 1997. Solution structure of the N-terminal domain of the delta subunit of the *E. coli* ATPsynthase [letter] Nat Struct Biol. **4:**198-201.

261. **Wingo, C. S.** 1989. Active proton secretion and potassium absorption in the rabbit outer medullary collecting duct J Clin Invest. **84:**361-365.

262. **Wingo, C. S.** 1987. Potassium transport by medullary collecting tubule of rabbit: effects of variation in K intake Am J Physiol. **253:**F1136-1141.

263. **Wingo, C. S., and B. D. Cain** 1993. The renal H-K-ATPase: physiological significance and role in potassium homeostasis Annu Rev Physiol. **55:**323-47.

264. **Wingo, C. S., K. M. Madsen, A. Smolka, and C. C. Tisher** 1990. H,K-ATPase immunoreactivity in cortical and outer medullary collecting duct Kidney Int. **38:**985-990.

265. **Wingo, C. S., and A. J. Smolka** 1995. Function and structure of H-K-ATPase in the kidney [editorial] Am J Physiol. **269:**F1-16.

266. **Xian, Y., and H. Hebert** 1997. Three-dimensional structure of the porcine gastric H,K-ATPase from negatively stained crystals J Struct Biol. **118:**169-77.

267. **Xie, X. S.** 1996. Reconstitution of ATPase activity from individual subunits of the clathrin-coated vesicle proton pump. The requirement and effect of three small subunits J Biol Chem. **271:**30980-5.

268. **Yates, J. L., N. Warren, and B. Sugden** 1985. Stable replication of plasmids derived from Epstein-Barr virus in various mammalian cells Nature. **313:**812-5.

269. **Zamofing, D., B. C. Rossier, and K. Geering** 1989. Inhibition of *N*-glycosylation affects transepithelial Na+ but not Na+- K+-ATPase transport Am J Physiol. **256:**C958-66.

270. **Zhang, J., M. Myers, and M. Forgac** 1992. Characterization of the V_0 domain of the coated vesicle (H+)-ATPase J Biol Chem. **267:**9773-8.

271. **Zhang, P., C. Toyoshima, K. Yonekura, N. M. Green, and D. L. Stokes** 1998. Structure of the calcium pump from sarcoplasmic reticulum at 8-A resolution Nature. **392:**835-9.

272. **Zhang, Y., and R. H. Fillingame** 1995. Changing the ion binding specificity of the *Escherichia coli* H(+)- transporting ATP synthase by directed mutagenesis of subunit *c* J Biol Chem. **270:**87-93.

273. **Zhang, Y., and R. H. Fillingame** 1995. Subunits coupling H+ transport and ATP synthesis in the *Escherichia coli* ATP synthase. Cys-Cys cross-linking of F_1 subunit epsilon to the polar loop of F_0 subunit *c* J Biol Chem. **270:**24609-14.

274. **Zhou, Y., T. M. Duncan, V. V. Bulygin, M. L. Hutcheon, and R. L. Cross** 1996. ATP hydrolysis by membrane-bound *Escherichia coli* F_0F_1 causes rotation of the gamma subunit relative to the beta subunits [published erratum appears in Biochim Biophys Acta 1996 Dec 18;1277(3):266] Biochim Biophys Acta. **1275:**96-100.

275. **Zhou, Y., T. M. Duncan, and R. L. Cross** 1997. Subunit rotation in *Escherichia coli* F_0F_1 ATP synthase during oxidative phosphorylation Proc Natl Acad Sci U S A. **94:**10583-7.

BIOGRAPHICAL SKETCH

Tamara Caviston Otto was born on May 8, 1971, in Havre de Grace, Maryland, to Dominic and Marsha Caviston. She grew up in Havre de Grace with her younger sister, Amy. Tamara graduated from The John Carroll School in May 1989. That fall she attended the University of Delaware where she received a Bachelor of Arts degree in biology in May 1993. After graduation, Tamara worked as a student contractor in a biochemistry laboratory at the United States Institute of Chemical Defense in Edgewood, Maryland, under the supervision of Dr. Charles Millard. She realized her strong interest in biochemistry and molecular biology, and Dr. Millard suggested that she attend graduate school. Tamara arrived at the University of Florida in August 1995 and in the spring of 1996, she joined Dr. Brian Cain's laboratory where she completed the work described in this dissertation. Once finishing the requirements for her degree, Tamara and her husband, Scott, will be returning to Maryland where she will study transcriptional control of adipogenesis with Dr. M. Daniel Lane at The Johns Hopkins University.

I certify that I have read this study and that in my opinion it conforms to acceptable standards of scholarly presentation and is fully adequate, in scope and quality, as a dissertation for the degree of Doctor of Philosophy.

Brian D. Cain, Chair
Professor of Biochemistry and
Molecular Biology

I certify that I have read this study and that in my opinion it conforms to acceptable standards of scholarly presentation and is fully adequate, in scope and quality, as a dissertation for the degree of Doctor of Philosophy.

Mary Jo Koroly
Associate Professor of Biochemistry and
Molecular Biology

I certify that I have read this study and that in my opinion it conforms to acceptable standards of scholarly presentation and is fully adequate, in scope and quality, as a dissertation for the degree of Doctor of Philosophy.

Michael S. Kilberg
Professor of Biochemistry and
Molecular Biology

I certify that I have read this study and that in my opinion it conforms to acceptable standards of scholarly presentation and is fully adequate, in scope and quality, as a dissertation for the degree of Doctor of Philosophy.

Daniel L. Purich
Professor of Biochemistry and
Molecular Biology

I certify that I have read this study and that in my opinion it conforms to acceptable standards of scholarly presentation and is fully adequate, in scope and quality, as a dissertation for the degree of Doctor of Philosophy.

Charles S. Wingo
Professor of Physiology and
Pharmacology

This dissertation was submitted to the Graduate Faculty of the College of Medicine and to the Graduate School and was accepted as partial fulfillment of the requirements for the degree of Doctor of Philosophy.

May 2001

Dean, College of Medicine

Dean, Graduate School

UNIVERSITY OF FLORIDA
3 1262 08554 3485